

**An investigation into the potential use of  
poly(vinylphosphonic acid-*co*-acrylic acid) in  
bone tissue scaffolds**

A thesis submitted to the University of Manchester for the degree  
of Doctor of Philosophy in the Faculty of Science and  
Engineering

**2017**

**Rebecca E. Dey**

**School of Chemistry**

# Table of Contents

<b>List of Figures</b> .....	<b>7</b>
<b>List of Tables</b> .....	<b>11</b>
<b>List of Schemes</b> .....	<b>12</b>
<b>List of Abbreviations</b> .....	<b>13</b>
<b>Abstract</b> .....	<b>15</b>
<b>Declaration</b> .....	<b>16</b>
<b>Copyright Statement</b> .....	<b>16</b>
<b>Acknowledgements</b> .....	<b>17</b>
<b>Chapter 1: Introduction</b> .....	<b>18</b>
1.1 Bone.....	18
1.1.1 Structure and properties of bone.....	18
1.1.2 Extracellular matrix of bone .....	19
1.1.3 Mineralisation of the ECM .....	20
1.1.4 Bone cells.....	21
1.1.5 The bone remodelling process .....	21
1.2 Bone Diseases and Current Treatments.....	22
1.2.1 Osteoporosis.....	22
1.2.2 Bone grafting techniques .....	23
1.2.3 Bisphosphonates .....	24
1.3 Materials used in Bone Repair .....	25
1.3.1 Metals.....	25
1.3.2 Ceramics .....	26
1.4 Bone Tissue Engineering.....	26
1.4.1 Tissue scaffolds for bone regeneration .....	27
1.5 Fabrication of Tissue Scaffolds .....	28
1.5.1 Freeze-drying .....	28
1.5.2 Solvent casting .....	28
1.5.3 Electrospinning .....	28
1.6 Polymeric Tissue Scaffolds .....	29
1.6.1 Poly(glycolic acid) and poly(lactic acid).....	30
1.6.2 Poly( $\epsilon$ -caprolactone).....	31
1.6.3 Functionalisation of scaffolds.....	32

1.6.4 Scaffolds for drug delivery .....	33
1.7 Hydrogels .....	34
1.7.1 Natural hydrogels.....	34
1.7.2 Synthetic hydrogels.....	35
1.8 Polyelectrolytes .....	36
1.8.1 Solution properties of polyelectrolytes .....	36
1.8.2 Polyelectrolyte conformation in solution.....	37
1.9 Poly(acrylic acid) .....	38
1.9.1 Hydrogels of PAA .....	38
1.10 Poly(vinylphosphonic acid).....	39
1.10.1 PVPA incorporation into tissue scaffolds.....	39
1.10.2 Hydrogels of PVPA .....	40
1.11 Poly(vinylphosphonic acid- <i>co</i> -acrylic acid).....	41
1.12 Aims and Objectives .....	43
<b>Chapter 2: Synthesis and characterisation of poly(vinylphosphonic acid-<i>co</i>-acrylic acid) .....</b>	<b>44</b>
2.1 Introduction .....	44
2.1.1 Free radical polymerisation .....	44
2.1.2 Monomer reactivity ratios.....	45
2.1.3 Synthesis of PAA.....	45
2.1.4 Synthesis of PVPA.....	46
2.1.5 Synthesis of PVPA- <i>co</i> -AA .....	47
2.1.6 Aims and Objectives .....	48
2.2 Experimental .....	49
2.2.1 Materials .....	49
2.2.2 Experimental methods .....	49
2.2.3 Synthesis of PVPA- <i>co</i> -AA .....	50
2.2.4 Synthesis of PVPA- <i>co</i> -AA for the evaluation of reactivity ratios.....	50
2.2.5 Synthesis of PVPA- <i>co</i> -AA using chain transfer agent (CTA) .....	51
2.2.6 Synthesis of PAA.....	51
2.2.7 Synthesis of PVPA.....	52
2.3 Results and Discussion .....	53
2.3.1 Effect of temperature and initiator concentration .....	53
2.3.2 Calculation of copolymer composition using elemental analysis.....	56

2.3.3 Calculation of copolymer composition using <sup>31</sup> P NMR spectroscopy .....	57
2.3.4 Effect of monomer feed ratio on the properties of the copolymers .....	58
2.3.5 Monomer reactivity ratios.....	60
2.3.6 Synthesis of PVPA- <i>co</i> -AA using chain transfer agent .....	65
2.4 Conclusions .....	70
<b>Chapter 3: Calcium binding affinity of PVPA-<i>co</i>-AA .....</b>	<b>72</b>
3.1 Introduction .....	72
3.1.1 Calcium binding to PAA and PVPA.....	73
3.1.2 Poly(vinylphosphonic acid- <i>co</i> -acrylic acid) .....	73
3.1.3 Composition of extracellular fluid .....	74
3.1.4 Aims and Objectives .....	75
3.2 Experimental .....	76
3.2.1 Materials .....	76
3.2.2 Potentiometric titrations.....	76
3.2.3 Assessment of calcium binding affinity.....	76
3.2.4 Rheology .....	78
3.2.5 Zeta-potential measurements .....	79
3.3 Results and Discussion .....	80
3.3.1 Potentiometric titrations.....	80
3.3.2 Assessment of calcium binding affinity.....	83
3.3.3 Rheological properties of PVPA- <i>co</i> -AA .....	89
3.3.4 Zeta-potential measurements .....	92
3.4 Conclusions .....	94
<b>Chapter 4: Incorporation of PVPA-<i>co</i>-AA into electrospun PCL scaffolds.....</b>	<b>96</b>
4.1 Introduction .....	96
4.1.1 Incorporation of bisphosphonates into tissue scaffolds .....	96
4.1.2 PCL/PVPA- <i>co</i> -AA composite scaffolds.....	96
4.1.3 Sterilisation of tissue scaffolds .....	98
4.1.4 Aims and Objectives .....	99
4.2 Experimental .....	100
4.2.1 Materials .....	100
4.2.2 Fabrication of PCL/PVPA- <i>co</i> -AA scaffolds by electrospinning.....	100
4.2.3 Uptake efficiency of PVPA- <i>co</i> -AA into PCL scaffolds .....	101
4.2.4 Sterilisation of PCL/PVPA- <i>co</i> -AA scaffolds .....	102

4.2.5 Calcium chelation of PCL/PVPA- <i>co</i> -AA scaffolds.....	103
4.2.6 Release of PVPA- <i>co</i> -AA from PCL scaffolds.....	103
4.2.7 Calcium chelation in osteogenic differentiation media .....	104
4.3 Results and Discussion .....	104
4.3.1 Uptake efficiency of PVPA- <i>co</i> -AA into PCL scaffolds .....	104
4.3.2 Effect of sterilisation on PCL/PVPA- <i>co</i> -AA scaffolds .....	106
4.3.3 Release of PVPA- <i>co</i> -AA from PCL scaffolds.....	108
4.3.4 Calcium chelation from osteogenic differentiation media.....	111
4.4 Conclusions .....	113
<b>Chapter 5: PVPA-<i>co</i>-AA hydrogels for bone regeneration .....</b>	<b>114</b>
5.1 Introduction .....	114
5.1.1 Biocompatibility studies .....	115
5.1.2 Aims and Objectives .....	116
5.2 Experimental .....	117
5.2.1 Materials .....	117
5.2.2 Preparation of PVPA- <i>co</i> -AA hydrogels .....	117
5.2.3 Elemental analysis .....	117
5.2.4 FT-IR spectroscopy.....	118
5.2.5 Swelling studies .....	118
5.2.6 Scanning Electron Microscope (SEM) analysis .....	118
5.2.7 Water contact angle measurements.....	119
5.2.8 Rheological properties of PVPA- <i>co</i> -AA hydrogels.....	119
5.2.9 Cell culture.....	119
5.2.10 Live/Dead® Staining .....	120
5.2.11 Determination of cell number .....	120
5.2.12 Cell metabolic activity .....	122
5.2.13 Statistical analysis.....	122
5.3 Results and Discussion .....	123
5.3.1 Synthesis and characterisation of PVPA- <i>co</i> -AA hydrogels .....	123
5.3.2 Swelling capacity of PVPA- <i>co</i> -AA hydrogels .....	128
5.3.3 SEM analysis .....	129
5.3.4 Water contact angle measurements.....	131
5.3.5 Rheology .....	133
5.3.6 Cell proliferation and metabolic activity .....	137

5.4 Conclusions .....	142
<b>Chapter 6: PVPA-co-AA for fluoride removal from groundwater .....</b>	<b>144</b>
6.1 Introduction .....	144
6.1.1 Dental fluorosis.....	144
6.1.2 Current methods for fluoride removal .....	145
6.1.3 Common adsorbents .....	146
6.1.4 Aims and Objectives.....	147
6.2 Experimental .....	148
6.2.1 Materials .....	148
6.2.2 Assessment of fluoride uptake by HA .....	148
6.2.3 Synthesis of PVPA-HA composite hydrogels .....	149
6.2.4 Swelling of PVPA-HA hydrogels.....	150
6.2.5 FT-IR spectroscopy.....	150
6.2.6 Rheology.....	150
6.2.7 Assessment of fluoride uptake by PVPA-HA hydrogels.....	151
6.2.8 Effect of pH on fluoride uptake .....	151
6.2.9 Effect of contact time on fluoride uptake .....	151
6.2.10 Effect of the presence of other ions on fluoride uptake.....	151
6.2.11 Regeneration of PVPA-HA hydrogels.....	152
6.3 Results and Discussion .....	153
6.3.1 Fluoride uptake by HA .....	153
6.3.2 Synthesis and characterisation of PVPA-HA hydrogels.....	155
6.3.3 Fluoride uptake by PVPA-HA hydrogels .....	157
6.3.4 Effect of pH on fluoride uptake .....	158
6.3.5 Effect of contact time.....	159
6.3.6 Effect of common ion interference .....	160
6.3.7 Regeneration of PVPA-HA hydrogels.....	161
6.4 Conclusions .....	162
<b>7.0 Conclusions and Future Work.....</b>	<b>164</b>
7.1 Conclusions .....	164
7.2 Recommendations for Future Work .....	167
<b>8.0 References .....</b>	<b>169</b>
<b>Appendix.....</b>	<b>178</b>

Final word count: 48,851

## List of Figures

<b>Figure 1.1</b> – Hierarchical structure of bone.....	19
<b>Figure 1.2</b> – A schematic representation of the native extracellular matrix (ECM) of bone and its components.....	20
<b>Figure 1.3</b> – A comparison between healthy bone and osteoporotic bone.....	23
<b>Figure 1.4</b> – Structural comparison of (a) inorganic pyrophosphate and (b) bisphosphonate.....	24
<b>Figure 1.5</b> – Typical electrospinning setup.....	29
<b>Figure 1.6</b> – Chemical structure of (a) poly(glycolic acid) (PGA) and (b) poly(lactic acid) (PLA).....	30
<b>Figure 1.7</b> – Chemical structure of poly( $\epsilon$ -caprolactone) (PCL).....	31
<b>Figure 1.8</b> – SEM micrographs of MSCs seeded onto PCL scaffolds. (a) Scaffold prior to seeding. (b) Low magnification view of the cell-polymer constructs after 1 week of culture.....	32
<b>Figure 1.9</b> – Schematic diagram of the electrical double layer of polyelectrolytes formed in aqueous media.....	37
<b>Figure 1.10</b> – (a) Adhesion and (b) proliferation of MC3T3-E1 subclone 4 pre-osteoblast cells adhered to acrylamide substrates modified with graft copolymers created from feed compositions of increasing VPA content (mol %)......	40
<b>Figure 1.11</b> – Calcium chelation by the carboxylate groups of acrylic acid (AA) and the phosphonate groups of vinylphosphonic acid (VPA).....	41
<b>Figure 1.12</b> – (a) Bone fill percentage after 35 days of culture on PCL and PCL/PVPA scaffolds (b) Micro-CT images of PCL and PCL/PVPA scaffolds after 7 and 35 days of culture.....	42
<b>Figure 2.1</b> – $^1\text{H}$ NMR spectrum of P2 (30 mol % VPA) prior to purification.....	54
<b>Figure 2.2</b> – $^{31}\text{P}$ NMR spectrum of P2 (30 mol % VPA) prior to purification.....	58
<b>Figure 2.3</b> – Weight distributions of $\log[\text{molar mass}/(\text{g mol}^{-1})]$ for PVPA- <i>co</i> -AA copolymers with VPA feed contents of 10, 30, 50 and 70 mol %.....	60
<b>Figure 2.4</b> – Fineman-Ross plot for the evaluation of monomer reactivity ratios for the copolymerisation of AA with VPA.....	64
<b>Figure 2.5</b> – Kelen-Tüdös plot for the evaluation of monomer reactivity ratios for the copolymerisation of AA with VPA.....	65
<b>Figure 2.6</b> – $^1\text{H}$ NMR spectra of (a) PVPA-0, (b) PVPA-30, (c) PVPA-60 and (d) PVPA-100.....	68
<b>Figure 2.7</b> – $^{31}\text{P}$ NMR spectra of (a) PVPA-30 and (b) PVPA-100.....	69
<b>Figure 2.8</b> – FT-IR spectra of (a) PVPA-0, (b) PVPA-30 and (c) PVPA-100.....	70
<b>Figure 3.1</b> – Calibration curve for the determination of calcium chelation by PVPA- <i>co</i> -AA copolymers, over a range of copolymer compositions and pH values.....	77
<b>Figure 3.2</b> – Storage ( $G'$ ) and loss ( $G''$ ) modulus of PVPA-30 in deionised water, at pH 7.3, across a strain range of 10.0 to 500%.....	78

<b>Figure 3.3</b> – pH titration curves of VPA monomer, PAA and PVPA homopolymers, and PVPA- <i>co</i> -AA copolymers with VPA contents of 20, 40, 60 and 80 mol %.....	81
<b>Figure 3.4</b> – pH titration curves of PVPA-0, PVPA-30, PVPA-30 with added NaCl (0.1 M) and PVPA-100.....	83
<b>Figure 3.5</b> – Calcium chelation capacity of PVPA- <i>co</i> -AA copolymers, at pH 5.0, with increasing VPA content in the copolymer.....	84
<b>Figure 3.6</b> – Calcium chelation capacity of PVPA- <i>co</i> -AA copolymers, at pH 7.3 and 9.0, with increasing VPA content in the copolymer.....	85
<b>Figure 3.7</b> – Calcium chelation capacity of PVPA-30 with increasing polymer concentration.....	86
<b>Figure 3.8</b> – Calcium chelation capacity of PVPA-0, PVPA-30 and PVPA-100 with increasing NaCl concentration.....	88
<b>Figure 3.9</b> – Effect of increasing NaCl concentration on the complex viscosity ( $\eta^*$ ) of PVPA-0, PVPA-30 and PVPA-100 in deionised water at pH 7.3.....	90
<b>Figure 3.10</b> – (a) Storage ( $G'$ ) and (b) loss ( $G''$ ) modulus of PVPA-30, with different calcium concentrations, across a frequency sweep of 1.0 to 20.0 Hz.....	91
<b>Figure 3.11</b> – Complex viscosity ( $\eta^*$ ) of PVPA-30, with different calcium concentrations, across a frequency sweep of 1.0 to 20.0 Hz.....	92
<b>Figure 3.12</b> – Dependence of zeta-potential on $\text{CaCl}_2$ concentration for aqueous solutions of PVPA-30 in deionised water at pH 7.3.....	93
<b>Figure 4.1</b> – (a) SEM micrograph of PCL fibres treated with PVPA- <i>co</i> -AA. (b) The phosphorus concentration on the surface of the polymeric scaffolds examined through energy-dispersive X-ray spectroscopy (EDX) over 21 days.....	97
<b>Figure 4.2</b> – Calibration curve for the determination of PVPA-30 uptake efficiency into PCL scaffolds by UV/Vis spectroscopy.....	102
<b>Figure 4.3</b> – FT-IR spectra of (a) PVPA-30 and (b) PVPA- $\text{Cu}^{2+}$ complex.....	105
<b>Figure 4.4</b> – Calcium chelation capacity of electrospun nanofibrous scaffolds before and after sterilisation with 70% ethanol.....	108
<b>Figure 4.5</b> – Cumulative percentage of PVPA-30 released, in deionised water at 37 °C, from PCL scaffolds. Scaffolds were produced by dip-coating with (PVPA-H) and without (PVPA-D) heat treatment.....	109
<b>Figure 4.6</b> – Cumulative percentage of PVPA-30 released, in deionised water at 37 °C, from PCL scaffolds. Scaffolds were produced by co-spinning PCL with PVPA- <i>co</i> -AA at different concentrations (5.0, 7.0 and 10 wt %) with the use of span 80 as a surfactant.....	111
<b>Figure 4.7</b> – Calcium chelation of PCL electrospun nanofibrous scaffolds, with different concentrations of PVPA-30, in osteogenic differentiation media.....	112
<b>Figure 5.1</b> – Determination of cell metabolic activity for AA and VPA monomers over a 72 h culture period, for a range of monomer concentrations, compared with a PBS control.....	115
<b>Figure 5.2</b> – Calibration curve for the determination of dsDNA concentration of cells seeded onto PVPA- <i>co</i> -AA hydrogels.....	121

<b>Figure 5.3</b> – (a) Effect of crosslinker (EGDA) concentration on the dynamic swelling of PVPA- <i>co</i> -AA hydrogels in phosphate buffer solution at pH 7.3. (b) Effect of EGDA concentration on the storage ( $G'$ ) modulus of PVPA- <i>co</i> -AA hydrogels across a frequency range of 0.1 to 10 Hz. In each case, the VPA content was 30 mol %.....	124
<b>Figure 5.4</b> – (a) Effect of polymerisation time on the swelling of PVPA- <i>co</i> -AA hydrogels in phosphate buffer solution at pH 7.3. (b) Effect of polymerisation time on the storage modulus ( $G'$ ) of PVPA- <i>co</i> -AA hydrogels across a frequency range of 0.1 to 10 Hz. In each case, the VPA content was 30 mol %.....	126
<b>Figure 5.5</b> – FT-IR spectra of (a) VPA-0, (b) VPA-10, (c) VPA-30 and (d) VPA-50.....	128
<b>Figure 5.6</b> – Swelling of PVPA- <i>co</i> -AA hydrogels as a function of VPA content, at pH 5.0, 7.3 and 9.0.....	129
<b>Figure 5.7</b> – Scanning electron microscope (SEM) images to show the difference in morphology of freeze-dried PVPA- <i>co</i> -AA hydrogels with increasing VPA contents. (a) VPA-0, (b) VPA-10, (c) VPA-30 and (d) VPA-50.....	130
<b>Figure 5.8</b> – Schematic representation of the hierarchical structure of hydrogels with both micro- and nanoscale pores.....	131
<b>Figure 5.9</b> – Photograph images of 10 $\mu$ L water droplet on (a) VPA-0, (b) VPA-10, (c) VPA-30 and (d) VPA-50 hydrogels.....	132
<b>Figure 5.10</b> – (a) Storage ( $G'$ ) and (b) loss ( $G''$ ) modulus of PVPA- <i>co</i> -AA hydrogels, with different copolymer compositions, across a frequency sweep of 0.1 to 10 Hz.....	134
<b>Figure 5.11</b> – Change in complex viscosity ( $\eta^*$ ) of PVPA- <i>co</i> -AA hydrogels, with different copolymer compositions, across a frequency sweep of 0.1 to 10 Hz.....	135
<b>Figure 5.12</b> – Storage ( $G'$ ) and loss ( $G''$ ) modulus of PVPA- <i>co</i> -AA hydrogels, with different copolymer compositions, across a strain range of 1.0-100%. (a) VPA-0, (b) VPA-10, (c) VPA-30 and (d) VPA-50.....	136
<b>Figure 5.13</b> – Live/Dead® imaging of SaOS-2 cells to illustrate cell viability on PVPA- <i>co</i> -AA hydrogels, as a function of copolymer composition, over 72 h.....	138
<b>Figure 5.14</b> – (a) Osteoblast proliferation and (b) cell spreading on PVPA- <i>co</i> -AA hydrogels, with increasing VPA content, over 72 h.....	139
<b>Figure 5.15</b> – Osteoblast proliferation on PVPA- <i>co</i> -AA hydrogels, with increasing VPA content, over 14 days.....	140
<b>Figure 5.16</b> – (a) Fluorescence intensity of SaOS-2 cells (measured using the AlamarBlue® assay) and (b) osteoblast metabolic activity on PVPA- <i>co</i> -AA hydrogels, with increasing VPA content, over 14 days.....	141
<b>Figure 6.1</b> – Moderate and severe effects of dental fluorosis as a result of fluoridated water.....	145
<b>Figure 6.2</b> – Calibration curve for the determination of fluoride uptake by HA powder.....	149
<b>Figure 6.3</b> – Effect of concentration on the fluoride uptake affinity of HA dispersed in NaF solution (10 mg L <sup>-1</sup> ) at pH 7.0 and 20.0 °C.....	153

<b>Figure 6.4</b> – Effect of solution pH on the fluoride uptake affinity of HA, at a concentration of 2.5 mM, dispersed in NaF solution (10 mg L <sup>-1</sup> ) at 20.0 °C.....	154
<b>Figure 6.5</b> – Storage ( <i>G'</i> ) and loss ( <i>G''</i> ) modulus of PVPA-HA hydrogels, with different HA concentrations, across a frequency sweep of 0.1 to 25 Hz at 20.0 °C.....	156
<b>Figure 6.6</b> – FT-IR spectra of (a) PVPA- <i>co</i> -AA hydrogel, with a VPA content of 30 mol %, and (b) PVPA-HA composite hydrogel, with a HA concentration of 0.25 mM.....	157
<b>Figure 6.7</b> – Effect of HA concentration on the fluoride uptake affinity of PVPA-HA hydrogels and HA powder in NaF solution (10 mg L <sup>-1</sup> ) at 20.0 °C.....	158
<b>Figure 6.8</b> – Effect of solution pH on the fluoride uptake affinity of PVPA-HA hydrogel (HA concentration of 0.25 mM) in NaF solution (10 mg L <sup>-1</sup> ) at 20.0 °C.....	159
<b>Figure 6.9</b> – Fluoride uptake affinity of PVPA-HA hydrogel (HA concentration of 0.25 mM), in NaF solution (10 mg L <sup>-1</sup> ) at 20.0 °C, as a function of contact time over 30 h.....	160
<b>Figure 6.10</b> – Effect of competitor ions (NaCl, Na <sub>2</sub> SO <sub>4</sub> , NaNO <sub>3</sub> and NaHCO <sub>3</sub> ) on the fluoride uptake affinity of PVPA-HA hydrogels (HA concentration of 0.25 mM) in NaF solution (10 mg L <sup>-1</sup> ) at 20.0 °C.....	161
<b>Figure 6.11</b> – Effect of repeated regeneration cycles on the fluoride uptake affinity of PVPA-HA hydrogel (HA concentration of 0.25 mM) in NaF solution (10 mg L <sup>-1</sup> ) at 20.0 °C.....	162

## List of Tables

<b>Table 1.1</b> – Desirable properties of a tissue engineered scaffold used for bone regeneration.....	27
<b>Table 2.1</b> – Experimental conditions for the copolymerisation of AA with VPA...	52
<b>Table 2.2</b> – Effect of temperature and initiator concentration on yield, monomer conversion, weight-average molar mass ( $M_w$ ), number-average molar mass ( $M_n$ ) and molar mass distribution ( $M_w/M_n$ ) for the copolymerisation of VPA with AA.....	56
<b>Table 2.3</b> – Elemental analysis data for PVPA- <i>co</i> -AA samples with different feed compositions.....	56
<b>Table 2.4</b> – Effect of monomer feed ratio on monomer conversion, copolymer composition (VPA content as determined by elemental analysis and $^{31}\text{P}$ NMR spectroscopy), weight-average molar mass ( $M_w$ ), number-average molar mass ( $M_n$ ) and molar mass distribution ( $M_w/M_n$ ) for the copolymerisation of VPA with AA.....	59
<b>Table 2.5</b> – Effect of monomer feed ratio on copolymer composition, yield, monomer conversion, weight-average molar mass ( $M_w$ ), number-average molar mass ( $M_n$ ) and molar mass distribution ( $M_w/M_n$ ) for the copolymerisation of VPA with AA at low conversion.....	62
<b>Table 2.6</b> – Parameters used for the Fineman-Ross and Kelen-Tüdös methods.....	63
<b>Table 2.7</b> – Effect of monomer feed ratio and chain transfer agent (CTA) on copolymer composition (mol % VPA in copolymer) as determined by $^{31}\text{P}$ NMR spectroscopy and elemental analysis.....	66
<b>Table 2.8</b> – Effect of monomer feed ratio and chain transfer agent (CTA) on yield, monomer conversion, weight-average molar mass ( $M_w$ ), number-average molar mass ( $M_n$ ) and molar mass distribution ( $M_w/M_n$ ).....	67
<b>Table 3.1</b> – Ionic concentrations of simulated body fluid (SBF) and human blood plasma.....	74
<b>Table 4.1</b> – Relative mass ratios of PCL:Span 80:PVPA-30 of the electrospun nanofibres.....	101
<b>Table 4.2.</b> The absorbance of PVPA- $\text{Cu}^{2+}$ complexes, PVPA- <i>co</i> -AA concentrations and their uptake efficiencies into PCL scaffolds.....	106
<b>Table 4.3</b> – The change in PVPA- <i>co</i> -AA concentration in the PCL scaffolds, as measured by UV/Vis spectroscopy, after undergoing sterilisation with 70% ethanol.....	107
<b>Table 5.1</b> – Experimental conditions for the preparation of PVPA- <i>co</i> -AA hydrogels.....	117
<b>Table 5.2</b> – Elemental analysis data for PVPA- <i>co</i> -AA hydrogels with different monomer feed ratios.....	127
<b>Table 5.3</b> – Water contact angle of PVPA- <i>co</i> -AA hydrogels with increasing VPA content.....	133
<b>Table 6.1</b> – Experimental conditions and swelling ratio of PVPA-HA hydrogels with increasing HA concentration.....	155

## List of Schemes

<b>Scheme 2.1</b> – Suggested mechanism of cyclopolymerisation involving vinylphosphonic acid anhydride by (a) intramolecular and (b) intermolecular propagation.....	47
<b>Scheme 2.2</b> – Free radical polymerisation of AA and VPA to produce PVPA- <i>co</i> -AA.....	53
<b>Scheme 2.3</b> – (a) Decomposition of AAPH initiator to form two stable carbon radicals and molecular nitrogen and (b) AAPH initiator radical combines with molecular oxygen to form a peroxy radical.....	54
<b>Scheme 2.4</b> – Mechanism of inhibition by MEHQ via hydrogen abstraction by (a) initiator peroxy radical or (b) initiator alkyl radical and (c) resonance stabilisation of MEHQ.....	61
<b>Scheme 2.5</b> – Mechanism of chain transfer to the growing polymer chain by hydrogen abstraction from 1-octanethiol.....	66
<b>Scheme 5.1</b> – Synthetic scheme for the production of PVPA- <i>co</i> -AA hydrogels from AA and VPA monomers, using EGDA as a crosslinking agent.....	123

## List of Abbreviations

AA	Acrylic acid
AAm	Acrylamide
AAPH	2,2'-Azobis(2-methylpropionamide)
ANOVA	Analysis of variance
ATP	Adenosine triphosphate
BMP	Bone morphogenetic protein
BP	Bisphosphonate
BSP	Bone sialoprotein
CTA	Chain transfer agent
DC	Defluoridation capacity
DCM	Dichloromethane
dH <sub>2</sub> O	Deionised water
DNA	Deoxyribonucleic acid
dsDNA	Double stranded DNA
ECM	Extracellular matrix
EDL	Electrical double layer
EDX	Energy-dispersive X-ray spectroscopy
EGDA	Ethylene glycol diacrylate
EGDMA	Ethylene glycol dimethacrylate
FBS	Foetal bovine serum
FCS	Foetal calf serum
FT-IR	Fourier transform infrared
GPC	Gel permeation chromatography
Ha	Hyaluronic acid
HA	Hydroxyapatite
ICP-MS	Inductively coupled plasma mass spectrometry
LVR	Linear viscoelastic region
MEHQ	Monomethyl ether of hydroquinone
MSC	Mesenchymal stem cell
NCP	Non-collagenous protein
NMR	Nuclear magnetic resonance
OPN	Osteopontin

ORP	Oxidation-reduction potential
PAA	Poly(acrylic acid)
PBS	Phosphate buffered saline
PCL	Poly( $\epsilon$ -caprolactone)
PEG	Poly(ethylene glycol)
PEVAc	Poly(ethylene- <i>co</i> -vinyl acetate)
PGA	Poly(glycolic acid)
PHEMA	Poly(2-hydroxyethyl methacrylate)
PLA	Poly(lactic acid)
PLGA	Poly(lactic- <i>co</i> -glycolic acid)
PPi	Inorganic pyrophosphate
PVA	Poly(vinyl alcohol)
PVPA	Poly(vinylphosphonic acid)
PVPA- <i>co</i> -AA	Poly(vinylphosphonic acid- <i>co</i> -acrylic acid)
PVSA	Poly(vinylsulfonic acid)
RO	Reverse osmosis
SaOS-2	Human osteosarcoma derived osteoblast cells
SBF	Simulated body fluid
SD	Standard deviation
SEM	Scanning electron microscope
TCP	Tissue culture plastic
TMP	Trimethyl phosphate
UE	Uptake efficiency
UV	Ultraviolet
Vac	Vinyl acetate
Vis	Visible
VPA	Vinylphosphonic acid
VSA	Vinylsulfonic acid
$\alpha$ -MEM	Alpha minimum essential media
$\Delta$	Chemical shift
$\lambda_{\max}$	Wavelength of maximum absorbance

## Abstract

Bone undergoes constant turnover throughout life and has the capacity to regenerate itself. However, the repair of critical size defects, caused by bone diseases such as osteoporosis, can be more problematic. Therefore, there is a clinical need for a bone graft substitute that can be used at sites of surgical intervention to enhance bone regeneration. Poly(vinylphosphonic acid-*co*-acrylic acid) (PVPA-*co*-AA) has recently been identified as a potential candidate for use in bone tissue scaffolds. It is hypothesised that PVPA-*co*-AA can mimic the action of bisphosphonates – a class of drugs used in the treatment of osteoporosis – by binding to calcium ions from bone mineral surfaces. In this way, bisphosphonates can affect bone turnover by increasing the activity of osteoblasts and reducing osteoclast activity. Although PVPA-*co*-AA has been shown to improve bone formation, the mechanism of action has so far not been fully elucidated. Therefore, this work aims to understand the effect of copolymer composition on the properties of PVPA-*co*-AA, and thus to determine its effect on osteoblast adhesion and proliferation.

PVPA-*co*-AA copolymers have been synthesised with a range of monomer feed ratios. It was found that a VPA content of 30 mol % led to the greatest calcium binding affinity of the copolymer and is thus expected to lead to enhanced bone formation and mineralisation of the matrix produced by osteoblast cells. The release profile of PVPA-*co*-AA from electrospun PCL scaffolds was investigated. It was shown that all of the PVPA-*co*-AA was released into aqueous media within 8 h of immersion. It was also found that the calcium chelation from osteogenic differentiation media significantly increased within the first 8 h. Therefore, it was concluded that PVPA-*co*-AA is released from the scaffolds, where it can then bind to calcium ions from the bone mineral surface to promote mineralisation, thus acting as a mimic of non-collagenous proteins, which are present in the extracellular matrix (ECM) of bone.

Hydrogels of PVPA-*co*-AA have been produced and the effect of monomer feed ratio (0-50 mol % VPA) on the properties of the gels was explored. It was found that an increase in VPA content led to greater hydrogel swelling and increased porosities. Hydrogels that contained 30 and 50 mol % VPA were shown to have similar morphologies to the native ECM of bone. Rheological testing showed that hydrogels with higher VPA contents were more flexible and could be deformed to a large extent without permanent deformation of their structure. An increase in osteoblast adhesion and proliferation was observed for hydrogels with 30 and 50 mol % VPA content as well as superior cell spreading. Osteoblast cell metabolic activity also increased as a function of VPA content in the hydrogels. This work indicates that hydrogels of PVPA-*co*-AA, with VPA contents of 30 or 50 mol %, are ideal for use as bone tissue scaffolds. Furthermore, the mechanical and cell adhesion properties of the gels can be tuned by altering the copolymer composition.

Finally, composite hydrogels of PVPA-*co*-AA and hydroxyapatite (HA) have been produced and investigated for their ability to remove fluoride ions from groundwater. It was found that the fluoride uptake ability of PVPA-HA hydrogels was significantly enhanced when compared with HA powder alone. Furthermore, the fluoride uptake was dependent on many factors, including pH, contact time and the presence of competing ions. It was possible to regenerate the hydrogel to remove the fluoride ions, and thus it was shown that the material can be used a number of times with only a slight reduction in its fluoride uptake capacity.

## DECLARATION

No portion of the work referred to in the thesis has been submitted in support of an application for another degree or qualification of this or any other university or other institute of learning.

## COPYRIGHT STATEMENT

- I. The author of this thesis (including any appendices and/or schedules to this thesis) owns certain copyright or related rights in it (the “Copyright”) and s/he has given The University of Manchester certain rights to use such Copyright, including for administrative purposes.
- II. Copies of this thesis, either in full or in extracts and whether in hard or electronic copy, may be made **only** in accordance with the Copyright, Designs and Patents Act 1988 (as amended) and regulations issued under it or, where appropriate, in accordance with licensing agreements which the University has from time to time. This page must form part of any such copies made.
- III. The ownership of certain Copyright, patents, designs, trademarks and other intellectual property (the “Intellectual Property”) and any reproductions of copyright works in the thesis, for example graphs and tables (“Reproductions”), which may be described in this thesis, may not be owned by the author and may be owned by third parties. Such Intellectual Property and Reproductions cannot and must not be made available for use without the prior written permission of the owner(s) of the relevant Intellectual Property and/or Reproductions.
- IV. Further Information on the conditions under which disclosure, publication and commercialisation of this thesis, the Copyright and any Intellectual Property and/or Reproductions described in it may take place is available in the University IP Policy (see <http://documents.manchester.ac.uk/DocuInfo.aspx?DocID=24420>), in any relevant Thesis restriction declarations deposited in the University Library, The University Library’s regulations (see <http://www.manchester.ac.uk/library/aboutus/regulations/>) and in The University’s policy on Presentation of Theses.

## ACKNOWLEDGEMENTS

Firstly, I would like to thank my supervisor Professor Peter Budd and my co-supervisors and collaborators Professor Julie Gough, Professor David Watts, Professor Sandra Downes and Professor Judith Hoyland for giving me the opportunity to undertake these PhD studies and for their impeccable support and supervision throughout.

I owe special thanks to Dr. Ian Wimpenny for his advice and assistance with the biomaterials aspects of the project. I would like to take this opportunity to thank my project collaborators from the School of Chemistry, Peter J. Youle and Dr. Xia Zhong, and from the School of Medical Sciences, Dr. Qi Guang Wang. I would also like to thank Keith Nixon for help with the GPC measurements and Dr. Louise Carney for cell culture training.

I would like to thank everyone in OMIC for making this an enjoyable place to work. There are too many people to mention adequately here, but this has been a challenging and rewarding experience that has been made much easier with the support of friends and colleagues.

Finally, I would like to thank my mum, Jeanette, and my sister, Lauren, for their endless support and patience throughout the past 3.5 years and my friends, Julia Cannon, Hannah Peters and Robert Woolfson for their continued encouragement and advice.

This thesis is dedicated to my dad, Mark Dey, for inspiring me to become a scientist.

# Chapter 1: Introduction

Tissue engineering is a rapidly expanding field that “applies the principles of engineering and life sciences toward the development of biological substitutes that restore, maintain or improve tissue function or a whole organ”.<sup>1</sup> The field of bone tissue engineering has attracted much attention in recent years in parallel with the rise in musculoskeletal disorders associated with increased life expectancies.<sup>2,3</sup>

Unlike other materials, bone undergoes constant turnover and has the ability to spontaneously regenerate itself up to a point. Critical size defects and non-union fractures are more difficult to treat and often require complex surgical intervention.<sup>4</sup> This can lead to an increased risk of fractures and the resulting low bone stock makes revision surgery much more problematic. Therefore, there is a need for a synthetic bone graft substitute, with bioactive properties, that can be used at the site of surgical intervention to promote bone regeneration.

## 1.1 Bone

### 1.1.1 Structure and properties of bone

Bone is a complex tissue that consists of a hierarchically organised structure (Figure 1.1).<sup>5</sup> At the nanostructural level, bone consists of a matrix of collagen fibres interspersed with calcium phosphate minerals, of which hydroxyapatite (HA) is the most common. These mineralised collagen fibres can form into planar arrangements, known as lamellae. The collagen fibres run in the same direction in each lamella and in opposite directions in adjacent lamellae to prevent cracks from occurring. The lamellae can then wrap in concentric layers around a central (Haversian) canal to form what is known as an osteon.<sup>6</sup>

At the macrostructural level, there are two main types of bone: cortical and trabecular. The type of bone present can be identified by the degree of porosity. Cortical bone is dense with few spaces for cells and blood vessels, whereas trabecular bone contains many large pores. The varying degrees of porosity can significantly alter the mechanical properties of bone.<sup>6</sup>

The varied arrangement of material structures within bone can work in concert to perform many diverse functions, such as mechanical support, protection of internal organs and blood cell production.<sup>6, 7</sup> Bone is also involved in maintaining mineral ion homeostasis as well as acting as a storage vessel for various minerals, proteins and growth factors.

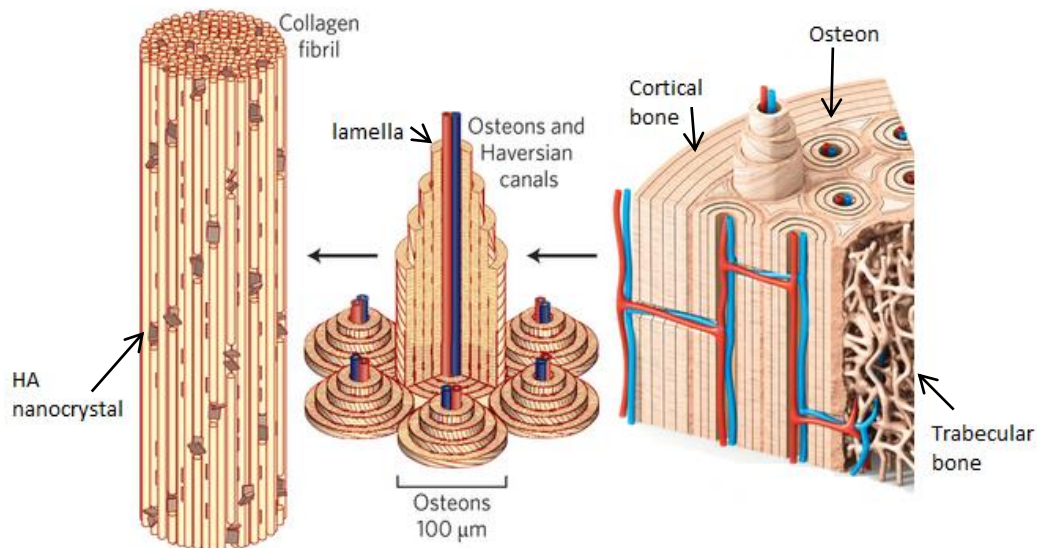


**Figure 1.1.** Hierarchical structure of bone. The macroscale arrangement involves both cortical and trabecular bone. Cortical bone is composed of osteons and Haversian canals which surround blood vessels. Osteons have a lamellar structure with individual lamella consisting of collagen fibres interspersed with hydroxyapatite (HA) nanocrystals. Image adapted from Wegst *et al.*<sup>5</sup>

### 1.1.2 Extracellular matrix of bone

Figure 1.2 shows a schematic representation of the nanoscale extracellular matrix (ECM) of bone.<sup>8</sup> This composite material is primarily composed of type I collagen with hydroxyapatite (HA) crystals, of formula  $[\text{Ca}_{10}(\text{PO}_4)_6(\text{OH})_2]$ , located within and between the fibres.<sup>9</sup> The collagen fibres are known to impart elasticity and flexibility to bone, whereas the mineral component provides mechanical rigidity and load-bearing strength. These properties combined give rise to the tensile behaviour of bone.

It is well known that the ECM plays a significant role in structural tissue support, acting as a scaffold for the attachment of bone cells. However, it has been recognised in recent years that the ECM also plays a more dynamic role in regulating cell function. The ECM serves as a reservoir for several non-collagenous proteins (NCPs), including osteocalcin and osteopontin, growth factors, such as bone morphogenetic proteins (BMPs), polysaccharides and cytokines. These macromolecules are known to perform many varied roles in supporting cell-matrix interactions and promoting the proliferation and differentiation of cells.

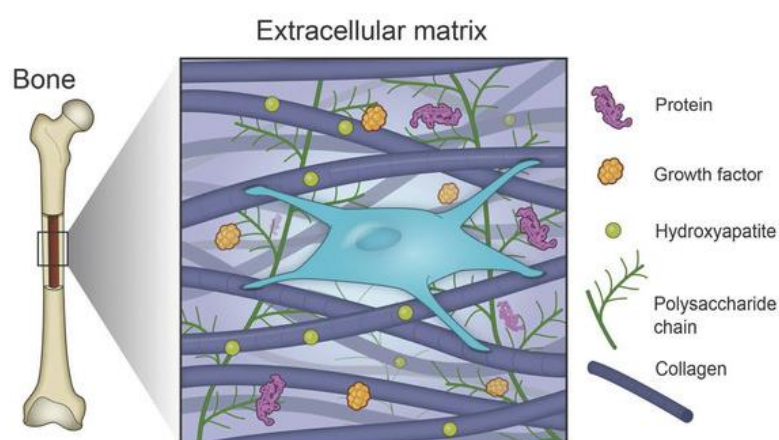


**Figure 1.2.** A schematic representation of the native extracellular matrix (ECM) of bone and its components, taken from Gaharwar *et al.*<sup>8</sup>

### 1.1.3 Mineralisation of the ECM

One of the main functions of non-collagenous proteins (NCPs), such as bone sialoprotein (BSP) and osteopontin (OPN), is to regulate the ordered deposition of mineral within the bone extracellular matrix. These proteins possess a high affinity for calcium ions due to the abundance of amino acids such as glutamic acid and aspartic acid. Thus, through binding to the  $\text{Ca}^{2+}$  ions of hydroxyapatite, BSP is thought to promote HA nucleation and growth, whereas OPN inhibits mineral growth and thus helps to control the size and orientation of mineral deposits.<sup>10</sup> It has been observed that the control of mineralisation is intimately associated with the degree of phosphorylation of proteins such as BSP and OPN.<sup>11, 12</sup> Therefore, it is suggested that a synergistic activity exists between the charged acidic groups of the protein, which is responsible for

HA binding and mineral growth. Furthermore, the binding of non-collagenous proteins to calcium ions, coupled with the enzymatic release of phosphorus, means that they can serve as a reservoir for calcium and phosphate ions to enhance mineral formation.

Maturation of the extracellular matrix is also associated with the expression of alkaline phosphatase.<sup>13</sup> Although the role of alkaline phosphatase is not fully understood, it is believed to hydrolyse the mineralisation inhibitor, inorganic pyrophosphate (PPi).<sup>14</sup> In this way, alkaline phosphatase can generate the optimal extracellular concentration of PPi that allows mineralisation to proceed. Therefore, the non-collagenous proteins can work co-operatively to promote mineralisation as well as to regulate the ordered deposition of mineral, and thus avoid ectopic calcification.

#### **1.1.4 Bone cells**

There are a number of specialised cells which permeate and line the bone and these can be divided into three main categories.<sup>10</sup> Osteoblasts are responsible for the formation of new bone by the synthesis and secretion of the organic extracellular matrix. They may eventually become embedded in the matrix and turn into osteocytes.

Osteocytes represent terminally differentiated osteoblasts. These cells express several matrix proteins to support intercellular adhesion and regulate the exchange of mineral in the bone fluid. Osteocytes can connect with other cells within the tissue, allowing for good cell-cell communication to regulate the activity of osteoblasts and osteoclasts.

Finally, osteoclasts are responsible for the resorption of old bone by breaking down the components of the extracellular matrix. This is critical for the maintenance, repair and remodelling of bone.

#### **1.1.5 The bone remodelling process**

Unlike other materials, bone undergoes constant turnover throughout life to adapt to changes in mechanical load and strain. The bone remodelling process also provides a mechanism for the repair and regeneration of micro-damaged tissue as well as maintaining a balance of calcium and phosphorus ions within the extracellular fluid.

During bone remodelling, bone formation is tightly coupled to bone resorption and direct contacts between osteoblasts and osteoclasts have been proposed to maintain this relationship.<sup>15</sup> Damage to the bone matrix, which leads to the formation of micro-

fractures, often results in osteocyte apoptosis which is a strong indicator of the location and size of the defect. Osteoblasts respond to the signals generated by osteocytes and recruit pre-osteoclasts to the remodelling site. These precursor cells then differentiate into multinucleated osteoclasts.

At an active resorption site, osteoclasts form a specialised cell membrane known as the ruffled border, which is in contact with the bone surface.<sup>16</sup> The ruffled border facilitates the removal of the bone matrix and is a morphological characteristic of an osteoclast that is actively resorbing bone. Osteoclasts resorb bone by the acidification of the space beneath the ruffled border, thus enabling dissolution of bone mineral. Enzymatic degradation of the collagen matrix and ECM proteins then occurs to complete the process.<sup>15</sup>

Following bone resorption, osteoblasts can begin the process of bone formation by the synthesis and secretion of the extracellular matrix as well as many non-collagenous proteins.<sup>10, 17</sup> Finally, hydroxyapatite is deposited during the mineralisation process. When an equal quantity of resorbed bone has been replaced, the remodelling cycle concludes.

Bone remodelling is carefully regulated by a number of hormones and growth factors. For example, studies of diseases associated with defects in bone formation have demonstrated the critical importance of local bone formation control by bone morphogenetic protein (BMP).<sup>16</sup> BMP-2 can act as a potent stimulator of bone formation and it is often used clinically to promote bone regeneration. In addition, oestrogen can promote the growth of new bone by preventing osteoclast formation and reducing the life span of these cells as well as stimulating osteoblast proliferation.<sup>17</sup>

## **1.2 Bone Diseases and Current Treatments**

### **1.2.1 Osteoporosis**

Perturbations of the activity of osteoblasts and osteoclasts can occur due to hormonal changes, such as those that occur in post-menopausal women. This can result in an imbalance between the two cell types, which is the origin for many bone metabolic diseases. Osteoporosis occurs when bone loss outpaces the growth of new bone. This results in a reduction in bone mineral density, with bones becoming increasingly porous

and brittle (Figure 1.3).<sup>18</sup> Literally meaning ‘porous bones’, osteoporosis is associated with an increased risk of fragility fractures, which cause substantial pain and disability for affected patients and, in extreme cases, can even lead to death.

It has been estimated in a recent report that 22 million women and 5.5 million men in the EU have osteoporosis, with the disease predominantly affecting post-menopausal women.<sup>19</sup> It is also estimated that 1 in 3 women and 1 in 5 men worldwide, over the age of 50, will sustain an osteoporotic fracture. With an increasingly ageing population, this represents a large scale problem with substantial costs to society.

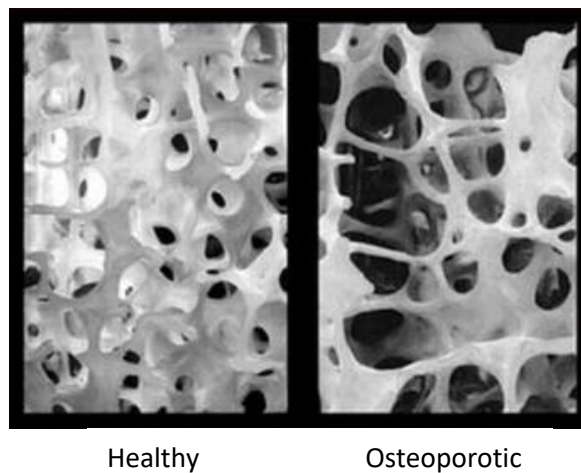


**Figure 1.3.** A comparison between healthy and osteoporotic bone. Osteoporotic bone is more porous and brittle than healthy bone. Image taken from Marcus *et al.*<sup>20</sup>

### 1.2.2 Bone grafting techniques

Current treatments for osteoporosis rely on bone grafting techniques; most commonly autografts and allografts are used. Autologous bone grafts use tissue taken from the patient’s own body (usually harvested from the iliac crest) and have osteoconductive and osteoinductive properties, i.e. they are able to support and promote bone growth.<sup>21</sup> Although this has been a popular technique, there are problems concerned with the limitation of supply and the procedure to harvest the material is associated with complications.<sup>22</sup>

Allografts, on the other hand, require tissue taken from a donor and are usually implanted in the form of demineralised bone matrix. Despite the potentially unlimited

supply, allografts are associated with certain risks, such as transmission of infectious diseases and rejection by the immune system.<sup>21</sup> Furthermore, the osteogenic properties of allografts are significantly reduced when compared with autografts. Therefore, autografts remain the current gold standard for bone grafting procedures.

### 1.2.3 Bisphosphonates

As opposed to bone grafts, bisphosphonate drugs are the most widely used and effective treatment for bone diseases where there is increased osteoclastic resorption. Bisphosphonates (BPs) are considered to be synthetic analogues of inorganic pyrophosphate (PPi), a physiological regulator of calcification and bone resorption.<sup>23</sup> A structural comparison of pyrophosphate and bisphosphonates can be seen in Figure 1.4. The non-hydrolysable P-O-P bond of pyrophosphate is replaced by a P-C-P bond in bisphosphonates. This backbone structure enables BPs to bind avidly to divalent calcium ions and as a result, BPs can bind to bone mineral surfaces *in vivo*.<sup>23</sup> This occurs via bidentate binding of  $\text{Ca}^{2+}$  by the phosphonate groups (Figure 1.4b) or tridentate binding involving the  $\text{R}_2$  side chain.

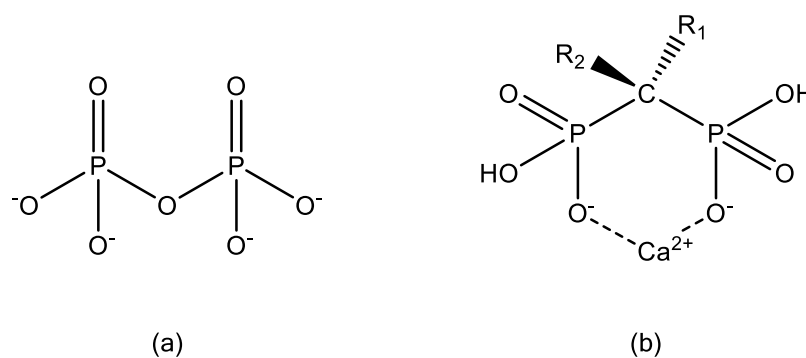


**Figure 1.4.** Structural comparison of (a) inorganic pyrophosphate (PPi) and (b) bisphosphonate (BP). The close proximity of the phosphonate groups allows the binding of  $\text{Ca}^{2+}$  ions *in vivo*.

There are two classes of bisphosphonates: non-nitrogen containing BPs (non-NBPs), such as clodronate and etidronate, and nitrogen-containing BPs (NBPs), such as alendronate.<sup>24</sup> Although the exact mechanism is not fully understood, it is thought that the uptake of BPs by osteoclasts occurs via fluid-phase endocytosis.<sup>25</sup> Once internalised,

NBPs act by disrupting essential metabolic pathways,<sup>26</sup> whereas non-NBPs are metabolically transformed into cytotoxic ATP analogues that inhibit ATP-dependent intracellular enzymes, eventually leading to osteoclast apoptosis.<sup>27-29</sup>

BPs can also prevent bone resorption through other biochemical pathways with subsequent different effects, such as inhibition of osteoclast formation<sup>30</sup> and/or by affecting the metabolic activity of osteoblasts.<sup>31</sup> A number of recent *in vitro* studies have shown that BPs can enhance the proliferation, differentiation and bone-forming activity of osteoblasts directly.<sup>32, 33</sup>

However, there are certain side effects associated with bisphosphonates, including osteonecrosis of the jaw and adverse gastrointestinal effects as well as local tissue damage and irritation at the injection site.<sup>34</sup> These effects can be improved by localised and controlled delivery of BPs to the target. Furthermore, it has been demonstrated that providing implantable bioresorbable systems with BP-releasing features can prevent many of these undesirable outcomes.<sup>35</sup>

### **1.3 Materials used in Bone Repair**

In situations where the bone defect occurs at a load-bearing site, such as the hip or knee, metal and ceramic implants are often required. A total hip or knee replacement is a common type of surgery where a damaged joint is replaced with an artificial implant.<sup>36</sup>

#### **1.3.1 Metals**

To date there are several biocompatible metallic materials used in orthopaedic surgery to replace damaged bone and provide immediate mechanical support at the defect site. Metals such as magnesium,<sup>37, 38</sup> cobalt-chromium alloys<sup>39</sup> and titanium<sup>40</sup> are among the most widely used materials for surgical implants. Although these metals possess excellent mechanical strength, they suffer from a lack of biological recognition on the material surface. They are also associated with the release of toxic metallic ions due to corrosion or wear, which can lead to inflammatory cascades and allergic reactions.<sup>41</sup>

The most commercially abundant metal for bone tissue engineering is tantalum,<sup>42, 43</sup> which has a similar elasticity to bone, sufficient strength to allow for load-bearing applications and is highly biocompatible. Tantalum also offers better osteoconduction than other materials and a recent study has shown a substantial filling of the material's

pores with new bone by 40 to 50% over the course of four weeks.<sup>42</sup> However, the main drawback to using tantalum in surgical implants lies in the removal of the metallic component during revision surgery, which can be very challenging and can lead to further bone loss around the implant.

### **1.3.2 Ceramics**

Ceramic implants usually take the form of hydroxyapatite ( $[\text{Ca}_{10}(\text{PO}_4)_6(\text{OH})_2]$ ) or tricalcium phosphate ( $[\text{Ca}_3(\text{PO}_4)_2]$ ); the inorganic components of native bone tissue.<sup>44, 45</sup> They are biocompatible, biodegradable and osteoconductive, with the additional advantage that calcium ions secreted from the scaffolds can enhance the mineralisation of osteoblasts and hence promote bone regeneration.<sup>46</sup> However, ceramics are brittle, have low tensile strength and difficult processability; the latter means they are usually only used as additives or coating materials.<sup>47, 48</sup>

Modern artificial hip or knee implants are designed to last for approximately 15 years. Most artificial implants will fail due to loosening, infection or instability. Hence, there is always a risk that revision surgery may be required to repair or replace the joint.<sup>49, 50</sup> Revision surgery tends to be a longer and more complicated operation. It is well known that an artificial joint becomes less effective every time it is replaced, mainly attributed to poorer stability due to bone loss around the prosthesis.<sup>50, 51</sup> Therefore, there is a clear clinical need for a synthetic bone graft substitute that can encourage bone regeneration, reducing the risk of further fracture or failure, and thus eliminating the need for revision surgery.

## **1.4 Bone Tissue Engineering**

Over the past few decades, the field of bone tissue engineering has been developed in order to overcome the various limitations associated with current grafting procedures and bone substitute biomaterials. The previous approach to bone tissue engineering was to provide a bioinert material that has no effect on the surrounding tissue. More recently, however, the focus has shifted to producing scaffolds that can act as a temporary substrate for cell attachment and proliferation and which maintain the differentiated function of the cells.<sup>52</sup>

### 1.4.1 Tissue scaffolds for bone regeneration

For successful bone repair to occur, the scaffold must possess certain attributes, which are summarised in Table 1.1. There are many other factors which also contribute to the scaffold's ability to promote bone regeneration, including surface area, electrical conductivity and surface properties, i.e. hydrophilicity and morphology.<sup>53</sup> The major challenge is to control all of these factors simultaneously. For example, while a higher porosity results in an increase in mass transport, it may also compromise the scaffold's mechanical strength. Achieving optimal scaffold performance therefore requires a delicate balance between many different factors.

It has been suggested that a scaffold which mimics the natural ECM of bone may aid in optimising the properties of scaffolds to improve bone formation.<sup>54</sup> Kikuchi *et al.*<sup>55</sup> have developed a composite of collagen and hydroxyapatite to be used as an artificial bone implant. They have demonstrated osteoclastic resorption followed by new bone formation by osteoblasts, which is very similar to the reaction in native bone tissue. Following on from this, there has been much research into composites of collagen, HA and polymeric materials, all of which have confirmed osteoblast adhesion, migration and proliferation and have proven to be promising materials for the repair of bone defects.<sup>56, 57</sup>

**Table 1.1.** Desirable properties of a tissue engineered scaffold used for bone regeneration.<sup>53, 58-60</sup>

<b>Desirable Properties</b>	<b>Advantages</b>
Biocompatibility	Lack of immunogenic response; Non-toxic.
Biodegradability	Degrades at an appropriate rate as new bone is formed; Degradation products should be non-toxic.
Porosity	Highly interconnected porous network for cell growth and transport of nutrients and waste; Ideal porosity = 90%; Increase surface area for cell attachment.
Mechanical Strength	Able to withstand the forces exerted by the body; Similar mechanical properties to surrounding tissue.
Osteoconductivity	Support bone growth by allowing cells to attach and proliferate; Supports migration of cells through structure.
Osteoinductivity	Induces the differentiation of stem cells into mature osteoblasts.

## **1.5 Fabrication of Tissue Scaffolds**

The technique of production of tissue scaffolds depends on the properties of the material, as well as the proposed function of the scaffold. While many different techniques exist, each one has its own advantages and disadvantages and the appropriate technique is selected to meet the requirements of the specific type of tissue.

### **1.5.1 Freeze-drying**

Among the different methods for scaffold production, freeze-drying has been widely utilised with many biocompatible polymers, including poly(propylene fumarate).<sup>61</sup> This technique uses rapid cooling to produce thermodynamic instability within a system and cause phase separation. The solvent (usually water) is then removed by sublimation under vacuum, leaving behind voids in the region it previously occupied. Scaffolds with highly interconnected pores and porosities of up to 90% are attainable by freeze-drying<sup>62</sup> and the final pore structure has been found to depend on the process conditions, such as pH, freezing rate and partial pressure.<sup>63</sup>

### **1.5.2 Solvent casting**

Solvent casting/particulate leaching involves casting a dissolved polymer around a suitable porogen, e.g. NaCl.<sup>64</sup> The polymer is dried and solidified and the porogen is leached out to yield a scaffold with an interconnected porous network. The major advantage of this technique is the effective control of porosity and pore size whereby the porosity is given by the amount of leachable particles and the pore size and shape can be modified by varying the leachable particle's characteristics.<sup>65, 66</sup> However, this method can only be used to produce thin scaffolds and is therefore not suitable for load-bearing applications.

### **1.5.3 Electrospinning**

Electrospinning has become a very popular technique for the production of tissue scaffolds comprising nanometre-scale nonwoven fibres. The principle of electrospinning is described in detail by Pham *et al.*<sup>67</sup> and is summarised in Figure 1.5. Briefly, the polymer is dissolved in a suitable solvent, loaded into a syringe and then expelled through a metal capillary. A high voltage (10-20 kV) is applied to the

capillary, charging the polymer and ejecting it toward a collecting plate. As the fibres assemble, the solvent evaporates, leaving a nonwoven porous scaffold.<sup>61,67</sup>

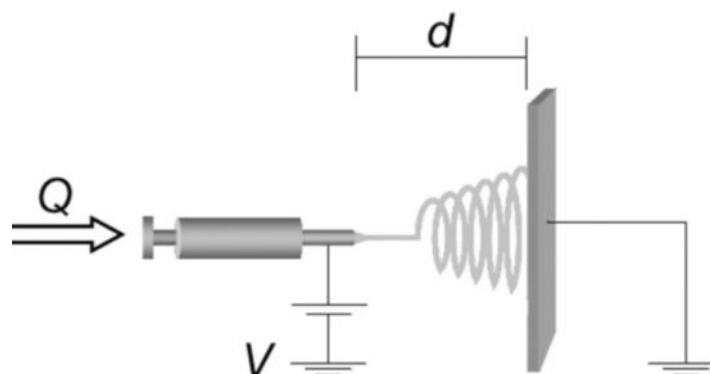


**Figure 1.5.** Typical electrospinning setup where  $Q$  is flow rate,  $d$  is distance between plate and needle and  $V$  is applied voltage. Image taken from Pham *et al.*<sup>67</sup>

The properties of the electrospun scaffold, i.e. fibre thickness, morphology and average pore diameter can be controlled by adjusting certain parameters.<sup>68, 69</sup> For example, solution viscosity (as controlled by polymer concentration) is considered to be one of the biggest determiners of fibre size and morphology when electrospinning polymeric fibres. At low polymer concentrations, defects in the form of beading and droplets have been observed.<sup>70</sup> For solutions that are too viscous, the droplet will dry out at the tip before the jet can be initiated, thus preventing electrospinning.<sup>71</sup> Other factors such as polymer molecular weight, choice of solvent, flow rate, applied voltage and the distance between the tip and collector have also been found to influence the extent of beading and uniformity of the fibres.<sup>67</sup>

## 1.6 Polymeric Tissue Scaffolds

Naturally occurring hydroxy acids such as glycolic, lactic and  $\epsilon$ -caproic acids are among the most widely used biodegradable polymers in regenerative medicine. This is partly due to the fact that the mechanical and degradation properties of the materials can be optimised to suit the required application.

### 1.6.1 Poly(glycolic acid) and poly(lactic acid)

Poly(glycolic acid) (PGA) is a highly crystalline, aliphatic polyester (Figure 1.6a). It has a high melting point and a low solubility in organic solvents. Due to its hydrophilic nature, surgical implants made of PGA tend to lose their mechanical strength as early as 2-4 weeks post-implantation.<sup>72</sup> To adapt the material properties for a wider range of applications, poly(lactic acid) (PLA) can be used. The extra methyl group (Figure 1.6b) increases the hydrophobicity, which limits water uptake and thus lowers the rate of backbone hydrolysis. It takes approximately 1-2 years for 50% of PLA to biodegrade.<sup>73</sup>

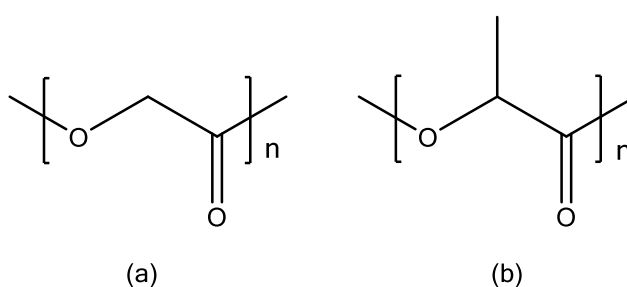


**Figure 1.6.** Chemical structure of (a) poly(glycolic acid) (PGA) and (b) poly(lactic acid) (PLA).

Among the most popular materials for bone tissue scaffolds is poly(lactic-*co*-glycolic acid) (PLGA), a copolymer of the above mentioned polymers.<sup>74, 75</sup> PLGA is biocompatible and its biodegradation rate can be tailored by altering the polymer molecular weight or copolymer ratio. However, clinical application of pure PLGA for bone regeneration is hindered by poor osteoconductivity and suboptimal mechanical properties. Furthermore, the degradation of PLGA results in acidic by-products, which can lead to an inflammatory reaction in the surrounding tissue.<sup>76</sup>

PLGA is often used in combination with other materials, such as ceramics, to improve the properties of the scaffolds for bone tissue engineering. Hydroxyapatite (HA) can be incorporated into PLGA scaffolds to increase their mechanical strength and osteoconductivity.<sup>77</sup> Yun *et al.*<sup>78</sup> have produced PLGA/HA composite nanofibres by electrospinning. Mesenchymal stem cells (MSCs) were deposited onto the fibres and their results showed that osteogenic differentiation and mineralisation of the cells

occurred. Therefore, these results suggest that the incorporation of HA results in a better biomimetic structure, which is more suitable for load-bearing applications.

### 1.6.2 Poly( $\epsilon$ -caprolactone)

Poly( $\epsilon$ -caprolactone) (PCL) is a semi-crystalline, linear polyester (Figure 1.7). The hydrophobic nature of PCL means that there is a low rate of diffusion of water into the scaffold material and hence the rate of degradation is remarkably slow. It has been found that PCL degrades by 50% in 4 years.<sup>73</sup> Therefore, PCL scaffolds are most suitable for the design of long-term implantable systems and are widely used for bone regeneration.

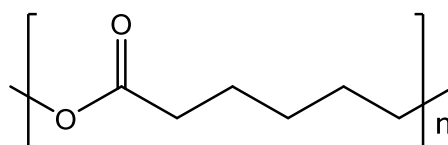


**Figure 1.7.** Chemical structure of poly( $\epsilon$ -caprolactone) (PCL).

The fabrication of PCL-based tissue scaffolds has generally focused on electrospinning techniques to produce fibres in the nanometre diameter range that are typically deposited as non-woven fabrics. As a result of the small fibre diameters and the overall porous structure, electrospun scaffolds have a high specific surface area that makes them ideal for tissue engineering applications. Yoshimoto *et al.*<sup>79</sup> have fabricated electrospun nanofibres of PCL (Figure 1.8a) and have seeded mesenchymal stem cells (MSCs) derived from the bone marrow of neonatal rats onto the material surface (Figure 1.8b). They have demonstrated cell migration within the scaffold and the production of an extracellular matrix (ECM) of collagen after one week. In addition, matrix mineralisation occurred throughout the construct after four weeks. This suggests that electrospun PCL is a promising candidate for bone tissue engineering.

PCL has the propensity to form compatible blends with a wide range of other materials, making it extremely useful for the production of composite scaffolds. The inclusion of hydroxyapatite (HA) has been shown to increase the tensile strength and elastic modulus of PCL scaffolds.<sup>80</sup> Furthermore, Venugopal *et al.*<sup>57</sup> have created a composite of electrospun PCL, collagen and HA. They have found that collagen imparts a greater

wettability of the scaffolds, which results in enhanced cell adhesion and proliferation. In addition, HA acts as a chelating agent to promote mineralisation of osteoblast cells. Therefore, it has been demonstrated that the production of composites of PCL can achieve the desirable characteristics of the ECM, leading to enhanced bone repair and regeneration.

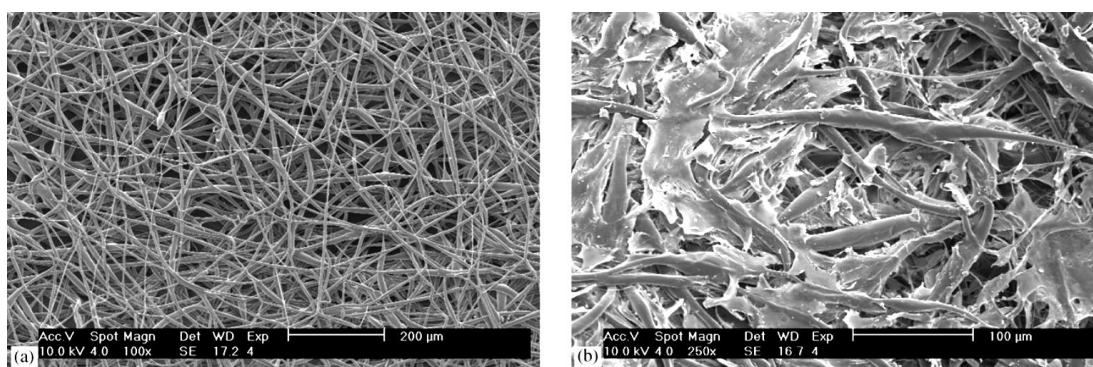


**Figure 1.8.** SEM micrographs of MSCs seeded onto PCL scaffolds. (a) Scaffold prior to seeding. The average fibre diameter is 400 nm ( $\pm$  200 nm). (b) Low magnification view of the cell-polymer constructs after 1 week of culture. The surface is partially covered with multilayers of cells. Images taken from Yoshimoto *et al.*<sup>79</sup>

### 1.6.3 Functionalisation of scaffolds

An effective method of improving the osteoinductive properties of a scaffold is through the incorporation of bioactive moieties such as DNA,<sup>81</sup> proteins<sup>82</sup> and growth factors.<sup>83</sup> By manipulating the scaffold's composition, controlled release of these bioactive factors is possible, allowing therapeutic doses to be delivered locally, for an appropriate duration.

There are a number of growth factors involved in bone formation and fracture repair. One important class of osteogenic growth factors is the bone morphogenetic proteins (BMPs). Recombinant human BMPs, including BMP-2 and BMP-7, are most often used to treat bone defects. Park *et al.*<sup>84</sup> have immobilised BMP-2 on a nanofibrous chitosan membrane. The results showed that BMP-2 was able to enhance osteoblast attachment and proliferation in a dose-dependent manner.

Alternatively, BMP-2 loaded into composite scaffolds could present a sustained release, which could accelerate the bone response process. Nie *et al.*<sup>85</sup> have produced

PLGA/HA/BMP-2 composite fibrous scaffolds and have evaluated the *in vitro* BMP-2 release kinetics. Scaffolds demonstrated controlled and sustained release of BMP-2, which was able to maintain its integrity. In addition, BMP-2 release rate was controllable by HA content, whereby an increase in HA led to an increased rate of release of BMP-2 that was deemed to be more suitable for bone tissue engineering.

Surface phosphorylation has been applied to many tissue scaffolds to act as a mimic of non-collagenous proteins, and thus to help promote bone formation. Partial phosphorylation of poly(vinyl alcohol) (PVA)<sup>86</sup> has been shown to significantly improve adhesion and proliferation of human osteoblast-like MG63 cells. In addition, the expression of alkaline phosphatase was increased in partially phosphorylated PVA nanofibres and cell-matrix calcium levels were about two times higher than in PVA alone. This study proved that partial phosphorylation of PVA nanofibres results in improved osteoconduction and expression of early markers of osteoinduction in MG63 cells. The extent of phosphorylation is important in terms of offering the best potential mimic of non-collagenous proteins for bone growth and repair.

#### **1.6.4 Scaffolds for drug delivery**

In recent years, there has been increasing interest in functionalising polymeric tissue scaffolds by loading them with therapeutic drugs, which can act on the surrounding tissues. Electrospun nanofibrous scaffolds offer many advantages for drug delivery systems owing to their high surface area to volume ratio and high pore connectivity. Furthermore, polymer degradation properties can be tailored for the specific application to control the release rate of the drugs.

Biodegradable polymeric scaffolds such as poly(lactic-*co*-glycolic acid) (PLGA),<sup>87</sup> poly(vinyl alcohol) (PVA)<sup>88</sup> and poly(ethylene-*co*-vinyl acetate) (PEVAc)<sup>89</sup> have gained significant attention in recent years for their use in drug delivery systems. It is thought that localised delivery of a drug to its target site can reduce side effects and limit the risk of overdose associated with systemic delivery. In addition, the scaffold may be designed to deliver a drug at a specific rate and for a specific period of time at the desired location, improving drug bioavailability.

A number of drugs, including antibiotics<sup>90</sup> and anti-inflammatories,<sup>88</sup> have been successfully introduced into biodegradable polymeric scaffolds, whilst maintaining their

structure and bioactivity. However, the choice of polymer may be dependent on the drug to be released and vice versa. For example, doxorubicin hydrochloride, a hydrophobic drug, was not well dispersed within electrospun PLA fibres until it was made lipophilic.<sup>91</sup>

The antibiotic drug, mefoxin, has been incorporated into electrospun PLGA nanofibrous scaffolds and the drug release kinetics have been investigated.<sup>92</sup> It was found that a burst release occurs, whereby most of the drug was released after 1 h of incubation in water. Although this type of release profile may be suitable for the prevention of postoperative infections, a more sustained release is often required. Therefore, it was demonstrated that the addition of a surfactant, in the form of a block copolymer (PEG-*b*-PLA), reduced the amount of released drug and prolonged the release rate.

Different release rates may be obtained by varying the fibre diameter or loading dosage.<sup>87</sup> Alternatively, blends of biodegradable polymers with different degradation rates can be used to control drug release. Release kinetics of the antibiotic, tetracycline hydrochloride, changed from a burst to a more sustained release when 50:50 blends of PLA:poly(ethylene-*co*-vinyl acetate) (PEVAc) were used compared to either polymer alone.<sup>89</sup> Finally, the drug can be mixed with the polymer solution prior to the electrospinning process.<sup>93</sup> Using this method, the drugs can be encapsulated within the fibres, as opposed to localisation on the surface, allowing for a more controlled release of the drug over time.

## **1.7 Hydrogels**

Hydrogels are crosslinked polymers with high water contents that are capable of capturing the characteristics of the native cellular microenvironment. As a result of their tuneable chemical and physical properties, hydrogels have been exploited in a variety of biomedical applications, including wound healing, drug delivery and tissue engineering.<sup>94</sup> Their ability to mimic the properties of the extracellular matrix has also meant that hydrogels have gained significant attention for use as bone tissue scaffolds.

### **1.7.1 Natural hydrogels**

Natural materials used in the preparation of hydrogels usually take the form of polysaccharides, proteins and ECM components, including collagen,<sup>95</sup> chitosan<sup>96, 97</sup> and

hyaluronic acid.<sup>98, 99</sup> Their inherent biocompatibility and bioactivity makes natural materials the first logical choice for use in tissue engineering. They also promote many cellular functions including adhesion, proliferation and differentiation owing to the many endogenous factors present. However, it can be difficult to tune the mechanics of natural polymers and there is always a risk of contamination and batch-to-batch variability.<sup>100</sup> Therefore, most research has focused on synthetic polymeric hydrogels.

### **1.7.2 Synthetic hydrogels**

Hydrogels formed of purely synthetic polymer materials, such as poly(ethylene glycol) (PEG),<sup>101</sup> poly(vinyl alcohol) (PVA)<sup>102</sup> or poly(2-hydroxyethyl methacrylate) (PHEMA)<sup>103</sup> have been studied extensively for tissue engineering applications. Synthetic hydrogels are highly reproducible and allow for fine tuning of their mechanical properties.

Although generally utilised in soft tissue applications, considerable research is currently being performed in the area of hydrogel mediated bone regeneration. A bioactive hydrogel scaffold is required that can provide mechanical support while directing cell adhesion, proliferation and differentiation and promoting expression of the ECM. Incorporation of hydroxyapatite (HA) into polymeric hydrogels has been shown to significantly increase their mechanical strength. In one such study, a composite of poly(acrylamide) (PAAm) and HA was produced that exhibited enhanced mechanical properties, namely higher tensile and compressive strength, compared to the as-synthesised PAAm hydrogels.<sup>104</sup> The composite also showed excellent osteoblast cell adhesion properties.

In addition, Song *et al.*<sup>105</sup> have developed a “bone-like” composite of PVA/collagen/HA and tested the response of osteoblasts to the material. They found that this composite material significantly improved the mechanical properties when compared with the individual components. The ductile collagen was also found to increase the poor fracture toughness of HA. Furthermore, the PVA composites enhanced cell adhesion, proliferation and differentiation *in vitro*.

## 1.8 Polyelectrolytes

Polyelectrolytes are polymers that contain ionisable groups, which dissociate in aqueous solution. The degree of dissociation of these groups, with regards to changes in pH, allows the classification of polyelectrolytes as ‘strong’ or ‘weak’. Strong polyelectrolytes, such as poly(vinylsulfonic acid) (PVSA),<sup>106</sup> are not sensitive to variations in pH and remain completely dissociated over a wide pH range. On the other hand, weak polyelectrolytes, of which poly(acrylic acid) (PAA) is an example,<sup>107</sup> are only partially dissociated at intermediate pH values.

### 1.8.1 Solution properties of polyelectrolytes

Due to the charged nature of polyelectrolytes, an electrical double layer (EDL) will develop in aqueous solution.<sup>108, 109</sup> Figure 1.9 shows a schematic diagram of the electrical double layer. The EDL can be thought of as existing in two layers: a fixed inner Stern layer and a diffuse outer layer. Within the Stern layer, counter-ions are adsorbed onto the polymer surface due to strong electrostatic attractive forces. The diffusive outer layer consists of accumulated counter-ions and depleted co-ions. Here, the ions are far enough from the polymer that they are only subjected to weak electrostatic forces; hence they remain mobile in solution.<sup>108</sup>

Double layer forces occur between charged species across liquids.<sup>110</sup> The differences in the ionic concentrations between the two objects, with respect to the bulk solution, create an osmotic pressure, which generates a force between the objects. For two similarly charged species, this force is repulsive and decays exponentially at larger distances. The strength of these forces increases with the magnitude of the surface charge density. Hence, the electrostatic repulsions between polyelectrolyte chains are a direct result of these double layer forces.<sup>110</sup>

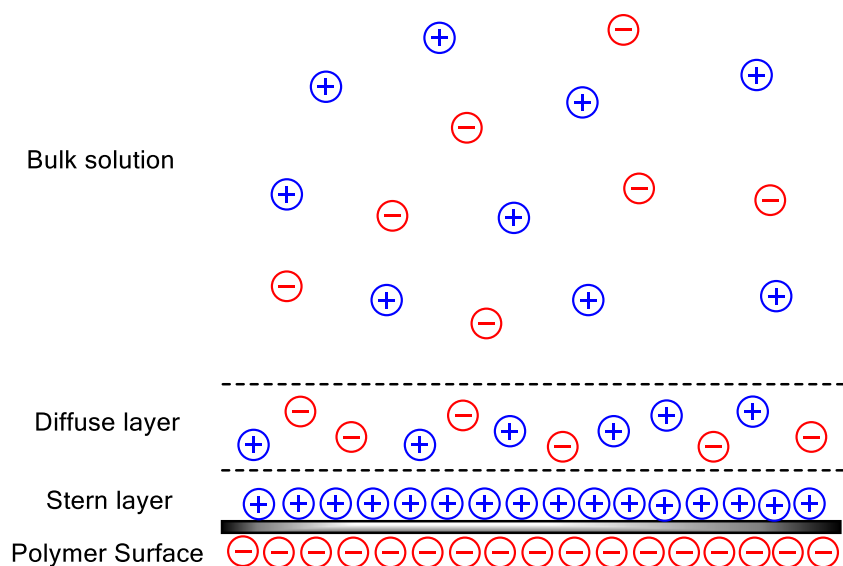


**Figure 1.9.** Schematic diagram of the electrical double layer of polyelectrolytes formed in aqueous media.

### 1.8.2 Polyelectrolyte conformation in solution

Neutral polymers have long been studied and are known to exist in a random coil conformation in solution. Polyelectrolytes, on the other hand, exhibit complex solution properties due to the presence of long-range electrostatic interactions. For this reason, the theoretical understanding of polyelectrolytes is less developed than that of neutral polymers. However, it is generally accepted that the charges along the polyelectrolyte chain will repel each other, causing the chain to adopt a more expanded configuration.<sup>111</sup> Furthermore, polyelectrolyte conformations are controlled by the fraction of ionised groups, which is influenced by many factors, including polymer concentration, molecular weight and chemical structure.

The effect of pH on polyelectrolyte conformation has been studied extensively and it has been found to have a much larger effect on the conformation of weak polyelectrolytes. Poly(acrylic acid) (PAA) is one example of a polyelectrolyte that can dramatically change its conformation in response to variations in the pH of the solution. Laguecir *et al.*<sup>112</sup> have demonstrated that as the chain is neutralised, the number of ionised groups increases, and thus the polyion transforms from a coiled to a more extended conformation.

Finally, while most solutions will not be completely salt-free, (depending on reaction conditions) the addition of low molecular weight salt can alter the polymer conformation dramatically. It has been observed by Valteau *et al.*<sup>113</sup> that the hydrodynamic size of a polyelectrolyte will decrease as the ionic strength of the medium is increased by the addition of monovalent salt. This is due to an increase in Coulombic screening of polyion charges, which reduces electrostatic repulsions within polymer chains and hence, causes a conformational change from an expanded to a coiled polymer chain.<sup>114</sup>

## **1.9 Poly(acrylic acid)**

Poly(acrylic acid) (PAA) is a hydrophilic polyelectrolyte that is often used in the production of nappies as well as for applications in many different areas, as diverse as cosmetics, agriculture and pharmacy.<sup>115</sup>

### **1.9.1 Hydrogels of PAA**

Hydrogels incorporating acrylic acid are heavily utilised in tissue engineering for wound healing and drug delivery. In a recent study, Hussain *et al.*<sup>116</sup> have produced hydrogels of poly(acrylic acid-*co*-vinylsulfonic acid) (PAA-*co*-VSA), using ethylene glycol dimethacrylate (EGDMA) as a crosslinking agent. They have demonstrated a greater swelling of the hydrogels as a result of an increase in the pH of the medium. This was attributed to enhanced ionisation of the carboxylic and sulfonic acid groups, which leads to greater electrostatic repulsions within the polymer network. Furthermore, the release of a model drug was found to be proportional to the pH of the medium. This suggests that (PAA-*co*-VSA) hydrogels are ideal for use as drug carriers, since the scaffold can release its contents in response to changes in the external environment.

Hydrogels comprising PCL and AA have also been investigated for their use as drug delivery systems.<sup>117, 118</sup> By modifying hydrophobic PCL with a hydrophilic polymer, such as AA, it is possible to incorporate drugs for controlled delivery. The inclusion of AA leads to a greater degree of swelling and a higher porosity, which allows for greater uptake of therapeutic drugs.<sup>117</sup> In addition, the slow rate of biodegradation of PCL allows for a more controlled release rate, which is desirable for long term therapeutic effects.

## 1.10 Poly(vinylphosphonic acid)

Poly(vinylphosphonic acid) (PVPA) is a negatively-charged polyelectrolyte that has been identified as a potential candidate for use in bone tissue scaffolds. PVPA can exhibit biomimetic functions by mimicking phosphorylated non-collagenous proteins (NCPs), such as bone sialoprotein (BSP), which are natural mediators of *in vivo* mineralisation. There have been a number of studies that have demonstrated the role of PVPA as a templating mechanism to guide biomimetic mineralisation of a demineralised bone matrix.<sup>119-122</sup> Therefore, it is expected that PVPA can offer osteoconductive and osteoinductive properties to scaffolds to enhance bone regeneration.

### 1.10.1 PVPA incorporation into tissue scaffolds

PVPA has been incorporated into electrospun nanofibres of poly(vinyl alcohol) (PVA). The hydrophilicity of both polymers means they are highly soluble in water. Therefore, stabilisation was performed by heat treatment to form physical crosslinks and thus prevent polymer dissolution in aqueous media. It was found that incorporation of PVPA into the electrospun scaffolds led to a large degree of swelling. Increased adhesion and proliferation of pre-osteoblast cells was observed on PVA/PVPA nanofibres when compared with PVA alone. Furthermore, *in vivo* implantation of membranes that contained PVPA showed more pronounced tissue growth than the pure PVA membrane.

PVPA has been entrapped and immobilised on chitosan prior to the formation of a porous three-dimensional matrix.<sup>123</sup> Higher surface and bulk protein adsorption was found for the matrices containing PVPA, which led to improved attachment and proliferation of MC3T3-E1 pre-osteoblast cells. The porous PVPA-chitosan matrix was able to promote bone formation after *in vivo* implantation into a rat calvarial defect, showing potential for bone tissue engineering applications.

Furthermore, Gemeinhart *et al.*<sup>124</sup> have grafted various concentrations of PVPA onto acrylamide surfaces. It was found that pre-osteoblasts successfully adhered and proliferated on surfaces grafted with PVPA. It is interesting to note that as the vinylphosphonic acid content approached 30 mol %, there was an increase in osteoblast-like cell adhesion and proliferation; higher VPA contents were accompanied by a steady decrease (Figure 1.10). It was suggested that this degree of phosphorylation was optimal

for protein-polymer interactions. In addition, all PVPA modified surfaces enhanced both differentiation and mineralisation of pre-osteoblast cells *in vitro*. Therefore, the results of this study further the potential use of PVPA in bone tissue scaffolds.

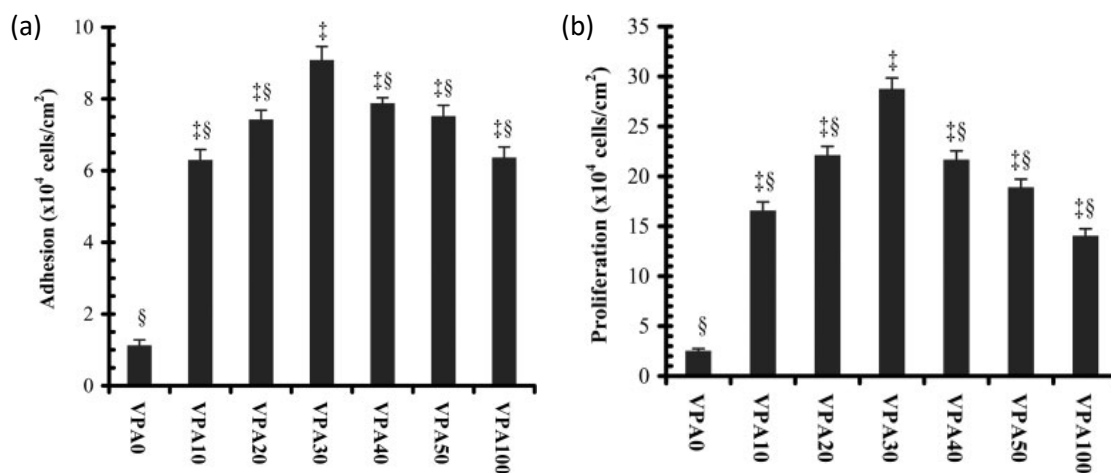


**Figure 1.10.** (a) Adhesion and (b) proliferation of MC3T3-E1 subclone 4 pre-osteoblast cells adhered to acrylamide substrates modified with graft copolymers created from feed compositions of increasing VPA content (mol %). Image taken from Gemeinhart *et al.*<sup>124</sup>

### 1.10.2 Hydrogels of PVPA

Synthetic hydrogels incorporating VPA have been investigated for various applications, including proton conducting membranes,<sup>125</sup> fuel cells<sup>126, 127</sup> and biomaterials.<sup>128, 129</sup> The superior swelling properties of PVPA hydrogels and the ability to manipulate their permeability make them ideal carriers for protein and drug delivery. In a recent study, a hydrogel composed of hyaluronic acid (Ha) and vinylphosphonic acid (VPA) was prepared, which serves as a binding site for calcium ions during the mineralisation process.<sup>130</sup> The VPA/Ha hydrogels were biomineralised to create functional polymer hydrogels that can act as a mimic of the bone extracellular matrix and can deliver a model protein drug. It was found that the hydrogels exhibited a high water content of > 90%, which was not significantly altered by biomineralisation. Furthermore, the release behaviour of protein drug molecules *in vitro* was shown to be controlled by the hydrogel composition, loading content and extent of biomineralisation.

Tan *et al.*<sup>131</sup> have produced hydrogels of VPA and acrylamide (AAm) and evaluated their potential for use in bone tissue scaffolds. They found that the swelling of the gels in culture medium increased with increasing VPA content. This was attributed to an increase in electrostatic repulsions, which is the major driving force for swelling of ionic gels. The presence of VPA also led to an increase in the protein uptake of the gels. The adhesion and proliferation of three cell types: NIH 3T3 fibroblasts, osteoblast-like MG 63 cells and SaOS-2 osteoblast cells, were significantly improved on hydrogels that contained 50 mol % VPA or higher. The results of this study indicate that it is possible to tune the adhesion and proliferation behaviour of bone-related cells by changing the composition of the hydrogels.

### 1.11 Poly(vinylphosphonic acid-*co*-acrylic acid)

Poly(vinylphosphonic acid-*co*-acrylic acid) (PVPA-*co*-AA) has been hypothesised to mimic the action of bisphosphonate drugs, due to a similar chemical structure. The phosphonate groups of VPA and the carboxylate groups of AA can bind to calcium ions (Figure 1.11) *in vivo*, forming a “bone hook” with the potential to enhance bone mineralisation. Previous studies have utilised PVPA-*co*-AA as a surface treatment of electrospun PCL scaffolds, demonstrating improved surface wettability, compressive strength and cell viability.<sup>132</sup>

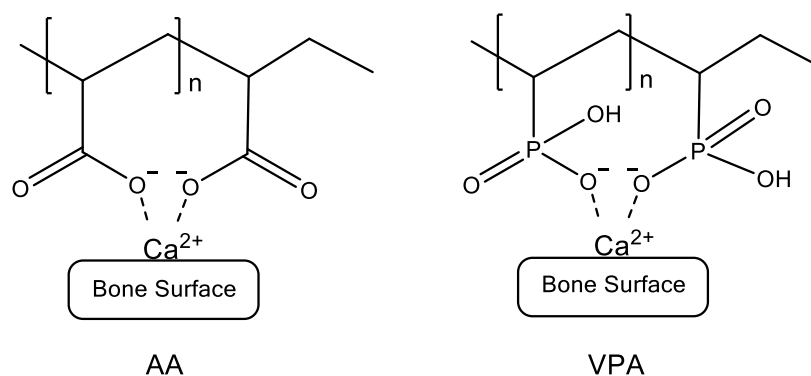


**Figure 1.11.** Calcium chelation by the carboxylate groups of acrylic acid (AA) and the phosphonate groups of vinylphosphonic acid (VPA), forming a “bone hook” to enhance mineralisation.

Bassi *et al.*<sup>133</sup> have demonstrated a significant increase in bone fill percentage in a critical size mouse parietal defect upon incorporation of a PCL/PVPA scaffold compared with PCL alone (Figure 1.12). The formation of tissue and deposition of extracellular matrix was confirmed by scanning electron microscopy. There was evidence of collagen fibre deposition and overall woven bone formation. Furthermore, a significant increase in calcium and phosphorus levels was observed in the presence of the PCL/PVPA scaffold, which suggests the potential formation of hydroxyapatite. These results show that the PCL/PVPA scaffold demonstrates osteoconductive properties, making it suitable for use as a bone graft substitute.

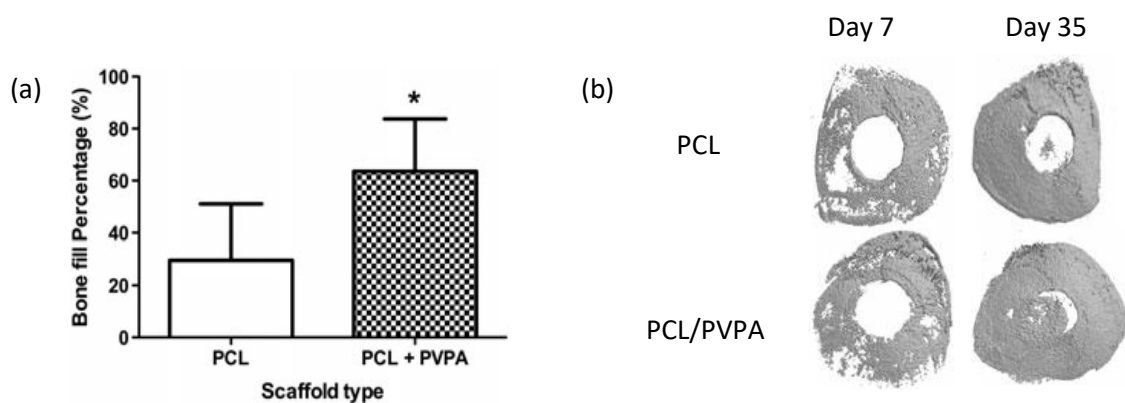


**Figure 1.12.** (a) Bone fill percentage after 35 days of culture on PCL and PCL/PVPA scaffolds (\* $p < 0.05$ ). (b) Micro-CT images of PCL and PCL/PVPA scaffolds after 7 and 35 days of culture. Images taken from Bassi *et al.*<sup>133</sup>

Ghag *et al.*<sup>134</sup> have further investigated the possibility of an osteoinductive effect of PCL/PVPA scaffolds. They have shown that the expression of type I collagen, osteocalcin and alkaline phosphatase is significantly higher on PCL/PVPA scaffolds when compared to PCL. In addition, there was a significant increase in mineralisation on PCL/PVPA substrates after 21 days of culture. The PCL/PVPA scaffold has been shown to increase osteoblast proliferation and matrix deposition. Furthermore, a significant decrease in osteoclast viability was found, with comparable results to Alendronate, a commercially available bisphosphonate. The combined effects of the PVPA-co-AA polymer on osteoblasts and osteoclasts may lead to active bone repair and healing. However, more research is needed to understand the mechanism of action of the polymer and to evaluate its potential for use in bone tissue scaffolds.

## 1.12 Aims and Objectives

The main aim of this study was to investigate the incorporation of poly(vinylphosphonic acid-*co*-acrylic acid) (PVPA-*co*-AA) into bone tissue scaffolds and to evaluate its potential to promote bone formation.

It is hypothesised that PVPA-*co*-AA can bind to calcium from bone mineral surfaces, and thus promote mineralisation of the ECM and enhance bone formation. However, to date there has been no detailed study on the calcium binding affinity of PVPA-*co*-AA and the effect of copolymer composition. Therefore, PVPA-*co*-AA copolymers were synthesised, with a range of VPA monomer feed contents, and fully characterised. The effect of monomer feed ratio on the solution properties of PVPA-*co*-AA was explored, with particular emphasis on the calcium binding affinity of the copolymers.

The *in vitro* release behaviour of PVPA-*co*-AA from electrospun PCL scaffolds was investigated in an attempt to determine the mechanism of action of the copolymer. Furthermore, the potential of PCL scaffolds to act as a carrier for the delivery of PVPA-*co*-AA to the application site was evaluated.

Hydrogels composed of PVPA-*co*-AA were prepared and evaluated for their use as bone tissue scaffolds. The properties of the hydrogels and their ability to promote osteoblast adhesion and proliferation were investigated, with regards to the effect of copolymer composition.

Finally, another potential application of PVPA-*co*-AA copolymers was investigated. The ability of the polymer-calcium complex to bind to fluoride ions and thus facilitate their removal from groundwater was explored. It is believed that this will contribute to improving the quality of drinking water in many parts of the world.

## Chapter 2: Synthesis and characterisation of poly(vinylphosphonic acid-co-acrylic acid)

### 2.1 Introduction

#### 2.1.1 Free radical polymerisation

Free radical polymerisation is a chain reaction consisting of three steps – initiation, propagation and termination. The first step involves the homolysis of an initiator molecule, either thermally or using UV light, to form two stable radicals. The rate of decomposition of a thermal initiator is significantly affected by the temperature of polymerisation and the initial concentration of initiator.<sup>135, 136</sup> Therefore, the rate of polymerisation and hence, monomer conversions and polymer molecular weights, can be controlled by adjusting the initial reaction conditions.

Propagation then occurs to allow growth of the polymer chain by the addition of monomer molecules. At some point during the polymerisation, the propagating polymer chain will be terminated. Termination can take place by many different methods, including combination, disproportionation or chain transfer.<sup>137</sup> Chain transfer involves the transfer of a hydrogen atom to the growing polymer chain from a species present in the system, i.e. monomer, initiator or solvent. This results in the premature termination of a growing polymer chain and thus produces polymers with low molecular weights. While this can be detrimental in some cases, much work has been carried out on the incorporation of a chain transfer agent to control the molecular weight at a specified level.<sup>138-140</sup>

Copolymerisation, where two different monomers are present in the polymerisation system, allows a wide range of polymers to be produced with properties that are tailored to specific applications. The behaviour of monomers in copolymerisation reactions has been found to depend on many factors including polarity, steric hindrance and resonance effects.<sup>141</sup> This, in turn, affects the relative reactivity of the monomers, which can have a significant impact on the structure and properties of the copolymer formed.

### 2.1.2 Monomer reactivity ratios

Monomer reactivity ratios provide a way of estimating the average composition of copolymers and the relative placement of functional monomers along the polymer chain. The type of copolymer produced during polymerisation is determined by statistical laws. For example, copolymers formed via Bernoulli processes,<sup>142</sup> known as random copolymers, have a random distribution of monomers along the polymer chain since the probability of adding any kind of monomer is independent of its predecessor.

Block and alternating copolymers follow the first-order Markov model,<sup>142, 143</sup> or terminal model, whereby the reactivity of a growing polymer chain is dependent only on the last monomer unit added and independent of the chain composition preceding the last monomer. Using this model, Mayo and Lewis developed a way to quantitatively measure the reactivity of each monomer by applying equation 2.1:<sup>144</sup>

$$\frac{d[M_1]}{d[M_2]} = \frac{[M_1](r_1[M_1] + [M_2])}{[M_2]([M_1] + r_2[M_2])} \quad (2.1)$$

where  $[M_1]$  and  $[M_2]$  are the concentrations of monomer 1 and monomer 2 and  $r_1$  and  $r_2$  are their reactivity ratios, i.e. the relative rate constants of a growing polymer chain toward adding itself (homo-propagation) versus adding the other monomer (cross-propagation) in the copolymerisation system. The tendency of two monomers to copolymerise is noted by  $r$  values between zero and one. An  $r_1$  value of greater than one means that  $M_1$  is more likely to homopolymerise, while an  $r_1$  value of less than one means that  $M_1$  preferentially adds  $M_2$ . An  $r_1$  value of zero would mean that  $M_1$  is incapable of undergoing homopolymerisation.<sup>141</sup> It should be noted that the reactivity of a monomer during homopolymerisation does not necessarily give an indication as to its ability to copolymerise.<sup>145</sup>

### 2.1.3 Synthesis of PAA

Poly(acrylic acid) (PAA) is a water-soluble polyelectrolyte. The synthesis of PAA has been studied extensively for use in many different applications. It is commonly used as a fluid thickener in various industries, such as pharmaceuticals, cosmetics and nuclear waste treatment.<sup>146, 147</sup> The rapid nature of the polymerisation means high molecular

weight PAA can easily be produced. It is also possible to copolymerise AA with many different monomers, including acrylamide<sup>148</sup> and vinylsulfonic acid.<sup>149</sup>

A study on the copolymerisation of AA and vinyl acetate (VAc) has identified  $r_{AA}$  as 1.4 and  $r_{VAc}$  as 0.039,<sup>150</sup> demonstrating the higher reactivity of AA in the copolymerisation system. This means that the composition of the copolymer will change throughout the course of the reaction, favouring the more active monomer species (in this case AA). This situation is known as a composition drift and it can have a profound effect on the properties of the copolymer. Therefore, many attempts have been made to alter the solvent system,<sup>150</sup> pH<sup>151, 152</sup> or ionic strength<sup>148</sup> of the reaction medium in order to limit the rate of polymerisation of acrylic acid and produce copolymers with more homogeneous compositions.

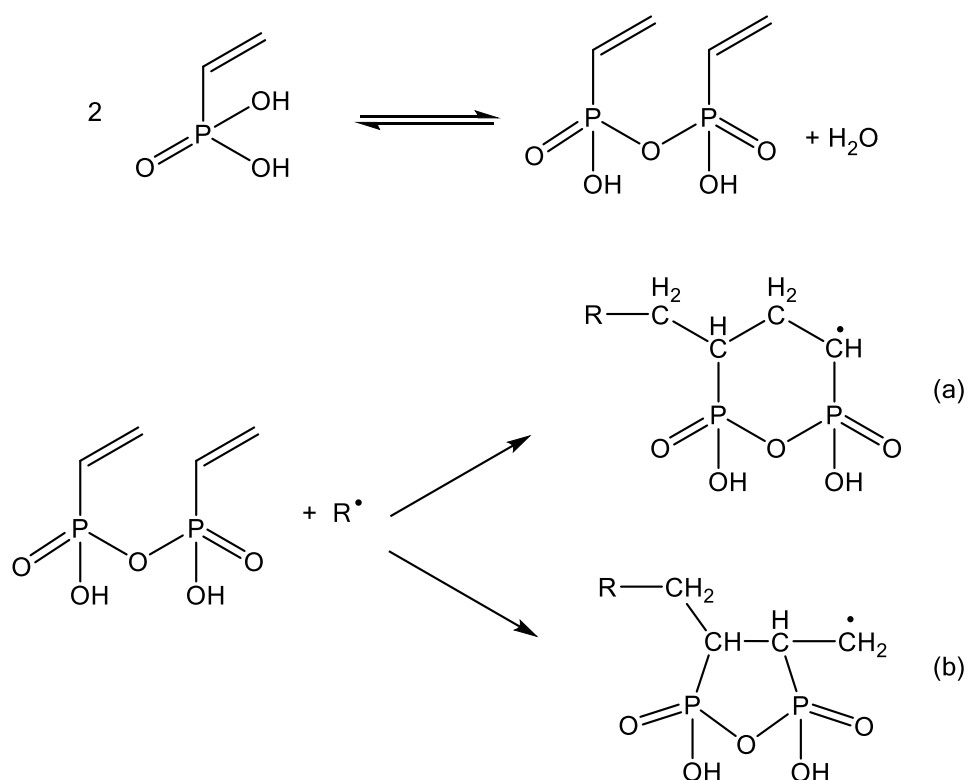
#### 2.1.4 Synthesis of PVPA

Poly(vinylphosphonic acid) (PVPA) has received relatively little attention, due to the difficulty and slow nature of its polymerisation. It is generally accepted that phosphonic acids readily form anhydrides in water at polymerisation temperatures. The steric bulk of the VPA anhydride makes it difficult for it to diffuse through the medium to the growing polymer chain, leading to a lower rate of reactivity. Bingöl *et al.*<sup>153</sup> have investigated the synthesis of PVPA homopolymer from vinylphosphonic acid (VPA). It was found that once the anhydride is formed in equilibrium with the free acid, the free radical polymerisation proceeds via two pathways (Scheme 2.1).<sup>153</sup>

Intramolecular propagation can occur to form a 6-membered ring, which produces head-tail linkages and a methine radical (Scheme 2.1a). Alternatively, propagation to form a 5-membered ring results in a pattern of head-head linkages and formation of a methylene radical (Scheme 2.1b). Attack of this radical to a further vinyl group in the  $\beta$ -position would lead to the formation of tail-tail links. This mechanism leads to defects in the polymer not exhibited in PAA, which is believed to be composed of head-tail links only and thus has a more regular structure. Furthermore, it is thought that a competition exists between the propagating radicals formed from VPA anhydride, which contributes to the low reactivity of VPA.<sup>154</sup>

Despite the difficult polymerisation, PVPA has been successfully copolymerised with monomers such as styrene,<sup>155</sup> acrylonitrile<sup>125</sup> and vinylpyrrolidone.<sup>126</sup> The

copolymerisation of VPA and styrene is not facile due to the different structures of the two monomers as well as the difference in their hydrophilicity. The reactivity ratios of the monomers have been calculated as 3.6 for styrene and 0.15 for VPA,<sup>155</sup> which confirms the much lower reactivity of VPA in the copolymerisation system and leads to a low incorporation of VPA into the final copolymer.



**Scheme 2.1.** Suggested mechanism of cyclopolymerisation involving vinylphosphonic acid anhydride to form (a) 6-membered ring and a methine radical or (b) 5-membered ring and a methylene radical, adapted from Bingöl *et al.*<sup>153</sup>

### 2.1.5 Synthesis of PVPA-*co*-AA

Research into copolymers of vinylphosphonic acid and acrylic acid is somewhat limited due to the stark difference in their reactivities. Kwak *et al.*<sup>156</sup> have synthesised PVPA-*co*-AA nanobeads using suspension polymerisation and investigated their properties for ion-exchange processes. They found that the synthetic yields were inversely dependent on the VPA content in the monomer feed and have attributed this to the lower reactivity of VPA when compared with AA. Furthermore, the phosphorus content – probed using energy-dispersive X-ray spectroscopy (EDX) – was determined to be much lower in the

nanobeads than was originally present in the monomer feed, confirming the low extent of VPA conversion.

Although this work provides some evidence to suggest that VPA is less reactive than AA, to date there has been no detailed synthetic study on the copolymerisation of AA and VPA, with regards to the effect of monomer feed ratio.

### **2.1.6 Aims and Objectives**

It was the aim of this work to investigate the copolymerisation of acrylic acid (AA) with vinylphosphonic acid (VPA).

Firstly, the effect of temperature and initiator concentration on the yield, monomer conversion and average molar masses was determined.

Copolymer compositions were calculated using elemental analysis and a new method has been developed using  $^{31}\text{P}$  NMR spectroscopy. Results from the two methods are compared. The effect of monomer feed ratio on copolymer composition, yield, monomer conversions and average molar masses was investigated.

The reactivity ratios for AA and VPA in the copolymerisation system were used to quantify the difference in reactivity of the two monomers and thus to gain an understanding of how the polymerisation proceeds and inform any improvements in the synthetic method.

PVPA-*co*-AA copolymers were produced with a range of copolymer compositions. The effect of the addition of chain transfer agent on the properties of the copolymers was investigated. The copolymers were then characterised by  $^1\text{H}$  NMR,  $^{31}\text{P}$  NMR and FT-IR spectroscopy.

## 2.2 Experimental

### 2.2.1 Materials

All chemicals were used without further purification unless otherwise stated. Vinylphosphonic acid (VPA), (97%) was purchased from Tokyo Chemical Industry (TCI), U.K. Acrylic acid (AA), (99%), 2,2'-azobis(2-methylpropionamide) dihydrochloride (AAPH), (97%), 1-octanethiol, ( $\geq 98.5\%$ ), trimethyl phosphate (TMP), (97%) and deuterium oxide ( $D_2O$ ), (99.9%) were all purchased from Sigma-Aldrich, U.K. Visking cellulose tubing (Scientific Laboratory Supplies, U.K.) was used for dialysis with a molecular weight cut off (MWCO) of 12000–14000  $g\ mol^{-1}$  and an inflated diameter of 17.5 mm.

### 2.2.2 Experimental methods

$^1H$  NMR spectra were recorded in solution (5 wt % in  $D_2O$ ) on a Bruker AV400 spectrometer operating at 400.13 MHz. The  $^1H$  NMR spectra were referenced to sodium 3-(trimethylsilyl)-propionate-2,2,3,3- $d_4$  ( $\delta_H = 0$  ppm). The pulse sequence consisted of a  $30^\circ$  pulse and a delay time of 1.0 s.

$^{31}P$  NMR spectra were recorded in solution (5 wt % in  $D_2O$ ) on a Bruker AV500 spectrometer operating at 202.48 MHz. The  $^{31}P$  NMR spectra were referenced to trimethyl phosphate (TMP) ( $\delta_P = 2.8$  ppm). 1.5 wt % TMP was added to the solution prior to the experiment. The pulse sequence consisted of a  $30^\circ$  pulse and a delay time of 2.0 s.

Fourier transform infrared (FT-IR) spectra were recorded using a Thermo Scientific Nicolet iS5 spectrometer with an iD5 diamond attenuated total reflectance (ATR) attachment over a wavenumber range of 4000–600  $cm^{-1}$  and a resolution of 4  $cm^{-1}$ . The spectra were obtained from 16 scans.

Elemental analyses were carried out using inductively coupled plasma mass spectrometry (ICP-MS), by the School of Chemistry Microanalysis Service, University of Manchester.

GPC measurements were performed with a Waters 515 HPLC pump, TSK gel columns (5000 and 6000 Å pore size) and an ERC-7515A refractive index detector. 0.1 M

aqueous disodium hydrogen phosphate ( $\text{Na}_2\text{HPO}_4$ ) was used as a mobile phase at a flow rate of  $0.5 \text{ mL min}^{-1}$ . A set of PAA-Na standards with  $\bar{M}_w$  between 1250 and  $1.1 \times 10^6 \text{ g mol}^{-1}$  were used for calibration with ethylene glycol as an internal marker. Solutions of  $1 \text{ g L}^{-1}$  PVPA-*co*-AA in  $\text{Na}_2\text{HPO}_4$  were measured at  $35 \text{ }^\circ\text{C}$ . Software was developed in house using LabVIEW.

### 2.2.3 Synthesis of PVPA-*co*-AA

The following method describes the synthesis of P2. Further details of the experimental conditions and procedures for the different compositions are presented in the appendix in Table A2.1. Their characterisation data are shown in section A2.1 of the appendix.

VPA (2.74 g, 25.4 mmol) was dissolved in deionised water ( $3.0 \text{ cm}^3$ ) and added to a 2-neck round-bottom flask equipped with a reflux condenser. The apparatus was purged with  $\text{N}_2$  before the polymerisation. The solution was heated to  $90 \text{ }^\circ\text{C}$  and left for 30 min. AA (4.20 g, 58.3 mmol) was dissolved in  $\text{H}_2\text{O}$  ( $4.0 \text{ cm}^3$ ) and AAPH (22.7 mg, 83.7  $\mu\text{mol}$ ) was dissolved in  $\text{H}_2\text{O}$  ( $3.0 \text{ cm}^3$ ). These were added to the reaction flask in equal portions, every 30 min, over the course of 6 h. After the last addition, the reaction was left for a further 18 h. The crude product was purified by dialysis for 24 h, using approximately 30 cm cellulose tubing. The resulting polymer was dried at  $55 \text{ }^\circ\text{C}$  under vacuum to afford a white solid (5.06 g, 73% yield).  $\delta_{\text{H}}$  (400 MHz;  $\text{D}_2\text{O}$ ) 4.29 (1 H, br.s, C-O-H), 2.80-2.22 (25 H, m, C-C-H), 2.19-1.27 (83 H, m, C- $\text{CH}_2$ ) ppm.  $\delta_{\text{P}}$  (202 MHz;  $\text{D}_2\text{O}$ ) 30.30 (s, C-P=O(OH) $_2$ ) ppm. Elemental analysis (calc.) (%): C 34.86 (36.32), P 9.17 (9.40), H 6.01 (5.90).

### 2.2.4 Synthesis of PVPA-*co*-AA for the evaluation of reactivity ratios

The following method details the synthesis of R40. Further details of the experimental conditions and procedures for the different compositions are presented in the appendix in Table A2.2. Their characterisation data are shown in section A2.2 of the appendix.

VPA (0.50 g, 4.63 mmol) was dissolved in deionised water ( $7.0 \text{ cm}^3$ ) and added to a 2-neck round-bottom flask equipped with a reflux condenser. The apparatus was purged with  $\text{N}_2$  prior to the polymerisation. The solution was heated to  $90 \text{ }^\circ\text{C}$  and left for 30 min. AA (0.50 g, 6.94 mmol) was dissolved in  $\text{H}_2\text{O}$  ( $10.0 \text{ cm}^3$ ) and AAPH (3.14 mg, 11.6  $\mu\text{mol}$ ) was dissolved in  $\text{H}_2\text{O}$  ( $2.0 \text{ cm}^3$ ). These were then added to the reaction flask

and the reaction was left for 30 min. The crude product was purified by dialysis for 24 h, using approximately 30 cm cellulose tubing. The resulting polymer was dried at 55 °C under vacuum to afford a white solid (0.66 g, 67% yield).  $\delta_{\text{H}}$  (400 MHz; D<sub>2</sub>O) 6.35-5.77 (30 H, m, C=CH<sub>2</sub>), 4.23 (1 H, br.s, C-O-H), 2.72-2.14 (6 H, m, C-C-H), 2.11-1.36 (12 H, m, C-CH<sub>2</sub>) ppm. Elemental analysis (calc.) (%): C 41.30 (39.20), P 4.03 (6.29), H 5.55 (5.46).

### 2.2.5 Synthesis of PVPA-co-AA using chain transfer agent (CTA)

The following method details the synthesis of PVPA-40. Further details of the experimental conditions and procedures for the different compositions are presented in Table 2.1. Their characterisation data are shown in section A2.3 of the appendix.

VPA (2.06 g, 19.1 mmol) was dissolved in deionised water (3.0 cm<sup>3</sup>) and added to a 2-neck round-bottom flask equipped with a reflux condenser. The apparatus was purged with N<sub>2</sub> before the polymerisation. The solution was heated to 90 °C and left for 30 min. AA (2.06 g, 28.6 mmol) was dissolved in H<sub>2</sub>O (3.0 cm<sup>3</sup>), AAPH (12.9 mg, 47.7  $\mu$ mol) was dissolved in H<sub>2</sub>O (3.0 cm<sup>3</sup>) and 1-octanethiol (6.9 mg, 47.7  $\mu$ mol) was dissolved in H<sub>2</sub>O (2.0 cm<sup>3</sup>). These were added to the reaction flask in equal portions, every 30 min, over the course of 6 h. After the last addition, the reaction was left for a further 18 h. The crude product was purified by dialysis for 24 h, using approximately 30 cm cellulose tubing. The resulting polymer was dried at 55 °C under vacuum to afford a white solid (1.40 g, 38% yield).  $\delta_{\text{H}}$  (400 MHz; D<sub>2</sub>O) 4.29 (1 H, br.s, C-O-H), 3.09-2.21 (10 H, m, C-C-H), 2.18-1.24 (32 H, m, C-CH<sub>2</sub>) ppm.  $\delta_{\text{P}}$  (202 MHz; D<sub>2</sub>O) 30.88 (s, C-P=O(OH)<sub>2</sub>) ppm. Elemental analysis (calc.) (%): C 31.59 (33.50), P 12.80 (12.36), H 5.61 (5.69).

### 2.2.6 Synthesis of PAA

The following method details the synthesis of PVPA-0 (Table 2.1). AA (2.10 g, 29.1 mmol) was dissolved in deionised water (26.0 cm<sup>3</sup>) and added to 2-neck round-bottom flask, equipped with a reflux condenser. The apparatus was purged with N<sub>2</sub> before the polymerisation. The solution was heated to 90 °C under reflux and left for 30 min. AAPH (8.0 mg, 29.1  $\mu$ mol) was dissolved in H<sub>2</sub>O (2.0 cm<sup>3</sup>) and 1-octanethiol (12.9 mg, 88.1  $\mu$ mol) was dissolved in H<sub>2</sub>O (2.0 cm<sup>3</sup>). These were then added to the reaction flask and the reaction was left to reach completion for 3 h. The crude product was purified by

dialysis for 24 h, using approximately 30 cm cellulose tubing. The resulting polymer was dried at 55 °C under vacuum to afford a white solid (1.74 g, 83% yield).  $\delta_{\text{H}}$  (400 MHz; D<sub>2</sub>O) 4.29 (1 H, br.s, C-O-H), 2.78-2.17 (7 H, m, C-C-H), 2.15-1.31 (12 H, m, C-CH<sub>2</sub>) ppm. Elemental analysis (calc.) (%): C 46.27 (50.0), H 5.75 (5.56).

### 2.2.7 Synthesis of PVPA

The following method details the synthesis of PVPA-100 (Table 2.1). VPA (1.37 g, 12.7 mmol) was dissolved in deionised water (3.0 cm<sup>3</sup>) and added to a 2-neck round-bottom flask, equipped with a reflux condenser. The apparatus was purged with N<sub>2</sub> before the polymerisation. The solution was heated to 90 °C under reflux and left for 30 min. AAPH (3.4 mg, 12.7  $\mu\text{mol}$ ) was dissolved in H<sub>2</sub>O (3.0 cm<sup>3</sup>) and added to the reaction flask. The reaction was left to reach completion for 24 h. The crude product was purified by dialysis for 24 h, using approximately 30 cm cellulose tubing. The resulting polymer was dried at 55 °C under vacuum to afford a white solid (0.15 g, 11% yield).  $\delta_{\text{H}}$  (400 MHz; D<sub>2</sub>O) 2.82-1.97 (10 H, m, C-C-H), 1.95-1.19 (12 H, m, C-CH<sub>2</sub>) ppm.  $\delta_{\text{P}}$  (202 MHz; D<sub>2</sub>O) 31.14 (s, C-P=O(OH)<sub>2</sub>) ppm. Elemental analysis (calc.) (%): C 19.76 (22.2), P 26.09 (29.6), H 4.59 (4.63).

**Table 2.1.** Experimental conditions for the copolymerisation of AA with VPA (where  $n$  is the number of moles, CTA is chain transfer agent and  $V$  is volume)\*.

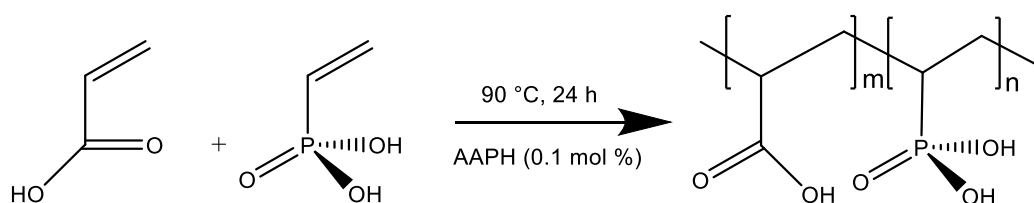
Sample Code	mol % VPA in the feed	$n_{\text{VPA}}$ (mmol)	mol % AA in the feed	$n_{\text{AA}}$ (mmol)	$n_{\text{AAPH}}$ ( $\mu\text{mol}$ )	$n_{\text{CTA}}$ ( $\mu\text{mol}$ )	$V_{\text{water}}$ (mL)
PVPA-0	0	0.00	100	29.1	29.1	88.1	30.0
PVPA-20	20	12.7	80	50.7	63.4	126.8	14.0
PVPA-30	30	12.7	70	29.2	41.9	83.8	12.0
PVPA-40	40	19.1	60	28.6	47.7	47.7	11.0
PVPA-60	60	19.0	40	12.7	31.7	0.00	10.0
PVPA-80	80	19.0	20	4.76	23.8	0.00	8.0
PVPA-100	100	12.7	0	0.00	12.7	0.00	6.0

\*The total monomer concentration was altered as a result of the large difference in polymerisation rate with varying copolymer composition.

## 2.3 Results and Discussion

### 2.3.1 Effect of temperature and initiator concentration

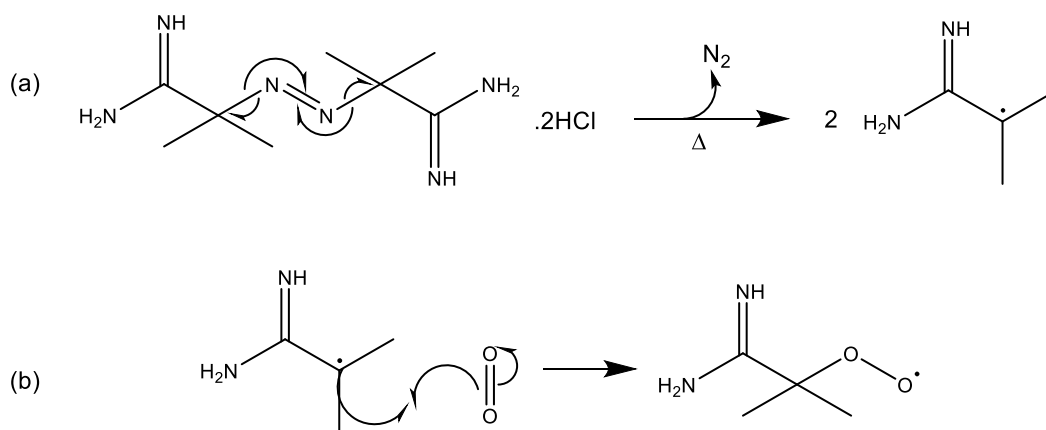
The free radical polymerisation of acrylic acid (AA) and vinylphosphonic acid (VPA) has been carried out in water, with various feed compositions, to produce PVPA-*co*-AA (Scheme 2.2). The synthetic procedure was adapted from a patent by Dürsch *et al.*,<sup>157</sup> whereby the VPA was added at the start of the reaction and the initiator (AAPH) and AA monomer were added batch-wise over the course of 6 h. The reaction was then left for a further 18 h to reach completion. Further additions of water were made where necessary, throughout the polymerisation, to prevent the viscosity from becoming too high, and thus to maintain sufficient stirring of the reaction mixture.



**Scheme 2.2.** Free radical polymerisation of AA and VPA to produce PVPA-*co*-AA.

AAPH, which has a half-life ( $t_{1/2}$ ) of 10 h at 56 °C and *ca.* 1.1 h at 73 °C,<sup>158</sup> was used as a water-compatible azo initiator. Decomposition of AAPH produces molecular nitrogen and two carbon radicals (Scheme 2.3a), which may combine to produce a stable by-product. The formation of the highly stable nitrogen molecule is the driving force for the thermal homolysis of AAPH.

The presence of oxygen in the polymerisation system can act as an inhibitor by reacting with initiator fragments to produce peroxy radicals (Scheme 2.3b), and thus preventing the polymerisation from occurring for a period of time (induction time).<sup>159, 160</sup> Once all the oxygen is consumed, the reaction will proceed at its normal rate. To prevent this, nitrogen gas was bubbled through the reaction apparatus prior to the polymerisation and continuously throughout to remove any oxygen present.



**Scheme 2.3.** (a) Decomposition of AAPH initiator to form two stable carbon radicals and molecular nitrogen and (b) AAPH initiator radical combines with molecular oxygen to form a peroxy radical.

Monomer conversions to copolymers were determined by taking  $^1\text{H}$  NMR spectra of the reaction mixtures prior to purification. Figure 2.1 shows the crude  $^1\text{H}$  NMR spectrum of P2. The methylene ( $\text{CH}_2$ ) and methine ( $\text{CH}$ ) protons of the polymer backbone show signals at 1.25–2.18 and 2.20–2.85 ppm, respectively and the vinyl protons, which occur due to unreacted monomer, show signals at 5.80–6.45 ppm. Hydrogen exchange can occur with the  $\text{D}_2\text{O}$  solvent to form HOD, which shows a signal at 4.8 ppm or  $\text{H}_2\text{O}$ , which could be responsible for the singlet peak at 4.29 ppm.

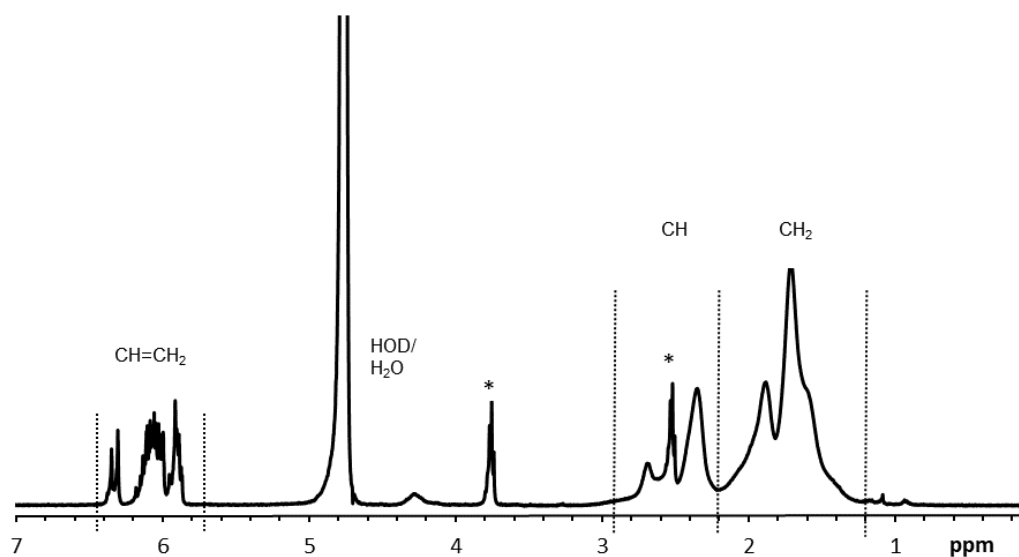


**Figure 2.1.**  $^1\text{H}$  NMR spectrum (in  $\text{D}_2\text{O}$ ) of P2 (30 mol % VPA) prior to purification (\*indicates monomer impurities).

Monomer conversions were calculated by comparing the relative intensities of the resonances of the polymer backbone protons with those of the vinyl protons, according to equation 2.2:

$$\text{monomer conversion (\%)} = \frac{I_{\text{CH}} + I_{\text{CH}_2}}{I_{\text{CH}=\text{CH}_2} + I_{\text{CH}} + I_{\text{CH}_2}} \quad (2.2)$$

where  $I_{\text{CH}}$ ,  $I_{\text{CH}_2}$  and  $I_{\text{CH}=\text{CH}_2}$  are the integrals under the CH, CH<sub>2</sub> and CH=CH<sub>2</sub> peaks, respectively.

The effect of temperature on the polymerisation of VPA with AA was investigated by my colleague, Peter J. Youle, and I then investigated the effect of initiator concentration.<sup>161</sup> The results are collated in Table 2.2. It was found that there was no significant change in the yield or monomer conversion to copolymers when the polymerisation temperature was increased, but a decrease in the average molar mass of the polymers was observed. It is generally accepted that an increase in temperature results in a higher rate of decomposition of initiator, which can then initiate many different monomers.<sup>135</sup> This results in an increase in the rate of polymerisation. However, above certain temperatures, the rate of termination increases, whereas the initiator efficiency remains relatively constant.<sup>162</sup> This means that while the yield and monomer conversion will not be affected, the rapid termination of growing chains will result in a decrease in polymer molar mass, as observed in Table 2.2.

Higher initiator concentrations were found to increase the yield and monomer conversion but decrease the average molar mass (Table 2.2). One possible explanation for this is that higher initiator concentrations result in shorter chain lengths due to the simultaneous initiation of many different monomers. Therefore, the viscosity of the medium is decreased, allowing for a greater rate of monomer diffusion and hence an increase in polymerisation rate and monomer conversion.<sup>162, 163</sup> The highest initiator concentration (1.0 mol %) resulted in a broad molar mass distribution. This is likely due to the initiation of many different chains, coupled with the effect of the batch-wise addition of initiator and acrylic acid monomer.

It is the aim of this work to produce copolymers of PVPA-*co*-AA with a high yield and monomer conversion and a reasonably high molecular weight. Therefore, it was decided that a temperature of 90 °C and an initiator concentration of 0.1 mol % are the optimum conditions for the copolymerisation of AA and VPA.

**Table 2.2.** Effect of temperature and initiator concentration on yield, monomer conversion, weight-average molar mass ( $M_w$ ), number-average molar mass ( $M_n$ ) and molar mass distribution ( $M_w/M_n$ ) for the copolymerisation of VPA with AA<sup>a</sup>.

$T$ (°C)	AAPH Concentration (mol %)	Yield (%)	Monomer Conversion (%)	$M_w$ (g mol <sup>-1</sup> )	$M_n$ (g mol <sup>-1</sup> )	$M_w/M_n$
80	0.1	72	87	310500	38600	8.04
90	0.1	73	86	284600	34800	8.18
100	0.1	73	84	259800	29600	8.77
90	0.3	78	93	145000	18600	7.78
90	1.0	95	98	142000	13600	10.4

<sup>a</sup>In each case, the monomer feed composition was 30 mol % VPA.

The effect of monomer feed ratio on copolymer composition was investigated using elemental analysis and <sup>31</sup>P NMR spectroscopy.

### 2.3.2 Calculation of copolymer composition using elemental analysis

Elemental analysis data, determined from ICP-MS, are shown in Table 2.3 for a range of PVPA-*co*-AA copolymer compositions.

**Table 2.3.** Elemental analysis data for PVPA-*co*-AA samples with different feed compositions.

Sample Code	Monomer feed ratio (VPA:AA)	C (%)	H (%)	P (%)	Copolymer Composition (VPA:AA)
P1	10:90	42.20	5.76	4.12	11:89
P2	30:70	34.86	6.01	9.17	28:72
P3	50:50	34.44	5.60	11.20	34:66
P4	70:30	30.20	5.30	15.80	51:49

The mole ratio,  $r_{P/C}$ , of P to C in the copolymer was calculated from the elemental analysis data using equation 2.3:

$$r_{P/C} = \frac{\%P \times M_C}{\%C \times M_P} \quad (2.3)$$

where  $M_C$  is the molar mass of carbon and  $M_P$  is the molar mass of phosphorus. The mole fraction of VPA,  $x_{VPA}$ , in the copolymer was calculated using equation 2.4:

$$x_{VPA} = \frac{1}{1 + \left(\frac{1 - 2r_{P/C}}{3r_{P/C}}\right)} \quad (2.4)$$

### 2.3.3 Calculation of copolymer composition using $^{31}\text{P}$ NMR spectroscopy

The crude  $^{31}\text{P}$  NMR spectrum of P2 is shown in Figure 2.2. The mole fraction of VPA in the copolymer was determined, first by calculating the moles per integral of TMP marker using equation 2.5:

$$n_{\text{TMP}} = \frac{m_{\text{TMP}}}{M_{\text{TMP}} \times \int \text{TMP}} \quad (2.5)$$

where  $n_{\text{TMP}}$  is the number of moles,  $m_{\text{TMP}}$  is the mass and  $M_{\text{TMP}}$  is the molar mass of TMP.  $\int \text{TMP}$  is the integral under the TMP peak at 2.8 ppm (Figure 2.2). This was then related to the moles of VPA using equation 2.6:

$$n_{\text{VPA}} = n_{\text{TMP}} \times \int \text{VPA} \quad (2.6)$$

Here,  $\int \text{VPA}$  is the integral under the polymer peak at 31.16 ppm. The number of moles of AA,  $n_{\text{AA}}$ , was determined by taking into account the total mass of polymer,  $m_{\text{PVPA-co-AA}}$ , using equation 2.7:

$$n_{\text{AA}} = \frac{(m_{\text{PVPA-co-AA}} - (n_{\text{VPA}} \times M_{\text{VPA}}))}{M_{\text{AA}}} \quad (2.7)$$

where  $M_{\text{VPA}}$  and  $M_{\text{AA}}$  are the molar masses of VPA and AA, respectively. Finally, the mol % VPA in the copolymer was calculated using equation 2.8:

$$\text{mol \% VPA} = \frac{n_{\text{VPA}}}{n_{\text{VPA}} + n_{\text{AA}}} \times 100 \quad (2.8)$$

Using these equations, it was possible to calculate the copolymer composition. Therefore, a new method has successfully been developed to calculate the VPA:AA mole ratio using  $^{31}\text{P}$  NMR spectroscopy. By comparison with elemental analysis, the values for VPA mol % differ slightly. However,  $^{31}\text{P}$  NMR spectroscopy is more

accurate than elemental analysis and so the values for copolymer composition will be quoted using this method from now on.

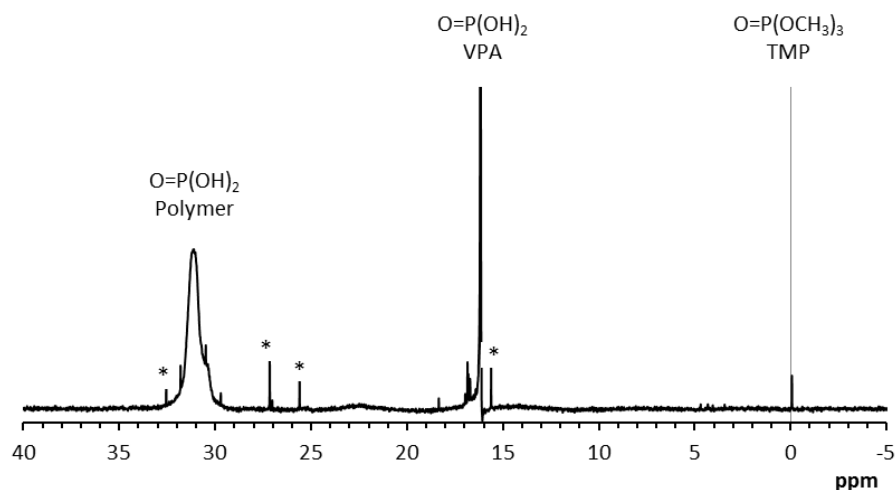


**Figure 2.2.**  $^{31}\text{P}$  NMR spectrum (in  $\text{D}_2\text{O}$ ) of P2 (30 mol % VPA) prior to purification (\*indicates monomer impurities).

### 2.3.4 Effect of monomer feed ratio on the properties of the copolymers

It was found that copolymer compositions, determined using either method, show a discrepancy from the monomer feed ratio. This difference is enhanced when the VPA content in the feed is increased (Table 2.4). Furthermore, there is a decrease in monomer conversions to copolymers and average molar masses with an increase in VPA feed content. The lower reactivity of VPA compared to AA, as explained by Bingöl *et al.*,<sup>153</sup> is a possible cause of the effects above. The formation of VPA anhydride in water produces two different propagating radicals, a 5- and a 6-membered ring, as shown in Scheme 2.1. It has been suggested that this polymerisation mechanism leads to a competition between the propagating radicals, which contributes to the lower reactivity of VPA when compared with AA.<sup>154</sup>

The extent to which the VPA anhydride forms has been found to depend on many factors, including solvent, temperature and the fraction of VPA in the feed.<sup>154</sup> Therefore, the inverse relationship between monomer conversion and VPA content may indicate

that the contribution of the VPA anhydride becomes more significant as the VPA content in the feed increases.

**Table 2.4.** Effect of monomer feed ratio on monomer conversion, copolymer composition (VPA content as determined by elemental analysis and  $^{31}\text{P}$  NMR spectroscopy), weight-average molar mass ( $M_w$ ), number-average molar mass ( $M_n$ ) and molar mass distribution ( $M_w/M_n$ ) for the copolymerisation of VPA with AA.

Sample Code	Monomer feed ratio (VPA:AA)	Monomer Conversion (%)	VPA mol % (EA)	VPA mol % ( $^{31}\text{P}$ NMR)	$M_w$ (g mol $^{-1}$ )	$M_n$ (g mol $^{-1}$ )	$M_w/M_n$
P1	10:90	90	11	8	307900	38700	7.95
P2	30:70	86	28	29	274100	24600	11.2
P3	50:50	73	34	38	85800	14900	5.77
P4	70:30	54	51	54	26000	6700	3.89

The effect of VPA feed content on the molar mass distribution of the copolymers is presented in Figure 2.3. It was shown by Strandberg *et al.*<sup>164</sup> that since PAA and PVPA have the same hydrodynamic structure, under a given set of solution conditions, identical GPC calibration curves are obtained. Therefore, the calibration curve for the determination of molar mass distributions was performed using a set of high molecular weight PAA-Na standards for both homopolymers and the PVPA-*co*-AA copolymers.

The molar mass distributions for P1 and P2 lie outside of the calibration range of the PAA-Na standards. If the calibration range was extended, a tail of very high molar masses is expected to be observed. In cases where the VPA content in the monomer feed is low, polymers are produced with very high molar masses and broad molar mass distributions due to the high reactivity of AA.

The difference in weight-average molar mass between the copolymers with 10 and 70 mol % VPA (P1 and P4) is substantial and so there is expected to be little consistency in the properties of the copolymers with different compositions. Therefore, the synthetic method must be altered to produce a set of copolymers with consistent molar masses and narrower molar mass distributions that lie within the calibration range.

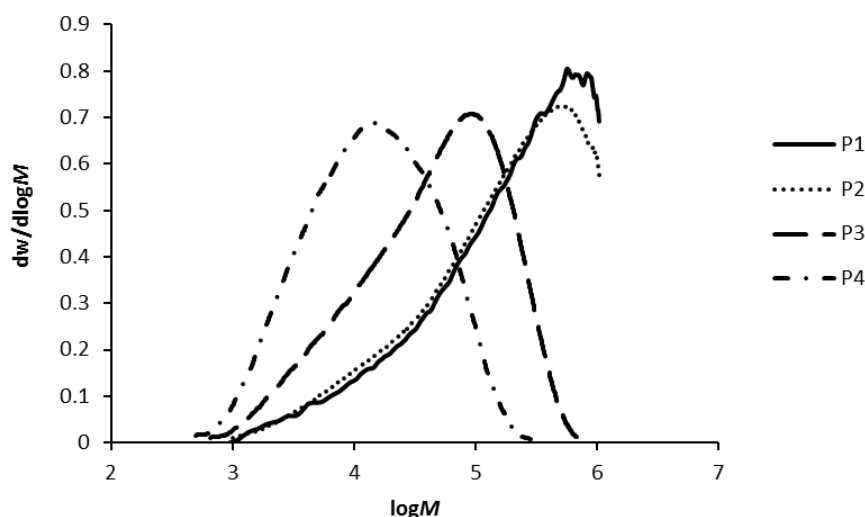


**Figure 2.3.** Weight distributions of  $\log[\text{molar mass}/(\text{g mol}^{-1})]$  for PVPA-co-AA copolymers with VPA feed contents of 10 (P1), 30 (P2), 50 (P3) and 70 (P4) mol %.

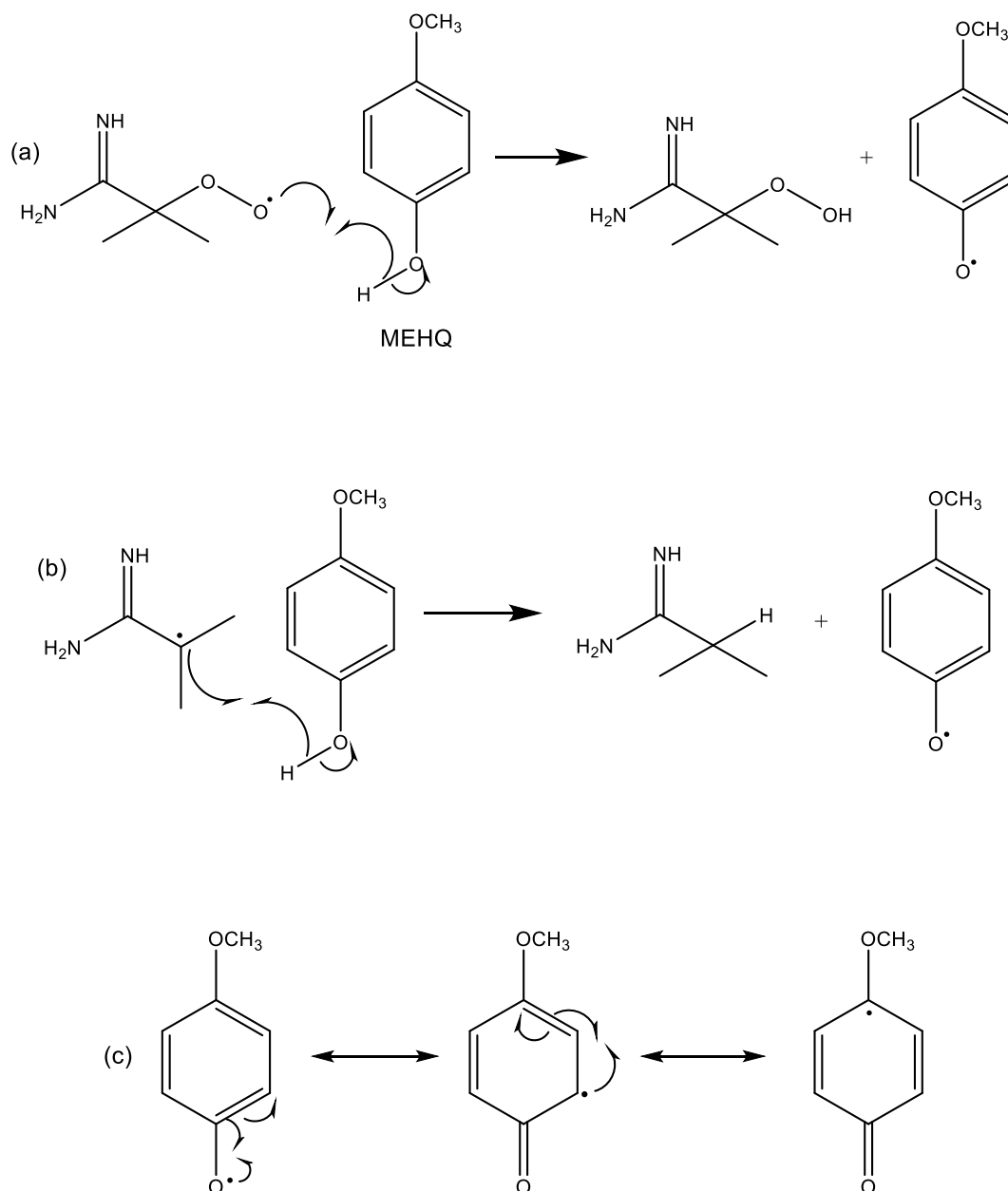
### 2.3.5 Monomer reactivity ratios

Although it has been determined that the reactivity of VPA is much lower than that of AA, a quantitative understanding of this difference would help to explain the mechanism of the copolymerisation. Therefore, monomer reactivity ratios were calculated.

Calculation of reactivity ratios is a kinetic study and so purification of monomers must be considered. Acrylic acid monomer contains the inhibitor 4-methoxyphenol (also known as the monomethyl ether of hydroquinone (MEHQ)) to prevent polymerisation from occurring during storage. The inhibition mechanism<sup>165, 166</sup> can occur via different methods and is summarised in Scheme 2.4. MEHQ can quench peroxy radicals, such as that formed from the reaction of AAPH initiator with molecular oxygen (shown in Scheme 2.3b). This occurs via a hydrogen abstraction mechanism to form a phenoxy radical (Scheme 2.4a). Thus, MEHQ and oxygen can work synergistically to inhibit the polymerisation.

Alternatively, in the absence of dissolved oxygen, the initiator can abstract a hydrogen atom from MEHQ to form the same phenoxy radical (Scheme 2.4b). This radical is much less reactive due to resonance stabilisation, as shown in Scheme 2.4c, so the rate of polymerisation is retarded. However, MEHQ has been shown to be ineffective as an

inhibitor without the presence of dissolved oxygen.<sup>160</sup> Since oxygen is removed from the polymerisation system by degassing with nitrogen, the presence of MEHQ should not have a large effect on the rate of polymerisation and so MEHQ was not removed prior to polymerisation.



**Scheme 2.4.** Mechanism of inhibition by MEHQ via hydrogen abstraction by (a) initiator peroxy radical or (b) initiator alkyl radical and (c) resonance stabilisation of MEHQ.

To calculate the monomer reactivity ratios, a range of copolymers was synthesised with different monomer feed ratios. The polymerisations were carried out to low conversion to minimise unequal monomer consumption throughout the course of the reaction. Total monomer concentrations were kept constant in each case. The effect of monomer feed ratio on copolymer composition (as determined by  $^{31}\text{P}$  NMR spectroscopy), yield, monomer conversion and average molar masses is summarised in Table 2.5. The yield and monomer conversion both show a general increase with a decrease in VPA content in the feed, as expected. As shown previously, the copolymer composition varied significantly from the monomer feed ratio. This effect is more pronounced with higher VPA contents in the feed.

It was not possible to obtain GPC data for R10, R80 and R90 samples. R10 had a VPA feed content of 90 mol %. The low reactivity of VPA meant that the monomer conversion was too low to achieve enough polymer sample for the measurement. On the other hand, R80 and R90 had low VPA feed contents, resulting in high monomer conversions. The polymers produced were of very high molecular weight and began to form a gel meaning that it was not possible to inject the sample into the GPC apparatus.

**Table 2.5.** Effect of monomer feed ratio on copolymer composition, yield, monomer conversion, weight-average molar mass ( $M_w$ ), number-average molar mass ( $M_n$ ) and molar mass distribution ( $M_w/M_n$ ) for the copolymerisation of VPA with AA at low conversion.

Sample Code	Monomer feed ratio (AA:VPA)	Copolymer Composition (AA:VPA)	Yield (%)	Monomer Conversion (%)	$M_w$ (g mol $^{-1}$ )	$M_n$ (g mol $^{-1}$ )	$M_w/M_n$
R10	10:90	60:40	17	3	-	-	-
R20	20:80	63:37	19	5	4200	2500	1.7
R30	30:70	73:27	16	7	17300	5500	3.18
R40	40:60	80:20	42	12	50700	11300	4.49
R50	50:50	86:14	41	17	122300	20500	5.96
R60	60:40	89:11	67	20	153200	28500	5.23
R70	70:30	91:9	54	33	180600	38000	4.76
R80	80:20	94:6	70	54	-	-	-
R90	90:10	96:4	78	65	-	-	-

A variety of methods for evaluation of the reactivity ratios have been proposed. The most common are linear fitting methods including that of Fineman and Ross.<sup>167</sup> This uses a linearized form of the copolymer equation, as shown in equation 2.9:

$$G = r_1 H + r_2 \quad (2.9)$$

where  $G$  is defined as  $X(Y-1)/Y$  and  $H$  as  $X^2/Y$ , with  $X = f_1/f_2$  (monomer feed ratio) and  $Y = F_1/F_2$  (copolymer ratio). A plot of  $G$  versus  $H$  allows  $r_1$  to be calculated from the slope and  $-r_2$  from the intercept. A slightly more accurate linearization method was developed by Kelen and Tüdös and is summarised in equation 2.10:<sup>168</sup>

$$\eta = \left[ r_1 + \frac{r_2}{\alpha} \right] \xi - \frac{r_2}{\alpha} \quad (2.10)$$

where  $\eta$  is equal to  $G/(\alpha + H)$  and  $\xi$  is equal to  $H/(\alpha + H)$ . A plot of  $\eta$  versus  $\xi$  yields a straight line with  $-r_2/\alpha$  and  $r_1$  as the intercept when extrapolating to  $\xi = 0$  and  $\xi = 1$ , respectively. The  $\alpha$  parameter corresponds to  $(Y_m \times Y_M)^{1/2}$  and corrects for the minimum ( $Y_m$ ) and maximum ( $Y_M$ ) values of  $Y$ , which, when using Fineman-Ross, can lead to differing  $r$  values depending on the choice of  $M_1$  and  $M_2$ . In this study, AA was chosen as  $M_1$  and VPA as  $M_2$ . The parameters used for both methods are presented in Table 2.6. The copolymers with monomer feed ratios of 80:20 and 90:10 (AA:VPA) had too high conversions to be included in the study.

**Table 2.6.** Parameters used for the Fineman-Ross and Kelen-Tüdös<sup>a</sup> methods.

$f_1$ (AA)	$f_2$ (VPA)	$F_1$ (AA)	$F_2$ (VPA)	$X$	$Y$	$G$	$H$	$\eta$	$\xi$
10	90	54	46	0.10	1.17	0.015	0.009	0.004	0.002
20	80	61	39	0.25	1.56	0.090	0.040	0.024	0.011
30	70	73	27	0.43	2.70	0.270	0.068	0.072	0.018
40	60	78	22	0.60	3.55	0.431	0.102	0.114	0.027
50	50	84	16	1.00	5.25	0.810	0.190	0.209	0.049
60	40	89	11	1.50	8.09	1.315	0.278	0.333	0.070
70	30	92	8	2.30	11.5	2.100	0.460	0.508	0.111

<sup>a</sup> $\alpha$  is 3.67.

The Fineman-Ross plot (Figure 2.4) yields a straight line which, from the slope and intercept, allows evaluation of the reactivity ratios:  $r_1$  is 4.725 and  $r_2$  is 0.0553. The Kelen-Tüdös plot (Figure 2.5) gave the value of  $r_1$  as 4.727 and  $r_2$  as 0.0558. These results demonstrate good correlation between the different methods. It can be seen here that  $r_1 \gg 1 \gg r_2$ , which means that, as predicted, acrylic acid ( $M_1$ ) is much more reactive than vinylphosphonic acid ( $M_2$ ) toward both propagating species. Hence, acrylic acid is incorporated into the polymer at a much faster rate and the corresponding copolymer contains a larger proportion of AA than VPA, which only becomes integrated into the polymer when AA is depleted. This behaviour is known as a composition drift, whereby the composition of the copolymer changes as the polymerisation proceeds.<sup>141</sup> Therefore, these results prove the lower reactivity of VPA and help to quantify the difference.

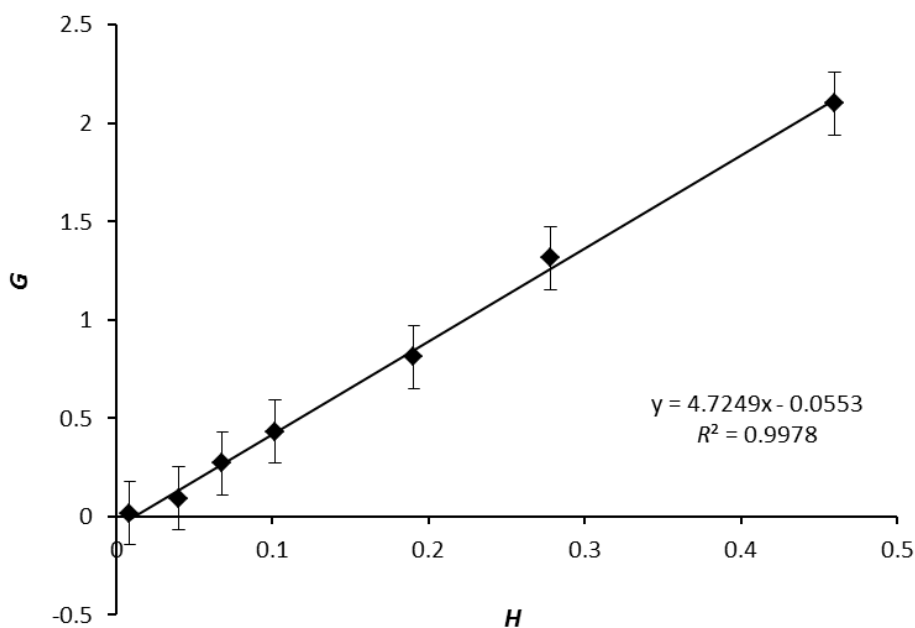


**Figure 2.4.** Fineman-Ross plot for the evaluation of monomer reactivity ratios for the copolymerisation of AA with VPA.

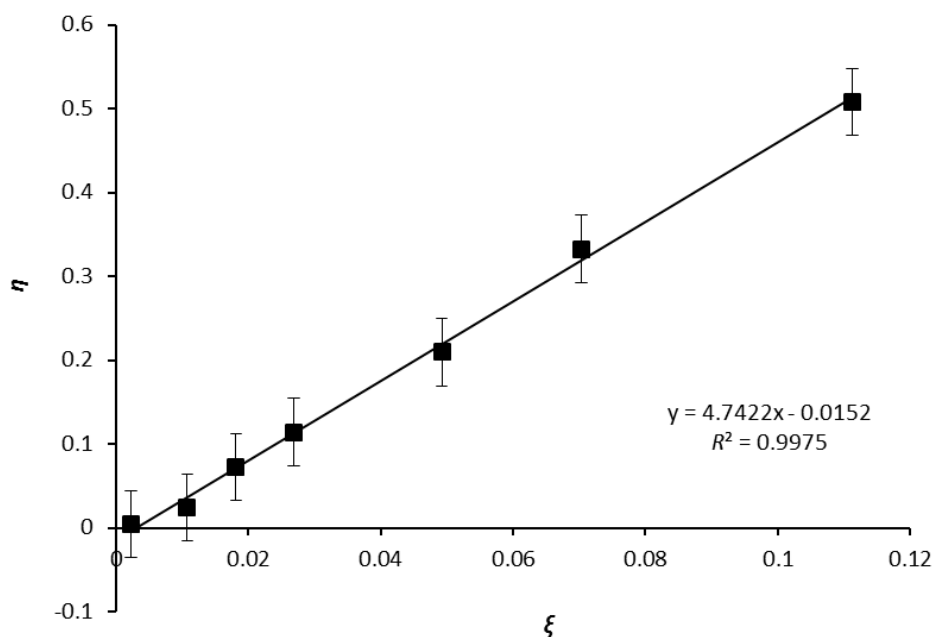
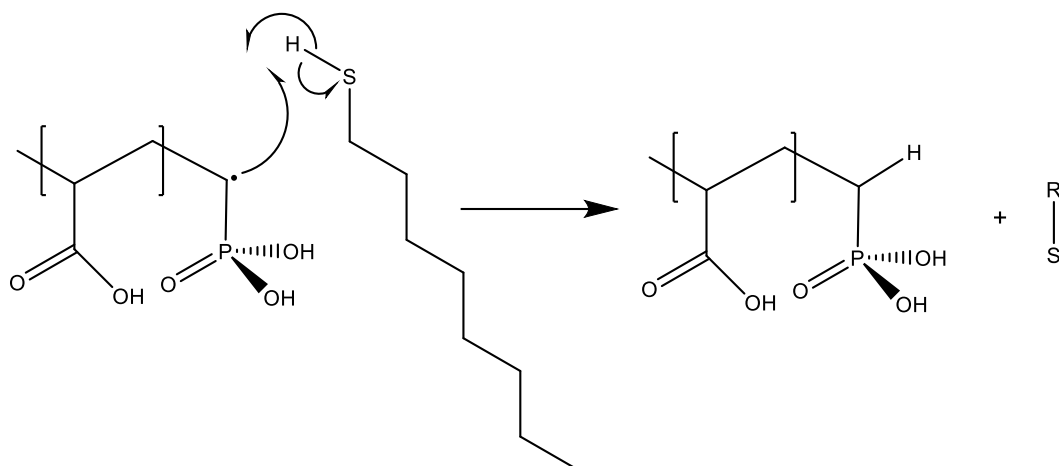


**Figure 2.5.** Kelen-Tüdös plot for the evaluation of monomer reactivity ratios for the copolymerisation of AA with VPA.

### 2.3.6 Synthesis of PVPA-*co*-AA using chain transfer agent

The batch-wise addition of AA monomer and initiator helps to offset the effects of the composition drift that occurs during the copolymerisation of AA and VPA. However, this method alone does not result in consistent average molar masses. When the VPA content in the monomer feed is low, very high molecular weight polymers are produced, with the tendency to form a gel. Conversely, high VPA feed contents result in very low molecular weight polymers. The difference in average molar mass between the different copolymer compositions could have profound effects on the properties of the copolymers.

Therefore, it was decided to alter the synthetic method to include a chain transfer agent (1-octanethiol) to curtail the molecular weight when the VPA content in the feed was low. In this way, it was hypothesised that a range of PVPA-*co*-AA copolymers could be produced with consistent molar masses, allowing for accurate comparisons to be made based on copolymer composition alone. The mechanism of chain transfer from 1-octanethiol to the growing chain is shown in Scheme 2.5.



**Scheme 2.5.** Mechanism of chain transfer to the growing polymer chain by hydrogen abstraction from 1-octanethiol.

Using this method, a range of copolymer compositions was produced. The effect of monomer feed ratio and concentration of chain transfer agent (CTA) on copolymer composition is summarised in Table 2.7. Copolymer compositions were determined using elemental analysis and  $^{31}\text{P}$  NMR spectroscopy and the methods compared. Although there is some variance in the values of VPA content determined by  $^{31}\text{P}$  NMR spectroscopy and elemental analysis, the trend is consistent. It can be observed that there is a slight discrepancy between copolymer composition and monomer feed ratio, in line with what was observed in the absence of chain transfer agent. Therefore, these results suggest that the CTA does not have any detrimental effects on the incorporation of VPA into the copolymer.

**Table 2.7.** Effect of monomer feed ratio and chain transfer agent (CTA) on copolymer composition (mol % VPA in copolymer) as determined by  $^{31}\text{P}$  NMR spectroscopy and elemental analysis.

Sample Code	Monomer feed ratio (VPA:AA)	CTA (mol %)	VPA mol % ( $^{31}\text{P}$ NMR)	VPA mol % (EA)
PVPA-0	0:100	0.3	0	0
PVPA-20	20:80	0.2	16	11
PVPA-30	30:70	0.2	27	26
PVPA-40	40:60	0.1	41	34
PVPA-60	60:40	0.0	59	61
PVPA-80	80:20	0.0	78	84
PVPA-100	100:0	0.0	100	100

Table 2.8 shows the effect of monomer feed ratio and concentration of chain transfer agent on the yield, monomer conversion and average molar masses of copolymers. It is generally accepted that chain transfer agents limit the molecular weight of polymers without affecting the overall rate of reaction if the CTA has negligible water solubility. Here, 1-octanethiol was used, which has a low solubility in water and it can be seen that there is a decrease in yield and monomer conversion with an increase in VPA content, which was also shown to be the case in the absence of CTA (Table 2.4).

The molecular weights of copolymers, with low VPA contents, have been reduced by the presence of CTA (Table 2.8). Furthermore, the molar mass distributions are lower due to the use of chain transfer agent. Therefore, despite the large difference in the reactivity of the monomers, it has proven possible to synthesise PVPA-*co*-AA with a range of copolymer compositions and relatively consistent molecular weights.

However, it proved to be challenging to produce high molecular weight copolymers with VPA contents greater than 60 mol %. The highest achievable weight-average molar mass for PVPA homopolymer was 29100 g mol<sup>-1</sup>, which is comparable to that of Bingöl *et al.*<sup>153</sup> The extremely low reactivity of VPA suggests there is a limit to how much VPA can be incorporated into the copolymer, whilst still maintaining the high molecular weights and consistent properties required.

**Table 2.8.** Effect of monomer feed ratio and chain transfer agent (CTA) on yield, monomer conversion, weight-average molar mass ( $M_w$ ), number-average molar mass ( $M_n$ ) and molar mass distribution ( $M_w/M_n$ ).

Sample Code	Monomer feed ratio (VPA:AA)	CTA (mol %)	Yield (%)	Monomer conversion (%)	$M_w$ (g mol <sup>-1</sup> )	$M_n$ (g mol <sup>-1</sup> )	$M_w/M_n$
PVPA-0	0:100	0.3	83	96	189500	18000	6.03
PVPA-20	20:80	0.2	75	90	185600	22600	8.21
PVPA-30	30:70	0.2	79	96	194800	24200	8.07
PVPA-40	40:60	0.1	38	80	156400	24100	6.47
PVPA-60	60:40	0.0	38	55	182700	13000	4.81
PVPA-80	80:20	0.0	35	22	15900	6500	2.43
PVPA-100	100:0	0.0	11	57	29100	9200	3.15

Further investigation into the structure of the copolymers was achieved using  $^1\text{H}$  NMR,  $^{31}\text{P}$  NMR and FT-IR spectroscopy. Figure 2.6 shows the  $^1\text{H}$  NMR spectra for PVPA-0, PVPA-100, PVPA-30 and PVPA-60; the latter two are shown as examples since all copolymers exhibit similar features. A signal at 4.8 ppm can be seen in all of the  $^1\text{H}$  NMR spectra, due to water impurities and hydrogen exchange with the  $\text{D}_2\text{O}$  solvent, forming HOD. The methylene ( $\text{CH}_2$ ) and methine ( $\text{CH}$ ) protons of the polymer backbone – which show signals at 1.3–2.1 and 2.2–2.8 ppm, respectively – are shifted upfield slightly in the spectrum of PVPA-100 due to the shielding effect of the phosphorus from the VPA side group.

The  $^{31}\text{P}$  NMR spectra of PVPA-100 and PVPA-30 are shown in Figure 2.7. The characteristic polymer peak ( $\text{O}=\text{P}(\text{OH}_2)$ ) is observed at 31.14 ppm for PVPA-100 and 30.38 ppm for PVPA-30. In the spectrum of PVPA-100, it is possible to see a broad peak at around 22.5 ppm which corresponds to the VPA anhydride and therefore corroborates the mechanism of polymerisation suggested by Bingol *et al.*<sup>153</sup> Furthermore, this peak is only present when the VPA content in the feed is high, which supports the theory that the contribution of the anhydride becomes more significant with higher VPA contents.<sup>154</sup> Thus, this offers further evidence for the polymerisation mechanism, which can help to explain the low reactivity of VPA.

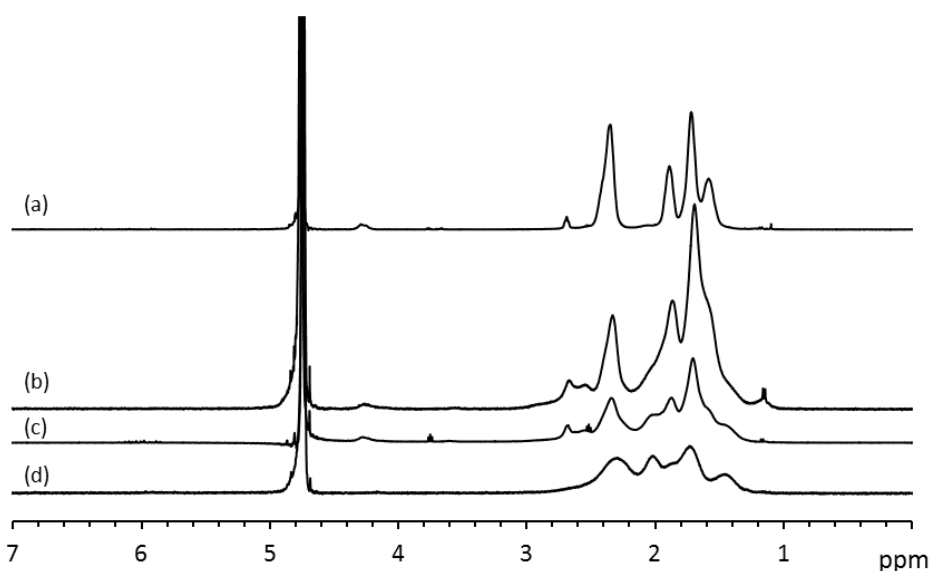


**Figure 2.6.**  $^1\text{H}$  NMR spectra (in  $\text{D}_2\text{O}$ ) of (a) PVPA-0, (b) PVPA-30, (c) PVPA-60 and (d) PVPA-100.

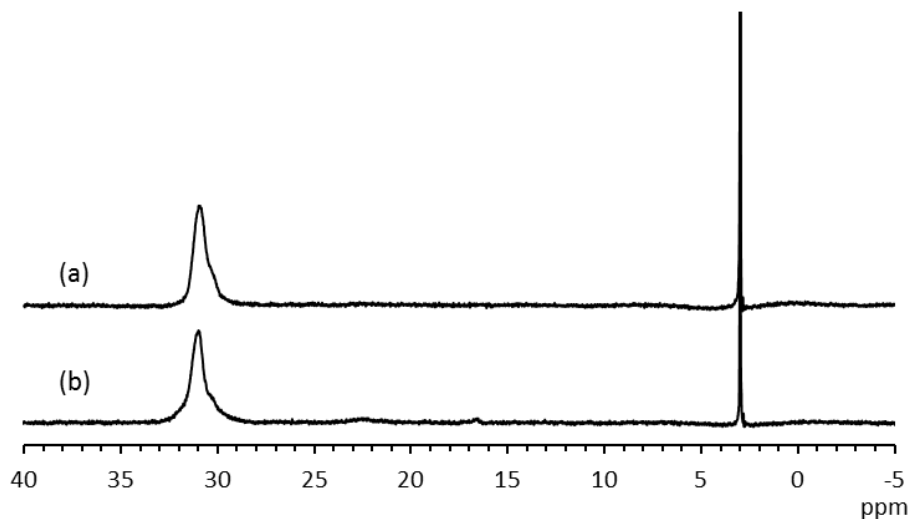


**Figure 2.7.**  $^{31}\text{P}$  NMR spectra (in  $\text{D}_2\text{O}$ ) of (a) PVPA-30 and (b) PVPA-100.

The FT-IR spectra of PVPA-*co*-AA and the respective homopolymers are shown in Figure 2.8. The FT-IR spectra of all the polymers exhibit bands of medium intensity at  $3300\text{--}2500\text{ cm}^{-1}$  and  $1500\text{--}1375\text{ cm}^{-1}$ , representing the methylene C-H stretch and bend, respectively. The O-H stretch appears as a broad band between  $3000$  and  $2300\text{ cm}^{-1}$  in all the spectra. The P-O-H bend can be seen in the spectrum of PVPA-100 at  $1647\text{ cm}^{-1}$ .

The strong IR band at  $1696\text{ cm}^{-1}$  was attributed to the C=O stretch of the carboxylic acid, found in the spectra of PVPA-0 and PVPA-30. This band is shifted to a lower wavenumber than expected due to the presence of hydrogen bonding between the acid groups. The signals which appear at  $1300\text{--}1050\text{ cm}^{-1}$ , of medium strong intensity, denote the C-O stretch of the same group. The spectra of PVPA-30 and PVPA-100 exhibit a band at  $1090\text{ cm}^{-1}$ , which represents the P=O stretch, whereas the P-O stretching bands can be seen at  $985\text{--}905\text{ cm}^{-1}$ . These bands do not appear in the spectrum of PVPA-0 and increase in intensity as the VPA content in the copolymer is increased (see appendix Figure A2.1). This coincides with a decrease in the C=O band of the carboxylic acid group. Therefore, the FT-IR results provide strong evidence for the successful synthesis of PVPA-*co*-AA as a true copolymer, as opposed to a mixture of homopolymers.

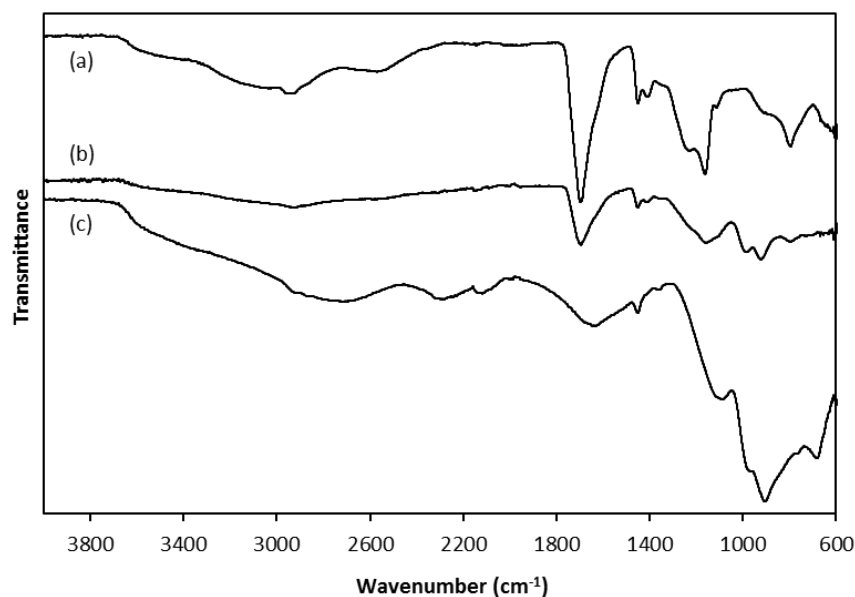


**Figure 2.8.** FT-IR spectra of (a) PVPA-0, (b) PVPA-30 and (c) PVPA-100.

## 2.4 Conclusions

The copolymerisation of AA and VPA has been investigated under a range of conditions. It was determined that a temperature of 90 °C and an initiator (AAPH) concentration of 0.1 mol % were the optimum conditions for the polymerisation, as a result of the high monomer conversions and large average molar masses of the copolymers produced.

The effect of monomer feed ratio on the synthetic yield and monomer conversion was investigated. It was found that an increase in the VPA feed content led to a general decrease in the yield and monomer conversion to copolymers. This also resulted in a decrease in the average molar masses of the copolymers produced, likely due to the lower reactivity of VPA when compared with AA.

A new method has been developed, utilising  $^{31}\text{P}$  NMR spectroscopy to accurately calculate the VPA content in the copolymer. This method was shown to be a more accurate alternative to elemental analysis. Copolymer compositions tended to deviate from monomer feed ratios, again likely due to the lower reactivity of VPA.

The difference in reactivity of AA and VPA was quantified by calculating monomer reactivity ratios. A range of copolymer compositions was produced with low monomer conversions and the reactivity ratios were evaluated using the Fineman-Ross and Kelen-Tüdös linear fitting methods. From the Fineman-Ross method,  $r_1(\text{AA})$  was calculated as 4.725 and  $r_2(\text{VPA})$  as 0.0553. The Kelen-Tüdös method yielded values of 4.727 and 0.0558 for  $r_1$  and  $r_2$ , respectively. Here,  $r_1 \gg 1 \gg r_2$ , which demonstrates the much higher reactivity of AA when compared with VPA. Composition drift occurs throughout the polymerisation, leading to low incorporation of VPA into the copolymer.

When producing polymers for biological applications, product homogeneity is important and composition drift must be eliminated. The batch wise addition of AA into the polymerisation over the course of 6 h contributes to offsetting this effect. Furthermore, a chain transfer agent (CTA) was included in the polymerisation to produce a set of copolymers with consistent molar masses. However, it was not possible to produce high molecular weight polymers from monomer feeds that contained higher than 60 mol % VPA.

PVPA-*co*-AA copolymers were successfully produced with a range of copolymer compositions and their structures were confirmed by  $^1\text{H}$  NMR and  $^{31}\text{P}$  NMR spectroscopy. FT-IR spectroscopy was used to prove the existence of a true copolymer as opposed to a mixture of homopolymers.

## Chapter 3: Calcium binding affinity of PVPA-co-AA

### 3.1 Introduction

The charged nature of polyelectrolytes allows them to bind to many ionic species in aqueous media. The interaction of polyelectrolytes with multivalent salts, such as  $\text{CaCl}_2$ , has been studied extensively and it has been found that two different mechanisms take place. The first is a non-specific electrostatic attraction, whereby divalent ions can screen the electrostatic repulsions within polymer chains and thus lead to a conformational change from an expanded to a coiled structure.<sup>169, 170</sup> For polyelectrolytes with a relatively high charge density along the backbone, some of the counter-ions remain in the vicinity of the polymer chain and when calcium is progressively added, they can displace monovalent counter-ions which are then released into the solution.

Secondly, if the polymer has a high affinity for an ion, a chemical association can occur between the negatively-charged groups of the polyelectrolyte and the  $\text{Ca}^{2+}$  ion. Entropically-driven complexation occurs between two neighbouring monomers of the polymer chain. This chemical association is thought to produce a hydrophobic complex by dehydration of the cation and charged group, which may lead to reversible precipitation of the polymer in solution, known as “salting out”.<sup>171</sup>

Sabbagh *et al.*<sup>172</sup> have investigated this phenomenon and they have suggested that the stability of polyelectrolytes in the presence of multivalent cations depends on the chemical nature of the charged side groups (carboxylate, sulfonate, phosphonate, etc.) as well as the distance between the charged groups and the counter-ion valency. It was found that for weak polyelectrolytes, such as PAA, complexes formed due to a chemical association between the carboxylate groups and the  $\text{Ca}^{2+}$  ions. However, for strong polyelectrolytes, such as poly(vinylsulfonic acid), no such chemical association occurs and the  $\text{Ca}^{2+}$  ions become localised in the vicinity of the polyelectrolyte chain due to electrostatic interactions alone.

### 3.1.1 Calcium binding to PAA and PVPA

Poly(acrylic acid) is often used in the detergent industry due to its high affinity for calcium ions.<sup>173</sup> The ability of PAA to bind to calcium ions is significantly affected by the pH of the medium. It was found by Kriwet *et al.*<sup>174</sup> that the calcium binding capacity of PAA increases linearly with pH, owing to the increased degree of neutralisation. This occurs as a result of electrostatic repulsions along the polymer chain, which result in chain expansion. Thus, the carboxylate anions are more available to bind to calcium. As mentioned previously, a site-specific interaction occurs between Ca<sup>2+</sup> ions and the carboxylate groups, which leads to a reduction in particle size.<sup>175</sup>

To date there is no detailed study investigating the calcium chelation capacity of poly(vinylphosphonic acid) (PVPA). However, PVPA bears structural similarity to PAA and is thus expected to exhibit a similar calcium binding affinity. In a recent study by Strandberg *et al.*,<sup>164</sup> it was shown that PVPA and PAA have the same hydrodynamic structure and demonstrate similar solution behaviour under certain conditions. However, whereas PAA is a weak polyelectrolyte and PVSA is strong, PVPA can be described as intermediate. Therefore, it is expected that calcium can bind to PVPA by both electrostatic attraction and chemical association.

### 3.1.2 Poly(vinylphosphonic acid-co-acrylic acid)

Poly(vinylphosphonic acid-co-acrylic acid) (PVPA-co-AA) is thought to mimic the action of many non-collagenous proteins (NCPs), present in the ECM. NCPs are a group of glycoproteins that contain many aspartic and glutamic acid side chains. The abundance of these amino acids allows NCPs to bind to calcium ions from the extracellular fluid. In this way, NCPs are believed to play a significant role in the mineralisation of bone.<sup>11, 176, 177</sup> NCPs are also phosphorylated to certain degrees and it has been shown that the degree of phosphorylation can affect the protein's ability to bind to calcium ions and hence promote mineralisation.

In addition, PVPA-co-AA has been identified by Bassi *et al.*<sup>133</sup> as an alternative to bisphosphonate drugs, owing to its ability to bind to calcium ions from bone mineral surfaces, essentially forming a "bone hook". In this way, the polymer-calcium complex can act as a templating mechanism to promote and direct mineralisation of the extracellular matrix (ECM) of bone as well as stimulating new bone formation.

Although it has been shown that PVPA-*co*-AA can help to promote bone formation and mineralisation,<sup>134</sup> the exact mechanism is as yet unclear. It is hypothesised that the copolymer composition will significantly affect the polymer's ability to bind to calcium ions owing to the varying concentration of phosphonate groups.

### 3.1.3 Composition of extracellular fluid

Extracellular calcium is the principal substrate for the mineralisation of bone; however, the extracellular fluid contains a multitude of ions, which play many crucial roles in the normal physiology of bone. Kokubo *et al.*<sup>178</sup> were the first to develop a simulated body fluid, which is prepared in the laboratory and contains ion concentrations similar to those of human blood plasma. Table 3.1 shows the ion concentration of SBF, prepared by the Kokubo method, and its comparison with human blood plasma.

**Table 3.1.** Ionic concentrations of simulated body fluid (SBF) and human blood plasma, adapted from Chavan *et al.*<sup>179</sup>

Electrolyte	Ionic concentration (mM)	
	Simulated body fluid	Human blood plasma
Na <sup>+</sup>	142.0	142.0
K <sup>+</sup>	5.00	5.00
Mg <sup>2+</sup>	1.50	1.50
Ca <sup>2+</sup>	2.50	2.50
Cl <sup>-</sup>	148.8	103.0
HCO <sub>3</sub> <sup>-</sup>	4.20	27.0
PO <sub>4</sub> <sup>2-</sup>	1.00	1.00

Therefore, it is important to consider the presence of other ions which may compete with and cause conformational changes within PVPA-*co*-AA, and thus have a substantial effect on its ability to bind to calcium ions *in vivo*.

### 3.1.4 Aims and Objectives

It was the aim of this work to investigate the calcium binding affinity of poly(vinylphosphonic acid-*co*-acrylic acid) (PVPA-*co*-AA) copolymers, and thus to evaluate their potential to aid in mineralisation of the bone extracellular matrix.

Firstly, pH titration curves were determined for PVPA-*co*-AA copolymers and their respective homopolymers. The effect of copolymer composition on the degree of ionisation was investigated. Furthermore, the changes in the pH titration curve of PVPA-*co*-AA with the addition of low molecular weight salt were also determined.

The calcium chelation capacity of PVPA-*co*-AA copolymers was explored in relation to copolymer composition, solution pH, polymer concentration and the ionic strength of the medium.

The rheological properties of the copolymers were investigated to understand the changes in polymer structure upon calcium binding. This was probed by observing the changes in the viscosity of the medium with regards to the concentration of added calcium chloride.

Finally, the change in the zeta-potential with regards to added CaCl<sub>2</sub> concentration was determined. This gives an indication as to the stability of the polymer in solution after binding to calcium.

## 3.2 Experimental

### 3.2.1 Materials

A range of PVPA-*co*-AA copolymers was prepared as outlined in Chapter 2 and their characterisation data are summarised in Tables 2.7 and 2.8. Sodium hydroxide (NaOH), sodium chloride (NaCl) and calcium chloride (CaCl<sub>2</sub>) were all purchased from ThermoFisher Scientific, U.K.

### 3.2.2 Potentiometric titrations

Potentiometric titrations were carried out using a HANNA pH meter (HI2211) and electrode (HI3311) at 20.0 °C. Solutions of PVPA-*co*-AA (1.0 mg mL<sup>-1</sup>) were prepared, with a range of copolymer compositions, in deionised water. The solutions were titrated with 0.1 M NaOH.

To test the effect of added salt on the titration curve of the PVPA-*co*-AA copolymers, 0.1 M NaCl was added to a solution of PVPA-30 in deionised water and the polymer solution was then titrated with 0.1 M NaOH.

### 3.2.3 Assessment of calcium binding affinity

#### 3.2.3.1 Effect of pH and copolymer composition

Solutions of PVPA-*co*-AA (5.0 mg mL<sup>-1</sup>) were prepared, with various copolymer compositions, in deionised water. The solutions were adjusted to the required pH (5.0, 7.3 or 9.0) using 0.1 M NaOH. CaCl<sub>2</sub> was added to the polymer solutions at a concentration of 0.1 M and they were stirred for 30 min. A calcium-selective electrode (ThermoFisher Scientific, U.K.) was immersed into the polymer solution to measure the free calcium concentration. A calibration curve was produced prior to the measurement using a range of CaCl<sub>2</sub> standard solutions (0.0001, 0.001, 0.01, 0.1 and 1 M). The oxidation-reduction potential (ORP) was plotted against the logarithm of Ca<sup>2+</sup> concentration (Figure 3.1).

The free calcium concentration was then calculated using the calibration curve and equation 3.1:

$$[\text{Ca}^{2+}]_{\text{free}} = 10^{\frac{\text{ORP}-412.1}{31.42}} \quad (3.1)$$

The calcium chelation was calculated by subtracting the free  $\text{Ca}^{2+}$  concentration measured from the total concentration of  $\text{Ca}^{2+}$  added.

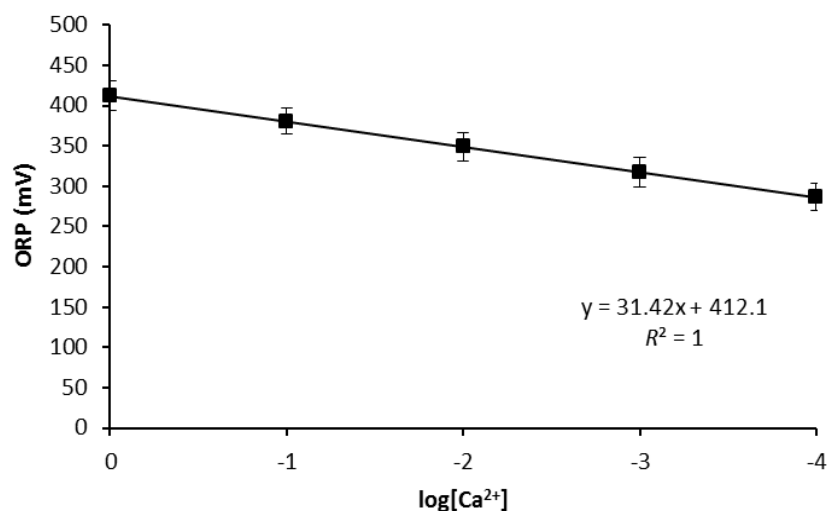


**Figure 3.1.** Calibration curve for the determination of calcium chelation by PVPA-*co*-AA copolymers, over a range of copolymer compositions and pH values. Data reported as mean  $\pm$  SD,  $n = 3$ .

### 3.2.3.2 Effect of polymer concentration

Solutions of PVPA-30 were prepared in deionised water at concentrations of 1.0, 2.5, 5.0, 7.5 and 10.0  $\text{mg mL}^{-1}$ . The solutions were adjusted to pH 7.3 using 0.1 M NaOH and  $\text{CaCl}_2$  was added at a concentration of 0.1 M. The solutions were stirred for 30 min and the calcium chelation was measured as described above. The calibration curve is presented in Figure A3.1 of the appendix.

### 3.2.3.3 Effect of ionic strength

Solutions of PVPA-0, PVPA-30 and PVPA-100 were prepared in deionised water, at a concentration of 5.0  $\text{mg mL}^{-1}$ . The pH of the solutions was adjusted to 7.3 using 0.1 M NaOH and various concentrations of NaCl were added (0.01, 0.05, 0.1, 0.5 or 1.0 M).  $\text{CaCl}_2$  was then added at a concentration of 0.1 M and the solutions were stirred for 30 min. The calcium chelation was measured as described above and the calibration curve is presented in Figure A3.2 of the appendix.

### 3.2.4 Rheology

Solutions of PVPA-30 were prepared in deionised water ( $10.0 \text{ mg mL}^{-1}$ ) and the pH was adjusted to 7.3 using 0.1 M NaOH. Rheological measurements were performed using an ARES LN2 rheometer (TA Instruments, Hertfordshire, U.K.) with parallel-plate geometry of 25 mm diameter. The tests were performed at a constant temperature of  $20.0 \text{ }^\circ\text{C}$  and a nominal gap of 0.5 mm. The strain sweep was performed at a frequency of 1.0 Hz while increasing the strain level from 10.0 to 500%. The linear viscoelastic region (LVR) from 100 to 500% was determined as a safe region without structural breakage from oscillatory strain (Figure 3.2).

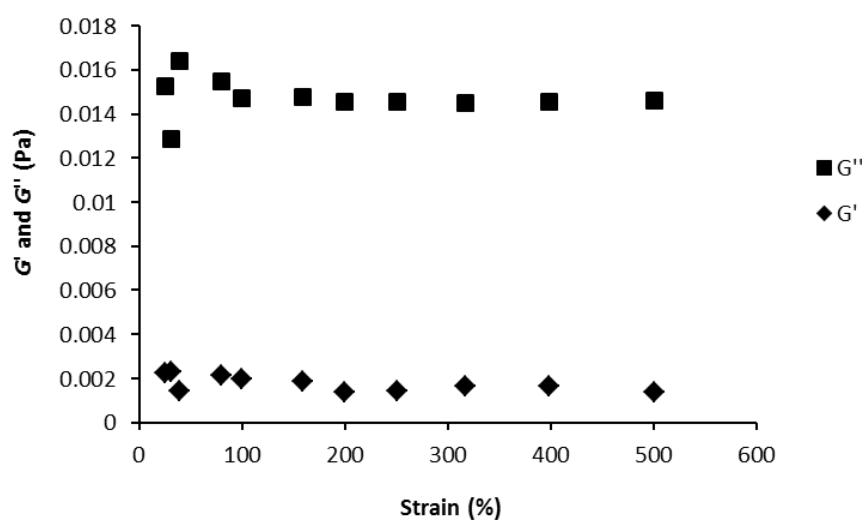


**Figure 3.2.** Storage ( $G'$ ) and loss ( $G''$ ) modulus of PVPA-30 in deionised water, at  $20.0 \text{ }^\circ\text{C}$  and pH 7.3, across a strain range of 10.0 to 500%.

#### 3.2.4.1 Effect of added NaCl

PVPA-30 was dissolved in deionised water ( $10.0 \text{ mg mL}^{-1}$ ) and the pH was adjusted to 7.3 using 0.1 M NaOH. NaCl was added to the polymer solutions at concentrations of 0.01, 0.05, 0.1, 0.5 or 1.0 M. The complex viscosity ( $\eta^*$ ) was measured from a single-point viscosity test at a frequency of 1.0 Hz and a strain of 250%, corresponding to a point in the middle of the LVR profile.

### 3.2.4.2. Effect of added CaCl<sub>2</sub>

PVPA-30 was dissolved in deionised water (10.0 mg mL<sup>-1</sup>) and the pH was adjusted to 7.3 using 0.1 M NaOH. CaCl<sub>2</sub> was then added to the polymer solutions at concentrations of 0.01, 0.05, 0.1, 0.5 or 1.0 M. A frequency sweep was performed at a constant strain of 250%. The oscillatory frequency was increased from 1.0 to 20 Hz and the plots of storage ( $G'$ ) and loss ( $G''$ ) modulus against frequency were obtained using the manufacturer's supplied software (TA Data Analysis, TA Instruments, U.K.). The complex viscosity ( $\eta^*$ ) was also plotted over the same frequency range.

### 3.2.5 Zeta-potential measurements

Solutions of PVPA-30 were prepared in deionised water (10.0 mg mL<sup>-1</sup>) and the pH was adjusted to 7.3 using 0.1 M NaOH. CaCl<sub>2</sub> was then added to the polymer solutions at concentrations of 0.01, 0.05, 0.1, 0.5 or 1.0 M. The solutions were filtered through mixed-ester membrane filters (Millex-GS, Merck Millipore, Hertfordshire, U.K.) with a pore size of 0.22  $\mu\text{m}$ . Each sample was filtered into a disposable capillary cell (DTS1070, Malvern Instruments, U.K.) The zeta-potential measurements were performed on a Malvern Zetasizer Nano-ZS instrument with a 633 nm laser. The capillary cell was placed into the Zetasizer and equilibrated at 20.0 °C for 2 min prior to the measurement. Tests were performed in triplicate and data are reported as mean  $\pm$  standard deviation.

For the zeta-potential measurement, the instrument uses a combination of laser Doppler velocimetry and phase analysis light scattering (PALS) in a technique called M3-PALS to measure the net electrophoretic mobility ( $U_E$ ) of the particles, which is then converted to the zeta-potential ( $\zeta$ ) using Henry's approximation (equation 3.2):

$$U_E = \frac{2\varepsilon\zeta f(\kappa r)}{3\eta} \quad (3.2)$$

where  $U_E$  is the electrophoretic mobility,  $\varepsilon$  is the dielectric constant,  $\zeta$  is the zeta-potential,  $\eta$  is the viscosity of the medium and  $f(\kappa r)$  is Henry's function, where  $\kappa$  is the Debye length and  $r$  is the radius of the particle. Therefore,  $\kappa r$  is the ratio of particle radius to Debye double layer thickness.

## 3.3 Results and Discussion

### 3.3.1 Potentiometric titrations

Poly(vinylphosphonic acid-*co*-acrylic acid) (PVPA-*co*-AA) copolymers were synthesised as detailed in Chapter 2, with various VPA feed contents, and their characterisation data are presented in Tables 2.7 and 2.8. The effect of copolymer composition on the solution properties of PVPA-*co*-AA has been investigated. Potentiometric titrations were carried out on the copolymers using 0.1 M NaOH. The nominal degree of neutralisation ( $\alpha$ ) was calculated by taking into account the analytical composition of the copolymer, revealed by elemental analysis. First, the molar mass of a hypothetical monomer ( $M_m$ ) was calculated using equation 3.3:

$$M_m = (M_{VPA} \times x_{VPA}) + (M_{AA} + x_{AA}) \quad (3.3)$$

where  $M_{VPA}$  and  $M_{AA}$  are the molar masses of VPA and AA, respectively, and  $x_{VPA}$  and  $x_{AA}$  are the mole fractions of VPA and AA in the copolymer, determined using elemental analysis data (see appendix section A2.3) and equations 2.3 and 2.4. The degree of neutralisation ( $\alpha$ ) is defined as the equivalents of base added per acid group, shown in equation 3.4:

$$\alpha = \frac{n_{OH^-}}{n_{H^+}} \quad (3.4)$$

where  $n_{OH^-}$  is the number of moles of base added and  $n_{H^+}$  is the number of moles of acid groups in the copolymer, which was calculated by dividing the mass of polymer by its hypothetical molar mass ( $M_m$ ).

The  $pK_a$  values for the dissociation of polymer hydroxyl groups were then calculated using equation 3.5, known as the Henderson-Hasselbach equation.

$$pK_a = pH + \log_{10} \left( \frac{\alpha}{1 - \alpha} \right) \quad (3.5)$$

The change in pH as a function of  $\alpha$  is presented in Figure 3.3 for PVPA-*co*-AA copolymers with various VPA contents (0, 20, 40, 60, 80 and 100 mol %) as well as for VPA monomer. The titration curve of the VPA monomer shows two dissociation steps with well-defined end points. These steps represent the consecutive dissociation of the two hydroxyl groups of VPA, with a  $pK_{a1}$  of 3.35 and a  $pK_{a2}$  of 8.27. The degree of

neutralisation ( $\alpha$ ) is defined as 1.0 for the first ionisation step and 2.0 for the second step to be completed.

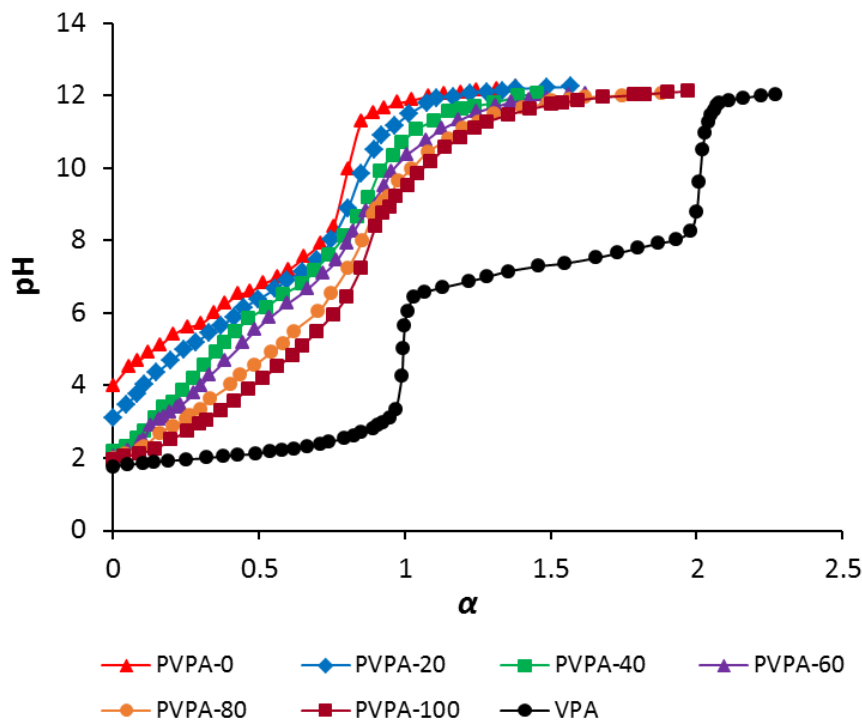


**Figure 3.3.** pH titration curves of VPA monomer, PAA (PVPA-0) and PVPA (PVPA-100) homopolymers, and PVPA-*co*-AA copolymers with VPA contents of 20, 40, 60 and 80 mol %. Polymer solutions ( $1.0 \text{ mg mL}^{-1}$ ) were prepared in deionised water at  $20.0 \text{ }^\circ\text{C}$ .  $\alpha$  is the nominal degree of neutralisation.

On the other hand, PVPA homopolymer shows an almost linear increase in pH with  $\alpha$ , up to a degree of neutralisation of 0.7. This is followed by a step increase in pH with increasing  $\alpha$  until the limiting value is reached, which represents the dissociation of one of the hydroxyl groups of phosphonic acid. These results are in agreement with previous literature on the topic, which have demonstrated that while the VPA monomer shows the two dissociation steps expected; PVPA behaves as a monoprotic acid.<sup>153, 180</sup> It has been suggested that a fully ionised PVPA polymer chain would have an unbearably high charge density, meaning that the remaining acid groups will hold on to the protons more tightly, which will prevent the second ionisation step from occurring.<sup>164</sup> Therefore,

PVPA should behave similarly to PAA in aqueous solution, as suggested by Strandberg *et al.*<sup>164</sup>

Despite their similarities, PVPA has a higher degree of neutralisation than PAA at certain pH values. The titration curve of PAA (PVPA-0) shows one neutralisation step, with a well-defined end point, at a  $pK_a$  of 8.37. This is due to the fact that PAA is a weak polyelectrolyte and so is only partially dissociated at intermediate pH values. Conversely, PVPA has intermediate strength and so has a higher degree of ionisation at certain pH values, and thus a greater charge density.

As opposed to the homopolymers, the titration curves of PVPA-*co*-AA copolymers show two neutralisation steps. This may be attributed to the different contributions of VPA and AA monomers with  $pK_a$  values of approximately 2.5 and 7.7, respectively, depending on the copolymer composition. However, these steps are not very distinct and there is no well-defined end point, indicating that the copolymers possess more protons than can be neutralised.

As the VPA content in the copolymer is increased, the degree of neutralisation of the polymers also increases at a given pH value. This occurs as a result of the increased acidity of PVPA when compared with PAA. Therefore, copolymers with higher VPA contents will have higher degrees of ionisation and higher charge densities, which may have profound effects on the properties of the copolymers in aqueous solution.

The effect of added NaCl on the titration curve of PVPA-*co*-AA, with a VPA content of 30 mol % (PVPA-30), is shown in Figure 3.4. It can be observed that the degree of neutralisation has increased with the addition of NaCl, indicating a substantial buffer effect of the salt. However, it can be seen that the addition of salt has no effect on the shape of the titration curve and it is not possible to discern two clear dissociation steps in the copolymer. This is in line with previous literature, such as that of Bingöl *et al.*,<sup>153</sup> who have also shown that even in the presence of a neutral salt, it is not possible to dissociate the second proton from PVPA homopolymer due to electrostatic effects.

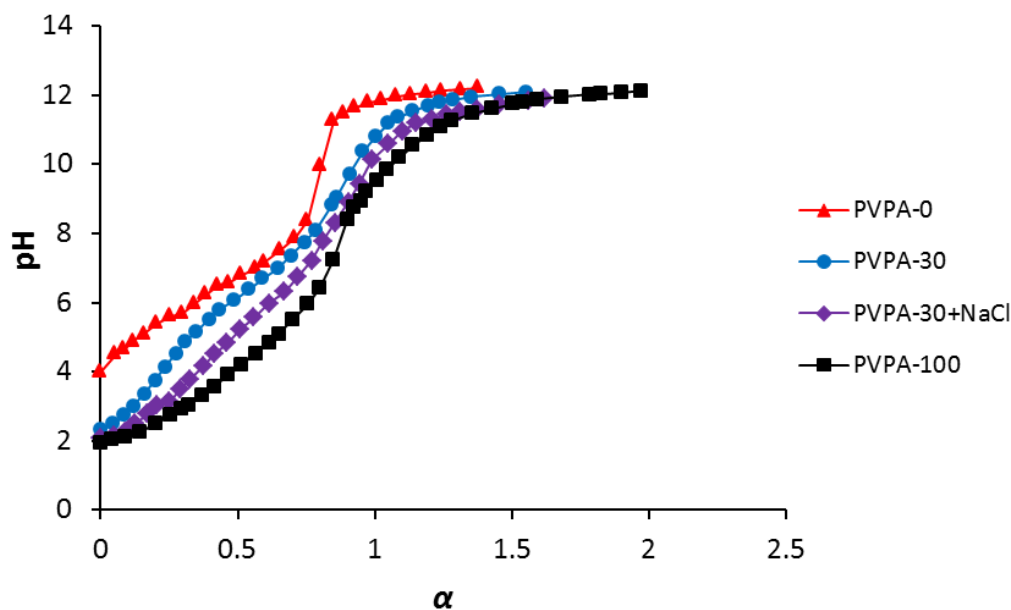


**Figure 3.4.** pH titration curves of PVPA-0, PVPA-30, PVPA-30 with added NaCl (0.1 M) and PVPA-100. Polymer solutions ( $1.0 \text{ mg mL}^{-1}$ ) were prepared in deionised water at  $20.0 \text{ }^\circ\text{C}$ .  $\alpha$  is the nominal degree of neutralisation.

### 3.3.2 Assessment of calcium binding affinity

#### 3.3.2.1 Effect of pH and copolymer composition

The degree of dissociation of a polyelectrolyte is important in terms of its ability to chelate metal ions from the surrounding environment. As discussed previously, PVPA behaves as a monoprotic acid in aqueous solution and is similar to PAA. It therefore requires two acid groups to chelate one  $\text{Ca}^{2+}$  ion.

Figure 3.5 shows the calcium chelation capacity of PVPA-*co*-AA, at pH 5.0, with copolymer compositions ranging from 0 to 100 mol % of VPA. It can be observed that there is an increase in calcium chelation with increasing VPA content in the copolymer. These results can be related to the polymer titration results, whereby an increase in VPA content leads to a higher degree of neutralisation of the polymer. Therefore, the increased fraction of charged groups along the polymer backbone leads to an increase in the calcium chelation capacity of the polymer.

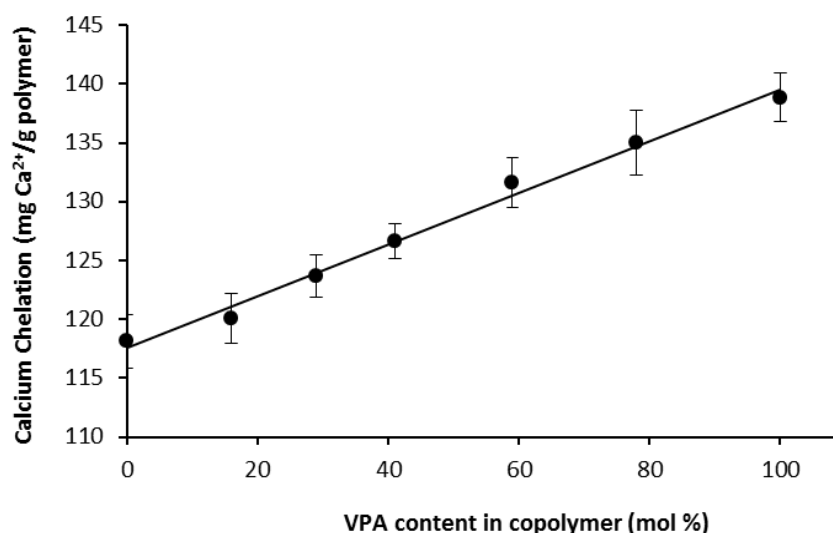


**Figure 3.5.** Calcium chelation capacity of PVPA-*co*-AA copolymers, at pH 5.0, with increasing VPA content in the copolymer. Polymer solutions (5.0 mg mL<sup>-1</sup>) were prepared in deionised water at 20.0 °C.

Figure 3.6 shows the calcium binding affinity of PVPA-*co*-AA copolymers, at pH 7.3 and 9.0, with VPA contents ranging from 0 to 100 mol %. As expected, the calcium chelation capacity is higher when the pH of the medium is increased. This occurs due to the increased deprotonation of the acid groups of the polymer backbone as the pH is increased. This also results in greater intramolecular repulsions within the polymer, which causes an expansion of the polymer chain, leading to more available binding sites for Ca<sup>2+</sup> ions.

With increasing VPA content in the copolymer, there is an increase in calcium chelation, reaching a maximum at *ca.* 30 mol %, after which there is a steady decrease up to PVPA-100. This is in stark contrast to the results presented in Figure 3.5, at pH 5.0, where the calcium chelation increases proportional to VPA content. It is worth noting that copolymers with high VPA contents (> 60 mol %) have much lower molar masses, which could affect the conformation of the polymer in aqueous solution at high pH values. Furthermore, the distribution of phosphonic acid groups along the polymer chain can also affect polymer conformation at physiological pH values and above and this may play a significant role in the polymer's ability to bind to calcium ions.

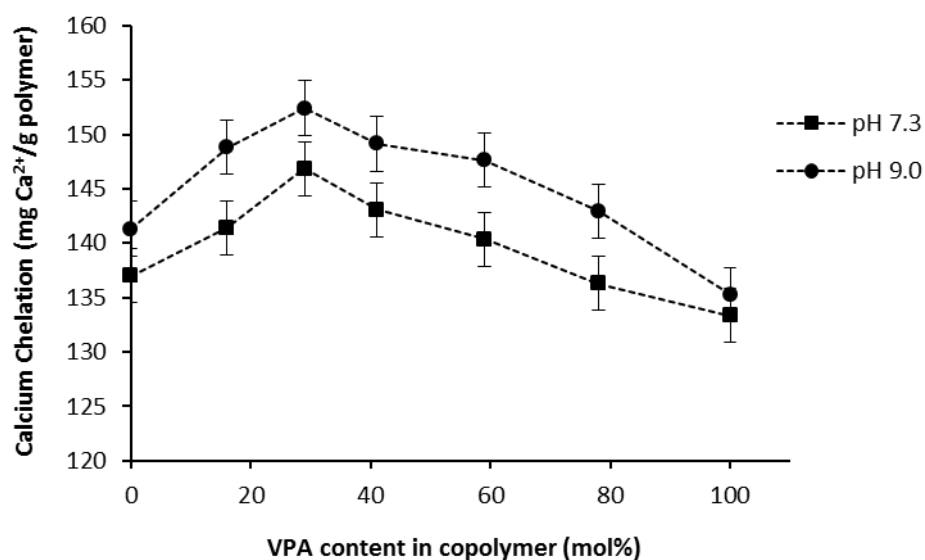


**Figure 3.6.** Calcium chelation capacity of PVPA-*co*-AA copolymers, at pH 7.3 and 9.0, with increasing VPA content in the copolymer. Polymer solutions ( $5.0 \text{ mg mL}^{-1}$ ) were prepared in deionised water at  $20.0 \text{ }^\circ\text{C}$ .

Natural bone contains many non-collagenous proteins (NCPs), which are phosphorylated to varying degrees. It has been suggested that variations in phosphorylation can significantly affect the mineralisation process, owing to the protein's ability to bind to calcium ions from the bone mineral surface.<sup>12, 86, 176, 177</sup> It is hypothesised that PVPA-30 offers the best potential mimic of NCPs in terms of the fraction of phosphonate groups along the polymer chain, which allows optimal calcium binding in solution.

In a recent study, Gemeinhart *et al.*,<sup>124</sup> have produced poly(vinylphosphonic acid-*co*-acrylamide) (PVPA-*co*-Am) as a graft-copolymer surface modification. They have investigated the effect of copolymer composition on osteoblast adhesion and proliferation and have found that a VPA content of 30 mol % resulted in the greatest increase. This composition was also found to significantly enhance mineralisation of the matrix produced by osteoblast cells. It was proposed that this was due to polymer-based calcification, i.e. the accumulation of calcium salts as a result of polymer-calcium chelation. These results are consistent with the results from the present work, in which acrylic acid rather than acrylamide was used as the comonomer. Here, it was found that PVPA-*co*-AA, with a VPA content of *ca.* 30 mol %, resulted in the highest levels of calcium chelation and so is expected to lead to increased matrix mineralisation.

In recent work by colleagues in the School of Medical Sciences, Wang *et al.*<sup>181</sup> have investigated the effect of copolymer composition on the ability of PVPA-*co*-AA copolymers to affect cell matrix mineralisation *in vitro*. They have demonstrated that PVPA-*co*-AA, with a VPA feed content of 30 mol %, led to the greatest mineralisation of SaOS-2 osteoblast-like cells *in vitro*. They have attributed this to the greater calcium chelation capacity of the copolymer. It has been shown that the effect of copolymer composition on the degree of mineralisation of SaOS-2 cells is directly related to the calcium chelation capacity of the different copolymers, and follows the exact trend shown in Figure 3.6. As a result, PVPA-30 is expected to be the most promising candidate for use in bone tissue scaffolds owing to its superior calcium binding affinity, which is hypothesised to mimic non-collagenous matrix proteins *in vivo*.

### 3.3.2.2 Effect of polymer concentration

The effect of polymer concentration on the calcium binding affinity of PVPA-30 was investigated and the results are shown in Figure 3.7. It can be seen that the calcium chelation capacity increases linearly with an increase in polymer concentration. This result is expected since a higher polymer concentration results in a greater amount of carboxylic and phosphonic acid groups, and thus more available binding sites for calcium ions.

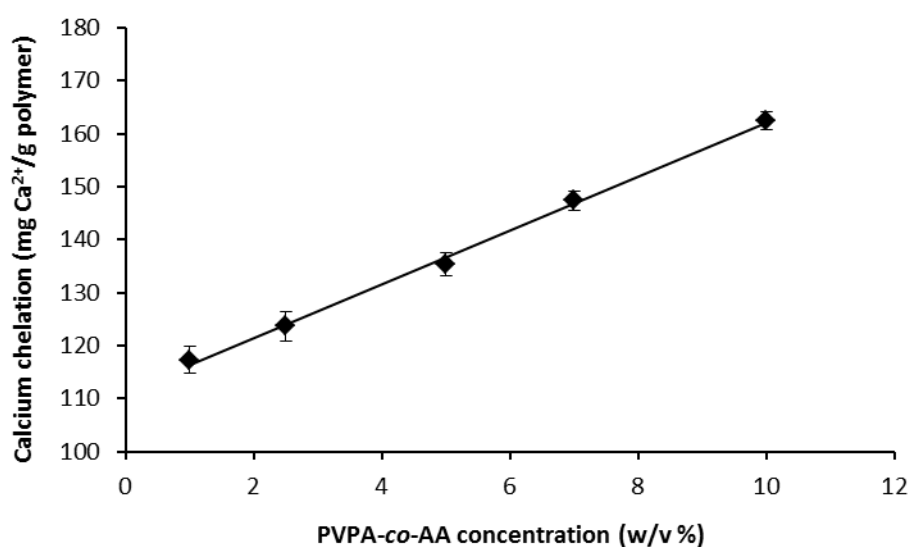


**Figure 3.7.** Calcium chelation capacity of PVPA-30 with increasing polymer concentration. Polymer solutions ( $5.0 \text{ mg mL}^{-1}$ ) were prepared in deionised water at pH 7.3 and  $20.0 \text{ }^\circ\text{C}$ .

Polymer concentration is important in terms of the formation of polymer-calcium complexes and their stability in solution. It has been suggested that PAA and PVPA can bind to calcium ions *in vivo* forming an amorphous, liquid-phase mineral precursor.<sup>120, 182</sup> These nanoprecursors can then be drawn into the spaces between the collagen fibrils of the ECM where they provide a template to control apatite formation. If the polymer concentration is low compared to the calcium concentration, inter-polymer-calcium complexes can form, which precipitate out of solution. This is hypothesised to be an undesirable process, since the precipitates can only deposit on the surface of the collagen matrix, which does not offer a suitable mimic of the native ECM.<sup>182</sup> However, at higher polymer concentrations, no such precipitation occurs and a stable, liquid-phase polymer-calcium complex is formed. Therefore, it is believed that higher polymer concentrations will be more beneficial for matrix mineralisation owing to their stability in solution, which allows them to become embedded within collagen fibrils, where they can act as a template to promote and control hydroxyapatite formation.

### 3.3.2.3 Effect of ionic strength

Natural cellular environments contain many ions, both mono- and multivalent, which can compete with the  $\text{Ca}^{2+}$  ions and cause a change in the polymer conformation. This must be considered when determining the calcium chelation capacity of the copolymer *in vivo*.

The effect of added salt (NaCl) on the calcium binding affinity of PVPA-0, PVPA-30 and PVPA-100 is shown in Figure 3.8. It was found that as the ionic strength of the medium is increased, the calcium chelation capacity decreases. As discussed earlier, polyelectrolytes adopt an expanded conformation in solution due to intramolecular electrostatic repulsions. Upon the addition of a monovalent salt, such as NaCl, an electrostatic attraction occurs between the negatively-charged acidic groups of the polymer and the  $\text{Na}^+$  ions. This causes a screening of the electrostatic repulsions and a collapse of the polymer chain into a coiled conformation. Therefore, the acid groups are less available for binding and so the calcium chelation capacity decreases.

It is noted that the change in ionic strength of the medium has a more significant effect on the calcium chelation capacity of PVPA-0 than for PVPA-30 or PVPA-100. PAA (PVPA-0) is a weak polyelectrolyte and so its conformation in solution is more affected

by changes in the medium i.e. pH and ionic strength, than for stronger polyelectrolytes, such as PVPA.

The effect of added divalent salt ( $\text{MgCl}_2$ ) on the calcium chelation of PVPA-30 was also investigated and the results are presented in Figure A3.3 of the appendix. It was found that the calcium chelation is reduced dramatically as the concentration of magnesium ions is increased. A  $\text{MgCl}_2$  concentration of 1.0 M reduced the calcium chelation capacity to almost zero. The reduction in calcium binding is significantly larger than in the presence of NaCl. This is expected since  $\text{Mg}^{2+}$  is a divalent ion, which can compete more readily with  $\text{Ca}^{2+}$  ions for the same binding sites. However, the concentration of  $\text{Mg}^{2+}$  in the extracellular fluid is relatively low compared to the concentration of  $\text{Na}^+$  ions and so it is thought that calcium binding by PVPA-co-AA will not be affected to a large extent.

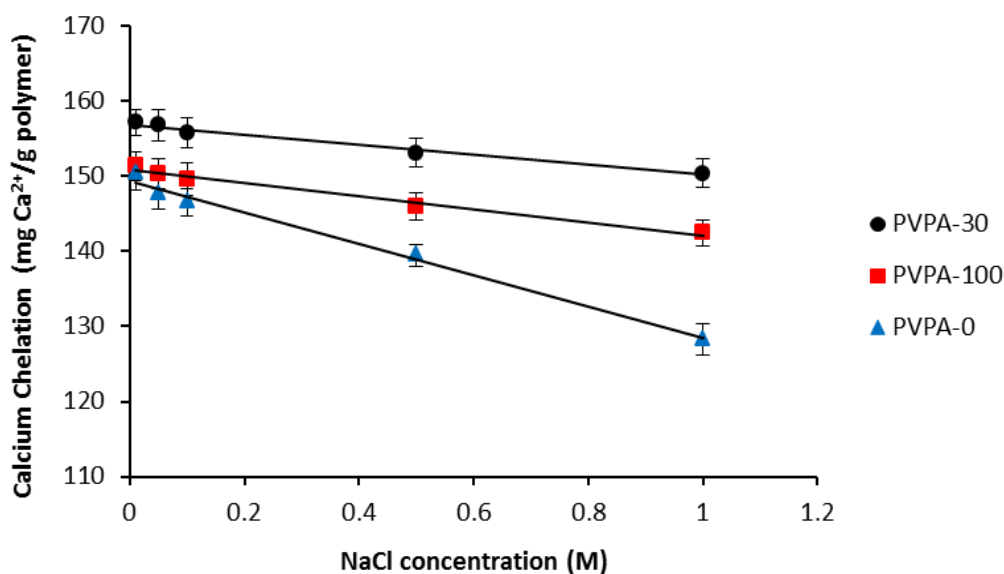


**Figure 3.8.** Calcium chelation capacity of PVPA-0, PVPA-30 and PVPA-100 with increasing NaCl concentration. Polymer solutions ( $5.0 \text{ mg mL}^{-1}$ ) were prepared in deionised water at pH 7.3 and  $20.0 \text{ }^\circ\text{C}$ .

### 3.3.3 Rheological properties of PVPA-co-AA

#### 3.3.3.1 Effect of added NaCl

The change in the conformation of the polymers, upon the addition of NaCl, was further investigated by rheology. Figure 3.9 shows the change in complex viscosity ( $\eta^*$ ) of PVPA-0, PVPA-30 and PVPA-100 as a function of NaCl concentration. It can be observed that in the absence of added salt, the complex viscosity is around 2.4–2.6 cP for all of the polymers. The addition of NaCl leads to an initial dramatic reduction in  $\eta^*$ , followed by a less significant decrease in viscosity with increasing NaCl concentration. These results can be explained in terms of the change in polymer conformation, discussed previously. In the absence of NaCl, the negatively-charged groups of the polymer chains repel each other, leading to an extended polymer conformation. However, when NaCl is added into the solution, the  $\text{Na}^+$  ions screen the electrostatic repulsions, causing the polymer chain to collapse into a coiled conformation, which significantly reduces the viscosity of the solution. The addition of higher concentrations of NaCl will cause a further decrease in the hydrodynamic size of the polymer, until eventually the size can decrease no further and the viscosity of the solution will remain the same.

It was observed that the viscosity of the polymer solution is higher for PVPA-30 than for PVPA-100. This is due to the higher molecular weight of PVPA-30, which results in greater chain entanglement, thus enhancing the viscosity of the solution. Furthermore, the viscosity of the PVPA-0 solution is lower than that of PVPA-30 and PVPA-100. This can be attributed to the greater expansion of the PVPA-30 and PVPA-100 polymer chains owing to their greater charge density. In addition, the reduction in viscosity, with increasing NaCl concentration is much greater for PVPA-0. This confirms that the conformation of PVPA-0 is most significantly affected by changes in the ionic strength of the medium.

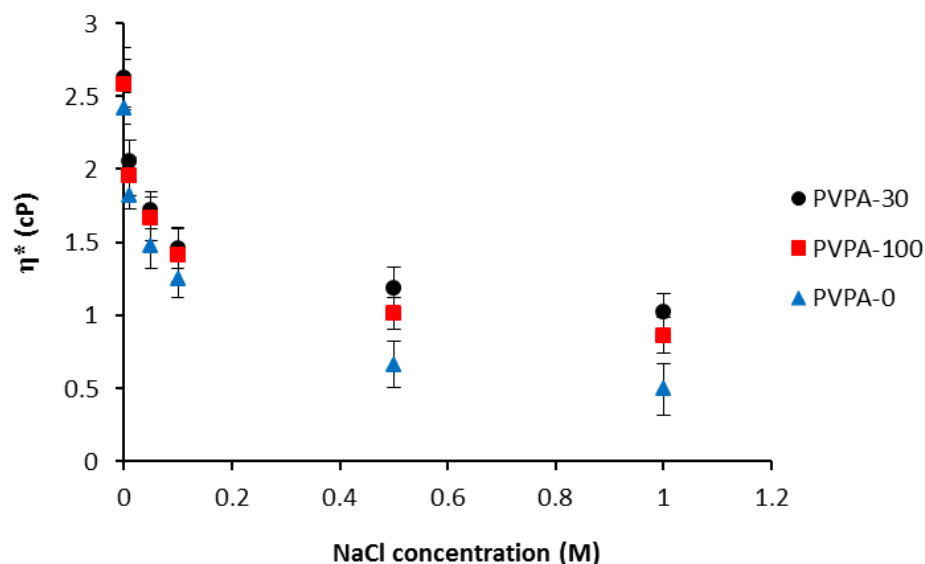


**Figure 3.9.** Effect of increasing NaCl concentration on the complex viscosity ( $\eta^*$ ) of PVPA-0, PVPA-30 and PVPA-100. Polymer solutions ( $10.0 \text{ mg mL}^{-1}$ ) were prepared in deionised water at pH 7.3 and  $20.0 \text{ }^\circ\text{C}$ .

### 3.3.3.2 Effect of added $\text{CaCl}_2$

The effect of added  $\text{CaCl}_2$  on the rheological properties of the copolymer in solution was then investigated. Figure 3.10 shows the change in storage ( $G'$ ) and loss modulus ( $G''$ ) for solutions of PVPA-30 with increasing frequency of oscillation. The  $\text{CaCl}_2$  concentration was increased from 0.01 to 1.0 M and the change in  $G'$  and  $G''$  was observed. For all calcium concentrations,  $G''$  is significantly larger than  $G'$ , indicating fluid-like behaviour, as expected. However, an increase in calcium concentration results in a significant decrease in  $G''$  and a small decrease in  $G'$ . This can be explained in terms of the conformational change in PVPA-*co*-AA upon the addition of  $\text{CaCl}_2$  into solution. As discussed earlier, the calcium ions can bind to the negatively-charged acid groups of the polymer chain. This leads to shrinkage of the polymer chain from an extended to a coiled structure. The large decrease in  $G''$  may be attributed to ionic crosslinks formed between PVPA-*co*-AA and  $\text{Ca}^{2+}$ , which leads to the formation of a compact intra- or intermolecular network structure, which reduces the fluidity of the solution.

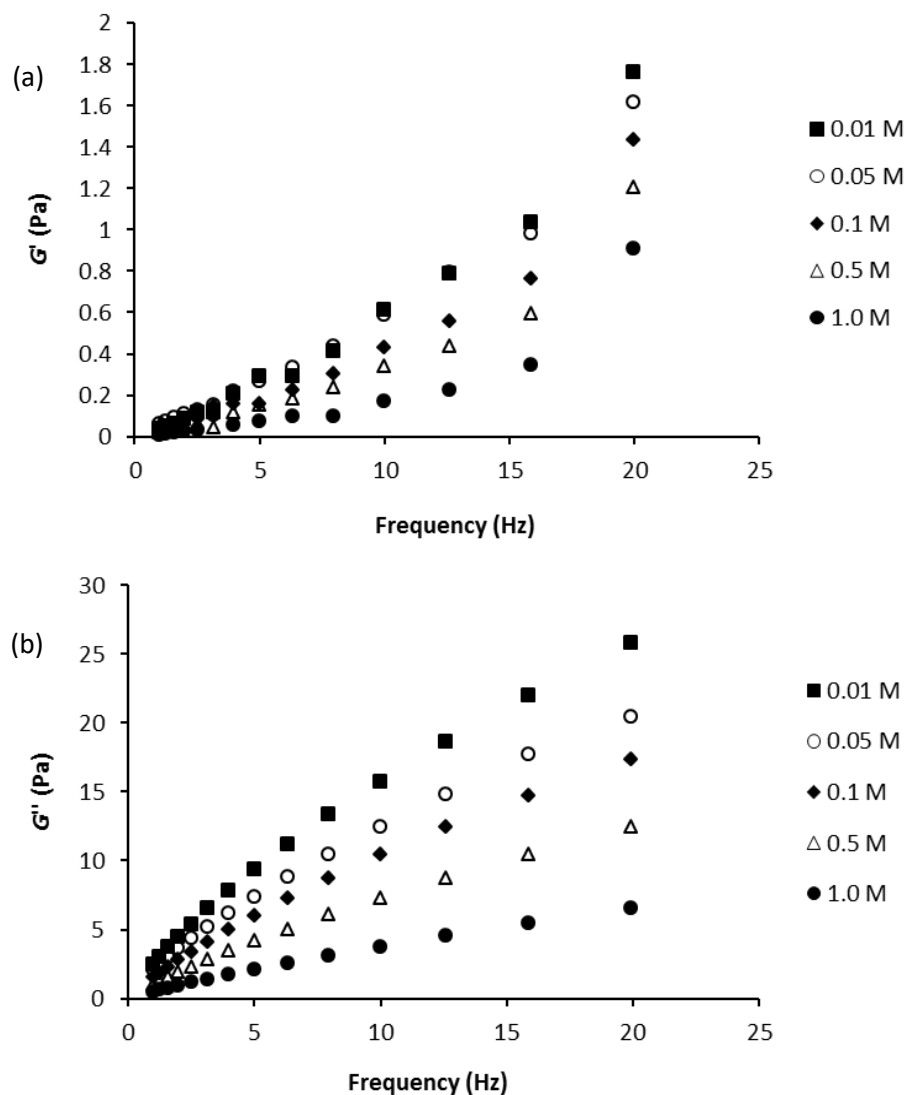


**Figure 3.10.** (a) Storage ( $G'$ ) and (b) loss ( $G''$ ) modulus of PVPA-30 across a frequency sweep of 1.0 to 20.0 Hz. Solutions of PVPA-30 ( $10.0 \text{ mg mL}^{-1}$ ) were prepared in deionised water at pH 7.3 and  $20.0 \text{ }^\circ\text{C}$  and  $\text{CaCl}_2$  was added at concentrations ranging from 0.01 to 1.0 M.

Figure 3.11 demonstrates the change in complex viscosity ( $\eta^*$ ) with increasing frequency of oscillation, for aqueous solutions of PVPA-30 ( $10 \text{ mg mL}^{-1}$ ) with different concentrations of added  $\text{CaCl}_2$ . It can be seen that there is a decrease in viscosity with increasing frequency, as typically observed for polyelectrolytes. This represents a breaking apart of the polymer chains and is known as shear thinning behaviour. A decrease in viscosity is also observed with increasing  $\text{CaCl}_2$  concentration. This offers further evidence of a conformational change of the polymer, forming a more compact network structure, which is induced by calcium binding.

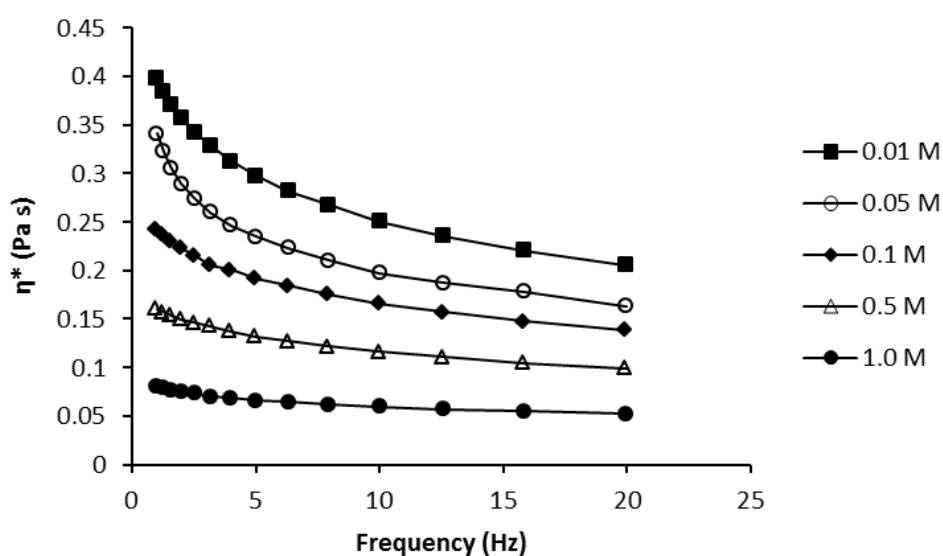


**Figure 3.11.** Complex viscosity ( $\eta^*$ ) of PVPA-30 across a frequency sweep of 1.0 to 20.0 Hz. Solutions of PVPA-30 ( $10.0 \text{ mg mL}^{-1}$ ) were prepared in deionised water at pH 7.3 and  $20.0 \text{ }^\circ\text{C}$  and  $\text{CaCl}_2$  was added at concentrations ranging from 0.01 to 1.0 M.

### 3.3.4 Zeta-potential measurements

To confirm the localisation of calcium ions within the vicinity of the polyelectrolyte chain, zeta-potential measurements were performed. Figure 3.12 shows the zeta-potential for aqueous solutions of PVPA-30 ( $10 \text{ mg mL}^{-1}$ ) as a function of calcium chloride concentration. It was found that the zeta-potential increases (becomes less negative) with increasing calcium concentration. This is due to the binding of calcium ions to the negatively-charged groups of PVPA-30, which reduces the effective charge

of the polymer. This also results in a decrease in the stability of the polymer in solution as a result of the screening of electrostatic repulsions within the polymer chains, which causes the polymer to collapse. Above concentrations of 0.1 M  $\text{CaCl}_2$ , a hydrophobic complex forms due to ionic crosslinking and the polymer precipitates out of solution. It is noted that as the calcium concentration was increased, the turbidity of the solution also increased until eventual precipitation occurred. This supports the previous results, which suggest that the polymer concentration, relative to the calcium concentration, is important in terms of the stability of the complex. It is preferable to have a high polymer concentration that can form a soluble complex with calcium ions. This can offer a better mimic of non-collagenous proteins, helping to promote and control the ordered deposition of mineral.

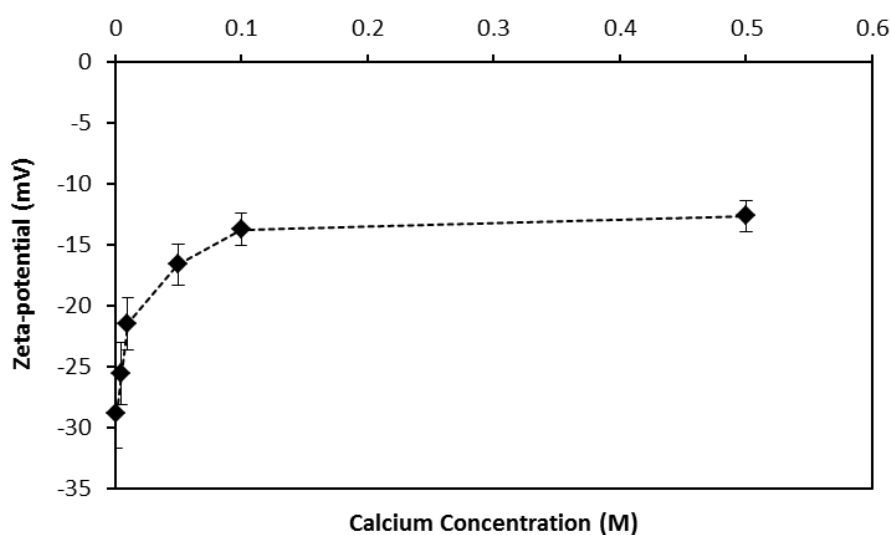


**Figure 3.12.** Dependence of zeta-potential on  $\text{CaCl}_2$  concentration for aqueous solutions of PVPA-30 ( $10.0 \text{ mg mL}^{-1}$ ) prepared in deionised water at pH 7.3 and  $20.0 \text{ }^\circ\text{C}$ .

### 3.4 Conclusions

The solution properties of poly(vinylphosphonic acid-*co*-acrylic acid) (PVPA-*co*-AA) have been investigated with regards to changes in copolymer composition, solution pH and the ionic strength of the medium.

Firstly, pH titration curves were determined for PVPA-*co*-AA copolymers and their respective homopolymers. It was found that although VPA monomer shows the two dissociation steps expected, PVPA behaves as a monoprotic acid in solution. In this way, the behaviour of PVPA is similar to that of PAA. As the VPA content in the copolymer was increased, the degree of neutralisation also increased. This was attributed to the greater acidity of VPA when compared with AA. Whereas AA is a weak polyelectrolyte, PVPA has been described as medium-strong. Therefore, PVPA will have a higher degree of dissociation of acidic groups, at any given pH, in aqueous solution. The addition of NaCl to a solution of PVPA-30, at a concentration of 0.1 M, led to an increase in the degree of neutralisation, as expected. However, even in the presence of added salt, it was still not possible to discern two clear dissociation steps, due to electrostatic effects.

The calcium chelation capacity of PVPA-*co*-AA copolymers was then investigated with regards to solution pH and copolymer composition. As expected, the calcium chelation increased with an increase in pH due to the enhanced ionisation of the polymers, which means there are more available negatively-charged groups to bind to calcium. At pH 5.0, the calcium chelation also increases with higher VPA contents in the copolymer, again due to a greater degree of neutralisation. However, at pH 7.3 and 9.0, calcium chelation capacity reaches a maximum at a VPA content of *ca.* 30 mol %. It is suggested that this copolymer composition contains the optimal distribution of phosphonate groups along the polymer chain, which offers the best mimic of NCPs and encourages greater calcium binding. Therefore, PVPA-*co*-AA, with a VPA content of 30 mol %, is expected to lead to the greatest cell matrix mineralisation *in vivo* and is thus the most suitable candidate for use in bone tissue scaffolds.

The calcium chelation capacity also increased with an increase in polymer concentration. This is due to the presence of more acidic groups, which are available for calcium binding. It is proposed that higher polymer concentrations will form stable,

amorphous, liquid-phase complexes that can embed within collagen fibrils and provide a template for matrix mineralisation.

An increase in the ionic strength of the medium, i.e. NaCl or MgCl<sub>2</sub> concentration, resulted in a decrease in calcium chelation capacity. This is due to the screening of electrostatic repulsions by the counter-ions, which causes the polymer to change from an extended to a collapsed conformation. Therefore, the acid groups are less available for calcium binding. Furthermore, the Mg<sup>2+</sup> ions can compete with Ca<sup>2+</sup> for the binding sites, reducing the calcium chelation capacity. Under physiological conditions, the ionic strength is relatively high and so this must be taken into account when considering the calcium binding affinity of PVPA-*co*-AA copolymers *in vivo*.

The effect of calcium binding on copolymer conformation was probed by measuring the rheological properties of PVPA-*co*-AA copolymers. It was found that by increasing the CaCl<sub>2</sub> concentration, the viscosity of the solution decreased. The loss modulus ( $G''$ ) decreased significantly and the storage modulus ( $G'$ ) also decreased to a lesser extent. These results are consistent with a conformational change from an extended to a collapsed structure. The Ca<sup>2+</sup> ions can form crosslinks within polymer chains, resulting in the formation of a compact network structure. This causes a large reduction in  $G''$ , consistent with a reduction in the fluid-like behaviour of the solution.

Finally, the zeta-potential of PVPA-*co*-AA copolymers was determined with respect to increasing calcium concentration. It was found that, as the CaCl<sub>2</sub> concentration increased, the zeta-potential increased, becoming less negative. This suggests a reduction in the stability of the polymer in solution. The binding of calcium to PVPA-30 causes the formation of a hydrophobic complex, which will precipitate out of solution at calcium concentrations above 0.1 M. This must be considered when considering the concentration PVPA-*co*-AA to be used in bone tissue scaffolds.

## Chapter 4: Incorporation of PVPA-*co*-AA into electrospun PCL scaffolds

### 4.1 Introduction

#### 4.1.1 Incorporation of bisphosphonates into tissue scaffolds

Bisphosphonates (BPs) have long been used in the treatment of bone metabolic diseases, such as osteoporosis and Paget's disease, due to their ability to inhibit osteoclastic activity. However, the systemic use of BPs has been associated with adverse gastrointestinal effects, local tissue damage and irritation at the injection site.<sup>34</sup> Therefore, much research has been carried out on the localised delivery of BP drugs to the target by incorporation into bioresorbable implants.

Bisphosphonates have been encapsulated into microspheres of chitosan<sup>183</sup> and poly(lactic-*co*-glycolic acid) (PLGA)<sup>184</sup> to allow for a more controlled and localised release of the drug. Most often an initial burst release occurs such has been observed for the release of a bisphosphonate drug from PLGA rods.<sup>185</sup> This type of release profile may be suitable for immediate osteoclast resorption. However, the burst release may also be indicative of the drug being attached only on the surface of the implant. Puppi *et al.*<sup>35</sup> have produced composite electrospun scaffolds of poly( $\epsilon$ -caprolactone) (PCL), hydroxyapatite (HA) and bisphosphonate (BP) drug and they found that the inclusion of the active agent influenced the fibre dimensions and scaffold porosity. Therefore, it is possible to assert a degree of control over the release kinetics of BP drugs from the electrospun fibres by varying fibre diameter or loading dosage.

#### 4.1.2 PCL/PVPA-*co*-AA composite scaffolds

In recent years, poly(vinylphosphonic acid-*co*-acrylic acid) (PVPA-*co*-AA) has been identified as a polymeric substitute for BP drugs. It is hypothesised that PVPA-*co*-AA can mimic the action of bisphosphonates by binding to calcium ions from the bone mineral surface. Moreover, PVPA-*co*-AA does not result in the well-documented side effects of bisphosphonates. Bassi *et al.*<sup>132-134</sup> have produced electrospun nanofibres of PCL and have functionalised them by dip-coating into a 15 w/v % solution of PVPA-

*co-AA*. The fibres were then heat treated at 55 °C for 24 h to immobilise the PVPA-*co-AA* onto the PCL fibres and prevent dissolution of the copolymer. The morphology of the fibres can be seen in Figure 4.1a.

The stability of the PVPA-*co-AA* coating was examined using energy-dispersive X-ray spectroscopy (EDX) analysis (Figure 4.1b).<sup>132</sup> The scaffolds were immersed in cell culture medium and the presence of phosphorus was monitored to give an indication as to the release of the copolymer. Scaffolds that had not undergone heat treatment were used as a control. They found that there was a sharp decrease in phosphorus content in the first two days, on both scaffold types. However, after day 2 there was a pronounced difference in phosphorus content between the two scaffold types; those that had undergone heat treatment had a significantly higher concentration. These results suggest that the heat treatment improves the stability of the PVPA-*co-AA* on the PCL scaffolds after an initial burst release. It is proposed that the initial release of phosphorus could be advantageous *in vivo* because it would lead to immediate osteoclast apoptosis, which would allow osteoblasts to secrete matrix. These results demonstrate that the incorporation of PVPA-*co-AA* into PCL scaffolds could behave as a drug delivery system, whereby the copolymer can mimic the action of bisphosphonates without the undesirable side effects.

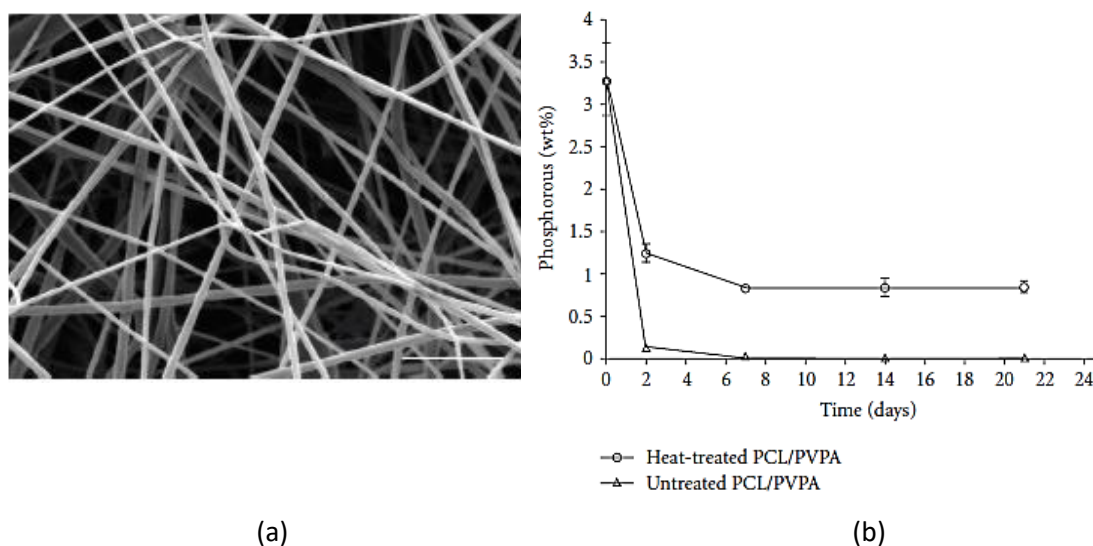


**Figure 4.1.** (a) SEM micrograph of PCL fibres treated with PVPA-*co-AA*, scale bar 5  $\mu\text{m}$ . (b) The phosphorus concentration on the surface of the polymeric scaffolds examined through energy-dispersive X-ray spectroscopy (EDX) over 21 days. Images taken from Bassi *et al.*<sup>132</sup>

### 4.1.3 Sterilisation of tissue scaffolds

The use of biodegradable polymeric scaffolds for bone tissue engineering offer many exciting possibilities. However, these scaffolds have the potential to become infected by a wide range of microorganisms such as viruses, bacteria and fungi, which can cause serious infections and diseases. Therefore, the scaffolds must be sterilised prior to implantation. When sterilising a biodegradable scaffold, it is vital to make sure that the structural and biochemical properties of the scaffold remain intact, thereby ensuring that the scaffolds will fulfil their intended purpose post-sterilisation.<sup>186</sup>

There are several sterilisation techniques that have regulatory approval for clinical use. These include gamma ( $\gamma$ ) and ultraviolet (UV) irradiation and chemical sterilisation using ethylene oxide or ethanol.<sup>187</sup> Gamma radiation sterilisation is simple, fast and effective and thus it is among the most commonly used techniques for scaffold sterilisation. However, it is known to result in changes in the scaffold's properties, i.e. reduced compressive mechanical properties and increased rates of degradation. Cottam *et al.*<sup>188</sup> have studied the effects of  $\gamma$ -irradiation on the properties of PCL scaffolds. It was found that the molecular weight of the polymer was significantly reduced and crosslinks had formed, which increased the mechanical yield stress of the material. However, this method of sterilisation had no effect on the ability of cells to grow on the scaffold.

Ethanol treatment is another widely used sterilisation procedure owing to its low cost and simplicity. Concentrations of ethanol ranging from 60 to 80% have the ability to destroy many forms of bacteria. However, there is some evidence to suggest that soaking poly(lactic-*co*-glycolic acid) (PLGA) scaffolds in 70% ethanol can significantly alter their mechanical properties and reduce surface porosity.<sup>189</sup> On the other hand, ethanol sterilisation treatment has been shown to have no effect on molecular weight or cell viability on PCL scaffolds and is therefore a viable technique.<sup>188</sup>

#### 4.1.4 Aims and Objectives

It was the aim of this work to investigate the incorporation of PVPA-*co*-AA into PCL tissue scaffolds. PVPA-*co*-AA, with a VPA content of 30 mol %, was used in this study since it has previously been shown to lead to the greatest calcium binding and is thus expected to enhance the bioactive properties of the scaffold.

PCL nanofibres were produced by electrospinning. PVPA-*co*-AA was then incorporated by dip-coating into a 15 w/v % solution of the copolymer or by co-spinning the PCL and PVPA-*co*-AA with the use of a surfactant (Span 80). The uptake efficiency of PVPA-*co*-AA into the PCL electrospun scaffolds was determined using UV/Vis spectroscopy and a comparison made between the different methods of scaffold production.

The scaffolds were sterilised using a 70% ethanol solution. This could have profound effects on the structure and properties of the fibres. Therefore, the calcium chelation capacity of the scaffolds was measured before and after sterilisation. Furthermore, the effect of PVPA-*co*-AA concentration on the calcium binding of the PCL scaffolds was investigated.

It is thought that PVPA-*co*-AA will be released from the PCL scaffolds after implantation. In this way, the PCL scaffolds may be used as a drug delivery system. Thus, UV/Vis spectroscopy was used to investigate the rate of release of PVPA-*co*-AA from PCL scaffolds. The difference between dip-coated samples and those that have been co-spun was determined. In order to understand the ability of the scaffolds to bind to calcium ions *in vivo*, the calcium chelation capacity was explored in osteogenic differentiation media. Therefore, the mechanism of calcium chelation by the scaffolds, i.e. pre- or post-release of PVPA-*co*-AA, was investigated.

## 4.2 Experimental

### 4.2.1 Materials

All chemicals were used as supplied unless otherwise stated. Poly( $\epsilon$ -caprolactone) (PCL) ( $M_n \approx 80\,000\text{ g mol}^{-1}$ ) and Span® 80 surfactant were purchased from Sigma-Aldrich, U.K. PVPA-*co*-AA, with a VPA content of 30 mol % (PVPA-30), was synthesised as described in Chapter 2 and its characterisation data are summarised in Tables 2.7 and 2.8. Osteogenic differentiation medium was prepared using Eagle's Minimum Essential Media ( $\alpha$ -MEM) (Sigma-Aldrich, U.K.), supplemented with 10% foetal calf serum (FCS), antibiotics (100 U mL<sup>-1</sup> penicillin, 100 mg mL<sup>-1</sup> streptomycin), 1% L-glutamine and 10  $\mu$ M ascorbic acid.

### 4.2.2 Fabrication of PCL/PVPA-*co*-AA scaffolds by electrospinning

PCL/PVPA-30 scaffolds were produced by Ian Wimpenny in the School of Materials, University of Manchester, U.K. Briefly, a 10 w/v % solution of PCL was prepared in DCM and the solution was electrospun using an applied voltage of 20 kV, a flow rate of 0.05 mL min<sup>-1</sup> and a needle collector distance of 15 cm. Fibres were collected on a grounded collector plate to give a randomly orientated morphology.

PCL electrospun fibres were then dip-coated in a solution of PVPA-30 (15 w/v %) in deionised water for 24 h, before being air-dried for 48 h. These scaffolds will be referred to as PVPA-D. Some of the scaffolds were then heat-treated at 55 °C for 24 h to immobilise the PVPA-30 onto the PCL fibres. These scaffolds will be referred to as PVPA-H. Solutions of PCL (10 w/v % in DCM) were also co-spun with PVPA-30 (10 w/v % in ethanol) using Span 80 as a surfactant. The relative mass ratios of PCL:Span 80:PVPA-30 in the electrospun fibres are presented in Table 4.1.

**Table 4.1.** Relative mass ratios of PCL:Span 80:PVPA-30 of the electrospun nanofibres.

Sample Code	Relative Mass Ratio		
	PCL	Span 80	PVPA- <i>co</i> -AA
PCL	100	0.0	0.0
PCL-SP	97.5	2.5	0.0
PVPA-1	96.5	2.5	1.0
PVPA-5	92.5	2.5	5.0
PVPA-7	90.5	2.5	7.0
PVPA-10	87.5	2.5	10.0

### 4.2.3 Uptake efficiency of PVPA-*co*-AA into PCL scaffolds

The amount of PVPA-30 incorporated into the scaffolds was determined using UV/Vis spectroscopy (Varian Cary 5000 UV/Vis spectrophotometer, Agilent Technologies, UK). Prior to the measurement, a calibration was performed using solutions of PVPA-30 (10-100  $\mu\text{g mL}^{-1}$ ) prepared in 1.5 mM  $\text{HNO}_3$  in deionised water, containing 0.5 mM  $\text{CuSO}_4$ , at a pH of 7.3. PVPA-*co*-AA can bind to  $\text{Cu}^{2+}$  ions through its acid groups, forming a polymer-metal complex. Kyuzou *et al.*<sup>190</sup> have previously demonstrated a strong UV band in the UV/Vis spectrum of PVPA- $\text{Cu}^{2+}$  complexes, which occurs at a wavelength of approx. 250-300 nm. This was attributed to a configuration interaction between the  $\sigma\text{-}\sigma^*$  transitions of the Cu-O bonds. In addition, this spectroscopic method has often been used for the determination of bisphosphonate (BP) content within tissue scaffolds.<sup>183-185</sup> Since it has been shown that PVPA-*co*-AA can mimic the action of BPs, the same method was applied to this system. Therefore, the absorbance was measured at  $\lambda_{\text{max}}$  270 nm and a calibration curve was produced as shown in Figure 4.2. The absorbance was corrected for that of pure  $\text{CuSO}_4$  solution.

PCL/PVPA-30 electrospun scaffolds were dissolved in dichloromethane (DCM) at a concentration of 3.0  $\text{mg mL}^{-1}$ . The organic solution was shaken with 10 mL of 1.5 mM  $\text{HNO}_3$  aqueous solution for 1 h to extract PVPA-30 in the aqueous phase, which was then separated. The solvent was partially evaporated using a Buchi (R-200) rotavapor and the aqueous medium was recovered and complexed with 0.5 mM  $\text{CuSO}_4$  in 1.5 mM  $\text{HNO}_3$  aqueous solution (pH 7.3). The PVPA- $\text{Cu}^{2+}$  complex was analysed at  $\lambda_{\text{max}}$  270 nm and the concentration determined using the pre-constructed calibration curve and equation 4.1:

$$[\text{PVPA} - 30] = \frac{\text{Absorbance} + 0.0063}{0.0032} \quad (4.1)$$

The measurement was repeated three times and an average recorded. The uptake efficiency (UE) of the copolymer into the scaffold was then calculated using equation 4.2:

$$\text{UE (\%)} = \frac{\text{Concentration of PVPA} - 30}{\text{Theoretical concentration of PVPA} - 30} \times 100 \quad (4.2)$$

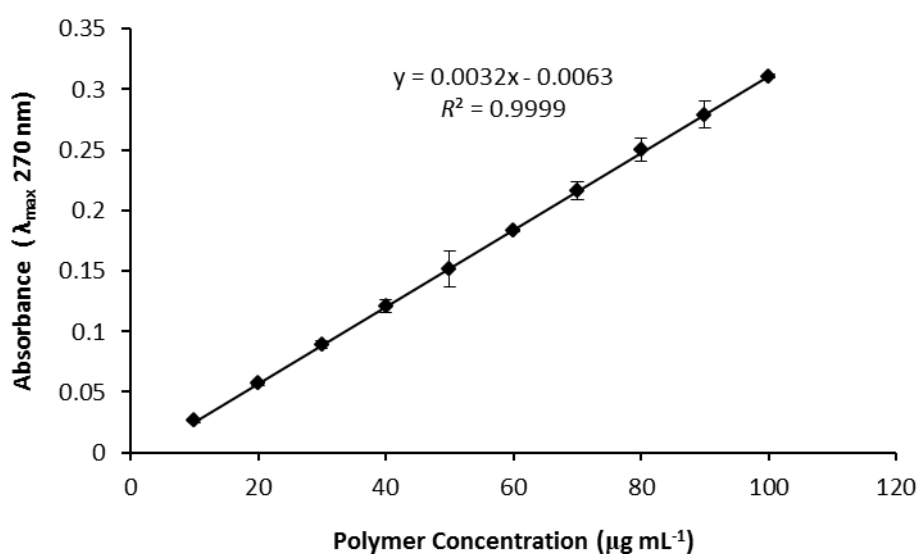


**Figure 4.2.** Calibration curve for the determination of PVPA-30 uptake efficiency into PCL scaffolds by UV/Vis spectroscopy. The absorbance of PVPA-Cu<sup>2+</sup> complexes is determined as a function of polymer concentration.

#### 4.2.4 Sterilisation of PCL/PVPA-co-AA scaffolds

The sterilisation procedure involved immersing the PCL/PVPA-30 scaffolds into a 70% ethanol solution for 2 h. The scaffolds were then immersed into phosphate buffered saline (PBS) for 5 min and this was repeated twice. The PVPA-30 concentration in the scaffolds was calculated pre- and post-sterilisation using UV/Vis spectroscopy and the method described above. The calibration curve is shown in Figure 4.2. The loss of PVPA-30 from the scaffolds, during sterilisation, was then calculated as a percentage.

#### 4.2.5 Calcium chelation of PCL/PVPA-co-AA scaffolds

The amount of calcium chelated by the scaffolds was measured using a calcium-selective electrode (ThermoFisher Scientific, U.K.). PCL/PVPA-30 scaffolds (1.0 mg mL<sup>-1</sup>) were immersed into a solution of deionised water, which was adjusted to pH 7.3 using 0.1 M NaOH. CaCl<sub>2</sub> was added at a concentration of 0.1 M and the scaffolds were left in the solutions for 24 h. The calcium-selective electrode was then immersed into the solution to measure the free Ca<sup>2+</sup> concentration. A calibration curve was produced prior to the measurement using a range of standard CaCl<sub>2</sub> solutions (0.0001, 0.001, 0.01, 0.1 and 1 M) (see appendix Figure A4.1). The samples were then quantified by means of the calibration curve ( $R^2 > 0.999$ ). The amount of calcium chelated by the scaffolds was calculated from the total amount of Ca<sup>2+</sup> added and the free Ca<sup>2+</sup> measured. Calcium chelation measurements were performed on the scaffolds before and after sterilisation.

#### 4.2.6 Release of PVPA-co-AA from PCL scaffolds

The PCL/PVPA-30 scaffolds (3.0 mg mL<sup>-1</sup>) were immersed in deionised water as a release medium, at a pH of 7.3 and a temperature of  $37.0 \pm 0.2$  °C. At fixed time intervals, 1.0 mL of release medium was removed and replaced with 1.0 mL deionised water to maintain sink conditions. Each sample withdrawn was added to 0.5 mM CuSO<sub>4</sub> in 1.5 mM HNO<sub>3</sub> aqueous solution (1.0 mL) and the PVPA-30 concentration was monitored spectrophotometrically at  $\lambda_{\max}$  270 nm. The amount of polymer released was calculated as described above, using a pre-constructed calibration curve (Figure 4.2). Dilution of the release medium due to successive sampling was corrected for using equation 4.3:<sup>185</sup>

$$C_1 = c_1 + c_1 \Delta t E \quad (4.3)$$

where  $C_1$  is the actual amount of polymer released after the correction;  $c_1$  is the uncorrected amount of polymer released;  $\Delta t$  is the time interval;  $E$  is the rate of sample withdrawal and  $c_1 \Delta t E$  is the amount of polymer eliminated from the solution during the time interval  $\Delta t$ .

#### 4.2.7 Calcium chelation in osteogenic differentiation media

The total calcium concentration in the osteogenic medium was first calculated by measuring a range of standard calcium concentrations (0.0001, 0.001, 0.01, 0.1 and 1 M) and producing a calibration curve (see appendix Figure A4.2). PCL/PVPA-30 scaffolds ( $1.0 \text{ mg mL}^{-1}$ ) were then immersed into the osteogenic medium, at a pH of 7.27 and a temperature of  $37.0 \pm 0.2 \text{ }^\circ\text{C}$ . The scaffolds were left in the media for a total of 7 days. At certain time points, the calcium-selective electrode was immersed into the solutions to measure the free  $\text{Ca}^{2+}$  concentration. The samples were then quantified by means of the calibration curve ( $R^2 > 0.999$ ). The amount of calcium chelated by the scaffolds was calculated from the initial amount of  $\text{Ca}^{2+}$  present in the osteogenic medium and the free  $\text{Ca}^{2+}$  measured at a given time point.

### 4.3 Results and Discussion

#### 4.3.1 Uptake efficiency of PVPA-*co*-AA into PCL scaffolds

The uptake efficiency of PVPA-*co*-AA into PCL scaffolds was determined using UV/Vis spectroscopy. It has been shown that the copolymer can bind to divalent metal ions. Hence, PVPA-30 was dissolved in copper sulphate solution to form a PVPA- $\text{Cu}^{2+}$  complex that was pale blue in colour. Figure 4.3 shows the FT-IR spectra for PVPA-30 and the PVPA- $\text{Cu}^{2+}$  complex. A difference in the two spectra is observed due to complex formation. PVPA-30 binds to  $\text{Cu}^{2+}$  in a bidentate manner via the oxygen atoms of its carboxylic and phosphonic acid side groups. Thus, the  $\text{H}^+$  counter-ions are released and so the O-H band, which appears between  $3000$  and  $2300 \text{ cm}^{-1}$  in PVPA-30, has disappeared following copper complexation. The position of the carbonyl stretching peak is a good indicator as to whether the carbonyl group is free, involved in hydrogen bonding or coordinated to a metal ion.<sup>191</sup> It can be seen in Figure 4.3 that the C=O band, which appears at  $1696 \text{ cm}^{-1}$  in the copolymer, has shifted to a lower wavenumber ( $1565 \text{ cm}^{-1}$ ) in the IR spectrum of the PVPA- $\text{Cu}^{2+}$  complex. The single sharp band at  $1565 \text{ cm}^{-1}$  suggests that the C–O bonds are approximately the same length and in both cases the oxygen is coordinated to a  $\text{Cu}^{2+}$  ion.<sup>191</sup> Therefore, the FT-IR spectra provide strong evidence of complexation between PVPA-30 and  $\text{Cu}^{2+}$  ions.

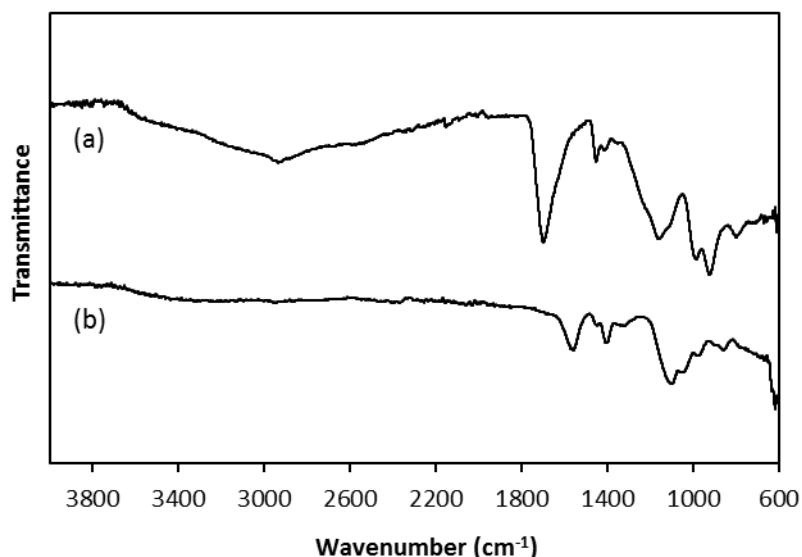


**Figure 4.3.** FT-IR spectra of (a) PVPA-30 and (b) PVPA-Cu<sup>2+</sup> complex.

Table 4.2 shows the absorbance of PVPA-Cu<sup>2+</sup>, the calculated polymer concentrations and uptake efficiencies for each of the PCL/PVPA-30 scaffolds. Polymer uptake efficiencies ranged from 63% to 72%, depending on the method of fabrication of the scaffolds and the initial concentration of PVPA-30. The lowest uptake efficiencies were found for samples that were prepared by dip-coating into a solution of PVPA-30, with (PVPA-H) or without (PVPA-D) heat treatment. This technique relies on the PVPA-30 attaching to the surface of the PCL fibres. However, PCL is hydrophobic and PVPA-co-AA is hydrophilic. Hence, the immiscibility of the polymers leads to a relatively low uptake of PVPA-30 onto the scaffold.

Scaffolds were also fabricated by co-spinning the polymers with the aid of a surfactant to increase their miscibility. This technique led to higher uptake efficiencies of PVPA-30 into the PCL scaffolds. It is noted that the uptake efficiency did not seem to depend on the initial concentration of PVPA-30. This suggests that it is possible to incorporate different concentrations of PVPA-30 into PCL scaffolds, depending on the amount required for the specific application.

**Table 4.2.** The absorbance of PVPA-Cu<sup>2+</sup> complexes which enables the calculation of PVPA-co-AA concentration and their uptake efficiencies into PCL scaffolds.

Sample Code	Absorbance ( $\lambda_{\max}$ 270 nm)	PVPA-30 Concentration ( $\mu\text{g mL}^{-1}$ )	Theoretical Concentration ( $\mu\text{g mL}^{-1}$ )	Uptake Efficiency (%)
PVPA-1	0.027	10.41	15.00	69.4
PVPA-5	0.167	53.96	75.00	71.9
PVPA-7	0.231	74.16	105.0	70.6
PVPA-10	0.325	103.6	150.0	69.1
PVPA-D	0.295	94.01	150.0	62.7
PVPA-H	0.318	101.4	150.0	67.6

### 4.3.2 Effect of sterilisation on PCL/PVPA-co-AA scaffolds

One of the most important factors when designing tissue scaffolds is their ability to undergo sterilisation with little effect on the properties of the scaffold. The scaffolds were sterilised by immersing into a 70% ethanol solution for 2 h. Table 4.3 shows the effect of sterilisation on the concentration of PVPA-30 in the scaffolds, as measured by UV/Vis spectroscopy. It is observed that the PVPA-D scaffold showed the greatest loss of PVPA-30 during sterilisation with 70% ethanol. The limited physical interactions between PVPA-30 and PCL mean that the majority of the PVPA-30 will likely be localised on the surface of the nanofibres due to the high ionic strength of the copolymer. Therefore, the PVPA-30 on the fibre surface can be washed off relatively easily by the ethanol, in which it is partially soluble. The loss of PVPA-30 was reduced for the heat treated sample (PVPA-H). It is thought that heat treatment takes the scaffold above its crystallisation temperature. This leads to movement of the polymer chains and cooling leads to subsequent crystallisation. Therefore, the PVPA-30 could become trapped during the heating and cooling of polymer chains, providing a stable scaffold.<sup>132</sup>

The scaffolds fabricated by co-spinning of the two polymers were able to retain the PVPA-30 more easily. This implies that some of the copolymer is located within the PCL fibres. It is also interesting to note that higher initial concentrations of PVPA-30 result in a greater loss during sterilisation. This could be due to aggregation of the copolymer on the fibre surface. Hence, the ethanol will wash off greater amounts of the PVPA-30 from the surface of the scaffolds.

**Table 4.3.** The change in PVPA-*co*-AA concentration in the PCL scaffolds, as measured by UV/Vis spectroscopy, after undergoing sterilisation with 70% ethanol.

Sample Code	Absorbance ( $\lambda_{\text{max}}$ 270 nm)	PVPA-30 Concentration Pre-Sterilisation ( $\mu\text{g mL}^{-1}$ )	PVPA-30 Concentration Post-Sterilisation ( $\mu\text{g mL}^{-1}$ )	Loss of PVPA-30 during sterilisation (%)
PVPA-1	0.020	10.41	8.312	20.1
PVPA-5	0.122	53.96	42.20	21.8
PVPA-7	0.168	74.16	54.52	26.5
PVPA-10	0.213	103.6	72.54	30.0
PVPA-D	0.164	94.01	55.08	41.4
PVPA-H	0.211	101.4	70.02	30.9

Incorporation of PVPA-*co*-AA into PCL scaffolds is believed to enhance calcium chelation and thus promote and direct mineralisation of the ECM. If, as proposed above, some of the PVPA-30 is dissolved by the ethanol and washed out of the scaffold, this may have a profound effect on its calcium binding affinity. Therefore, the calcium chelation capacity of the scaffolds was measured before and after sterilisation and the results are presented in Figure 4.4. It was found that the calcium chelation significantly increased when span 80 was incorporated into PCL scaffolds. This could possibly be due to a change in the structure of the scaffolds, which allows for greater water uptake, allowing the calcium to become embedded within the fibres. Furthermore, as the PVPA-30 concentration increased, the calcium chelation capacity also increased owing to the greater ability of PVPA-30 to bind to calcium ions.

Sterilisation with 70% ethanol led to a significant decrease in the calcium chelation capacity for all of the scaffolds, with the exception of PCL alone. It is thought that this occurs due to the loss of some of the PVPA-30 during ethanol sterilisation. The reduction in calcium binding was more pronounced for PVPA-D and PVPA-H. This is expected since the PVPA-30 is predominantly located on the surface of the PCL scaffolds after dip-coating and is washed off by the ethanol with relative ease. Heat treatment allowed greater retention of the copolymer than just dip-coating alone, but there was no significant difference in the calcium binding of these scaffolds post-sterilisation.

The scaffolds that were produced by co-spinning of the PCL and PVPA-*co*-AA also showed reduced calcium chelation capacities post-sterilisation, albeit to a lesser extent. This is due to the greater retention of PVPA-30 after sterilisation with ethanol. It is suggested that the copolymer could become encapsulated within the PCL fibres during the electrospinning process as a result of the surfactant, which acts as a compatibilizer between the PCL and PVPA-30. Therefore, this encapsulated polymer is shielded from the ethanol and thus, not washed out of the scaffolds.

However, it is not yet clear whether the PVPA-30 can bind to calcium ions whilst attached to the PCL fibres or if calcium binding occurs after the release of PVPA-*co*-AA into aqueous solution. The mechanism of action of polymer-calcium binding can significantly affect the mineralisation process and so this must be investigated further.

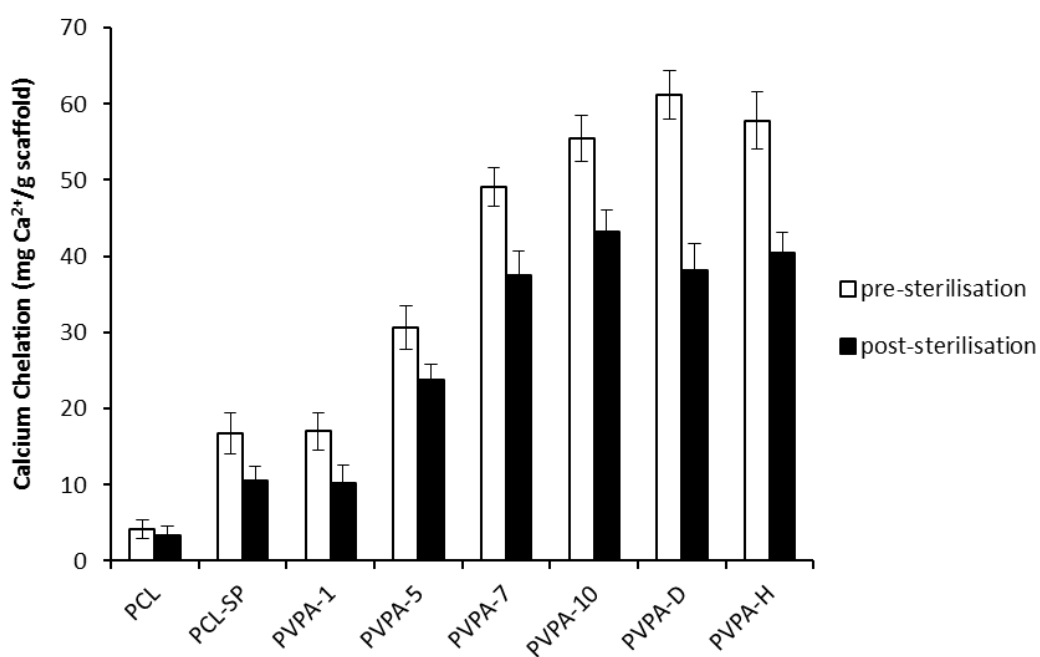


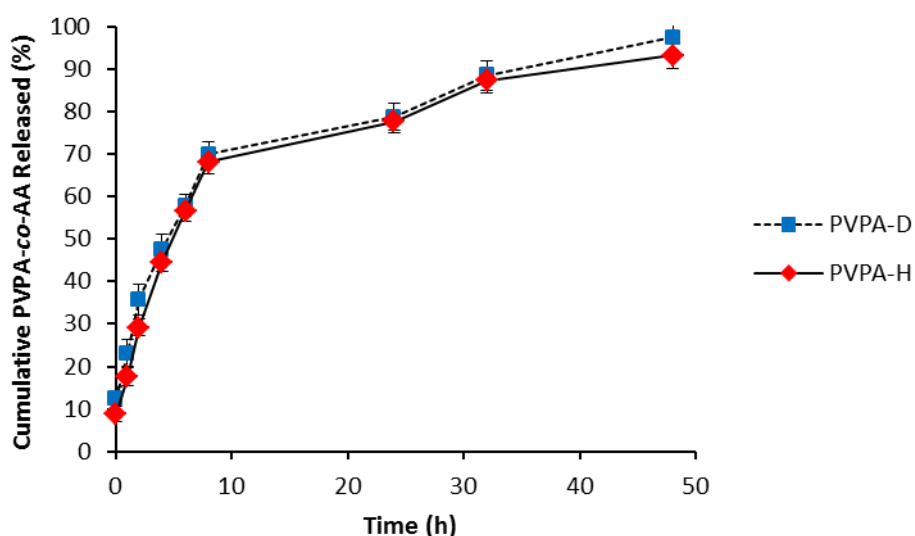
**Figure 4.4.** Calcium chelation capacity of electrospun nanofibrous scaffolds before and after sterilisation with 70% ethanol.

#### 4.3.3 Release of PVPA-*co*-AA from PCL scaffolds

Figure 4.5 shows the release profile of PVPA-*co*-AA from PCL scaffolds in aqueous media. The scaffolds were produced by dip-coating with (PVPA-H) and without (PVPA-D) heat treatment. The results show that the release of PVPA-30 from PVPA-D

scaffold was complete in approximately 48 h and was 93% complete for PVPA-H. There was an initial burst whereby 70% of the polymer was released within 8 h. Following this, there was a slower rate of release until all of the copolymer had been washed out of the scaffolds. This biphasic release profile occurs as a result of the nature of polymer uptake into the PCL scaffolds. The majority of the PVPA-*co*-AA is located on the surface of the PCL fibres due to the immiscibility of the polymers and the lack of interactions between them. Thus, the initial burst release represents the dissolution of this surface attached polymer. However, some of the PVPA-*co*-AA can diffuse through the pores in the PCL scaffold and become entrapped, which leads to the second more sustained release phase.

It is noted that heat treatment had almost no effect on the release rate of PVPA-30 from the PCL scaffolds. It was thought that heat treatment would immobilise the copolymer onto the PCL fibres, which would prevent the dissolution of PVPA-30 to a certain extent. However, it would appear that this process did not achieve the desired effect and does not lead to a slower release rate of the copolymer from the scaffolds.



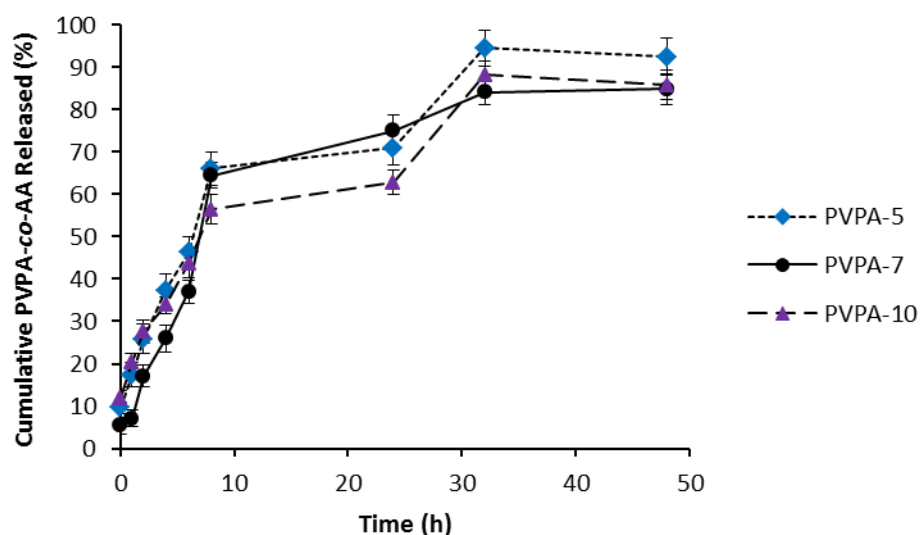
**Figure 4.5.** Cumulative percentage of PVPA-30 released, in deionised water at 37 °C, from PCL scaffolds. Scaffolds were produced by dip-coating with (PVPA-H) and without (PVPA-D) heat treatment. Data represented as mean  $\pm$  SD.

Figure 4.6 shows the release of PVPA-30 (at concentrations of 5.0, 7.0 and 10 wt %) from PCL scaffolds produced by co-spinning with the use of span 80 as a surfactant. PVPA-1 was excluded from the study due to the low initial concentration of the copolymer, which made it difficult to quantify. The release profile of PVPA-30 from all of the co-spun scaffolds is similar to that observed for PVPA-D and PVPA-H. As discussed previously, there is an initial burst release of surface attached PVPA-co-AA, followed by a slower release of the copolymer that had diffused through the scaffold and become entrapped.

The process of co-spinning, with the aid of a surfactant, increases the miscibility of the polymers and leads to greater interactions between them. Therefore, there is a prolonged polymer release due to a better dispersion of PVPA-30 in the PCL electrospun scaffold. This allows more of the PVPA-30 to become encapsulated within the PCL fibres as opposed to on the surface, when compared with the dip-coating method. Therefore, after the initial burst release of surface attached polymer, the second release phase is slightly slower for the co-spun samples.

The total amount of PVPA-30 released from the scaffolds was 85-92%, which is slightly lower than for PVPA-D and PVPA-H scaffolds. However, the difference is not significant. This could be due to the high surface area and porosity of PCL electrospun scaffolds, which allow the rapid diffusion of water into the scaffold and hence accelerate the rate of PVPA-30 release.

The scaffolds that contained higher concentrations of PVPA-30, demonstrated the lowest total amount of polymer released. It is hypothesised that higher concentrations of PVPA-30 in the initial emulsion resulted in more polymer becoming incorporated within the PCL fibres. Therefore, the rate of release of PVPA-30 from the PCL scaffold will be decreased. These results provide some evidence for the efficacy of this fabrication method, which can lead to slower rates of release and which can be tailored for the specific duration or dose required in drug delivery applications.



**Figure 4.6.** Cumulative percentage of PVPA-30 released, in deionised water at 37 °C, from PCL scaffolds. Scaffolds were produced by co-spinning PCL with PVPA-*co*-AA at different concentrations (5.0, 7.0 and 10 wt %) with the use of span 80 as a surfactant. Data is represented as mean  $\pm$  SD.

#### 4.3.4 Calcium chelation from osteogenic differentiation media

To determine the efficacy of the materials for use in bone tissue scaffolds, it is important to try to replicate the *in vivo* conditions. Cell culture medium contains many inorganic salts, proteins, vitamins, etc., which may affect the ability of the copolymer to bind to calcium ions. Furthermore, it is not yet clear whether PVPA-*co*-AA can bind to calcium ions from the culture medium when attached to the PCL scaffold or if the polymer is first released before calcium binding.

Figure 4.7 shows the calcium binding affinities of scaffolds, in osteogenic differentiation media, as a function of time. An initial sharp increase in calcium chelation was observed for all of the scaffolds in the first 6-8 h. After this point, there was a much slower rate of increase until the maximum capacity was reached. It is interesting to note that, from the results described above; most of the PVPA-30 is released from the PCL scaffolds within the first 8 h. As this is also the time frame where a rapid increase in calcium chelation is observed, it can be hypothesised that the PVPA-*co*-AA is first released from the scaffolds, after which calcium binding can occur in solution. It is proposed that PVPA-*co*-AA acts as a mimic of non-collagenous matrix

proteins by binding to calcium ions in solution to form stable polymer-calcium complexes, which can act as a template for HA nucleation and growth.

Calcium chelation increased with increasing PVPA-*co*-AA concentration in the co-spun scaffolds. The calcium binding affinity of PVPA-D and PVPA-H were similar to that of PVPA-7 and PVPA-10, respectively, owing to their similar PVPA-*co*-AA concentrations. Despite the presence of many competing ions in the osteogenic differentiation media, this does not seem to have had any significant effect on the ability of the scaffolds to bind to the calcium ions. The rapid release of PVPA-30 from the PCL scaffolds could be beneficial *in vivo* because the copolymer can immediately bind to calcium ions from the bone mineral surface to affect osteoclast activity. However, if the copolymer is to enhance the mineralisation of osteoblast cells, a more sustained release may be favourable. Therefore, the method of fabrication of PVPA-*co*-AA-containing scaffolds may need to be fine-tuned to allow for a more sustained release of the polymer over time depending on the specific application.

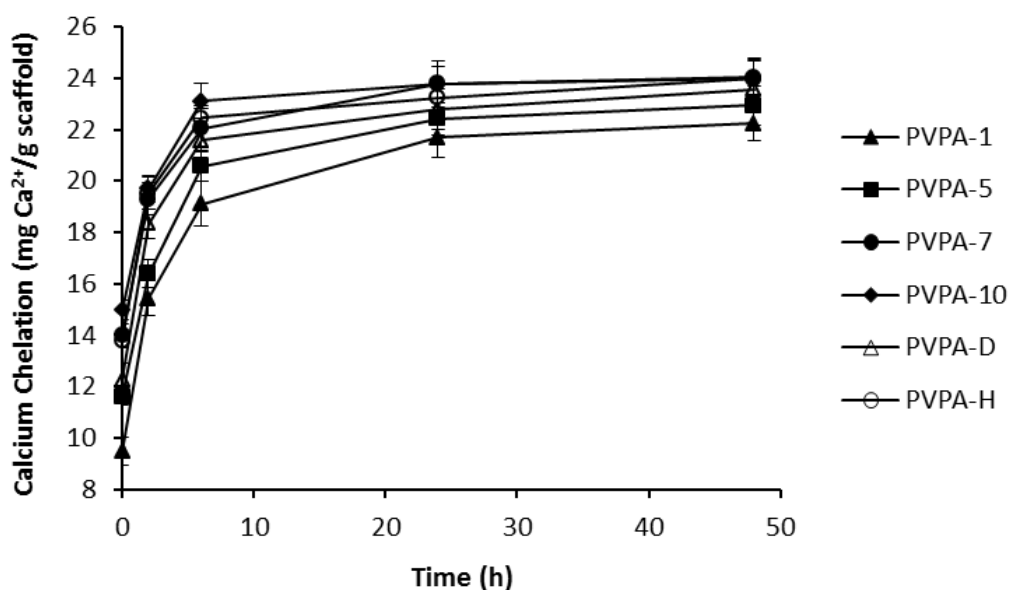


**Figure 4.7.** Calcium chelation of PCL electrospun nanofibrous scaffolds, with different concentrations of PVPA-30, produced by dip-coating or co-spinning with the aid of a surfactant, in osteogenic differentiation media.

## 4.4 Conclusions

The effectiveness of PCL/PVPA-*co*-AA electrospun scaffolds, produced by dip-coating or co-spinning techniques, has been investigated for use as a delivery device to improve mineralisation of the bone extracellular matrix. The uptake efficiency of PVPA-*co*-AA into PCL scaffolds varied depending on the fabrication method. Scaffolds produced by dip-coating had lower uptake efficiencies due to the immiscibility of the two polymers. Co-spinning of the PCL and PVPA-*co*-AA led to higher uptake efficiencies as a result of the use of a surfactant (Span 80) which helped to improve their compatibility. There was no significant difference between the uptake efficiencies of scaffolds with different initial PVPA-30 concentrations.

Scaffolds were sterilised by immersing in a 70% ethanol solution. It was found that this led to a decrease in the PVPA-30 concentration in the scaffolds due to the partial solubility of the copolymer in ethanol, which, in turn, resulted in a decrease in the calcium chelation capacity of the scaffolds. This effect was more pronounced in scaffolds that had been produced by dip-coating owing to the majority localisation of PVPA-30 on the surface of the PCL fibres.

The release profile of PVPA-30 from the PCL scaffolds was determined. It was shown that the majority of the copolymer was released within the first 8 h of immersion in aqueous media, regardless of the fabrication method. However, the release of PVPA-30 from the dip-coated and heat treated samples was complete within 48 h, whereas those produced by co-spinning had only released 85-92% of the copolymer in this time frame. Furthermore, the calcium chelation of the scaffolds was measured in osteogenic differentiation media over 48 h. It was found that most of the calcium had been chelated from the media within 6-8 h of immersion. This suggests that PVPA-*co*-AA binds to calcium when it is released into solution and not when it is immobilised onto the scaffolds. In this way, PVPA-*co*-AA can act as a mimic of NCPs and can form stable polymer-calcium complexes in solution.

These results have implications for the use of PCL scaffolds for the therapeutic delivery of PVPA-*co*-AA as an alternative to bisphosphonate drugs. It has been shown that by altering the fabrication method, the release rate of the copolymer can be tuned for the specific application. However, more work is needed to allow for a slower release of the polymer over time to provide long-term therapeutic effects.

## Chapter 5: PVPA-*co*-AA hydrogels for bone regeneration

### 5.1 Introduction

Polyelectrolytes have become increasingly utilised for the preparation of hydrogels due to the fact that the functional groups along the polymer chain can respond to changes in the external environment, such as temperature,<sup>192</sup> pH<sup>193</sup> and ionic strength<sup>194</sup> of the medium.

The extent of crosslinking is one of the most important factors that can significantly affect the properties of hydrogels. Weakly crosslinked hydrogels are soft and flexible, whereas an increase in the crosslink density produces stiffer gels that are also quite brittle. Thus, although a high degree of crosslinking is advantageous in terms of mechanical strength, a decrease in the dynamic swelling ratio of hydrogels is observed due to a more densely packed structure.<sup>116</sup> This also results in a lower tensile strength, toughness and resilience. Highly crosslinked hydrogels are therefore more likely to suffer from irreversible rupture at low deformations. This can significantly affect the ability of hydrogels to enhance cell adhesion and proliferation and so a delicate balance must be found between high mechanical strength and a large degree of swelling.

The microstructural properties of three-dimensional hydrogels, such as pore size and pore volume, can also affect cell growth. Lien *et al.*<sup>195</sup> have prepared gelatin scaffolds and have shown that as the pores become larger (50-500  $\mu\text{m}$ ), the rate of cell growth increases. In addition, ECM secretion was also found to increase proportional to pore size. It was suggested that larger pores allow for effective nutrient supply, gas diffusion and metabolic waste removal, which enables greater cell growth.

Hydrogels comprising acrylic acid (AA) or vinylphosphonic acid (VPA) have been studied extensively for many biomedical applications, including drug delivery and tissue regeneration. However, this is the first study to investigate a hydrogel that incorporates both monomers. It is believed that the polyelectrolyte nature and hydrophilicity of both monomers will lead to the production of a superabsorbent hydrogel. Furthermore, their mechanical and cell adhesion properties can be altered by varying the copolymer composition.

### 5.1.1 Biocompatibility studies

One of the most essential characteristics of a bone tissue scaffold is its ability to undergo biodegradation *in vivo* as new bone is deposited. Moreover, the degradation products should be non-toxic to avoid an inflammatory reaction in the surrounding tissue. When producing hydrogels of PVPA-*co*-AA, it is important to consider the biocompatibility of the constituent monomers. This was investigated in previous work.<sup>161</sup> Figure 5.1 shows the fold change in cell metabolic activity for AA and VPA monomers as a function of concentration, after 72 h of culture. Phosphate buffer solution (PBS) was used as a control. The results indicate that AA and VPA monomers, with concentrations ranging from 1-500  $\mu$ M, had no detrimental effect on SaOS-2 cell metabolic activity, when compared with the control, over a 72 h culture period.

Furthermore, the cytotoxicity of PVPA-*co*-AA copolymers was investigated *in vitro* as a function of VPA content.<sup>161</sup> The results showed that all PVPA-*co*-AA polymers had no detrimental effect on SaOS-2 cell metabolic activity. No statistical difference was found between each polymer treatment and the PBS control up to 24 h of culture. This suggests that PVPA-*co*-AA is biocompatible and not cytotoxic over this culture period, regardless of copolymer composition, and is therefore suitable for use in bone tissue scaffolds.

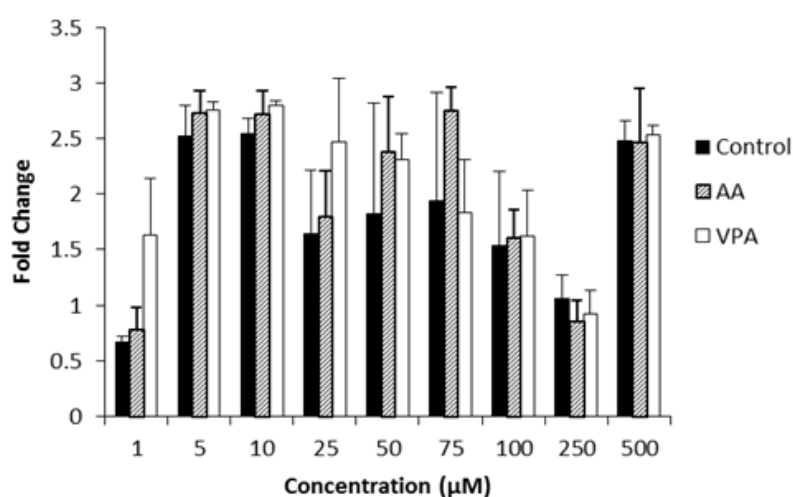


**Figure 5.1.** Determination of cell metabolic activity for AA and VPA monomers over a 72 h culture period, for a range of monomer concentrations, compared with a PBS control, image taken from Dey *et al.*<sup>161</sup>

### 5.1.2 Aims and Objectives

It was the aim of this work to produce hydrogels of PVPA-*co*-AA and to investigate the effect of copolymer composition on osteoblast adhesion and proliferation.

Firstly, the synthesis of PVPA-*co*-AA hydrogels was investigated to find the optimum conditions, i.e. polymerisation time and crosslinker concentration, to produce hydrogels with the desired properties for cell adhesion.

The effect of monomer feed ratio on the properties of the PVPA-*co*-AA hydrogels was investigated in terms of their physical morphology, swelling capacity and hydrophilicity.

The rheological properties of the gels were then explored. For example, their ability to resist high mechanical strain is an important property of hydrogels for use as bone graft substitutes if they are to be moulded into a bone defect site.

Finally, the effect of monomer feed ratio on osteoblast adhesion and proliferation was investigated.

## 5.2 Experimental

### 5.2.1 Materials

All chemicals were used without further purification unless otherwise stated. Vinylphosphonic acid (VPA), (97%) was purchased from Tokyo Chemical Industry (TCI), U.K. Acrylic acid (AA), (99%), 2,2'-azobis(2-methylpropionamide) dihydrochloride (AAPH), (97%) and ethylene glycol diacrylate (EGDA), (90%) were all purchased from Sigma-Aldrich Ltd., U.K.

### 5.2.2 Preparation of PVPA-*co*-AA hydrogels

The following method details the preparation of VPA-30. Further details of the experimental conditions for all of the hydrogels are presented in Table 5.1. VPA (0.35 g, 3.24 mmol), AA (0.54 g, 7.50 mmol), EGDA (3.5 mg, 0.21 mmol) and AAPH (2.9 mg, 0.01 mmol) were added together and dissolved in deionised water (4.0 cm<sup>3</sup>). The reaction mixture was purged with N<sub>2</sub> for 20 min and then 400 μL of the solution was aliquoted into a 24-well plate with a well diameter of 15.6 mm. This was heated to 80 °C for 30 min. The resulting gels were washed in dH<sub>2</sub>O for 48 h to remove any unreacted monomer. Gels were produced in triplicate and were stored in dH<sub>2</sub>O before use.

**Table 5.1.** Experimental conditions for the preparation of PVPA-*co*-AA hydrogels (where  $n$  is the number of moles and  $V$  is volume).

Sample Code	Monomer feed ratio (VPA:AA)	$n_{VPA}$ (mmol)	$V_{VPA}$ (mL)	$n_{AA}$ (mmol)	$V_{AA}$ (mL)	AAPH (mg)	$V_{EGDA}$ (mL)	$V_{H_2O}$ (mL)
VPA-0	0:100	0.00	0.00	10.7	0.74	2.9	0.035	8.0
VPA-10	10:90	1.07	0.08	9.67	0.67	2.9	0.035	6.0
VPA-30	30:70	3.24	0.23	7.50	0.51	2.9	0.035	4.0
VPA-50	50:50	5.37	0.42	5.37	0.37	2.9	0.035	2.0

### 5.2.3 Elemental analysis

PVPA-*co*-AA hydrogels were dried fully (as verified by no change in weight) under vacuum and then ground into a fine powder. Elemental analyses were carried out using

inductively coupled plasma mass spectrometry (ICP-MS), by the School of Chemistry Microanalysis Service at the University of Manchester.

#### 5.2.4 FT-IR spectroscopy

PVPA-*co*-AA hydrogels were dried fully (as verified by no change in weight) under vacuum and then ground into a fine powder. Fourier transform infrared (FT-IR) spectra were recorded using a Thermo Scientific Nicolet iS5 spectrometer with an iD5 diamond attenuated total reflectance (ATR) attachment over a wavenumber range of 4000–600  $\text{cm}^{-1}$  and a resolution of 4  $\text{cm}^{-1}$ . The spectra were obtained from 16 scans.

#### 5.2.5 Swelling studies

Before swelling, gels were fully dried (as verified by no change in weight) in air in a 24-well plate. The weight of the dry material ( $W_d$ ) was recorded. For the swelling experiment, 2 mL phosphate buffer ( $\sim 0.1$  M  $\text{Na}_2\text{HPO}_4$ ) solution (pH 5.0, 7.3 or 9.0) was added to the well plate and the gels were left to swell for 24 h at 37.0 °C. The supernatant was discarded and the gels were blotted with filter paper to remove any excess water. The weight of the swollen hydrogel ( $W_s$ ) was then recorded. Thus, the swelling was calculated using equation 5.1. The swelling experiment was repeated in triplicate for each hydrogel composition and the results are expressed as mean  $\pm$  SD.

$$\text{Swelling (\%)} = \frac{W_s - W_d}{W_d} \times 100 \quad (5.1)$$

#### 5.2.6 Scanning Electron Microscope (SEM) analysis

The as-synthesised hydrogels were allowed to swell in deionised water for 24 h before being placed into a freezer, set at -80 °C, for 1 h. The frozen samples were subsequently freeze-dried in an Edwards EF4 Modulyo vacuum freeze-dryer (ThermoFisher Scientific, U.K.). The freeze-dried samples were mounted onto aluminium stubs using carbon tabs (Agar Scientific, U.K.) and then gold-coated using an Emitech K550X sputter-coater set at 40 mA for 1 min. The morphology of the freeze-dried sample was then observed with a Zeiss EVO 50 field emission scanning electron microscope, using an acceleration voltage of 20.0 kV, a spot size of 400 and a working distance of 24.5 mm.

### **5.2.7 Water contact angle measurements**

The water contact angle of the scaffolds was tested using the OneAttention Theta optical tensiometer (Biolin Scientific, U.K.). The wettability was tested on three separate hydrogel samples. A 10  $\mu\text{L}$  droplet of deionised water was released onto each hydrogel using an 8-gauge needle (BD Plastics, U.K.). The advancing contact angle was measured over 7.20 seconds.

### **5.2.8 Rheological properties of PVPA-*co*-AA hydrogels**

An ARES LN2 rheometer (TA instruments, Hertfordshire) with parallel-plate geometry of 25 mm diameter was used for the rheological characterisation of PVPA-*co*-AA hydrogels. Test methods of oscillatory strain sweep and frequency sweep were used. The tests were performed at a constant temperature (20.0  $^{\circ}\text{C}$ ) and a nominal gap of 2.5 mm. The strain sweep was performed at a frequency of 1.0 Hz. The strain level was increased from 1.0 to 100% and the change in storage ( $G'$ ) and loss ( $G''$ ) modulus was recorded. The linear viscoelastic region (LVR) from 5 to 15% was determined as a safe region without structural breakage from oscillatory strain.

The frequency sweep was performed at a constant strain of 10%, corresponding to a point in the middle of the LVR profile. The oscillatory frequency was increased from 0.1 to 10 Hz and plots of  $G'$  and  $G''$  against frequency were obtained using the manufacturer's supplied software. The complex viscosity ( $\eta^*$ ) was also plotted against the same frequency range.

### **5.2.9 Cell culture**

Human osteosarcoma derived osteoblast (SaOS-2) cells were purchased from the European Collection of Authenticated Cell Cultures, U.K. (ECACC 89050205). Cells were cultured in McCoy's 5A medium (Sigma-Aldrich, U.K.) supplemented with 10% foetal bovine serum (FBS), antibiotics (100 U  $\text{mL}^{-1}$  penicillin, 100 mg  $\text{mL}^{-1}$  streptomycin) and 1% L-glutamine. Culture medium was replenished every 24 h. Hydrogels were placed on glass coverslips (13 mm diameter, Scientific Laboratory Supplies, U.K.) in 24-well plates and sterilised using UV-irradiation for 1 h. Cells were counted and seeded onto scaffolds at a density of 50 000 cells per  $\text{cm}^2$ . Plates were cultured at 37  $^{\circ}\text{C}$  and 5%  $\text{CO}_2$  for up to 14 days.

### **5.2.10 Live/Dead® Staining**

Live/Dead® staining solution (Invitrogen, U.K.) was prepared by adding ethidium homodimer-1 (4  $\mu\text{M}$ ) and calcein-AM (2  $\mu\text{M}$ ) to sterile phosphate buffered saline (PBS). Cells were cultured on the various hydrogels and glass coverslips were used as a control. At certain time points (4, 24 and 72 h) the culture medium was removed from the samples and the wells were washed with sterile PBS. The prepared staining solution (150  $\mu\text{L}$ ) was added to each well and incubated for 30 min at 37 °C and 5%  $\text{CO}_2$ . The hydrogels were then mounted onto glass microscope slides and viewed under the Nikon Eclipse 50i fluorescence microscope with a camera attachment. Cell spreading and proliferation was quantified using ImageJ software (<https://imagej.nih.gov/ij/>).<sup>196</sup>

### **5.2.11 Determination of cell number**

Cells were cultured on the various hydrogels and tissue culture plastic (TCP) was used as a control. At certain time points (1, 3, 7 and 14 days) the culture medium was removed and samples were washed with sterile PBS. The samples were immersed in 1 mL lysis buffer (0.1% Triton X-100 in  $\text{dH}_2\text{O}$ ) and 3 freeze-thaw cycles were performed. The PicoGreen® dsDNA stain solution was prepared as outlined by the manufacturer (ThermoFisher Scientific, U.K.). 100  $\mu\text{L}$  of each sample and 100  $\mu\text{L}$  of the PicoGreen® stain solution were added to a flat-bottomed 96-well plate (Nunc®, U.K.). The fluorescence was measured at an excitation of 485 nm and an emission at 520 nm using a Fluostar Optima Fluorescence Microplate Reader (BMG Labtech, Germany). A calibration curve (Figure 5.2) was produced prior to the measurement using a set of dsDNA standards (0-2  $\mu\text{g mL}^{-1}$ ), prepared in TE (Tris EDTA) buffer.

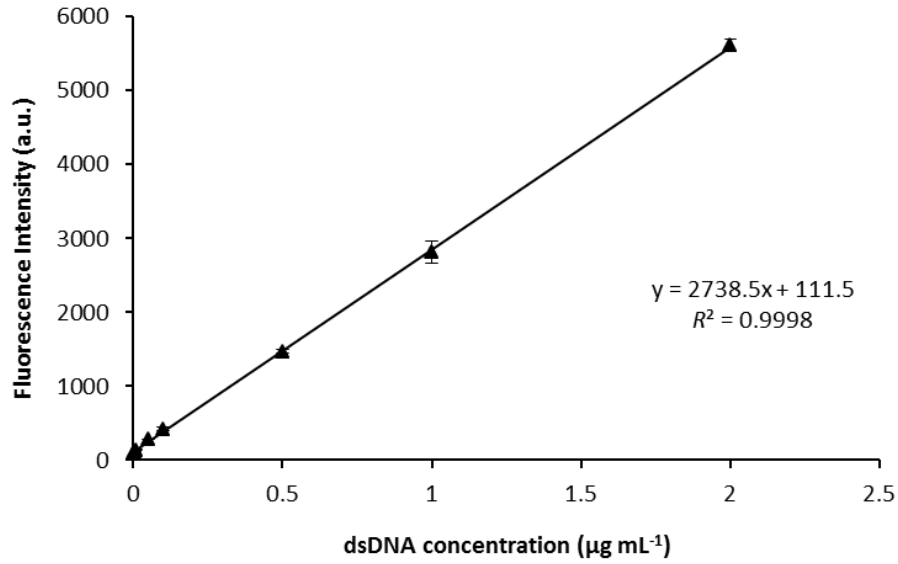


**Figure 5.2.** Calibration curve for the determination of dsDNA concentration of cells seeded onto PVPA-*co*-AA hydrogels. Mean  $\pm$  standard deviation ( $n = 3$ ).

The dsDNA concentration was quantified by using the calibration curve ( $R^2 > 0.999$ ) and equation 5.2:

$$\text{dsDNA concentration } (\mu\text{g mL}^{-1}) = \frac{\text{Fluorescence Intensity} - 111.5}{2738.5} \quad (5.2)$$

The cell number could then be estimated by assuming that each cell contains approximately 5 pg dsDNA<sup>197</sup> and using equation 5.3:

$$\text{Cell number} = \frac{M_{\text{dsDNA}}}{5 \times 10^{-6}} \quad (5.3)$$

where  $M_{\text{dsDNA}}$  is the mass of dsDNA in 1 mL lysis buffer.

### **5.2.12 Cell metabolic activity**

Metabolic activity was determined using the AlamarBlue® assay. Cells were cultured on the various hydrogels and tissue culture plastic (TCP) was used as a control. At certain time points (1, 3, 7 and 14 days) the culture medium was removed and samples were washed with sterile PBS. 1 mL of fresh culture medium was added along with 100 µL of AlamarBlue® solution (8.0 mg mL<sup>-1</sup> resazurin salt in PBS). The plates were incubated at 37 °C and 5% CO<sub>2</sub> for 4 h. The fluorescence was then measured at an excitation of 544 nm and an emission at 590 nm using a Fluostar Optima Fluorescence Microplate Reader (BMG Labtech, Germany). The fluorescence was recorded as a function of dsDNA content (measured using the PicoGreen® assay) to give an indication as to the metabolic activity relative to the number of cells.

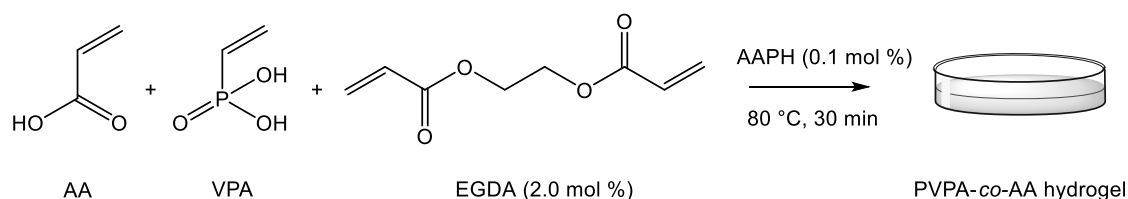
### **5.2.13 Statistical analysis**

Statistical evaluation of data was performed using GraphPad Prism™ software package. Tests were carried out in triplicate ( $n = 6$ ) and all data are reported as mean  $\pm$  standard deviation at a significance level of  $*p \leq 0.05$ ,  $**p \leq 0.01$ ,  $***p \leq 0.001$ . The data was tested for normality and a one-way analysis of variance (ANOVA) was carried out with the Tukey test to compare the groups of the SaOS-2 cell culture.

## 5.3 Results and Discussion

### 5.3.1 Synthesis and characterisation of PVPA-*co*-AA hydrogels

Hydrogels of poly(vinylphosphonic acid-*co*-acrylic acid) (PVPA-*co*-AA) were synthesised from AA and VPA monomers (Scheme 5.1). Water was used as a common solvent and AAPH was used as a water-compatible initiator at a concentration of 0.1 mol %, with respect to the total monomer concentration. The polymerisation was carried out at 80 °C to give the optimal decomposition of initiator. Ethylene glycol diacrylate (EGDA) was utilised as a difunctional crosslinking agent since it has previously been shown to be successful in the production of PVPA hydrogels.<sup>154</sup> The synthetic conditions were first investigated for the production of hydrogels with optimal properties for use in bone tissue scaffolds.



**Scheme 5.1.** Synthetic scheme for the production of PVPA-*co*-AA hydrogels from AA and VPA monomers, using EGDA as a crosslinking agent.

#### 5.3.1.1 Effect of crosslinker concentration

Firstly, the effect of crosslinker (EGDA) concentration on the properties of the hydrogels was investigated. Figure 5.3a shows the effect of EGDA concentration on the swelling of the hydrogels. The VPA content was maintained at 30 mol % in each case and the polymerisation was carried out for 30 min. It was found that the swelling decreased with an increase in crosslinker concentration. This is to be expected since a greater concentration of crosslinker leads to a more densely packed structure with less space available for water uptake. This is supported by the increase in the storage modulus ( $G'$ ) with increased EGDA concentration, as shown in Figure 5.3b, which

represents a reinforced crosslinked network. For applications in bone tissue scaffolds, it is important for the material to have a relatively high mechanical strength. However, a high porosity and a large degree of swelling are vital for cell infiltration and the transport of nutrients. Therefore, a delicate balance must be found between these two factors. An EGDA concentration of 2.0 mol % was chosen for the production of hydrogels with a good mechanical strength and a reasonable degree of swelling. This crosslinker concentration was used to produce hydrogels in subsequent work.

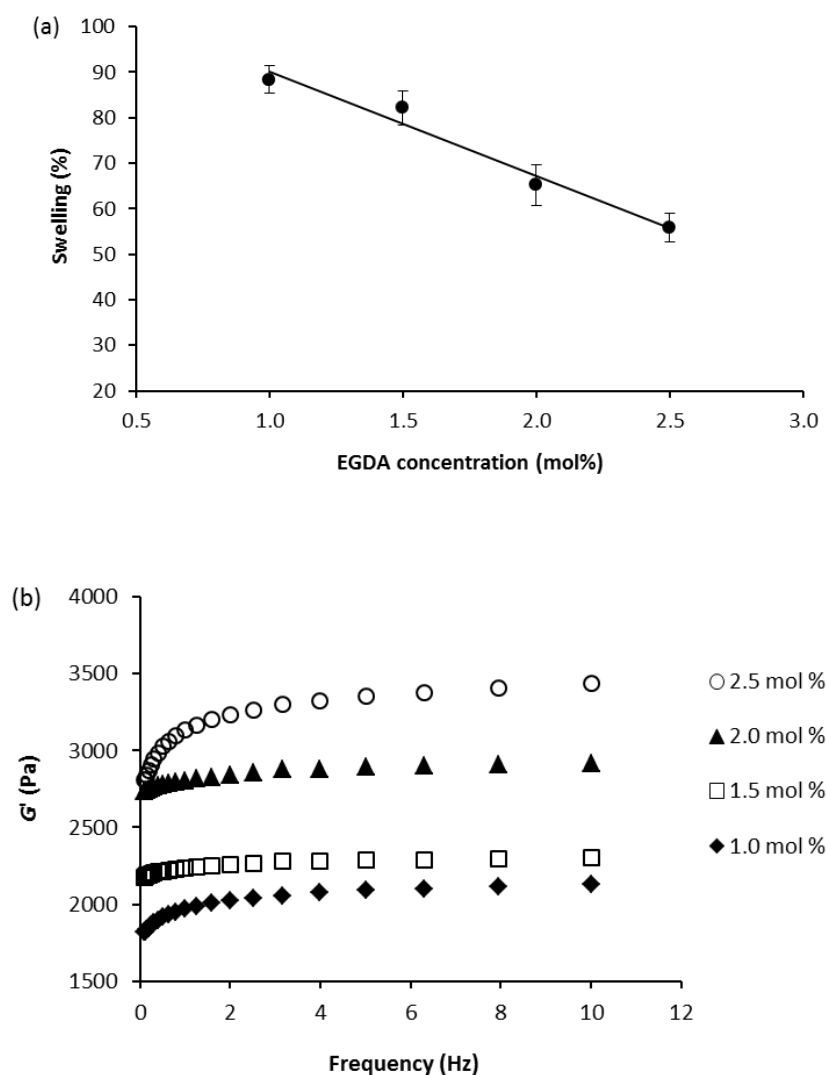


**Figure 5.3.** (a) Effect of crosslinker (EGDA) concentration on the dynamic swelling of PVPA-co-AA hydrogels in phosphate buffer solution at pH 7.3. (b) Effect of EGDA concentration on the storage ( $G'$ ) modulus of PVPA-co-AA hydrogels across a frequency range of 0.1 to 10 Hz. In each case, the VPA content was 30 mol %.

### 5.3.1.2 Effect of polymerisation time

Figure 5.4a shows the effect of polymerisation time on the dynamic swelling of PVPA-*co*-AA hydrogels. The VPA content was 30 mol % in each case. It can be observed that the swelling of the gels decreases with longer polymerisation times. This can be attributed to the increase in the degree of polymerisation with time, which leads to a more highly crosslinked structure. Therefore, there is less available space for water uptake and the swelling will decrease. The decrease in the swelling capacity is not linear and starts to level after 120 min. At this point, the hydrogel is fully polymerised and the extent of crosslinking cannot increase any further and so the swelling remains the same.

Figure 5.4b shows the effect of polymerisation time on the storage modulus ( $G'$ ) of PVPA-*co*-AA hydrogels. As expected, an increase in polymerisation time results in an increase in  $G'$ . As discussed previously, the higher degree of polymerisation leads to a greater extent of crosslinking, which reinforces the hydrogel network, causing an increase in  $G'$ . Again, a balance must be found between a high mechanical strength of the gels and a high degree of swelling. Therefore, a polymerisation time of 30 min was chosen to obtain hydrogels with optimal properties for cell adhesion.

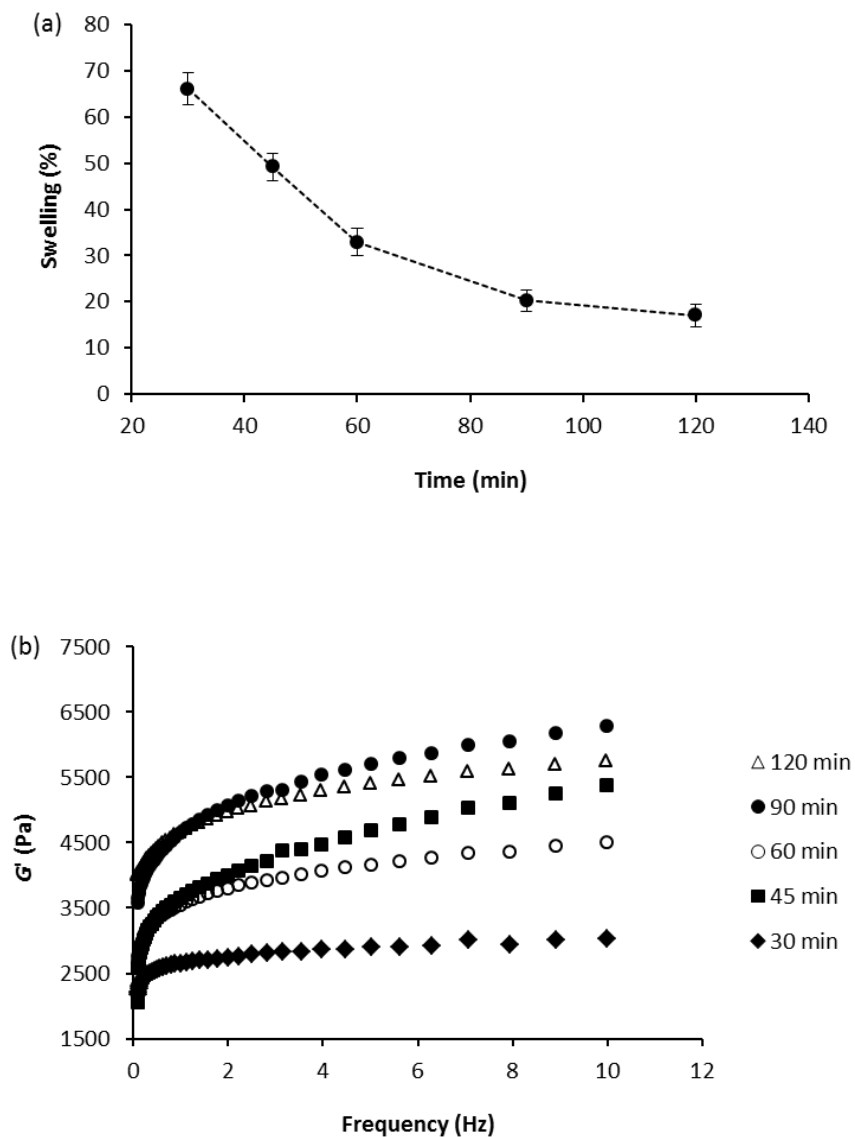


**Figure 5.4.** (a) Effect of polymerisation time on the dynamic swelling of PVPA-*co*-AA hydrogels in phosphate buffer solution at pH 7.3. (b) Effect of polymerisation time on the storage modulus ( $G'$ ) of PVPA-*co*-AA hydrogels across a frequency range of 0.1 to 10 Hz. In each case, the VPA content was 30 mol %.

### 5.3.1.3 Effect of monomer feed ratio

Using the optimised synthetic conditions, hydrogels were produced with VPA monomer feed contents of 0, 10, 30 and 50 mol % and copolymer compositions were calculated using elemental analysis data (Table 5.2) and equations 2.3 and 2.4. The copolymer ratio (VPA:AA) in the hydrogels differed slightly from the monomer feed ratios and this was more pronounced when the VPA content in the monomer feed was higher. This effect occurs as a result of the lower reactivity of VPA when compared with AA and thus, the incorporation of VPA into the hydrogels is reduced.

**Table 5.2.** Elemental analysis data for PVPA-*co*-AA hydrogels with different monomer feed ratios.

Sample Code	Monomer Feed Ratio (VPA:AA)	C (%)	H (%)	P (%)	Copolymer Ratio (VPA:AA)
VPA-0	0:100	46.8	6.09	0.00	0:100
VPA-10	10:90	44.1	5.96	2.60	7:93
VPA-30	30:70	36.4	5.91	8.08	24:76
VPA-50	50:50	31.2	5.89	12.6	41:59

The hydrogels were also characterised by FT-IR spectroscopy (Figure 5.5). It can be observed that all hydrogels exhibit characteristic signals between 2800 and 2400  $\text{cm}^{-1}$ , representing the O-H stretch of the acrylic acid and phosphonic acid side groups. The C-H stretch and bend signals are observed at 3000–2800 and 1500–1375  $\text{cm}^{-1}$ , respectively. The strong band at 1696  $\text{cm}^{-1}$  was attributed to the C=O stretch of the acrylic acid side group. This band is shifted to lower wavenumber than is expected for carboxylic acids due to the presence of hydrogen bonding within the polymer network. Furthermore, the signals which are observed at 1300–1050  $\text{cm}^{-1}$ , of medium-strong intensity, denote the C-O stretch of the same group. When VPA is incorporated into the hydrogels, as in the spectra of (b), (c) and (d), two new bands appear between 1090 and 905  $\text{cm}^{-1}$  (indicated on Figure 5.5), which represent the P-O stretch of the phosphonic acid side group. These signals increase in intensity as the VPA content in the feed is increased. Therefore, this provides strong evidence for the successful synthesis of PVPA-*co*-AA hydrogels, with increasing VPA contents.

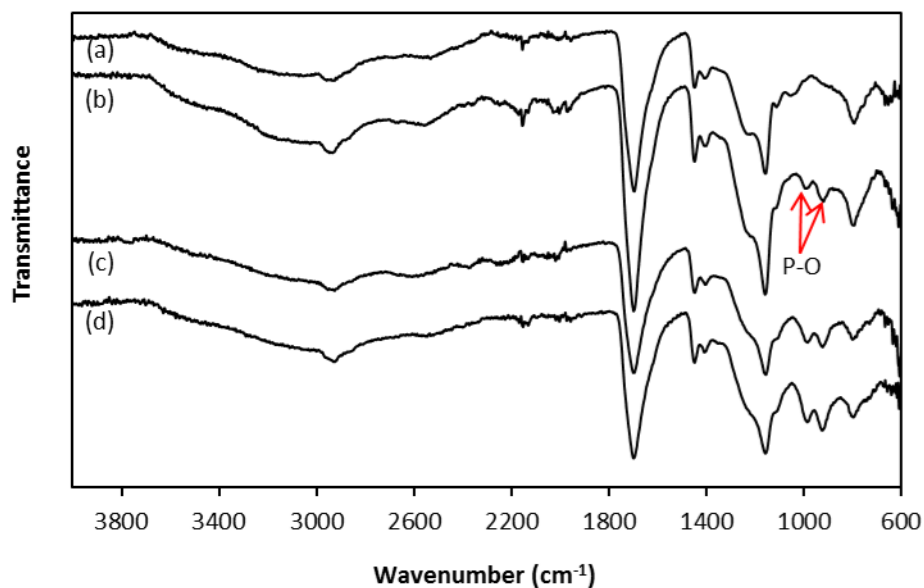


**Figure 5.5.** FT-IR spectra of (a) VPA-0, (b) VPA-10, (c) VPA-30 and (d) VPA-50.

### 5.3.2 Swelling capacity of PVPA-*co*-AA hydrogels

The swelling behaviour of hydrogels in response to external stimuli, such as pH and ionic strength, can give an indication as to their effectiveness in biomaterials applications. Therefore, in this study, the swelling of the hydrogels was determined gravimetrically in phosphate buffer solutions of pH 5.0, 7.3 and 9.0.

As can be seen in Figure 5.6, the swelling increased with an increase in VPA content in the hydrogels. This can be attributed to the properties of the respective homopolymers. Both PAA and PVPA are negatively-charged polyelectrolytes; PAA is considered to be a weak polyelectrolyte ( $pK_a \sim 4.50$ ),<sup>198</sup> whereas PVPA has been described as medium-strong ( $pK_a \sim 2.75$ ).<sup>153</sup> This means that there is greater dissociation of phosphonic acid groups in aqueous media, resulting in enhanced electrostatic repulsions within the polymer network and hence, an increase in the swelling of the gels. It is hypothesised that a greater degree of swelling will result in optimal cell infiltration and transport of nutrients, waste products and growth factors.<sup>199, 200</sup> Furthermore, the degree of ionisation of the hydrogel may affect the transport and adsorption of charged molecules, such as proteins.<sup>131</sup>

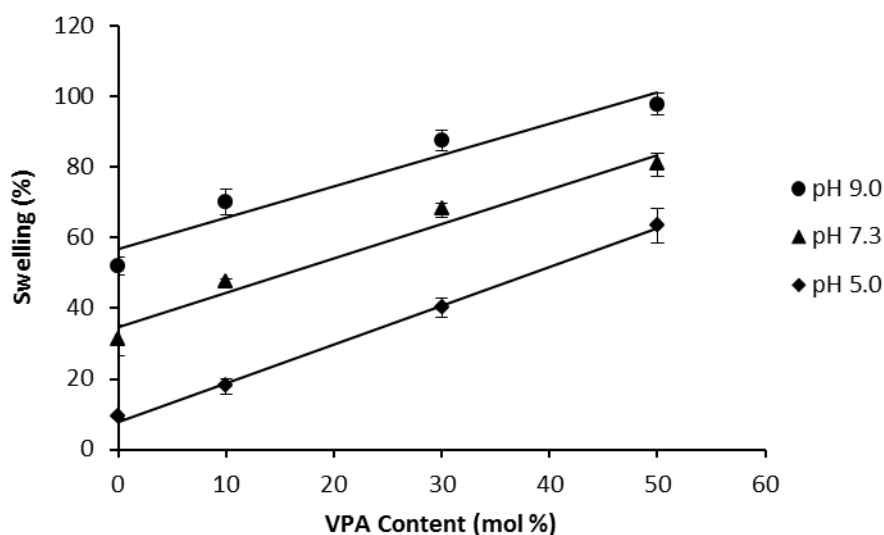


**Figure 5.6.** Swelling of PVPA-*co*-AA hydrogels as a function of VPA content, at pH 5.0, 7.3 and 9.0. Lines are added as a guide to the eye.

An increase in the pH of the buffer solution also resulted in greater swelling capacities (Figure 5.6). Buffer solutions with higher pH values promote enhanced ionisation of carboxylic and phosphonic acid groups and thus, increased electrostatic repulsions occur which leads to greater swelling of the hydrogels.

### 5.3.3 SEM analysis

PVPA-*co*-AA hydrogels were freeze-dried and then investigated using a scanning electron microscope (SEM). A difference in their physical morphology can be observed with different monomer feed compositions (Figure 5.7). It can be seen that the freeze-dried hydrogel composed of poly(acrylic acid) (VPA-0) has a flaky structure, whereas the addition of low amounts of VPA, such as in VPA-10, produced a porous structure with an average pore diameter of  $49 \pm 20 \mu\text{m}$ . Freeze-dried hydrogels with higher VPA contents formed structures with larger pores and an interconnected pore network. For example, VPA-30 hydrogels had an average pore diameter of  $84 \pm 37 \mu\text{m}$  and for VPA-50, the average diameter was  $100 \pm 32 \mu\text{m}$ .

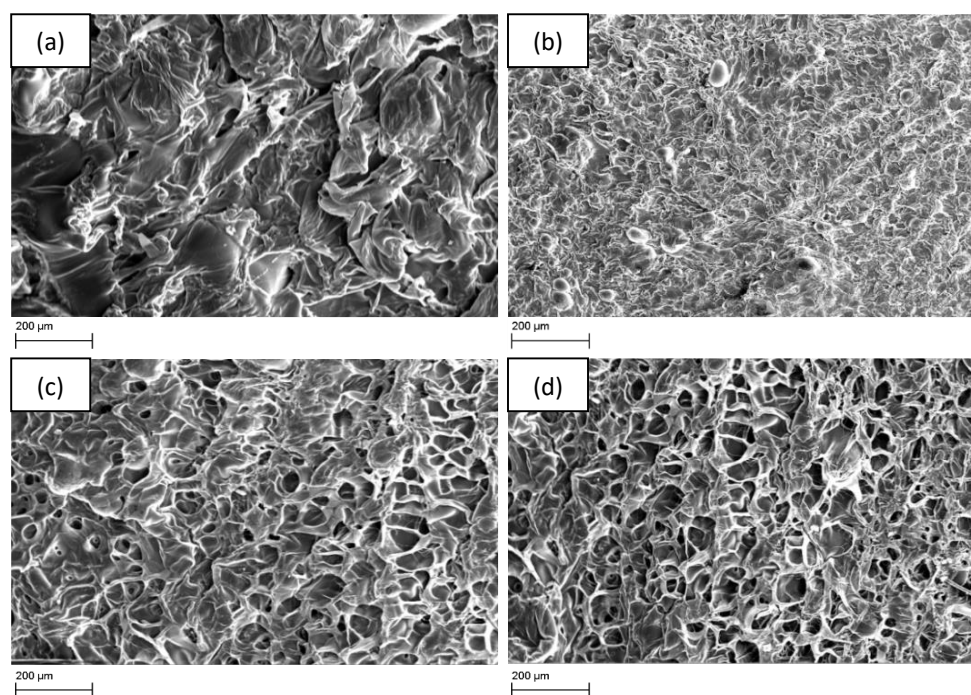


**Figure 5.7.** Scanning electron microscope (SEM) images to show the difference in morphology of freeze-dried PVPA-*co*-AA hydrogels with increasing VPA contents. (a) VPA-0, (b) VPA-10, (c) VPA-30 and (d) VPA-50.

The morphology of the freeze-dried hydrogels, observed under SEM, can be attributed to their hierarchical porous structure, depicted in Figure 5.8. The hydrogel network is formed due to crosslinks between polymer chains. The spaces between polymer chains are on the nanoscale and allow the infiltration of water, which results in swelling of the gels. As the hydrogels swell, there is an increase in the size of the nanopores. This effect is greater for gels that contain higher VPA contents, owing to the increased acidity of VPA when compared with AA.

However, micropores are also observed in the structure of freeze-dried hydrogels with VPA contents of 30 and 50 mol %. It is suggested that the low reactivity of VPA in the polymerisation system results in a low degree of crosslinking and inhomogeneously distributed crosslinks with dangling chain ends. This creates large voids in the hydrogel structure, which allows the infiltration of large droplets of water. This results in the creation of the microscale pores observed in the freeze-dried samples. These larger pores are not observed in the structure of VPA-0 due to the high degree of crosslinking. Therefore, the swelling of VPA-0 is purely as a result of the infiltration of water into the nanoscale pores between polymer chains.

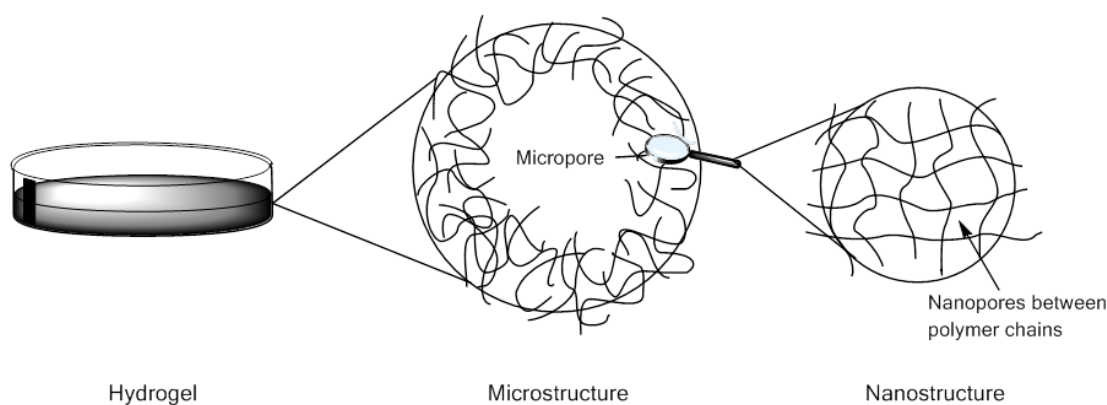


**Figure 5.8.** Schematic representation of the hierarchical structure of hydrogels with both micro- and nanoscale pores.

The porosity and pore architecture of hydrogels used in bone tissue engineering play a significant role in cell adhesion, migration and proliferation. A high degree of porosity is required for angiogenesis to occur, which is a key requirement for vascularised tissue. Furthermore, the extent of ECM secretion increases by increasing the pore size within the microstructure of three-dimensional scaffolds.<sup>195</sup> It has been noted that a pore size of 100-350  $\mu\text{m}$  is ideal for bone regeneration.<sup>201, 202</sup> Therefore, it can be hypothesised that VPA-30 and VPA-50 will be the most effective for this application owing to their structure and average pore diameter. Although there are differences between the freeze-dried and swollen hydrogels, the pore size is still likely to be greater in VPA-30 and VPA-50 gels when swollen in cell culture media. Furthermore, the structure of these gels is believed to be very similar to the native extracellular matrix (ECM) of bone.

### 5.3.4 Water contact angle measurements

The difference in the swelling capacity of PVPA-*co*-AA hydrogels, as a function of VPA content, can be further explained by the change in hydrophilicity of the gels. The wettability of PVPA-*co*-AA hydrogels was determined by water contact angle measurements (Figure 5.9). The contact angle is defined as the angle formed by a liquid at the three phase boundary where a liquid, gas and solid intersect. This is represented by the dashed lines on Figure 5.9 for the different hydrogels. It is generally accepted that if the contact angle is less than 90°, the water droplet spreads out and the surface

can be described as being hydrophilic. Contact angles of greater than  $90^\circ$  show that the surface is non-wetting, i.e. hydrophobic.

The results suggest that all of the PVPA-*co*-AA hydrogels are hydrophilic, as proven by contact angles of less than  $90^\circ$ . Furthermore, it was found that the water contact angle decreases with increasing VPA content from  $79.2 \pm 2.2^\circ$  for VPA-0 hydrogels to  $38.0 \pm 1.3^\circ$  for VPA-50 hydrogels (Table 5.3). Hence, it can be concluded that the incorporation of greater amounts of VPA significantly increases the wettability of the hydrogels. The phosphonic acid groups of VPA can exhibit greater hydrogen bonding with water than the carboxylic acid groups of AA, owing to the increased electronegativity. Thus, the surface becomes more hydrophilic, which will lead to enhanced water uptake into the polymer network.

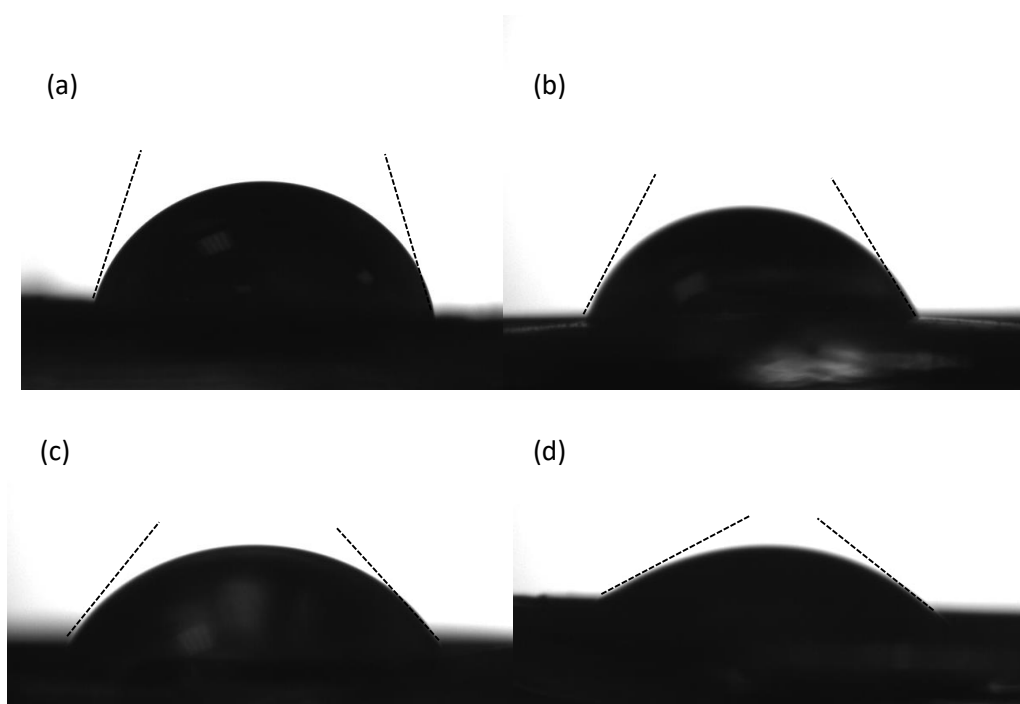


**Figure 5.9.** Photograph images of 10  $\mu\text{L}$  water droplet on (a) VPA-0, (b) VPA-10, (c) VPA-30 and (d) VPA-50 hydrogels ( $n = 3$  different hydrogel samples).

The hydrophilic surface of PVPA-*co*-AA hydrogels, coupled with their strong negative charge can allow the adsorption of positively-charged extracellular matrix proteins *in vivo*, which helps to modulate cell adhesion and consequently cell biochemical mechanisms via interactions with cell-surface molecules, such as integrins.<sup>203</sup> It has

been demonstrated that VPA can attract positively-charged proteins from cell culture media, which, in turn, led to enhanced SaOS-2 cell adhesion and proliferation.<sup>203</sup> Therefore, it is expected that hydrogels with higher VPA contents will lead to greater cell adhesion and proliferation.

**Table 5.3.** Water contact angle of PVPA-*co*-AA hydrogels with increasing VPA content.

Sample Code	Monomer Feed Ratio	Water Contact Angle (°)
VPA-0	0:100	79.2 ± 2.2
VPA-10	10:90	67.8 ± 1.3
VPA-30	30:70	57.4 ± 1.4
VPA-50	50:50	38.0 ± 1.3

### 5.3.5 Rheology

Another important property of hydrogels is their rheological behaviour. While it is important to have high porosities and swelling characteristics, hydrogels should also have sufficient mechanical integrity to provide an ECM-like architecture. Furthermore, it is desirable to produce flexible hydrogels that may be moulded into the shape of the bone defect site in a clinical setting.

Figure 5.10 shows the change in storage ( $G'$ ) and loss ( $G''$ ) modulus for PVPA-*co*-AA hydrogels with increasing frequency of oscillation. It was found that an increase in VPA content in the hydrogels led to a decrease in  $G'$  and a general increase in  $G''$ , indicating the dominance of viscous fluid behaviour in gels with high VPA contents. This behaviour is expected since the water content increases proportional to the amount of VPA in the hydrogels.

The difference in mechanical properties of the hydrogels can be explained as a result of the differences in the structure of the gels with increasing VPA contents, as shown in Figure 5.8. It has been shown that hydrogels with lower VPA contents, i.e. VPA-0 and VPA-10, have a higher mechanical strength, which may be attributed to the higher degree of crosslinking and more uniform structure of these gels. VPA-30 and VPA-50 gels demonstrated more viscous fluid behaviour as a result of their greater swelling capacities and highly porous structure. Hydrogels with higher VPA contents consist of inhomogeneously distributed crosslinks with dangling chain ends and large micropores.

This may contribute to the lower mechanical strength of VPA-30 and VPA-50 gels. Therefore, these results suggest that VPA-0 and VPA-10 hydrogels would be more suitable for load-bearing applications.

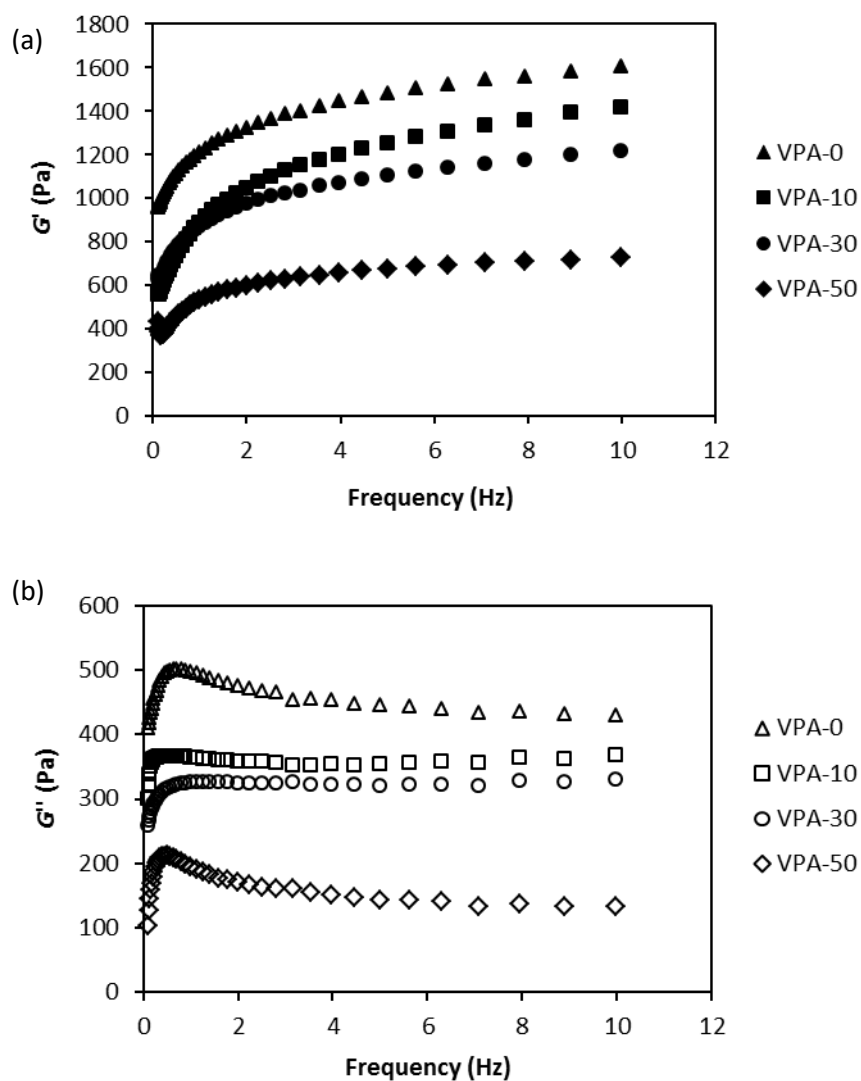


**Figure 5.10.** (a) Storage ( $G'$ ) and (b) loss ( $G''$ ) modulus of PVPA-*co*-AA hydrogels, with different copolymer compositions, across a frequency sweep of 0.1 to 10 Hz.

Figure 5.11 shows the change in complex viscosity ( $\eta^*$ ) across a frequency range of 0.1 to 10 Hz. The complex viscosities of the hydrogels all show a decrease with an increase in frequency, which indicates pseudoplastic behaviour of the materials. This decrease in  $\eta^*$  represents a deformation of the network structure of the hydrogels at high

frequencies of shear strain. The complex viscosity is lower for hydrogels with higher VPA contents, which suggests a weaker network structure, corroborating the results presented above.

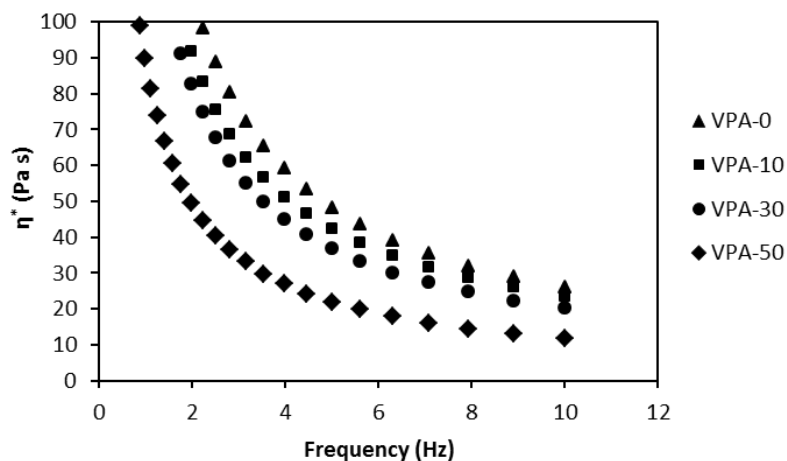


**Figure 5.11.** Change in complex viscosity ( $\eta^*$ ) of PVPA-*co*-AA hydrogels, with different copolymer compositions, across a frequency sweep of 0.1 to 10 Hz.

The change in  $G'$  and  $G''$  with increasing strain is presented in Figure 5.12 for all of the PVPA-*co*-AA hydrogels. The  $G'$  and  $G''$  crossover point, where viscous fluid behaviour starts to dominate over elastic behaviour, gives an indication as to the yield strain of the materials. This point occurs at a strain rate of 60% for VPA-0 and 80% for VPA-10. For VPA-30 and VPA-50 hydrogels, this point is not reached within the strain range of this experiment. This indicates that hydrogels with lower or no VPA content are more brittle, with their crosslinked structure being broken down under lower values of strain. VPA-30 and VPA-50 hydrogels are more flexible and are thus able to resist high values of strain before failure.

It is suggested that although VPA-0 and VPA-10 gels demonstrate greater mechanical integrity, their highly crosslinked structure will allow for little cell infiltration. Hydrogels with higher VPA contents (VPA-30 and VPA-50) demonstrate superior swelling capacities and greater porosities, offering a better mimic of the native ECM. Furthermore, the ductile behaviour of these hydrogels will allow them to be moulded into a bone defect site. The gels can then be reinforced by a support material to increase the mechanical strength of the implant for use in load-bearing applications.

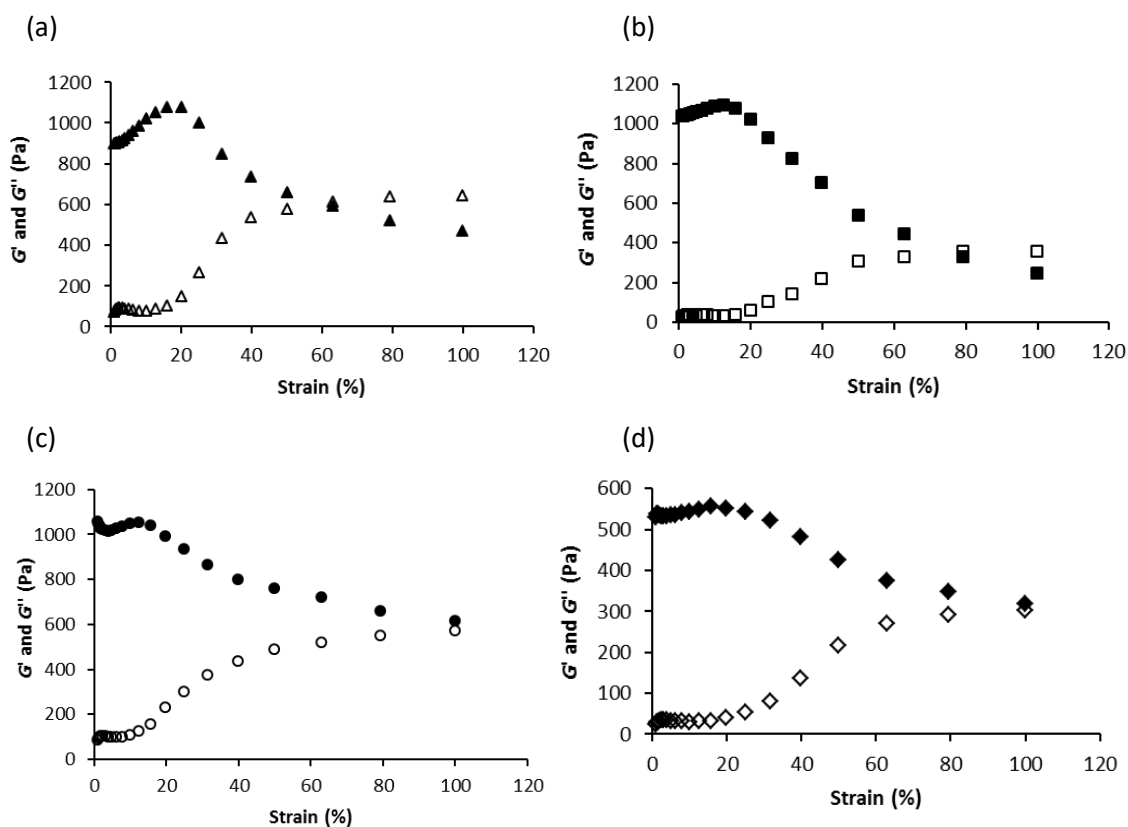


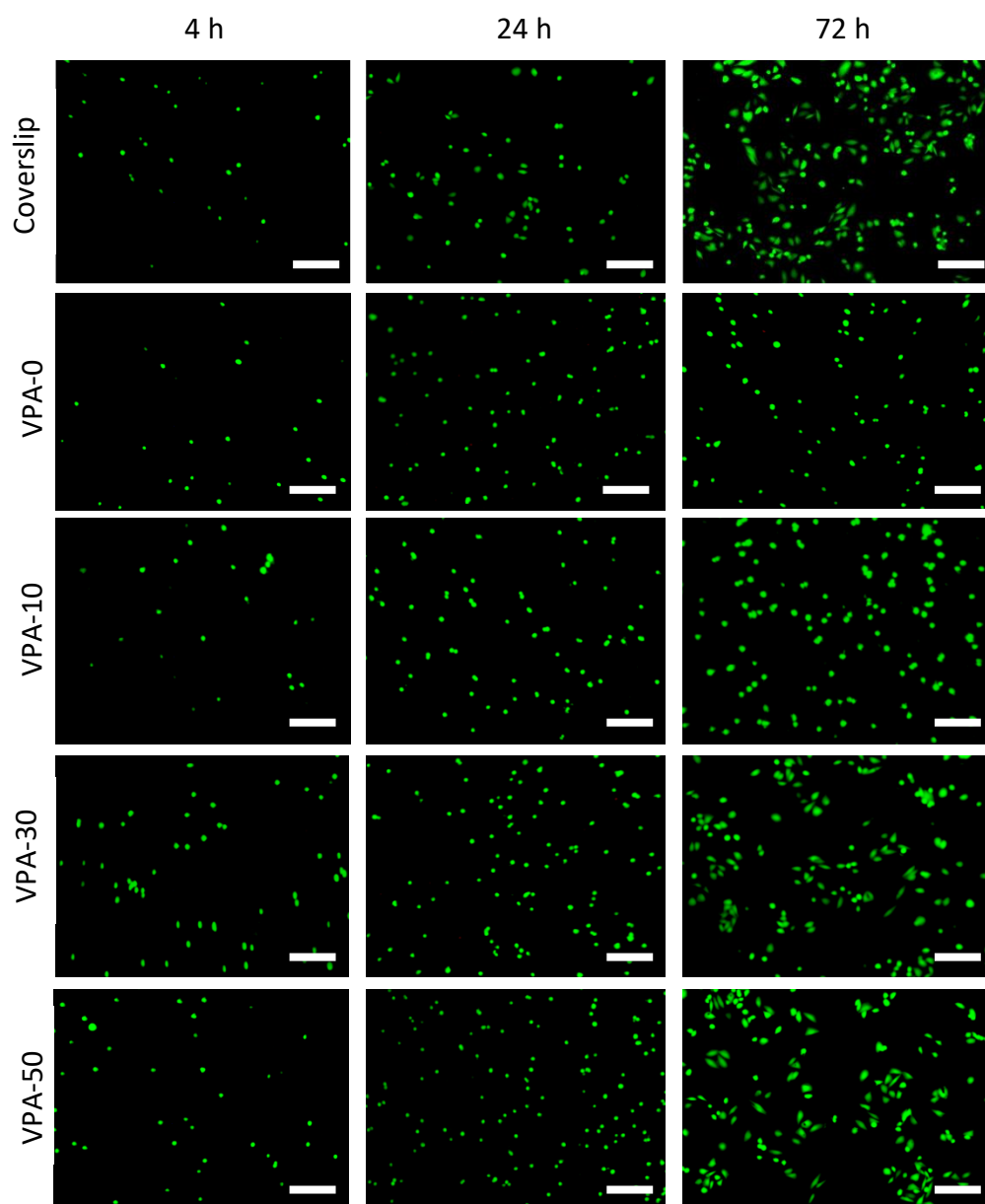
**Figure 5.12.** Storage ( $G'$ ) and loss ( $G''$ ) modulus of PVPA-*co*-AA hydrogels, with different copolymer compositions, across a strain range of 1.0-100%. (a) VPA-0, (b) VPA-10, (c) VPA-30 and (d) VPA-50.  $G'$  is represented by closed symbols and  $G''$  is represented by open symbols.

### 5.3.6 Cell proliferation and metabolic activity

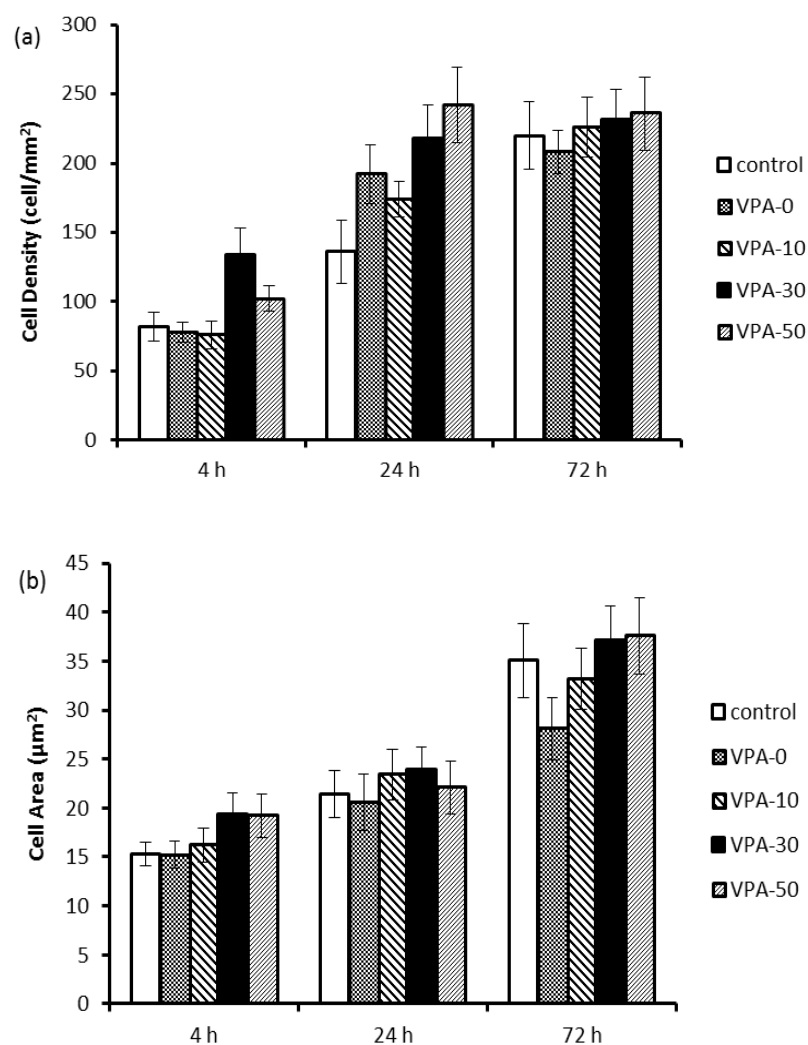
The effect of VPA content on the osteoblast response to PVPA-*co*-AA hydrogels was investigated. Live/Dead® cell staining was used to study osteoblast viability for up to 72 h of cell culture (Figure 5.13). Tests were performed in accordance with international standard ISO 10993-5 for *in vitro* cytotoxicity for the biological evaluation of medical devices.<sup>204</sup> The attachment and proliferation of live (green) SaOS-2 cells can be visualised on all hydrogels, with a complete lack of dead (red) cells. This confirms the biocompatibility of PVPA-*co*-AA hydrogels, which was not affected by copolymer composition. However, the density and morphology of the growing cells differed depending on the VPA content in the gels. A general increase in cell proliferation was found on hydrogels with higher VPA contents. Furthermore, VPA-0 and VPA-10 hydrogels showed little cell spreading, whereas cells seeded onto VPA-30 and VPA-50 gels demonstrated enhanced spreading morphologies after 72 h in culture medium. At this point, cell spreading was comparable to that of the control.

Figure 5.14 shows the cell density (cell/mm<sup>2</sup>) and average cell area (µm<sup>2</sup>) of SaOS-2 cells seeded onto PVPA-*co*-AA hydrogels, quantified using ImageJ analysis. Figure 5.14a shows that there was a general increase in cell proliferation with increasing VPA content. This effect is more pronounced at 4 h and 24 h. At 4 h, VPA-30 shows significantly higher cell proliferation than any of the other substrates. This demonstrates that the cells initially grew more rapidly on this hydrogel. At 24 h, VPA-30 and VPA-50 hydrogels demonstrated rapid cell proliferation, which was significantly higher than that of the control. After 72 h the cells had reached confluence on all of the substrates. Therefore, it can be postulated that VPA-30 and VPA-50 hydrogels are associated with the most rapid cell proliferation and may also form mineralised tissue sooner.

Furthermore, enhanced cell spreading was observed on hydrogels with higher VPA contents (Figure 5.14b). At 4 h and 24 h, there was no significant difference in cell spreading between hydrogels with different compositions. However, at 72 h, a clear increase in cell area can be seen with an increase in VPA content, which confirms the superior cell spreading capabilities of these hydrogels.



**Figure 5.13.** Live/Dead® imaging of human osteoblast (SaOS-2) cells to illustrate cell viability on PVPA-*co*-AA hydrogels, as a function of copolymer composition, over 72 h. Glass coverslips were used as a control. Live cells stained green, dead cells stained red.  $n = 6$ , scale bar 100  $\mu\text{m}$ .



**Figure 5.14.** (a) Osteoblast proliferation and (b) cell spreading on PVPA-co-AA hydrogels, with increasing VPA content, over 72 h. Mean  $\pm$  SD,  $n = 6$  triplicates.

The increased cell adhesion and proliferation on VPA-30 and VPA-50 hydrogels can be attributed to the increase in swelling and porosity of the gels, which results in enhanced cell infiltration. In addition, gels with higher VPA contents are more hydrophilic, as confirmed by a decrease in water contact angle (Figure 5.9). The hydrophilic surface, coupled with the strong negative charge of these gels can attract extracellular matrix proteins, which can help to modulate cell attachment and spreading.<sup>131, 203</sup> The increase in cell adhesion was confirmed in Figure 5.15, where there was an increase in cell number as a function of VPA content, up to 7 days of culture. By day 14, the highest cell number was observed on VPA-30 gels, although the difference between hydrogels was not statistically significant ( $p > 0.05$ ). It can be concluded that all cells had reached confluence after 14 days.

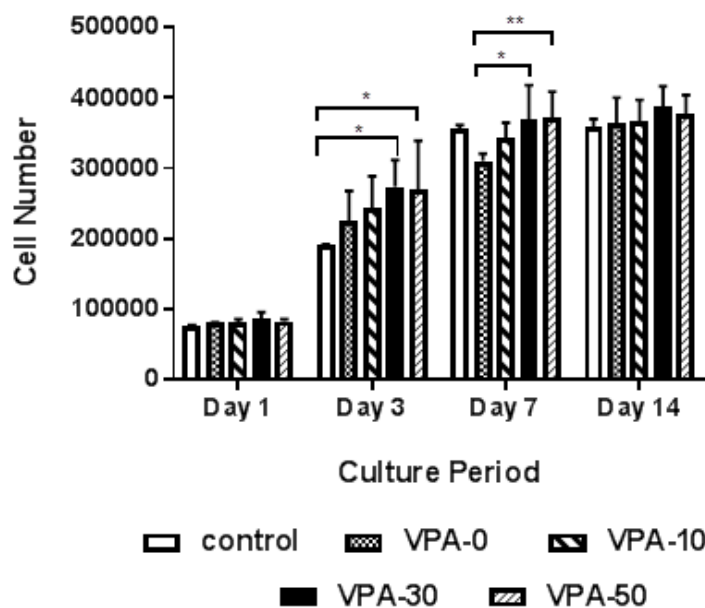


**Figure 5.15.** Osteoblast proliferation on PVPA-*co*-AA hydrogels, with increasing VPA content, over 14 days. Mean  $\pm$  SD,  $n = 6$  triplicates ( $*p \leq 0.05$ ,  $**p \leq 0.01$ ,  $***p \leq 0.001$ ).

The metabolic activity of SaOS-2 cells, seeded onto PVPA-*co*-AA hydrogels, was measured using the AlamarBlue® assay. The data are represented in Figure 5.16 as raw fluorescence intensity (Figure 5.16a) and as a function of dsDNA concentration, calculated using the PicoGreen® assay (Figure 5.16b). This gives an indication of the metabolic activity relative to the number of cells present. At day 1, there was a clear increase in cell metabolic activity with higher VPA contents. SaOS-2 cells growing on VPA-30 and VPA-50 hydrogels demonstrated the highest metabolic activities, which were comparable to that of the control. This suggests that these cells can more easily perform essential functions such as the transport of nutrients and removal of waste and this, in turn, will lead to more rapid cell growth and proliferation.

However, at days 3, 7 and 14, there was no significant difference between the different hydrogels. This indicates that at this point the metabolic activity is proportional to the cell number. Therefore, after 3 days of culture, the hydrogels have no significant effect on the cell metabolic activity.

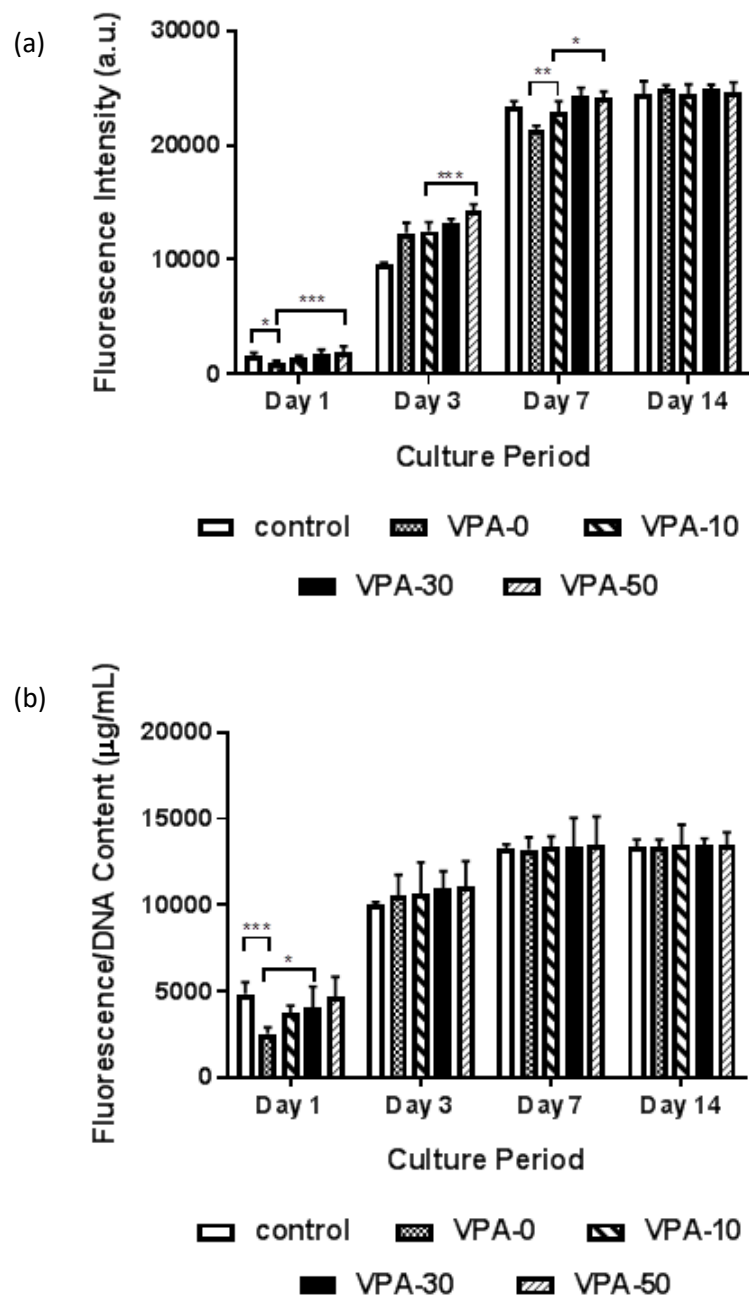


**Figure 5.16.** (a) Fluorescence intensity of SaOS-2 cells (measured using the AlamarBlue® assay) and (b) osteoblast metabolic activity on PVPA-co-AA hydrogels, with increasing VPA content, over 14 days. Mean  $\pm$  SD,  $n = 6$  triplicates ( $*p \leq 0.05$ ,  $**p \leq 0.01$ ,  $***p \leq 0.001$ ).

## 5.4 Conclusions

In this study, hydrogels of poly(vinylphosphonic acid-*co*-acrylic acid) have been produced and investigated for their potential use in bone tissue scaffolds. Firstly, the effect of crosslinker (EGDA) concentration and polymerisation time on the swelling and rheological properties of the gels was investigated. It was found that an increase in crosslinker concentration or polymerisation time led to hydrogels with greater mechanical strength but lower swelling capacities. Therefore, it is likely that the best compromise would be a material with sufficient mechanical integrity and a high enough porosity to allow for cell infiltration and nutrient exchange. Thus, hydrogels were produced with an EGDA concentration of 2.0 mol % and the polymerisation was performed for 30 min.

The effect of monomer feed ratio on the properties of the hydrogels was then explored. It was found that an increase in VPA content led to greater hydrogel swelling, which may be attributed to enhanced electrostatic repulsions between polymer chains. Hydrogels with higher VPA contents resulted in a hierarchical hydrogel structure with microscale pores, as confirmed by SEM analysis of the freeze-dried samples. Hydrogels with 30 and 50 mol % VPA contents were shown to have similar morphologies to the native ECM of bone. The increase in swelling capacity was thought to be partly influenced by the greater hydrophilicity of VPA when compared with AA. This was proven by water contact angle testing. The contact angle decreased on hydrogels with greater amounts of VPA.

Natural bone is both porous and mechanically durable. Therefore, when designing bone tissue scaffolds, it is important to have high porosities and swelling characteristics as well as sufficient mechanical strength to provide an ECM-like architecture. It was found that hydrogels with lower VPA contents, i.e. VPA-0 and VPA-10 had a greater mechanical strength, which was attributed to their higher degree of crosslinking. VPA-30 and VPA-50 gels demonstrated more viscous fluid behaviour as a result of their greater swelling capacities and highly porous structure (Figure 7). This implies that VPA-0 hydrogels would be more suitable for load-bearing applications. However, VPA-30 and VPA-50 gels were shown to be more ductile and could resist large amounts of strain without permanent deformation of their structure. This is desirable for clinical applications where they can be moulded into a bone defect site.

An increase in SaOS-2 cell adhesion and proliferation was observed on hydrogels with 30 and 50 mol % VPA contents. It was found that cells proliferated much more rapidly on these hydrogels, which suggests that they are likely to form mineralised tissue sooner, which will enhance the rate of bone regeneration. Additionally, cells that were seeded onto VPA-30 and VPA-50 hydrogels demonstrated superior spreading morphologies, comparable to that of the control. This was attributed to the increase in swelling and porosity of these gels, which, can lead to enhanced protein adsorption to facilitate cell attachment and proliferation.

The metabolic activity of the SaOS-2 cells was measured relative to the number of cells. Initially, the cell metabolic activity was higher on VPA-30 and VPA-50 hydrogels, which will allow for transport of nutrients and removal of waste as well as enhancing the rate of cell proliferation. However, after 3 days, there was no significant difference between metabolic activity on hydrogels with different VPA contents, which indicates that the metabolic activity is proportional to the cell number.

This work suggests that hydrogels with 30 or 50 mol % VPA are ideal for use in bone tissue scaffolds. The hydrophilic nature of these gels encourage high swelling, which allows for increased cell attachment and proliferation. Furthermore, the structure of these hydrogels provides the ideal mechanical properties for use in bone defect sites to promote repair and regeneration. In addition, this work shows that the mechanical and cell adhesion properties of the gels can be tuned by altering the copolymer composition.

## Chapter 6: PVPA-co-AA for fluoride removal from groundwater

### 6.1 Introduction

The presence of fluoride ions in drinking water can lead to both beneficial and detrimental effects on health, depending on the relative quantities. Ingestion of low fluoride concentrations ( $1.0\text{-}1.5\text{ mg L}^{-1}$ ) can help to protect against dental caries.<sup>205</sup> However, excessive fluoride ingestion at concentrations above  $1.5\text{ mg L}^{-1}$  can lead to dental fluorosis: a developmental disturbance that makes tooth enamel more porous. It has been suggested that long-term exposure to fluoride concentrations above  $3\text{ mg L}^{-1}$  can result in skeletal fluorosis, a debilitating illness which is characterised by severe joint pain and crippled limbs.<sup>205</sup>

#### 6.1.1 Dental fluorosis

Although the exact mechanism of fluorosis is unknown, it has been suggested that fluoride may affect the cell/matrix/mineral interactions as the teeth are forming.<sup>206, 207</sup> Fluoride appears to enhance mineral precipitation in forming teeth, resulting in hypermineralised bands of enamel, which are then followed by hypomineralised bands. The white opaque appearance of fluorosed enamel is caused by a hypomineralised enamel surface (Figure 6.1). More severe dental fluorosis causes pitting and a loss of the enamel surface, leading to staining and discolouration. Specific cellular effects of fluoride, including effects on the ameloblasts (enamel forming cells), have also been implicated in dental fluorosis. However, more research is needed to determine the exact mechanism for the formation of fluorosed teeth.

Dental fluorosis is a serious problem in places such as India, Tanzania and parts of North Africa, where groundwater is the principal source of drinking water. In some regions of Tanzania, fluoride concentrations as high as  $45\text{ mg L}^{-1}$  have been reported.<sup>208</sup> Groundwater contamination arises primarily due to weathering of igneous and sedimentary rocks. The most common fluoride bearing minerals are fluorite ( $\text{CaF}_2$ ), cryolite ( $\text{Na}_3\text{AlF}_6$ ) and fluorosilicates, e.g. sodium fluorosilicate ( $\text{Na}_2[\text{SiF}_6]$ ) and ammonium fluorosilicate ( $(\text{NH}_4)_2\text{SiF}_6$ ). In addition, many phosphate fertilisers contain

fluoride as an impurity, which is leached into the groundwater as a result of heavy rainfall.

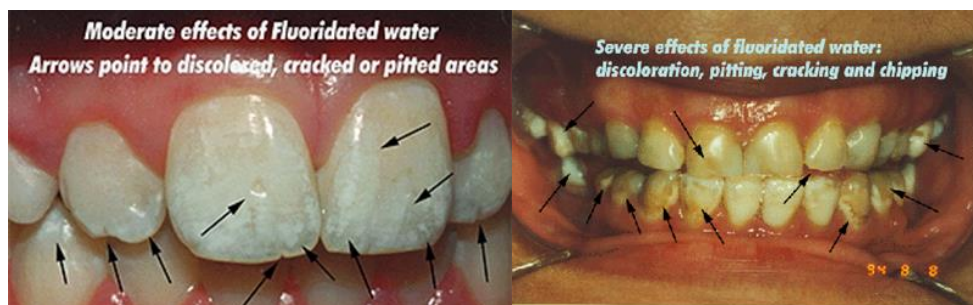


**Figure 6.1.** Moderate and severe effects of dental fluorosis as a result of fluoridated water.

### 6.1.2 Current methods for fluoride removal

There are many possible techniques for the removal of fluoride ions from groundwater. These can be broadly classified into two categories, namely membrane and adsorption techniques. Membrane techniques comprising reverse osmosis and nanofiltration are briefly discussed in the following section.

Reverse osmosis (RO) is the process of forcing a solvent (water) from a region of high solute concentration, through a semipermeable membrane, to a region of low solute concentration. This is achieved by applying a pressure in excess of the osmotic pressure to the concentrated side of the membrane. Reverse osmosis has a high efficiency of around 98% for fluoride removal.<sup>209</sup> However, it is not a selective technique, which means that all of the ions present are removed.

Nanofiltration makes use of the same overall technique as reverse osmosis,<sup>210, 211</sup> although the semipermeable membrane contains larger pores and offers less resistance to the passage of both solvent and solute molecules. As a result, the pressures required are lower, flows are faster and the removal of solutes is much less exhaustive. The main advantage of nanofiltration over RO is the greater selectivity of the former technique as a result of solute retention. Retention of solutes is attributed mainly to steric and charge effects.<sup>212, 213</sup> Despite the small size of fluoride ions, they are very strongly hydrated due to their high charge density. The consequent steric effects of this hydration shell leads to

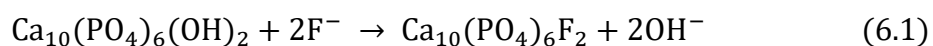
a high retention of fluoride ions when compared with other monovalent ions such as chloride or nitrate.

The main advantages of membrane process are: very high removal capacity, one step purification and no chemical usage. However, these techniques are not entirely appropriate since all ions are removed from the water and so remineralisation is required. Moreover, the initial cost of the membranes is very high and disposal of concentrated fluoride sludge can be a major problem.

### 6.1.3 Common adsorbents

Although membrane methods have been successful in reducing fluoride concentrations to acceptable levels, surface adsorption is still a desirable alternative due to its lower cost and greater accessibility. Adsorption is a simple technique with moderate efficiencies (up to 90%). However, the efficiency is strongly dependent on the capacity of the adsorbent as well as on the pH of the medium. Furthermore, regeneration of the adsorbent may reduce its capacity and thus decrease its efficiency.

A wide range of adsorbents have been tested for fluoride uptake, including zeolites,<sup>214</sup> activated alumina<sup>215</sup> and titanium hydroxide.<sup>216</sup> Stanić *et al.*<sup>217</sup> have conducted a comprehensive review of the many and varied materials that have been investigated for fluoride removal from groundwater. The most widely used and commercially available adsorbent is bone char.<sup>218, 219</sup> Bone char is a porous, granular material produced by the carbonisation of animal bones. It consists mainly of hydroxyapatite (HA), calcium carbonate and activated carbon. Bone char works by ion exchange adsorption between fluoride ions from the water and the hydroxyl groups of hydroxyapatite, as shown in equation 6.1:



Bone char is often used due to its low cost and availability. In a recent work, it was found that the adsorption capacity of bone char was approximately three times greater than those of activated alumina and activated carbon, both of which are commercially available.<sup>220</sup> However, the adsorption capacity is highly dependent on the pH of the solution. It has been found that the adsorption of fluoride onto bone char decreases significantly when the pH of the medium is increased from pH 3 to 12.<sup>220</sup> It has also been shown that the presence of other anions, such as  $\text{Cl}^-$ ,  $\text{NO}_3^-$  and  $\text{SO}_4^{2-}$  can compete

with the fluoride for adsorption sites of bone char, affecting the adsorption capacity of bone char toward fluoride ions.<sup>221</sup>

The active component of bone char, hydroxyapatite, has often been utilised as an adsorbent to improve the efficiency of fluoride uptake. It has been suggested that fluoride removal by HA occurs by both an ion-exchange process and adsorption onto the surface as a result of electrostatic interactions.<sup>222</sup> Therefore, the fluoride capacity has been shown to be dependent on solution pH, contact time and the presence of other competing anions.<sup>223</sup>

In recent years, there have been many attempts to create composite materials consisting of natural polymers, such as cellulose,<sup>224</sup> chitin<sup>225</sup> and chitosan,<sup>226</sup> with nano-hydroxyapatite powder. These composite materials have the advantage of a high specific surface area, imparted by the polymer, as well as the strong affinity for fluoride ions by hydroxyapatite. Studies have shown that the composite materials have a higher defluoridation capacity (DC) than hydroxyapatite alone.<sup>225, 226</sup> Furthermore, Sundaram *et al.*<sup>225</sup> have conducted a field study in a fluoride endemic area. Their results showed an almost complete reduction in the fluoride level without much alteration in other water quality parameters.

#### **6.1.4 Aims and Objectives**

It was the aim of this study to investigate the efficacy of a poly(vinylphosphonic acid-co-acrylic acid)-hydroxyapatite (PVPA-HA) composite hydrogel for fluoride removal from groundwater.

PVPA-HA hydrogels were produced and their fluoride uptake capacity was investigated and compared to that of hydroxyapatite alone.

The effects of solution pH, contact time and the presence of other ions on the fluoride uptake ability of the hydrogels were also explored.

Finally, regeneration of the PVPA-HA hydrogels was attempted by immersing into a solution of NaOH. The effect of repeated regeneration cycles on the defluoridation capacity of the gels was then investigated.

## 6.2 Experimental

### 6.2.1 Materials

All chemicals were used without further purification unless otherwise stated. Vinylphosphonic acid (VPA), (97%) was purchased from Tokyo Chemical Industry (TCI), U.K. Acrylic acid (AA), (99%), 2,2'-azobis(2-methylpropionamide) dihydrochloride (AAPH), (97%) and nano-hydroxyapatite (HA) powder (particle size < 200 nm) ( $\geq 97\%$ ) were all purchased from Sigma-Aldrich Ltd., U.K. Calcium chloride ( $\text{CaCl}_2$ ), sodium hydroxide (NaOH), sodium fluoride (NaF), sodium chloride (NaCl), sodium sulphate ( $\text{Na}_2\text{SO}_4$ ), sodium nitrate ( $\text{NaNO}_3$ ) and sodium bicarbonate ( $\text{NaHCO}_3$ ) were all purchased from ThermoFisher Scientific Ltd., U.K.

### 6.2.2 Assessment of fluoride uptake by HA

Hydroxyapatite powder (HA) was suspended in a solution of NaF ( $10 \text{ mg L}^{-1}$ ) at concentrations ranging from 0.25-5.0 mM. The pH was adjusted to 7.0 using 0.1 M NaOH. The  $\text{F}^-$  uptake was measured after 24 h using a fluoride-selective electrode (ThermoFisher Scientific, U.K.). The fluoride-selective electrode was immersed into the solutions to measure the free  $\text{F}^-$  concentration. A calibration curve was produced prior to the measurement using a range of NaF standard solutions (100, 10, 1.0 and  $0.1 \text{ mg L}^{-1}$ ). The oxidation-reduction potential (ORP) is plotted against the logarithm of fluoride ion concentration (Figure 6.2).

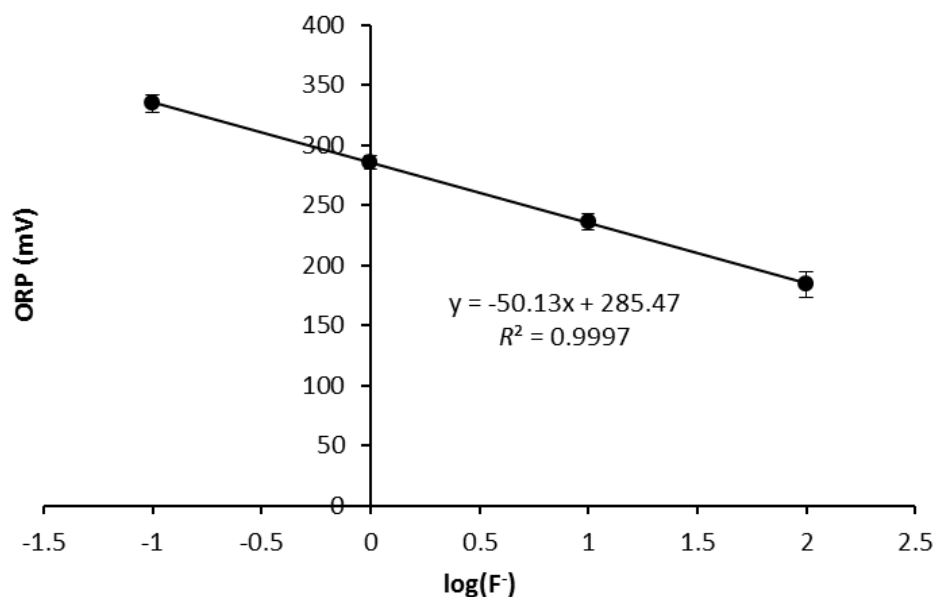


**Figure 6.2.** Calibration curve for the determination of fluoride uptake by HA powder.

The free fluoride concentration was then calculated using the calibration curve and equation 6.1:

$$[F^-]_{\text{free}} = 10^{\frac{\text{ORP}-285.47}{-50.13}} \quad (6.1)$$

Fluoride uptake was calculated from the total amount of  $F^-$  present initially and the amount of free  $F^-$  measured after 24 h.

To test the effect of pH on the fluoride uptake of HA, suspensions of HA in NaF (10 mg  $L^{-1}$ ) were produced at a concentration of 0.25 mg  $mL^{-1}$ . The pH was adjusted to 3.0, 5.0, 7.0, 9.0 or 11.0 using 0.1 M NaOH. The fluoride uptake was measured after 24 h using the calibration curve (Figure 6.2) and the method described above.

### 6.2.3 Synthesis of PVPA-HA composite hydrogels

The following method details the synthesis of PVPA-HA hydrogel, with a HA concentration of 0.25 mM. A range of PVPA-HA hydrogels were produced with varying HA concentrations (0.05, 0.10 and 0.50 mM). The monomer feed ratio of VPA:AA was kept at 30:70 in all cases.

VPA (0.35 g, 3.2 mmol) was dissolved in H<sub>2</sub>O (3.0 cm<sup>3</sup>), AA (0.54 g, 7.5 mmol) was dissolved in H<sub>2</sub>O (2.0 cm<sup>3</sup>), EGDA (0.037 g, 0.21 mmol) was dissolved in H<sub>2</sub>O (0.5 cm<sup>3</sup>), AAPH (2.9 mg, 0.01 mmol) was dissolved in H<sub>2</sub>O (0.5 cm<sup>3</sup>) and HA (0.13 g, 0.25 mmol) was dissolved in H<sub>2</sub>O (2.0 cm<sup>3</sup>). The reactants were added together and the solution was purged with N<sub>2</sub> for 20 min. The reaction mixture (1 mL) was aliquoted into a 12-well plate and heated to 60 °C for 2 h. The resulting gel was soaked in deionised water for 48 h to remove any unreacted monomer. The hydrogel was then dried under vacuum to constant weight.

#### **6.2.4 Swelling of PVPA-HA hydrogels**

Before swelling, gels were fully dried (as verified by no change in weight). The weight of the dry hydrogel ( $W_d$ ) was recorded. For the swelling experiment, hydrogels were immersed in deionised water that had been adjusted to pH 7.0 using 0.1 M NaOH. The gels were left to swell for 24 h. The supernatant was discarded and the gels were blotted with filter paper to remove any excess water. The weight of the swollen hydrogel ( $W_s$ ) was then recorded. Thus, the swelling was calculated using equation 5.1. The swelling experiment was repeated in triplicate for each hydrogel composition and the results are expressed as mean  $\pm$  SD.

#### **6.2.5 FT-IR spectroscopy**

PVPA-HA hydrogels were dried fully (as verified by no change in weight) and then ground into a fine powder. Fourier transform infrared (FT-IR) spectra were recorded using a Thermo Scientific Nicolet iS5 spectrometer with an iD5 diamond attenuated total reflectance (ATR) attachment over a wavenumber range of 4000–600 cm<sup>-1</sup> and a resolution of 4 cm<sup>-1</sup>. The spectra were obtained from 16 scans.

#### **6.2.6 Rheology**

An ARES LN2 rheometer (TA instruments, Hertfordshire) with parallel-plate geometry of 25 mm diameter was used for the rheological characterisation of PVPA-HA hydrogels. Test methods of oscillatory strain sweep and frequency sweep were used. The tests were performed at a constant temperature (20.0 °C) and a nominal gap of 2.5 mm. The strain sweep was performed at a frequency of 1.0 Hz. The strain level was increased from 1.0 to 100% and the change in storage ( $G'$ ) and loss ( $G''$ ) modulus was

recorded (Figure A6.1). The linear viscoelastic region (LVR) from 20 to 100% was determined as a safe region without structural breakage from oscillatory strain.

The frequency sweep was performed at a constant strain of 60%, corresponding to a point in the middle of the LVR profile. The oscillatory frequency was increased from 0.1 to 25 Hz and the plots  $G'$  and  $G''$  against frequency were obtained using the manufacturer's supplied software.

### **6.2.7 Assessment of fluoride uptake by PVPA-HA hydrogels**

PVPA-HA hydrogels ( $5.0 \text{ mg mL}^{-1}$ ), with different HA concentrations (0.05-0.5 mM), were immersed into a solution of NaF ( $10 \text{ mg L}^{-1}$ ) in deionised water. The pH was adjusted to 7.0 using 0.1 M NaOH. The fluoride uptake was measured after 24 h using the method described above. The calibration curve for the calculation of fluoride uptake is presented in Figure A6.2.

### **6.2.8 Effect of pH on fluoride uptake**

HA-0.25 hydrogels ( $5.0 \text{ mg mL}^{-1}$ ) were immersed into a solution of NaF ( $10 \text{ mg L}^{-1}$ ) in deionised water. The pH was adjusted to the desired value (3.0, 5.0, 7.0 or 9.0) using 0.1 M NaOH. The  $F^-$  uptake was measured after 24 h using the method described above. The calibration curve for the calculation of fluoride uptake is presented in Figure A6.3.

### **6.2.9 Effect of contact time on fluoride uptake**

HA-0.25 hydrogel ( $5.0 \text{ mg mL}^{-1}$ ) was immersed into a solution of NaF ( $10 \text{ mg L}^{-1}$ ) in deionised water. The pH was adjusted to 7.0 using 0.1 M NaOH. After the desired period of time, the fluoride uptake was measured by immersing the fluoride selective electrode into the solution and using the method described above. Fluoride uptake was measured intermittently over a period of 30 h. The calibration curve for the calculation of fluoride uptake is presented in Figure A6.4.

### **6.2.10 Effect of the presence of other ions on fluoride uptake**

HA-0.25 hydrogels ( $5.0 \text{ mg mL}^{-1}$ ) were immersed into a solution of NaF ( $10 \text{ mg L}^{-1}$ ) in deionised water. The pH was adjusted to 7.0 using 0.1 M NaOH. NaCl was added at various concentrations ( $100\text{-}500 \text{ mg L}^{-1}$ ) and the solution was left for 24 h. The fluoride

uptake was then measured using the method described above. This process was then repeated using the same concentrations of  $\text{Na}_2\text{SO}_4$ ,  $\text{NaNO}_3$  and  $\text{NaHCO}_3$ . The calibration curve for the calculation of fluoride uptake is presented in Figure A6.5.

#### **6.2.11 Regeneration of PVPA-HA hydrogels**

HA-0.25 hydrogel ( $5.0 \text{ mg mL}^{-1}$ ) was immersed into a solution of NaF ( $10 \text{ mg L}^{-1}$ ) in deionised water. The pH was adjusted to 7.0 using 0.1 M NaOH. The  $\text{F}^-$  uptake was measured after 24 h using a fluoride-selective electrode and the method described above. The hydrogel was then dried under vacuum to constant weight before being immersed into an excess solution of 0.1 M NaOH. The gel was left for 24 h for complete removal of the fluoride ions and was then dried under vacuum to constant weight. It was then re-immersed into a solution of NaF ( $10 \text{ mg L}^{-1}$ ). This cycle was repeated 4 times to see the effect of regeneration on the fluoride uptake capacity of the hydrogel. The calibration curve for the calculation of fluoride uptake is presented in Figure A6.6.

## 6.3 Results and Discussion

### 6.3.1 Fluoride uptake by HA

In the first instance, the fluoride uptake by nano-hydroxyapatite (HA) powder was investigated. It was found that the fluoride uptake increased with an increase in HA concentration (Figure 6.3). As shown in equation 6.1, fluoride ions can exchange with the hydroxyl ions of hydroxyapatite. Therefore, greater concentrations of HA lead to increased ion exchange processes and thus, a greater fluoride uptake. However, at high concentrations of HA (5.0 mM), the HA particles are poorly dispersed in the medium and sediment to the bottom of the flask. Thus, the fluoride uptake no longer increases. The maximum defluoridation capacity was found to be 1.92 mg F<sup>-</sup>/g HA, which occurred at a HA concentration of 2.5 mM. Hence, this concentration was used for further experiments.

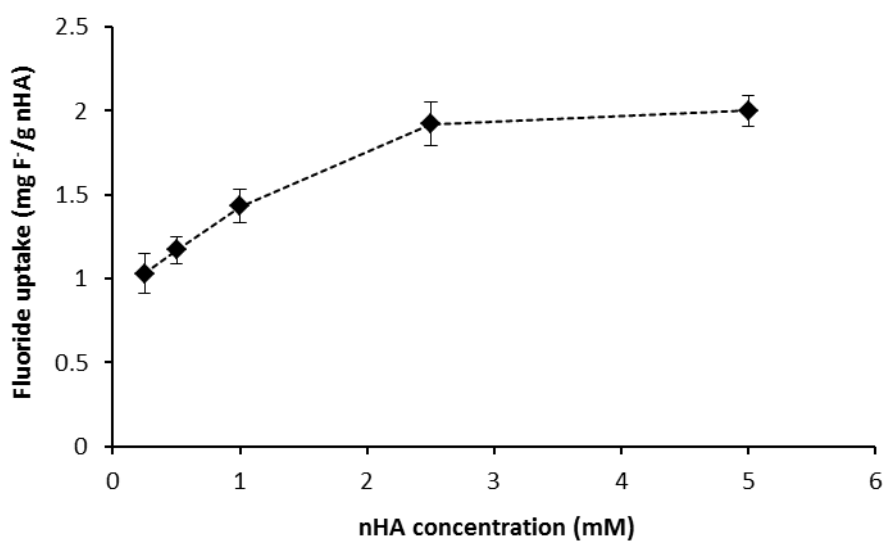


**Figure 6.3.** Effect of concentration on the fluoride uptake affinity of HA dispersed in NaF solution (10 mg L<sup>-1</sup>) at pH 7.0 and 20.0 °C.

It is well known that the pH of the aqueous solution can significantly affect adsorption. Therefore, the influence of pH on the fluoride uptake of HA was investigated over a pH range of 3 to 11 and the results are shown in Figure 6.4. The pH of the solution was controlled by adding dilute NaOH. Maximum fluoride removal was achieved at pH 3 (2.76 mg F<sup>-</sup>/g HA) and the fluoride uptake decreased with increasing pH of the medium. The lowest fluoride uptake was found to be 0.61 mg F<sup>-</sup>/g HA at pH 11.

These results are comparable to those found in the literature and can be explained due to the change in surface charge of the adsorbent.<sup>222, 223</sup> The surface of HA is highly protonated in acidic medium and therefore the maximum fluoride removal can be attributed to the net electrostatic attraction between the positively-charged surface and the negatively charged fluoride ions. As the pH increases, the HA becomes increasingly deprotonated and the surface acquires a negative charge. Thus, there is an electrostatic repulsion between the fluoride ions and the negatively-charged surface, which leads to a decrease in the fluoride uptake affinity of HA adsorbent.

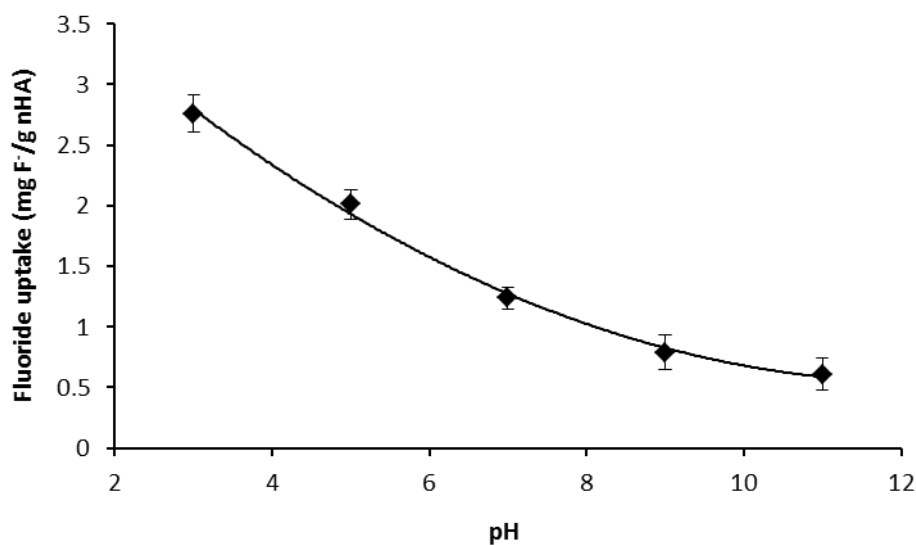


**Figure 6.4.** Effect of solution pH on the fluoride uptake affinity of HA, at a concentration of 2.5 mM, dispersed in NaF solution (10 mg L<sup>-1</sup>) at 20.0 °C.

### 6.3.2 Synthesis and characterisation of PVPA-HA hydrogels

It has been shown that by incorporating HA into a polymeric substrate, an increase in fluoride uptake is observed. Therefore, composite hydrogels were produced, consisting of nano-hydroxyapatite (HA) and poly(vinylphosphonic acid-*co*-acrylic acid) (PVPA-*co*-AA). It was previously shown that a VPA content of 30 mol % results in the greatest calcium binding and thus, this composition was chosen to lead to enhanced incorporation of HA.

The effect of HA concentration on the swelling properties of the PVPA-*co*-AA hydrogels was investigated and the results are presented in Table 6.1. It was found that an increase in the HA concentration in the gels led to a decrease in their swelling capacity. This occurs as a result of the decrease in porosity in the hydrogels owing to the occupation of free space by the HA. However, at concentrations above 0.5 mM, the HA led to a breaking apart of the polymer network and the production of a hydrogel was not possible, instead a viscous liquid formed.

**Table 6.1.** Experimental conditions and swelling ratio of PVPA-HA hydrogels with increasing HA concentration.

Sample Code	HA concentration (mM)	Mass of HA (g)	Swelling Ratio (%)
HA-0.05	0.05	0.025	55.01 ± 4.23
HA-0.1	0.10	0.05	47.01 ± 3.84
HA-0.25	0.25	0.13	37.44 ± 3.45
HA-0.5	0.50	0.25	33.16 ± 2.95

The effect of HA incorporation on the mechanical properties of the hydrogels was then investigated. Figure 6.5 shows the change in storage ( $G'$ ) and loss ( $G''$ ) modulus of PVPA-HA composite hydrogels with increasing HA concentration. It was observed that there is a large increase in  $G'$  and a smaller increase in  $G''$  with greater HA concentrations, which implies that HA reinforces the network. For all samples,  $G'$  is much greater than  $G''$ , suggesting that the bulk response of the PVPA-HA hydrogels is nearly elastic. Therefore, these results show that HA significantly improves the

mechanical properties of the hydrogels but leads to a reduction in the swelling capacities, as a function of HA concentration. Hence, it was decided that a HA concentration of 0.25 mM offers the best balance between these properties.

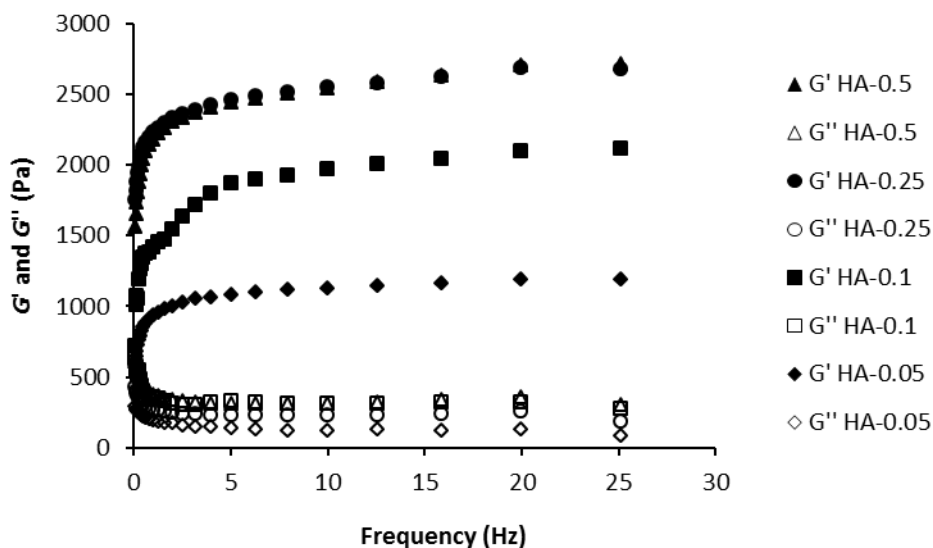


**Figure 6.5.** Storage ( $G'$ ) and loss ( $G''$ ) modulus of PVPA-HA hydrogels, with different HA concentrations, across a frequency sweep of 0.1 to 25 Hz at 20.0 °C.  $G'$  is represented by closed symbols and  $G''$  by open symbols.

The improvement in the mechanical properties of the PVPA-HA composite hydrogels suggests that there are some interactions between the polymer matrix and the HA particles. Some obvious differences can be found in the FT-IR spectra of the as-synthesised hydrogel and the hydrogel-HA composite, as show in Figure 6.6. The spectrum of PVPA-30 hydrogel (Figure 6.6a) shows two bands between 1090 and 905  $\text{cm}^{-1}$ , which represent the P-O stretch of the phosphonic acid side group. However, these bands are significantly reduced in the spectrum of the PVPA-HA composite hydrogel (Figure 6.6b). This indicates a weakening of the P-O bonds due to the formation of chelating bonds between the  $\text{Ca}^{2+}$  of hydroxyapatite and the phosphonate groups of PVPA-*co*-AA.

There is also a slight broadening of the O-H band between 3200 and 2400  $\text{cm}^{-1}$ , which occurs as a result of hydrogen bonding interactions between HA and the PVPA-*co*-AA

hydrogel. These interactions within the polymer network lead to the increase in the elastic modulus and mechanical strength of the hydrogel-HA composite.

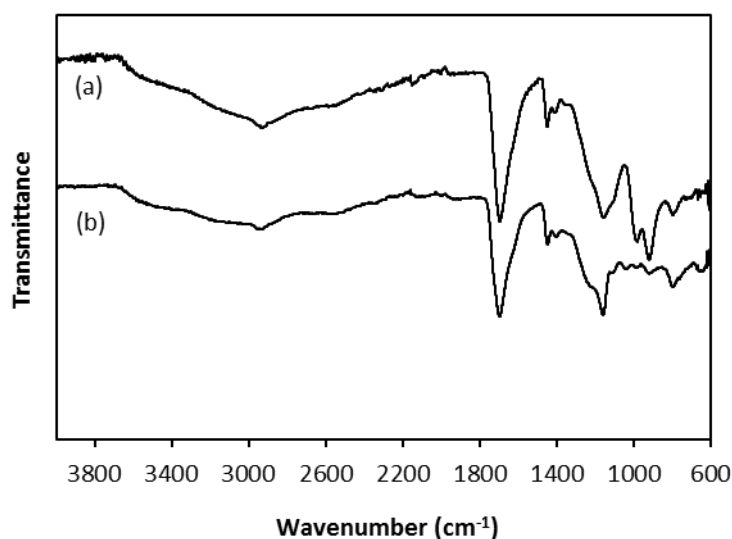


**Figure 6.6.** FT-IR spectra of (a) PVPA-co-AA hydrogel, with a VPA content of 30 mol %, and (b) PVPA-HA composite hydrogel, with a HA concentration of 0.25 mM.

### 6.3.3 Fluoride uptake by PVPA-HA hydrogels

The fluoride uptake affinity of the PVPA-HA composite hydrogels was then investigated and compared with that of HA powder. The results are presented in Figure 6.7. It can be seen that the fluoride uptake ability of the hydrogels increases with an increase in HA concentration, as was the case for the HA powder. It is interesting to note that the fluoride uptake is increased in the PVPA-HA hydrogels when compared with HA powder alone, at the same concentration of HA. This can be explained as a result of the high specific surface area of the polymer network, which allows for enhanced fluoride adsorption. Furthermore, the inherent swelling capacity of hydrogels allows for the uptake of large amounts of water. Therefore, some of the fluoride may become trapped within the pores of the hydrogel, providing another method for fluoride uptake. Finally, the HA binds to the phosphonic acid and carboxylic acid groups of the polymer chain, immobilising the HA within the hydrogel network. This prevents any sedimentation of the HA particles, allowing greater uptake of fluoride ions from solution.

As mentioned previously, it was not possible to incorporate large amounts of HA into the PVPA-*co*-AA hydrogels, since this led to a decrease in the extent of crosslinking as a result of the large HA particles forcing the polymer chains apart. Therefore, it was decided that a HA concentration of 0.25 mM would lead to optimal mechanical properties of the PVPA-HA hydrogels as well as a high degree of fluoride uptake and so this concentration was used for further experiments.

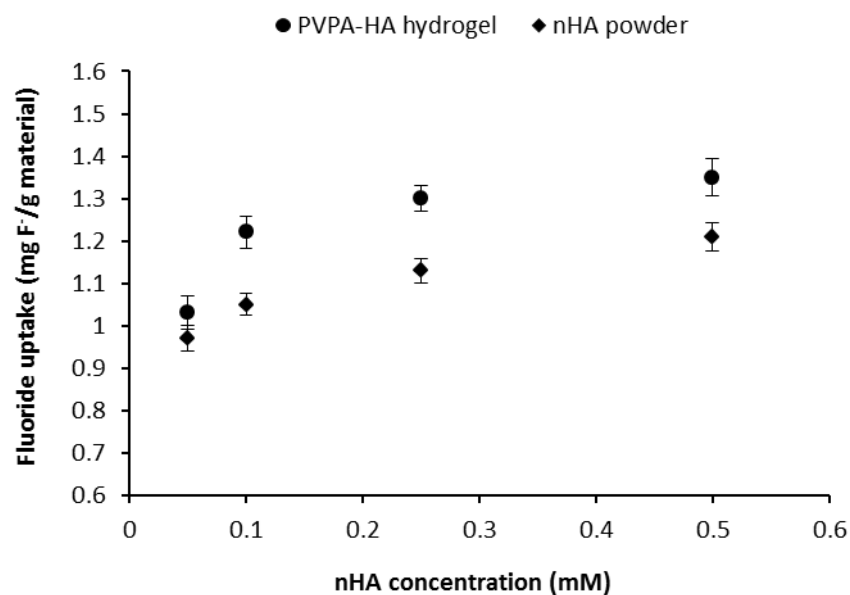


**Figure 6.7.** Effect of HA concentration on the fluoride uptake affinity of PVPA-HA hydrogels and HA powder in NaF solution ( $10 \text{ mg L}^{-1}$ ) at  $20.0 \text{ }^\circ\text{C}$ .

### 6.3.4 Effect of pH on fluoride uptake

Figure 6.8 shows the effect of pH on the fluoride uptake ability of PVPA-HA hydrogel, with a HA concentration of 0.25 mM. It was found that fluoride uptake decreases with an increase in the pH of the solution. This occurs as a result of the acquired negative charge of the adsorbent, which leads to electrostatic repulsions with the fluoride ions. However, the change in fluoride uptake with increasing pH is less pronounced in PVPA-HA hydrogels than for HA powder. This could possibly be due to the lower concentration of HA incorporated into the hydrogels. Furthermore, the formation of hydrogen bonds between the hydroxyl groups of HA and the PVPA-*co*-AA polymer chain may lead to a reduction in the effective charge and thus, a decreased repulsive

effect felt by the fluoride ions. These results show that PVPA-HA hydrogel is a promising candidate for fluoride removal from groundwater (pH 7.0), since the solution pH does not significantly affect its fluoride uptake affinity.

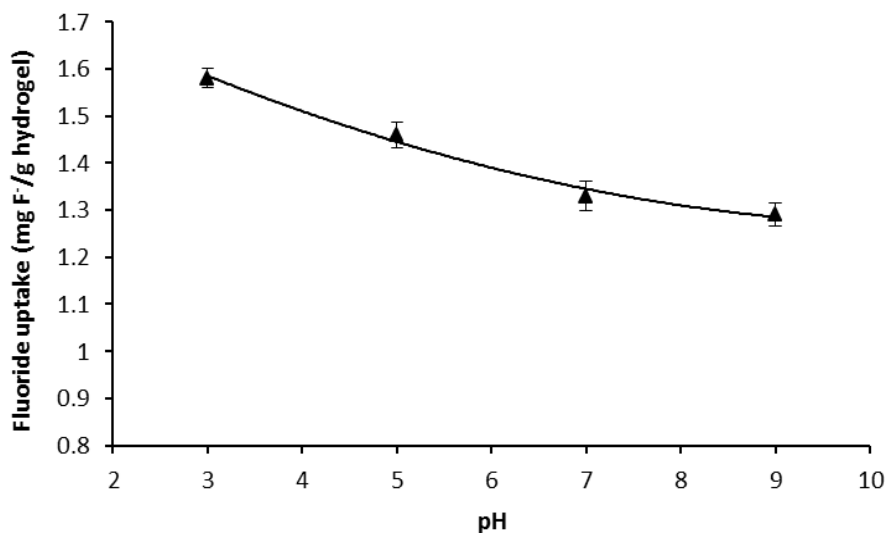


**Figure 6.8.** Effect of solution pH on the fluoride uptake affinity of PVPA-HA hydrogel (HA concentration of 0.25 mM) in NaF solution (10 mg L<sup>-1</sup>) at 20.0 °C.

### 6.3.5 Effect of contact time

The adsorption of fluoride ions onto PVPA-HA hydrogel was investigated as a function of contact time, over a period of 30 h, with 10 mg L<sup>-1</sup> as initial NaF concentration at 20.0 °C. The effect of defluoridation capacity (DC) with contact time is shown in Figure 6.9. It can be seen that there is an initial sharp increase in fluoride uptake within 1 h of immersion. This is followed by a slower rate of increase until saturation is reached after 8 h of immersion in NaF solution. It has been suggested that the slow rate of fluoride uptake is indicative of an adsorption process, which is rather slower than ion-exchange processes.<sup>222</sup> The maximum defluoridation capacity was found to be 1.55 mg F<sup>-</sup>/g hydrogel, which occurred after 8 h in solution. These results may have significant implications for the commercial use of PVPA-HA hydrogel for fluoride removal from groundwater. After a period of 8 h, the gel will have reached maximum capacity for fluoride ions and must be removed and potentially regenerated.

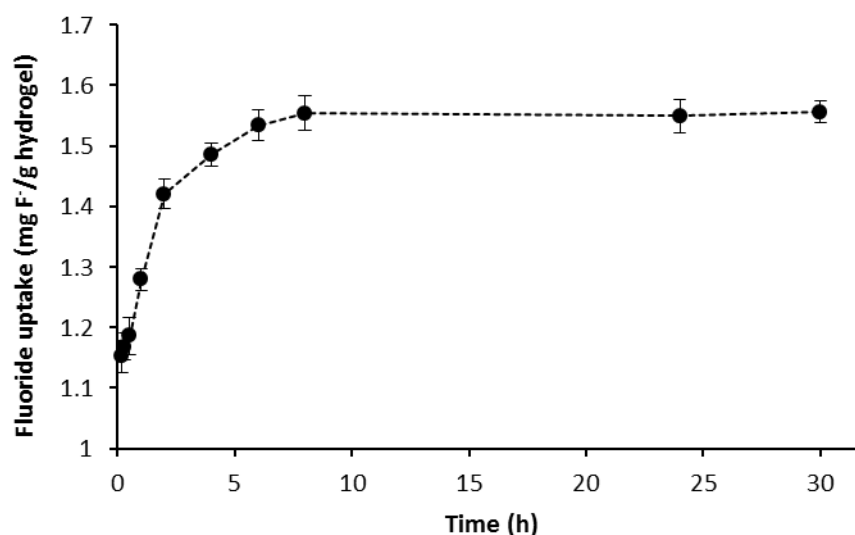


**Figure 6.9.** Fluoride uptake affinity of PVPA-HA hydrogel (HA concentration of 0.25 mM), in NaF solution ( $10 \text{ mg L}^{-1}$ ) at  $20.0 \text{ }^{\circ}\text{C}$ , as a function of contact time over 30 h.

### 6.3.6 Effect of common ion interference

The defluoridation capacity of PVPA-HA hydrogel, in the presence of competing anions, such as chloride, sulphate, nitrate and bicarbonate, was studied and the results are presented in Figure 6.10. These ions are usually present in groundwater at concentrations ranging from  $100\text{-}500 \text{ mg L}^{-1}$  and so the effect of the presence of the anions within this concentration range was investigated with an initial NaF concentration of  $10 \text{ mg L}^{-1}$ . It was observed that the presence of  $\text{Cl}^-$ ,  $\text{SO}_4^{2-}$  and  $\text{NO}_3^-$  ions had no significant influence on the defluoridation capacity of the PVPA-HA hydrogel. However, the presence of bicarbonate ( $\text{HCO}_3^-$ ) ions led to a dramatic reduction in the fluoride removal capacity of the hydrogel. This may be attributed to a competition between the bicarbonate and fluoride ions during adsorption onto the active sites of hydroxyapatite. Furthermore, it has been suggested that the release of  $\text{OH}^-$  ions from the hydrolysis of  $\text{NaHCO}_3$  will increase the solution pH, thus leading to enhanced coulombic repulsive forces between the adsorbent and the fluoride ions.<sup>223</sup>

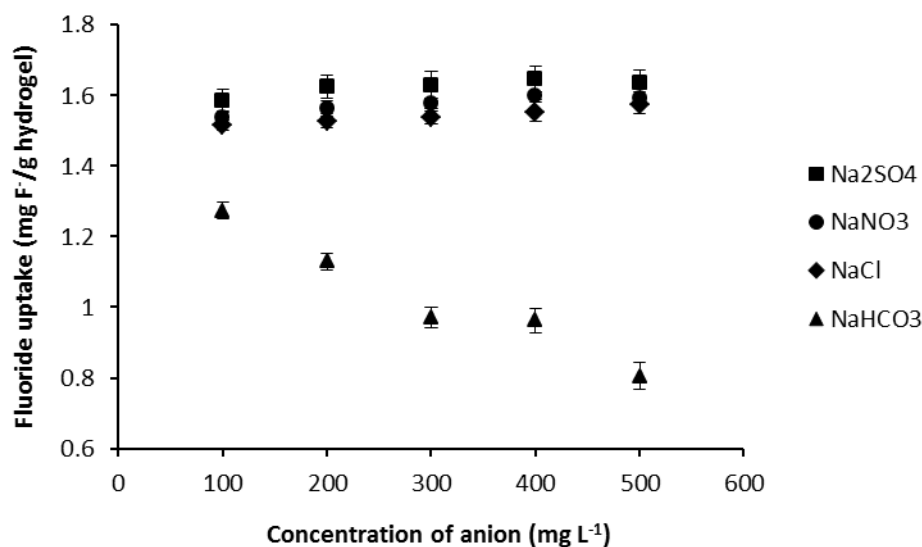


**Figure 6.10.** Effect of competitor ions (NaCl, Na<sub>2</sub>SO<sub>4</sub>, NaNO<sub>3</sub> and NaHCO<sub>3</sub>) on the fluoride uptake affinity of PVPA-HA hydrogels (HA concentration of 0.25 mM) in NaF solution (10 mg L<sup>-1</sup>) at 20.0 °C.

### 6.3.7 Regeneration of PVPA-HA hydrogels

Once the maximum fluoride capacity of an adsorbent has been reached, the material should be able to undergo a regeneration process to remove the adsorbed fluoride and thus enhance the cost effectiveness of the adsorbent. Therefore, the PVPA-HA hydrogels were immersed into a solution of excess NaOH to return the HA to its original state for re-use. However, this process is not 100% effective and repeated regeneration cycles may have a significant effect on the defluoridation capacity of the hydrogels. Figure 6.11 shows the change in fluoride uptake affinity of the PVPA-HA hydrogels after repeated regeneration of the material by immersion in NaOH. The initial fluoride uptake affinity of PVPA-HA was 1.69 mg F<sup>-</sup>/g hydrogel. After regeneration of the material, there was a significant reduction in the fluoride removal capacity, to 1.35 mg F<sup>-</sup>/g hydrogel. With further regeneration cycles, the fluoride uptake affinity of the hydrogel decreases to a lesser extent. After the fourth regeneration cycle, the fluoride removal capacity was 1.27 mg F<sup>-</sup>/g hydrogel. Although this is lower than the initial removal capacity, this is a relatively high fluoride uptake affinity for an adsorbent that has undergone four regeneration cycles. Therefore, these results demonstrate the

potential of PVPA-HA hydrogel for fluoride removal from groundwater over multiple cycles, without any appreciable loss in its removal capacity over repeated use.

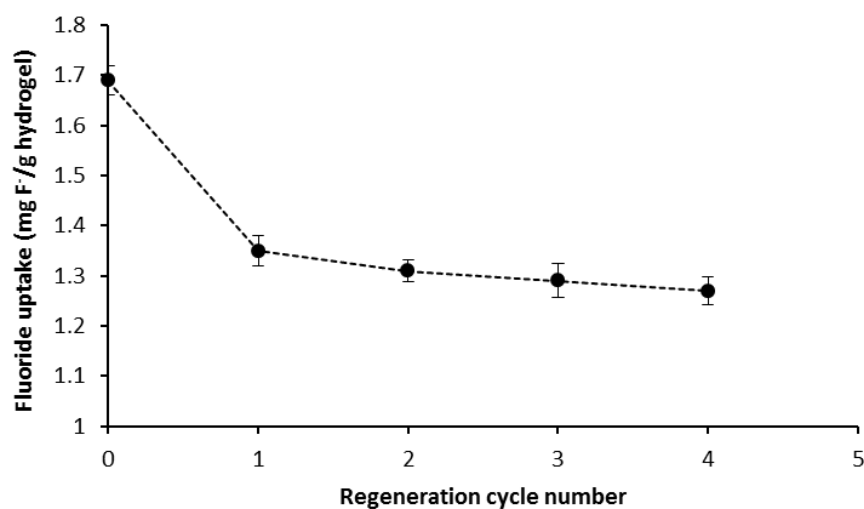


**Figure 6.11.** Effect of repeated regeneration cycles on the fluoride uptake affinity of PVPA-HA hydrogel (HA concentration of 0.25 mM) in NaF solution (10 mg L<sup>-1</sup>) at 20.0 °C.

## 6.4 Conclusions

Composite hydrogels of poly(vinylphosphonic acid-*co*-acrylic acid) (PVPA-*co*-AA) and nano-hydroxyapatite (HA) have been produced and investigated for their potential use as an adsorbent for fluoride removal from groundwater.

It was found that the PVPA-HA hydrogels enhance fluoride removal capacity when compared with HA powder alone. Furthermore, the fluoride uptake affinity of the hydrogels was shown to be dependent on many factors, including pH, contact time and the presence of competing anions.

The fluoride removal capacity decreased with increasing pH of the medium, owing to the acquisition of a negative charge on the surface of the adsorbent, which led to electrostatic repulsions between the hydrogel and the fluoride ions. It was found that maximum defluoridation capacity of the PVPA-HA hydrogels was reached after 8 h of

immersion in NaF solution ( $10 \text{ mg L}^{-1}$ ). Furthermore, while  $\text{Cl}^-$ ,  $\text{SO}_4^{2-}$  and  $\text{NO}_3^-$  ions had no significant influence on the defluoridation capacity of the PVPA-HA hydrogels, the fluoride removal capacity was reduced in the presence of bicarbonate ( $\text{HCO}_3^-$ ) ions. This was attributed to a competition between the bicarbonate and fluoride ions for the adsorption sites on HA.

After the maximum defluoridation capacity of the PVPA-HA hydrogel was reached, the material could be returned to its original state by immersing it in excess NaOH solution. It was found that upon regeneration of the hydrogel, the fluoride removal capacity was reduced. However, the decrease in fluoride uptake ability was relatively small (1.69 to 1.27 mg F/g hydrogel). Therefore, these results demonstrate the potential use of PVPA-HA hydrogels for fluoride removal from groundwater over many repeated cycles. Hence, this adsorbent has a desirable cost effectiveness that will make it ideal for commercial use.

## 7.0 Conclusions and Future Work

### 7.1 Conclusions

There is a clinical need for a bone graft substitute that can be used at sites of surgical intervention to promote bone regeneration. Poly(vinylphosphonic acid-*co*-acrylic acid) (PVPA-*co*-AA) has recently been identified as a potential candidate for use in bone tissue scaffolds. PVPA-*co*-AA can act as a mimic of bisphosphonates – a class of drugs used to treat osteoporosis - owing to its ability to bind to calcium ions from bone mineral surfaces. Therefore, it was hypothesised that PVPA-*co*-AA could enhance mineralisation of the extracellular matrix (ECM) of bone and could lead to an increase in bone formation.

The synthesis of PVPA-*co*-AA was first investigated with regards to the effect of monomer feed ratio. It was found that an increase in VPA content in the feed led to a reduction in the yield, monomer conversion and average molar masses of the copolymers produced. This was attributed to the lower reactivity of vinylphosphonic acid (VPA) compared to acrylic acid (AA), which was confirmed by calculation of their reactivity ratios. Using the Fineman-Ross method,  $r_1(\text{AA})$  was calculated as 4.725 and  $r_2(\text{VPA})$  as 0.0553. The Kelen-Tüdös method yielded values of 4.727 and 0.0558 for  $r_1$  and  $r_2$ , respectively. Here,  $r_1 \gg 1 \gg r_2$ , which demonstrates the much higher reactivity of AA when compared with VPA. Composition drift may occur throughout the polymerisation, leading to low incorporation of VPA into the final copolymer. This was controlled by the batch wise addition of AA monomer and initiator. Furthermore, a chain transfer agent (CTA) was included in the polymerisation system to produce a range of PVPA-*co*-AA copolymers, with different compositions yet consistent molar masses. The copolymers were characterised by  $^1\text{H}$  NMR,  $^{31}\text{P}$  NMR and FT-IR spectroscopy.

The affinity of the copolymers towards calcium ions, and thus their ability to promote mineralisation *in vivo*, was then investigated. By determination of the pH titration curves, it was shown that the degree of neutralisation increases proportional to the VPA content in the copolymers. VPA is a medium-strong polyelectrolyte and AA is a weak polyelectrolyte and so copolymers with higher VPA contents show a greater dissociation in aqueous media. It would therefore be expected that the calcium chelation

would increase linearly with VPA content in the copolymers. However, at pH 7.3 and 9.0, calcium chelation capacity reaches a maximum at a VPA content of *ca.* 30 mol %. It is suggested that this copolymer composition contains the optimal distribution of phosphonate groups along the polymer chain, which offers the best potential mimic of non-collagenous matrix proteins and leads to the greatest calcium binding. Therefore, it is expected that PVPA-*co*-AA, with a VPA content of 30 mol %, will lead to enhanced bone formation and mineralisation and is thus the best potential candidate for use in bone tissue scaffolds.

The incorporation and release of PVPA-*co*-AA from electrospun scaffolds of poly( $\epsilon$ -caprolactone) (PCL) has been explored. The scaffolds were produced, prior to this work, by dip-coating the PCL scaffold into a 15 w/v % solution of PVPA-*co*-AA or by co-spinning of the two polymers with the aid of a surfactant. It was found that the uptake efficiency of PVPA-*co*-AA into PCL scaffolds varied depending on the fabrication method. Scaffolds produced by dip-coating had lower uptake efficiencies due to the immiscibility of the two polymers. Co-spinning of the PCL and PVPA-*co*-AA led to higher uptake efficiencies as a result of the use of a surfactant (Span 80) which helped to improve their compatibility.

The scaffolds were sterilised by immersion into a 70% ethanol solution. This led to a reduction in the PVPA-*co*-AA concentration in the scaffolds due to the partial solubility of the copolymer in ethanol, which, in turn, resulted in a decrease in the calcium chelation capacity of the scaffolds.

The release profile of PVPA-*co*-AA from the PCL scaffolds was determined. It was shown that the majority of the copolymer was released within the first 8 h of immersion in aqueous media, regardless of the fabrication method. However, a larger total amount of PVPA-*co*-AA was released from the dip-coated samples as opposed to those that had been co-spun. Furthermore, the calcium chelation of the scaffolds was measured in osteogenic differentiation media over 48 h. It was found that most of the calcium from the media had been chelated within 6-8 h of immersion. This suggests that PVPA-*co*-AA binds to calcium when it is released into solution and not when it is immobilised onto the scaffolds. These results have implications for the mechanism of mineralisation *in vivo*. It can be hypothesised that the copolymer does not promote nucleation on the surface of the scaffold but instead acts as a mimic of non-collagenous proteins by

binding to the calcium ions in solution, and thus helping to direct and control the process of mineralisation.

Hydrogels of PVPA-*co*-AA have been produced and the effect of monomer feed ratio on the properties of the hydrogels was investigated. It was shown that an increase in VPA content led to greater swelling of the hydrogels and a higher degree of porosity. This was attributed to enhanced electrostatic repulsions between polymer chains and the greater hydrophilicity of VPA when compared with AA, which was confirmed by a decrease in water contact angle. It was also found that hydrogels with higher VPA contents were more flexible and could be deformed to large extents without permanent deformation of their structure, as shown by rheological measurements. Therefore, these gels are most suitable for use in clinical settings where they can be moulded into a defect site during surgical intervention.

An increase in osteoblast adhesion and proliferation was observed as a function of VPA content in the hydrogels. Furthermore, cells that were seeded onto VPA-30 and VPA-50 hydrogels demonstrated superior cell spreading, comparable to that of the control. Cell metabolic activity increased proportionally to cell number and so it can be concluded that the hydrogels had no significant effect on cell metabolic activity. Therefore, this work proves that hydrogels with 30 or 50 mol % VPA are ideal for use in bone tissue scaffolds. The structures of these gels encourage high swelling and increased cell attachment and proliferation. Furthermore, it has been demonstrated that the mechanical and cell adhesion properties of the gels can be tuned by altering copolymer compositions.

Finally, another potential application of PVPA-*co*-AA has been explored; fluoride removal from groundwater. Composite hydrogels of PVPA-*co*-AA and hydroxyapatite (HA) have been produced and were shown to enhance fluoride removal capacity when compared with HA powder alone. Furthermore, the fluoride uptake affinity of the hydrogels was shown to be dependent on many factors, including pH, contact time and the presence of competing anions. After the maximum defluoridation capacity of the PVPA-HA hydrogel was reached, the material could be returned to its original state by immersing it in excess NaOH solution. However, it was found that upon regeneration of the hydrogel, the fluoride removal capacity was reduced.

## 7.2 Recommendations for Future Work

The current study was undertaken to understand the role of PVPA-*co*-AA in bone formation and thus, to evaluate its potential for use in bone tissue scaffolds. Although this was largely successful, there still remain a number of unanswered questions that require further investigation.

It was determined that the PVPA-*co*-AA shows a burst release from PCL scaffolds and can then bind to calcium ions in solution to promote mineralisation. In order to understand the location and morphology of the mineral crystals that are formed, the PCL/PVPA scaffolds could be immersed into simulated body fluid (SBF). The ions present in SBF are believed to mimic the natural extracellular bodily fluid and so mineralisation can occur in line with what would be expected *in vivo*. The size and shape of the crystals formed could then be probed using scanning electron microscopy (SEM). This would give a clearer picture of the mechanism of mineralisation and the role of PVPA-*co*-AA in this process.

Hydrogels of PVPA-*co*-AA have been produced and have been shown to promote osteoblast adhesion and proliferation. However, the mechanical properties of the gels may be insufficient for load-bearing applications. One way to improve their mechanical strength is to produce a composite hydrogel of PVPA-*co*-AA and hydroxyapatite (HA). HA is a natural component of bone mineral and it is often used to improve the osteoconductive and osteoinductive properties of tissue scaffolds. Furthermore, the alkaline properties of HA may help to neutralise the acidic PVPA-*co*-AA to provide a less harsh environment for cells to adhere and proliferate.

The incorporation of PVPA-*co*-AA into PCL scaffolds has proven to be challenging due to the immiscibility of the two polymers. In addition, the hydrophilic nature of PVPA-*co*-AA leads to a burst release of the copolymer from the PCL scaffolds that is complete within 8 h. This could be improved by the production of an electrospun fibre-hydrogel composite. The crosslinked nature of the hydrogel renders it insoluble in water, which could allow for a more controlled release of PVPA-*co*-AA, providing longer release times and a smaller initial burst. Furthermore, the immobilisation of PVPA-*co*-AA onto the electrospun nanofibrous scaffold may provide a better templating surface for mineral nucleation and growth.

It has been shown that PVPA-*co*-AA hydrogels can encourage osteoblast adhesion and proliferation. However, the effect of the hydrogels on osteoclast viability has not been investigated. It is hypothesised that PVPA-*co*-AA can act as a mimic of bisphosphonates and so studies need to be carried out to determine if osteoclasts undergo apoptosis in the presence of PVPA-*co*-AA, thus leading to a net increase in bone formation.

There are a number of other cell culture assays that could be carried out *in vitro* to evaluate not only the osteoconductive effect of PVPA-*co*-AA but also if there are any signs of osteoinductivity. For example, the expression of alkaline phosphatase is an early marker of mineralisation and the deposition of type I collagen indicates the production of new extracellular matrix by osteoblast cells. Furthermore, non-collagenous proteins, such as osteocalcin and osteoprotegerin, are produced by osteoblasts and are a good indication of the osteoinductive properties of a scaffold.

Finally, the degradation properties of the PVPA-*co*-AA scaffolds should be investigated. A long-term degradation study should be carried out to determine the length of time that the scaffold will remain intact. The change in the mechanical properties of the scaffold, as it is degrading, will need to be investigated since it is important for an implantable system to maintain its biomechanical properties whilst new bone is being deposited, particularly for load-bearing applications. Moreover, the breakdown products of the PVPA-*co*-AA scaffolds will need to be explored in terms of their cytotoxicity. Acidic breakdown products can cause inflammatory reactions in patients and can enhance the degradation rate of the scaffolds.

## 8.0 References

1. R. Langer and J. P. Vacanti, *Science*, 1993, **260**, 920-926.
2. C. Laurencin, A. Ambrosio, M. Borden and J. Cooper, *Annu. Rev. Biomed. Eng.*, 1999, **1**, 19-26.
3. R. Lanza, R. Langer and J. Vacanti, in *Principles of Tissue Engineering*, 4th edn., Elsevier, California, 2014, Ch. 5, pp. 1201-1216.
4. M. Doblaré, J. M. García and M. J. Gómez, *Eng. Fract. Mech.*, 2004, **71**, 1809-1840.
5. U. G. K. Wegst, H. Bai, E. Saiz, A. P. Tomsia and R. O. Ritchie, *Nat. Mater.*, 2015, **14**, 23-36.
6. J.-Y. Rho, L. Kuhn-Spearing and P. Zioupos, *Med. Eng. Phys.*, 1998, **20**, 92-102.
7. J. D. Currey, in *Bones: Structure and Mechanics*, Princeton University Press, Oxford, 2002, Ch. 1, pp. 11-24.
8. A. K. Gaharwar, A. Arpanaei, T. L. Andresen and A. Dolatshahi-Pirouz, *Adv. Mater.*, 2016, **28**, 771-781.
9. L. Módis, in *Organisation of the Extracellular Matrix*, CRC Press, Inc., Florida, 1991, Ch. 5, pp. 99-122.
10. B. Clarke, *Clin. J. Am. Soc. Nephrol.*, 2008, **3**, 131-139.
11. A. George and A. Veis, *Chem. Rev.*, 2008, **108**, 4670-4693.
12. E. Salih, J. Wang, J. Mah and R. Fluckiger, *Biochem. J.*, 2002, **364**, 465-474.
13. M. P. Whyte, *Endocr. Rev.*, 1994, **15**, 439-461.
14. D. Harmey, L. Hessle, S. Narisawa, K. A. Johnson, R. Terkeltaub and J. L. Millán, *Am. J. Pathol.*, 2004, **164**, 1199-1209.
15. L. J. Raggatt and N. C. Partridge, *J. Biol. Chem.*, 2010, **285**, 25103-25108.
16. J. C. Crockett, M. J. Rogers, F. P. Coxon, L. J. Hocking and M. H. Helfrich, *J. Cell Sci.*, 2011, **124**, 991-998.
17. D. J. Hadjidakis and I. I. Androulakis, *Ann. N. Y. Acad. Sci.*, 2006, **1092**, 385-396.
18. M. T. Drake, B. L. Clarke and E. M. Lewiecki, *Clin. Ther.*, 2015, **37**, 1837-1850.
19. E. Hernlund, A. Svedbom, M. Ivergård, J. Compston, C. Cooper, J. Stenmark, E. V. McCloskey, B. Jönsson and J. A. Kanis, *Arch. Osteoporos.*, 2013, **8**, 1-115.
20. R. Marcus, D. Feldman, D. A. Nelson and C. J. Rosen, in *Osteoporosis*, 3rd edn., Elsevier, Massachusetts, 2008.
21. C. G. Finkemeier, *J. Bone Joint Surg.*, 2002, **84**, 454-464.
22. H. Burchardt, *Clin. Orthop. Relat. Res.*, 1983, **174**, 28-42.
23. F. P. Coxon, K. Thompson and M. J. Rogers, *Curr. Opin. Pharmacol.*, 2006, **6**, 307-312.
24. J. P. Cattalini, A. R. Boccaccini, S. Lucangioli and V. Mouriño, *Tissue Eng., Part B*, 2012, **18**, 323-340.
25. K. Thompson, M. J. Rogers, F. P. Coxon and J. C. Crockett, *Mol. Pharmacol.*, 2006, **69**, 1624-1632.

26. J. Fisher, M. Rogers, J. Halasy, S. Luckman, D. Hughes, P. Masarachia, G. Wesolowski, R. Russell, G. Rodan and A. Reszka, *Proc. Natl. Acad. Sci. USA*, 1999, **96**, 133-140.
27. J. C. Frith, J. Mönkkönen, G. M. Blackburn, R. G. G. Russell and M. J. Rogers, *J. Bone Miner. Res.*, 1996, **12**, 1358-1367.
28. J. C. Frith, J. Mönkkönen, S. Auriola, H. Mönkkönen and M. J. Rogers, *Arthritis Rheum.*, 2001, **244**, 2201-2210.
29. P. P. Lehenkari, M. Kellinsalmi, J. P. Näpänkangas, K. V. Ylitalo, J. Mönkkönen, M. J. Rogers, A. Azhayevev, H. K. Väänänen and I. E. Hassinen, *Mol. Pharmacol.*, 2002, **61**, 1255-1262.
30. M. J. Rogers, S. Gordon, H. L. Benford, F. P. Coxon, S. P. Luckman, J. Mönkkönen and J. C. Frith, *Cancer*, 2000, **88**, 2961-2978.
31. D. Horie, M. Takahashi, K. Aoki and K. Ohya, *J. Med. Dent. Sci.*, 2003, **50**, 121-132.
32. G. G. Reinholz, B. Getz, L. Pederson, E. S. Sanders, M. Subramaniam, J. N. Ingle and T. C. Spelsberg, *Cancer Res.*, 2000, **60**, 6001-6007.
33. G. Im, S. A. Qureshi, J. Kenney, H. E. Rubash and A. S. Shanbhag, *Biomaterials*, 2004, **25**, 4105-4115.
34. A. Ezra and G. Golomb, *Adv. Drug Del. Rev.*, 2000, **42**, 175-195.
35. D. Puppi, A. M. Piras, F. Chiellini, E. Chiellini, A. Martins, I. B. Leonor, N. Neves and R. Reis, *J. Tissue Eng. Regen. Med.*, 2011, **5**, 253-263.
36. J. S. Siopack and H. E. Jergesen, *West J. Med.*, 1995, **162**, 243-249.
37. M. P. Staiger, A. M. Pietak, J. Huadmai and G. Dias, *Biomaterials*, 2006, **27**, 1728-1734.
38. Z. Li, X. Gu, S. Lou and Y. Zheng, *Biomaterials*, 2008, **29**, 1329-1344.
39. C. Yao, J. Lu and T. J. Webster, *Biomater. Artif. Organs*, 2011, 34-55.
40. J. A. Jansen, J. W. M. Vehof, P. Q. Ruhé, H. Kroeze-Duetman, Y. Kuboki, H. Takita, E. L. Hedberg and A. G. Mikos, *J. Controlled Release*, 2005, **101**, 127-136.
41. J. J. Jacobs, A. K. Skipor, L. M. Patterson, N. J. Hallab, W. G. Paprosky, J. Black and J. O. Galante, *J. Bone Joint Surg.*, 1998, **80**, 1447-1458.
42. J. D. Bobyn, G. J. Stackpool, S. A. Hacking, M. Tanzer and J. J. Krygier, *J. Bone Joint Surg.*, 1999, **81B**, 907-914.
43. R. M. Meneghini, D. G. Lewallen and A. D. Hanssen, *J. Bone Joint Surg. Am.*, 2008, **90**, 78-84.
44. D. G. Guo, K. W. Xu and Y. Han, *J. Biomed. Mater. Res. A*, 2009, **88A**, 43-52.
45. H. R. R. Ramay and M. Zhang, *Biomaterials*, 2004, **25**, 5171-5180.
46. G. Y. Jung, Y. J. Park and J. S. Han, *J. Mater. Sci. Mater. Med.*, 2010, **21**, 1649-1654.
47. D. Lickorish, J. A. M. Ramshaw, J. A. Werkmeister, V. Glattauer and C. R. Howlett, *J. Biomed. Mater. Res. A*, 2004, **68A**, 19-27.
48. R. E. Neuendorf, E. Saiz, A. P. Tomsia and R. O. Ritchie, *Acta Biomater.*, 2008, **4**, 1288-1296.
49. S. Kurtz, K. Ong, E. Lau, F. Mowat and M. Halpern, *J. Bone Jt. Surg., Am. Vol.*, 2007, **89**, 780-785.

50. N. N. Mahomed, J. A. Barrett, J. N. Katz, C. B. Phillips, E. Losina, R. A. Lew, E. Guadagnoli, W. H. Harris, R. Poss and J. A. Baron, *J. Bone Joint Surg. Am.*, 2003, **85-A**, 27-32.
51. P. F. Sharkey, P. M. Lichstein, C. Shen, A. T. Tokarski and J. Parvizi, *J. Arthroplasty*, 2014, **29**, 1774-1778.
52. N. Sultana, in *Biodegradable Polymer-Based Scaffolds for Bone Tissue Engineering*, Springer, Heidelberg, 2013, Ch. 1, pp. 4-7.
53. Y. Luo, G. Engemayr, D. T. Auguste, L. da Silva Ferreira, J. M. Karp, R. Saigal and R. Langer, in *Principles of Tissue Engineering*, Elsevier, Boston, MA, 3<sup>rd</sup> edn., 2007, Ch. 25, pp. 359-373.
54. K. E. M. Benders, P. R. v. Weeren, S. F. Badylak, D. B. F. Saris, W. J. A. Dhert and J. Malda, *Trends Biotechnol.*, 2013, **31**, 169-176.
55. M. Kikuchi, T. Ikoma, S. Itoh, H. N. Matsumoto, Y. Koyama, K. Takakuda, K. Shinomiya and J. Tanaka, *Compos. Sci. Technol.*, 2004, **64**, 819-825.
56. S. S. Liao, F. Z. Cui and Y. Zhu, *J. Bioact. Compat. Polym.*, 2004, **19**, 117-130.
57. J. Venugopal, P. Vadgama, T. S. S. Kumar and S. Ramakrishna, *Nanotechnol.*, 2007, **18**, 1-8.
58. A. Boger, K. Wheeler, A. Montali and E. Gruskin, *J. Biomed. Mater. Res., Part B: Appl. Biomater.*, 2009, **90B**, 760-766.
59. J. M. Pachence, M. P. Bohrer and J. Kohn, in *Principles of Tissue Engineering*, 3<sup>rd</sup> edn., Elsevier, 2007, Ch. 23, pp. 323-339.
60. C. M. Agrawal and R. B. Ray, *J. Biomed. Mater. Res.*, 2001, **55**, 141-150.
61. M. B. Murphy and A. G. Mikos, in *Principles of Tissue Engineering*, 3<sup>rd</sup> edn., Elsevier, USA, 2007, Ch. 22, pp. 311-314.
62. N. Annabi, J. W. Nichol, X. Zhong, C. Ji, S. Koshy, A. Khademhosseini and F. Dehghani, *Tissue Eng.*, 2010, **16**, 371-383.
63. C. J. Doillon, C. F. Whyne, S. Brandwein and F. H. Silver, *J. Biomed. Mater. Res.*, 1986, **20**, 19-28.
64. J. Reignier and M. A. Huneault, *Polymer*, 2006, **47**, 4703-4717.
65. J. M. Saldanha and T. Kyu, *Macromolecules*, 1987, **20**, 2840-2847.
66. W. Lin, Q. Li and T. Zhu, *J. Ind. Eng. Chem.*, 2012, **18**, 941-947.
67. Q. P. Pham, U. Sharma and A. G. Mikos, *Tissue Eng.*, 2006, **12**, 1197-1211.
68. P. Gupta, C. Elkins, T. E. Long and G. L. Wilkes, *Polymer*, 2005, **46**, 4799-4810.
69. C. Zhang, X. Yuan, L. Wu, Y. Han and J. Sheng, *Eur. Polym. J.*, 2005, **41**, 423-432.
70. J. M. Deitzel, J. Kleinmeyer, D. Harris and N. C. B. Tan, *Polymer*, 2001, **42**, 261-272.
71. X. H. Zong, K. Kim, D. F. Fang, S. F. Ran, B. S. Hsiao and B. Chu, *Polymer*, 2002, **43**, 4403-4412.
72. A. M. Reed and D. K. Gilding, *Polymer*, 1981, **22**, 494-498.
73. Y. Ikada and H. Tsuji, *Macromol. Rapid Commun.*, 2000, **21**, 117-132.
74. R. P. F. Lanao, A. M. Jonker, J. G. C. Wolke, J. A. Jansen, J. C. M. v. Hest and S. C. G. Leeuwenburgh, *Tissue Eng.*, 2013, **19**, 380-390.

75. P. Gentile, V. Chiono, I. Carmagnola and P. V. Hatton, *Int. J. Mol. Sci.*, 2014, **15**, 3640-3659.
76. O. M. Böstman, *J. Bone Joint Surg.*, 1991, **73**, 148-153.
77. M. V. Jose, V. Thomas, K. T. Johnson, D. R. Dean and E. Nyairo, *Acta Biomater.*, 2009, **5**, 305-315.
78. Y. P. Yun, S. E. Kim, J. B. Lee, D. N. Heo, M. S. Bae, D.-R. Shin, S.-B. Lim, K. K. Choi, S. J. Park and I. K. Kwon, *Tissue Eng. Regener. Med.*, 2009, **6**, 336-345.
79. H. Yoshimoto, Y. M. Shin, H. Terai and J. P. Vacanti, *Biomaterials*, 2003, **24**, 2077-2082.
80. V. Thomas, S. Jagani, K. Johnson, M. V. Jose, D. R. Dean, Y. K. Vohra and E. Nyairo, *J. Nanosci. Nanotechnol.*, 2006, **6**, 487-493.
81. Y. K. Luu, K. Kim, B. S. Hsiao, B. Chu and M. Hadjiargyrou, *J. Controlled Release*, 2003, **89**, 341-353.
82. W. Xue, A. Bandyopadhyay and S. Bose, *J. Biomed. Mater. Res., Part B: Appl. Biomater.*, 2009, **91**, 831-838.
83. N. Y. C. Yu, A. Schindeler, D. G. Little and A. J. Ruys, *J. Biomed. Mater. Res., Part B: Appl. Biomater.*, 2010, **93B**, 285-295.
84. Y. J. Park, K. H. Kim, J. Y. Lee, Y. Ku, S. J. Lee, B. M. Min and C. P. Chung, *Biotechnol. Appl. Biochem.*, 2006, **43**, 17-24.
85. H. Nie, B. Soh, Y.-C. Fu and C.-H. Wang, *Biotechnol. Bioeng.*, 2008, **99**, 223-234.
86. P. Datta, J. Chatterjee and S. Dhara, *Colloids Surf., B*, 2012, **94**, 177-183.
87. J. J. Yoon, J. H. Kim and T. G. Park, *Biomaterials*, 2003, **24**, 2323-2329.
88. P. Taepaibon, V. Rungsardthang and P. Supapol, *Nanotechnology*, 2006, **17**, 2317-2329.
89. E.-R. Kenawy, G. L. Bowlin, K. Mansfield, J. Layman, D. S. Simpson, E. H. Sanders and G. E. Wnek, *J. Controlled Release*, 2002, **81**, 57-64.
90. K. Feng, H. Sun, M. A. Bradley, E. J. Dupler, W. V. Giannobile and P. X. Ma, *J. Controlled Release*, 2010, **146**, 363-369.
91. J. Zeng, X. Xu, X. Chen, Q. Liang, X. Bian, L. Yang and X. Jing, *J. Controlled Release*, 2003, **92**, 227-231.
92. K. Kim, Y. K. Luu, C. Chang, D. Fang, B. S. Hsiao, B. Chu and M. Hadjiargyrou, *J. Controlled Release*, 2004, **98**, 47-56.
93. S. Tungprapa, I. Jangchud and P. Supaphol, *Polymer*, 2007, **48**, 5030-5041.
94. J. A. Hunt, R. Chen, T. v. Veen and N. Bryan, *J. Mater. Chem. B*, 2014, **2**, 5319-5338.
95. J. T. Butcher and R. M. Nerem, *J. Heart Valve Dis.*, 2004, **13**, 478-485.
96. N. Bhattarai, J. Gunn and M. Zhang, *Adv. Drug Del. Rev.*, 2010, **62**, 83-99.
97. F. Croisier and C. Jérôme, *Eur. Polym. J.*, 2013, **49**, 780-792.
98. X. Xu, A. K. Jha, D. A. Harrington, M. C. Farach-Carson and X. Jia, *Soft Matter*, 2012, **8**, 3280-3294.
99. C. B. Highley, G. D. Prestwich and J. A. Burdick, *Curr. Opin. Biotechnol.*, 2016, **40**, 35-40.
100. M. W. Tibbit and K. S. Anseth, *Biotechnol. Bioeng.*, 2009, **103**, 655-663.

101. A. S. Sawhney, C. P. Pathak and J. A. Hubbel, *Macromolecules*, 1993, **26**, 581-587.
102. P. Martens, T. Holland and K. S. Anseth, *Polymer*, 2002, **43**, 6093-6100.
103. T. V. Chirila, I. J. Constable, G. J. Crawford, S. Vijayasekaran, D. E. Thompson, Y.-C. Chen and W. A. Fletcher, *Biomaterials*, 1993, **14**, 26-38.
104. Z. Li, Y. Su, B. Xie, H. Wang, T. Wen, C. He, H. Shen, D. Wu and D. Wang, *J. Mater. Chem. B*, 2013, **1**, 1755-1764.
105. W. Song, D. C. Markel, X. Jin, T. Shi and W. Ren, *J. Biomed. Mater. Res., Part A*, 2012, **100A**, 3071-3079.
106. W. Kern, W. Herold and B. Scherlag, *Makromol. Chem.*, 1956, **17**, 231-239.
107. R. Speiser, C. H. Hills and C. R. Eddy, *J. Phys. Colloid Chem.*, 1945, **49**, 334-340.
108. D. P. J. Barz and P. Erhrard, *Lab Chip*, 2005, **5**, 949-958.
109. R. Ni, D. Cao and W. Wang, *J. Phys. Chem. B*, 2006, **110**, 26232-26239.
110. P. C. Hiemenz and R. Rajagopalan, in *Principles of Colloid and Surface Chemistry*, 3rd edn., Marcel Dekker, New York, 1991.
111. A. V. Dobrynin and M. Rubinstein, *Prog. Polym. Sci.*, 2005, **30**, 1049-1118.
112. A. Laguecir, S. Ulrich, J. Labille, N. Fatin-Rouge, S. Stoll and J. Buffle, *Eur. Polym. J.*, 2006, **42**, 1135-1144.
113. J. P. Valteau, *Chem. Phys.*, 1989, **129**, 163-175.
114. H. Schiessel, *Macromolecules*, 1999, **32**, 5673-5680.
115. M. J. Zohuriaan-Mehr, H. Omidian, S. Doroudiani and K. Kabiri, *J. Mater. Sci.*, 2010, **45**, 5711-5735.
116. T. Hussain, M. Ansari, N. M. Ranjha, I. U. Khan and Y. Shahzad, *Sci. World J.*, 2013, **2013**, 1-9.
117. N. M. Ranjha, J. Mudassir and S. Majeed, *Bull. Mater. Sci.*, 2011, **34**, 1537-1547.
118. S. K. Bajpai, N. Chand and S. Soni, *J. Biomater. Sci. Polym. Ed.*, 2015, **26**, 947-962.
119. J. Kim, D. D. Arola, L.-S. Gu, Y. K. Kim, S. Mai, Y. Liu, D. H. Pashley and F. R. Tay, *Acta Biomater.*, 2010, **6**, 2740-2750.
120. Y. K. Kim, L.-S. Gu, T. E. Bryan, J. R. Kim, L. Chen, Y. Liu, J. C. Yoon, L. Breschi, D. H. Pashley and F. R. Tay, *Biomaterials*, 2010, **31**, 6618-6627.
121. L.-S. Gu, Y. K. Kim, Y. Liu, K. Takahashi, S. Arun, C. E. Wimmer, R. Osorio, J.-Q. Ling, S. W. Looney, D. H. Pashley and F. R. Tay, *Acta Biomater.*, 2011, **7**, 268-277.
122. K. Schöller, A. Ethirajan, A. Zeller and K. Landfester, *Macromol. Chem. Phys.*, 2011, **212**, 1165-1175.
123. C. D. G. Abueva and B.-T. Lee, *Int. J. Biol. Macromol.*, 2014, **64**, 294-301.
124. R. A. Gemeinhart, C. M. Bare, R. T. Haasch and E. J. Gemeinhart, *J. Biomed. Mater. Res., Part A*, 2006, **78A**, 433-440.
125. C. H. Park, S. Y. Nam and Y. M. Lee, *J. App. Polym. Sci.*, 1999, **74**, 83-89.
126. H. Erdemi and A. Bozkurt, *Eur. Polym. J.*, 2004, **40**, 1925-1929.
127. T. Kusunoki, M. Oshiro, F. Hamasaki and T. Kobayashi, *J. Appl. Polym. Sci.*, 2011, **119**, 3072-3079.

128. R. A. Franco, Y.-K. Min, H.-M. Yang and B.-T. Lee, *J. Nanomater.*, 2012, **2012**, 1-9.
129. J. D. Kretlow, M. C. Hacker, L. Klouda, B. B. Ma and A. G. Mikos, *Biomacromolecules*, 2010, **11**, 797-805.
130. S. Y. Kim and J.-S. Park, *J. App. Polym. Sci.*, 2014, **131**, 41194-41205.
131. J. Tan, R. A. Gemeinhart, M. Ma and W. M. Saltzman, *Biomaterials*, 2005, **26**, 3663-3671.
132. A. K. Bassi, J. E. Gough, M. Zakikhani and S. Downes, *J. Tissue Eng.*, 2011, **2011**, 1-9.
133. A. K. Bassi, J. E. Gough and S. Downes, *J. Tissue Eng. Regen. Med.*, 2012, **6**, 833-840.
134. A. K. Ghag, J. E. Gough and S. Downes, *Biomater. Sci.*, 2014, **2**, 233-241.
135. S. G. Cohen, *J. Am. Chem. Soc.*, 1945, **67**, 17-20.
136. C. K. Ober and M. L. Hair, *J. Polym. Sci., Part A: Polym. Chem.*, 1987, **25**, 1395-1407.
137. G. Odian, *Principles of Polymerisation*, 4th edn., John Wiley & Sons, Inc., New Jersey, 2004, Ch. 3, pp. 198-291.
138. L. M. Gugliotta, A. Salazar, J. R. Vega and G. R. Meira, *Polymer*, 2001, **42**, 2719-2726.
139. M. F. Cunningham and T. Witty, *Polym. React. Eng.*, 2003, **11**, 519-540.
140. A. Valdebenito and M. V. Encinas, *Polymer*, 2005, **46**, 10658-10662.
141. G. Odian, *Principles of Polymerisation*, 4th edn., John Wiley & Sons, Inc., New Jersey, 2004, Ch. 6, pp. 464-506.
142. Z. Wang and F. R. W. McCourt, *Macromolecules*, 1989, **22**, 2788-2795.
143. N. Striebeck, *Polymer*, 1992, **33**, 2792-2795.
144. F. R. Mayo and F. M. Lewis, *J. Am. Chem. Soc.*, 1944, **66**, 1594-1601.
145. H. Staudinger and J. Schneiders, *Ann. Chem.*, 1939, **541**, 151-195.
146. J. Chun, A. P. Poloski and E. K. Hansen, *J. Colloid Interface Sci.*, 2010, **348**, 280-288.
147. Y. Wang, R. A. Pethrick, N. E. Hudson and C. J. Schaschke, *Ind. Eng. Chem. Res.*, 2012, **51**, 16196-16208.
148. M. Riahi-zhad, N. Kazemi, N. McManus and A. Penlidis, *J. App. Polym. Sci.*, 2014, **131**, 40949-40955.
149. B. L. Rivas and N. Schiappacasse, *J. Appl. Polym. Sci.*, 2003, **88**, 1698-1704.
150. C. Zaldívar, O. d. Sol and G. D. Iglesias, *Polymer*, 1997, **39**, 245-246.
151. A. Paril, A. Giz and H. Catalgil-Giz, *J. App. Polym. Sci.*, 2013, **127**, 3530-3536.
152. I. Rintoul and C. Wandrey, *Polymer*, 2005, **46**, 4525-4532.
153. B. Bingöl, W. H. Meyer, M. Wagner and G. Wegner, *Macromol. Rapid Commun.*, 2006, **27**, 1719-1724.
154. B. Bingöl, C. Strandberg, A. Szabo and G. Wegner, *Macromolecules*, 2008, **41**, 2785-2790.
155. L. E. P. Santos, L. S. Hanamoto, R. P. Pereira, A. M. Rocco and M. I. Felisberti, *J. App. Polym. Sci.*, 2011, **119**, 460-471.
156. N.-S. Kwak, H.-M. Park and T. S. Hwang, *Chem. Eng. J.*, 2012, **191**, 579-587.
157. *US Pat.*, 4,749,758, 1988.

158. T. Perchyonok, I. N. Lykakis and A. Postigo, *Streamlining Free Radical Green Chemistry*, Royal Society of Chemistry, Cambridge, 2011, Ch. 6, p. 130.
159. V. A. Bhanu and K. Kishore, *Chem. Rev.*, 1991, **91**, 99-117.
160. S. S. Cutié, D. E. Henton, C. Powell, R. E. Reim, P. B. Smith and T. L. Staples, *J. Appl. Polym. Sci.*, 1997, **64**, 577-589.
161. R. E. Dey, X. Zhong, P. J. Youle, Q. G. Wang, I. Wimpenny, S. Downes, J. A. Hoyland, D. C. Watts, J. E. Gough and P. M. Budd, *Macromolecules*, 2016, **49**, 2656-2662.
162. P. B. Zetterlund, S. Yamauchi and B. Yamada, *Macromol. Chem. Phys.*, 2004, **205**, 778-785.
163. H. Yamazoe, P. B. Zetterlund, B. Yamada, D. J. T. Hill and P. J. Pomery, *Macromol. Chem. Phys.*, 2001, **202**, 824-829.
164. C. Strandberg, C. Rosenauer and G. Wegner, *Macromol. Rapid Commun.*, 2010, **31**, 374-379.
165. L. B. Levy, *J. Polym. Sci., Part A: Polym. Chem.*, 1985, **23**, 1505-1515.
166. L. B. Levy, *J. App. Polym. Sci.*, 1996, **60**, 2481-2487.
167. M. Fineman and S. D. Ross, *J. Polym. Sci.*, 1949, **5**, 259-265.
168. T. Kelen and F. Tüdös, *J. Macromol. Sci. Chem.*, 1975, **9**, 1-27.
169. M. Olvera de la Cruz, L. Belloni, M. Delsanti, J. P. Dalbiez, O. Spalla and M. Drifford, *J. Chem. Phys.*, 1995, **103**, 5781-5791.
170. F. J. Solis and M. Olvera de la Cruz, *Macromolecules*, 1998, **31**, 5502-5506.
171. T. Arakawa and S. N. Timasheff, *Biochemistry*, 1984, **23**, 5912-5923.
172. I. Sabbagh and M. Delsanti, *Eur. Phys. J.*, 2000, **1**, 75-86.
173. D. Kuila, G. A. Blay, R. E. Borjas, S. Hughes, P. Maddox, K. Rice, W. Stansbury and N. Laurel, *J. App. Polym. Sci.*, 1999, **73**, 1097-1115.
174. B. Kriwet and T. Kissel, *Int. J. Pharm.*, 1996, **127**, 135-145.
175. J.-P. Boisvert, A. Malgat, I. Pochard and C. Daneault, *Polymer*, 2002, **43**, 141-148.
176. A. Gericke, C. Qin, L. Spevak, Y. Fujimoto, W. T. Butler, E. S. Sørensen and A. L. Boskey, *Calcif. Tissue Int.*, 2005, **77**, 45-54.
177. K. Alvares, *Connect. Tissue Res.*, 2014, **55**, 34-40.
178. T. Kokubo, H. Kushitani and S. Sakka, *J. Biomed. Mater. Res.*, 1990, **24**, 721-734.
179. P. N. Chavan, M. M. Bahir, R. U. Mene, M. P. Mahabole and R. S. Khairnar, *Mater. Sci. Eng.*, 2010, **168**, 224-230.
180. Y. A. Levin, V. G. Romanov and B. Y. Ivanov, *Polym. Sci. U.S.S.R.*, 1975, **17**, 880-886.
181. Q. G. Wang, I. Wimpenny, R. E. Dey, X. Zhong, P. J. Youle, S. Downes, D. C. Watts, P. M. Budd, J. A. Hoyland and J. E. Gough, *J. Biomed. Mater. Res.*, 2017, In preparation.
182. T. T. Thula, F. Svedlund, D. E. Rodriguez, J. Podschun, L. Pendi and L. B. Gower, *Polymers*, 2011, **3**, 10-35.
183. S. Patashnik, L. Rabinovich and G. Golomb, *J. Drug Targeting*, 1997, **4**, 371-380.

184. E. H. Nafea, M. A. El-Massik, L. K. El-Khordagui, M. K. Marei and N. M. Khalafallah, *J. Microencapsulation*, 2007, **24**, 525-538.
185. R. Huolman and N. Ashammakhi, *J. Craniofac. Surg.*, 2007, **18**, 295-301.
186. C. E. Holy, C. Cheng, J. E. Davies and M. S. Shoichet, *Biomaterials*, 2001, **22**, 25-31.
187. Z. Dai, J. Ronholm, Y. Tian, B. Sethi and X. Cao, *J. Tissue Eng.*, 2016, **7**, 1-13.
188. E. Cottam, D. W. L. Hukins, K. Lee, C. Hewitt and M. J. Jenkins, *Med. Eng. Phys.*, 2009, **31**, 221-226.
189. H. Shearer, M. J. Ellis, S. P. Perera and J. B. Chaudhuri, *Tissue Eng.*, 2006, **12**, 2717-2727.
190. M. Kyuzou, W. Mori and J. Tanaka, *Inorg. Chim. Acta*, 2010, **363**, 930-934.
191. S. Lodhia, A. Turner, M. Papadaki, K. D. Demadis and G. B. Hix, *Cryst. Growth Des.*, 2009, **9**, 1811-1822.
192. Y. L. Lo, C. Y. Hsu and H. R. Lin, *J. Drug Targeting*, 2013, **21**, 54-66.
193. N. M. Ranjha, G. Ayub, S. Naseem and M. T. Ansari, *J. Mater. Sci.*, 2010, **21**, 2805-2816.
194. J. E. Elliott, M. MacDonald, J. Nie and C. N. Bowman, *Polymer*, 2004, **45**, 1503-1510.
195. S.-M. Lien, L.-Y. Ko and T.-J. Huang, *Acta Biomater.*, 2009, **5**, 670-679.
196. M. D. Abramoff, P. J. Magalhaes and S. J. Ram, *Biophotonics Int.*, 2004, **11**, 36-42.
197. J. Serth, M. A. Kuczyk, U. Paeslack, R. Lichtinghagen and U. Jonas, *Am. J. Pathol.*, 2000, **156**, 1189-1196.
198. R. Arnold, *J. Colloid Sci.*, 1957, **12**, 549-556.
199. B. V. Slaughter, S. S. Khurshid, O. Z. Fisher, A. Khademhosseini and N. A. Peppas, *Adv. Mater.*, 2009, **21**, 3307-3329.
200. A. S. Hoffman, *Adv. Drug Del. Rev.*, 2002, **54**, 3-12.
201. B. P. Robinson, J. O. Hollinger, E. H. Szachowicz and J. Brekke, *Otolaryngol. Head Neck Surg.*, 1995, **112**, 707-713.
202. K. Whang, K. E. Healy, D. R. Elenz, E. K. Nam, D. C. Tsai, C. H. Thomas, G. W. Nuber, F. H. Glorieux, R. Travers and S. M. Sprague, *Tissue Eng.*, 1999, **5**, 35-51.
203. P. M. López-Pérez, R. M. P. d. Silva, R. A. Sousa, I. Pashkuleva and R. L. Reis, *Acta Biomater.*, 2010, **6**, 3704-3712.
204. ISO, *Biological evaluation of medical devices - Tests for in vitro cytotoxicity (ISO 10993-5)*, 2009.
205. J. Fawell, K. Bailey, J. Chilton, E. Dahi, L. Fewtrell and Y. Magara, *Fluoride in Drinking-water*, World Health Organisation, 2006.
206. A. L. J. J. Bronckers, D. M. Lyaruu and P. K. DenBesten, *J. Dent. Res.*, 2009, **88**, 877-893.
207. P. DenBesten and W. Li, *Monogr. Oral Sci.*, 2011, **22**, 81-96.
208. M. C. Latham and P. Gretch, *J. Public Health*, 1967, **57**, 651-660.
209. P. I. Ndiaye, P. Moulin, L. Dominguez, J. C. Millet and F. Charbit, *Desalination*, 2005, **173**, 25-32.
210. X. Lefebvre, J. Palmeri and P. David, *J. Phys. Chem. B*, 2004, **108**, 16811-16824.

211. K. Hu and J. M. Dickson, *J. Membr. Sci.*, 2006, **279**, 529-538.
212. C. K. Diawara, *Sep. Purif. Rev.*, 2008, **37**, 303-325.
213. A. Szymczyk and P. Fievet, *J. Membr. Sci.*, 2005, **252**, 77-88.
214. M. S. Onyango, Y. Kojima, O. Aoyi, E. C. Bernardo and H. Matsuda, *J. Colloid Interf. Sci.*, 2004, **279**, 341-350.
215. O. J. Hao, A. M. Asce, C. P. Huang and M. Asce, *J. Environ. Eng.*, 1986, **112**, 1054-1069.
216. T. Wajima, Y. Umeta, S. Narita and K. Sugawara, *Desalination*, 2009, **249**, 323-330.
217. M. Habuda-Stanić, M. E. Ravančić and A. Flanagan, *Materials*, 2014, **7**, 6317-6366.
218. M. E. Kaseva, *J. Water Health*, 2006, **4**, 139-147.
219. I. Abe, S. Iwasaki, T. Tokimoto, N. Kawasaki, T. Nakamura and S. Tanada, *J. Colloid Interf. Sci.*, 2004, **275**, 35-39.
220. N. A. Medellin-Castillo, R. Leyva-Ramos, R. Ocampo-Perez, R. F. G. d. l. Cruz, A. Aragon-Piña, J. M. Martinez-Rosales, R. M. Guerrero-Coronado and L. Fuentes-Rubio, *Ind. Eng. Chem. Res.*, 2007, **46**, 9205-9212.
221. N. A. Medellin-Castillo, R. Leyva-Ramos, E. Padilla-Ortega, R. Ocampo-Perez, J. V. Flores-Cano and M. S. Berber-Mendoza, *J. Ind. Eng. Chem.*, 2014, **20**, 4014-4021.
222. C. S. Sundaram, N. Viswanathan and S. Meenakshi, *J. Hazard. Mater.*, 2008, **155**, 206-215.
223. S. M. Prabhu and S. Meenakshi, *Powder Technol.*, 2014, **268**, 306-315.
224. X. Yu, S. Tong, M. Ge and J. Zuo, *Carbohydr. Polym.*, 2013, **92**, 269-275.
225. C. S. Sundaram, N. Viswanathan and S. Meenakshi, *J. Hazard. Mater.*, 2009, **172**, 147-151.
226. C. S. Sundaram, N. Viswanathan and S. Meenakshi, *Bioresour. Technol.*, 2008, **99**, 8226-8230.

## Appendix

### Chapter 2: Synthesis and characterisation of poly(vinylphosphonic acid-*co*-acrylic acid)

#### A2.1 Synthesis of PVPA-*co*-AA

The experimental conditions for the copolymerisation of AA and VPA, with a range of monomer feed ratios, are shown in Table A2.1.

**Table A2.1.** Experimental conditions for the copolymerisation of AA with VPA.

Sample Code	mol% VPA in the feed	$n_{\text{VPA}}$ (mmol)	mol% AA in the feed	$n_{\text{AA}}$ (mmol)	$n_{\text{AAPH}}$ ( $\mu\text{mol}$ )	$V_{\text{water}}$ (mL)
P1	10	5.07	90	45.7	50.7	16.0
P3	50	12.7	50	12.7	25.4	6.00
P4	70	25.4	30	10.9	36.3	4.50

The characterisation data for PVPA-*co*-AA copolymers synthesised with different monomer feed ratios, are presented below:

**P1 (10:90):** (2.55 g, 86% yield).  $\delta_{\text{H}}$  (400 MHz; D<sub>2</sub>O) 4.30 (1 H, br.s, C-O-H), 2.83-2.17 (8 H, m, C-C-H), 2.16-1.27 (17 H, m, C-CH<sub>2</sub>) ppm.  $\delta_{\text{P}}$  (202 MHz; D<sub>2</sub>O) 30.45 (s, C-P=O(OH)<sub>2</sub>) ppm. Elemental analysis (calc.) (%): C 42.20 (42.74), P 4.12 (3.69), H 5.76 (5.60).

**P3 (50:50):** (0.99 g, 22% yield).  $\delta_{\text{H}}$  (400 MHz; D<sub>2</sub>O) 4.29 (1 H, br.s, C-O-H), 2.81-2.20 (13 H, m, C-C-H), 2.18-1.25 (47 H, m, C-CH<sub>2</sub>) ppm.  $\delta_{\text{P}}$  (202 MHz; D<sub>2</sub>O) 29.89 (s, C-P=O(OH)<sub>2</sub>) ppm. Elemental analysis (calc.) (%): C 34.44 (32.24), P 11.20 (10.94), H 5.60 (5.46).

**P4 (70:30):** (0.47 g, 13% yield).  $\delta_{\text{H}}$  (400 MHz; D<sub>2</sub>O) 4.30 (1 H, br.s, C-O-H), 3.06-2.22 (11 H, m, C-C-H), 2.20-1.23 (49 H, m, C-CH<sub>2</sub>) ppm.  $\delta_{\text{P}}$  (202 MHz; D<sub>2</sub>O) 30.61 (s, C-P=O(OH)<sub>2</sub>) ppm. Elemental analysis (calc.) (%): C 30.20 (30.90), P 15.80 (16.10), H 5.30 (5.40).

## A2.2 Synthesis of PVPA-*co*-AA for the evaluation of reactivity ratios

The experimental conditions for the copolymerisation of AA and VPA, for the evaluation of reactivity ratios, are shown in Table A2.2.

**Table A2.2.** Experimental conditions for the copolymerisation of AA with VPA for the evaluation of reactivity ratios.

Sample Code	mol % VPA	<i>n</i> <sub>VPA</sub> (mmol)	mol % AA	<i>n</i> <sub>AA</sub> (mmol)	<i>n</i> <sub>AAPH</sub> (μmol)	<i>V</i> <sub>water</sub> (mL)
R10	10	1.85	90	16.7	18.6	24.0
R20	20	3.70	80	14.8	18.5	22.0
R30	30	4.63	70	10.6	15.2	20.0
R50	50	6.29	50	6.29	12.6	18.0
R60	60	4.63	40	3.08	7.71	16.0
R70	70	6.48	30	2.82	9.30	14.0
R80	80	7.41	20	1.85	9.26	12.0
R90	90	8.33	10	0.93	9.26	10.0

The characterisation data for PVPA-*co*-AA copolymers, synthesised for the evaluation of reactivity ratios, are presented below:

**R10 (10:90):** (1.10 g, 78% yield).  $\delta_{\text{H}}$  (400 MHz; D<sub>2</sub>O) 6.37-5.72 (6 H, m, C=CH<sub>2</sub>), 4.24 (1 H, br.s, C-O-H), 2.72-2.14 (5 H, m, C-C-H), 2.09-1.41 (9 H, m, C-CH<sub>2</sub>) ppm. Elemental analysis (calc.) (%): C 43.75 (41.26), P 1.59 (3.70), H 5.49 (5.55).

**R20 (20:80):** (1.02 g, 70% yield).  $\delta_{\text{H}}$  (400 MHz; D<sub>2</sub>O) 6.35-5.75 (13 H, m, C=CH<sub>2</sub>), 4.23 (1 H, br.s, C-O-H), 2.71-2.14 (7 H, m, C-C-H), 2.07-1.33 (15 H, m, C-CH<sub>2</sub>) ppm. Elemental analysis (calc.) (%): C 41.88 (41.20), P 2.31 (4.21), H 5.55 (5.49).

**R30 (30:70):** (0.70 g, 55% yield).  $\delta_{\text{H}}$  (400 MHz; D<sub>2</sub>O) 6.38-5.74 (17 H, m, C=CH<sub>2</sub>), 4.24 (1 H, br.s, C-O-H), 2.74-2.12 (4 H, m, C-C-H), 2.09-1.35 (11 H, m, C-CH<sub>2</sub>) ppm. Elemental analysis (calc.) (%): C 41.21 (39.20), P 3.17 (5.31), H 5.63 (5.54).

**R50 (50:50):** (0.47 g, 41% yield).  $\delta_{\text{H}}$  (400 MHz; D<sub>2</sub>O) 6.33-5.75 (34 H, m, C=CH<sub>2</sub>), 4.26 (1 H, br.s, C-O-H), 2.71-2.14 (5 H, m, C-C-H), 2.11-1.33 (14H, m, C-CH<sub>2</sub>) ppm. Elemental analysis (calc.) (%): C 38.71 (38.10), P 5.00 (6.80), H 5.09 (5.00).

**R60 (60:40):** (0.30 g, 42% yield).  $\delta_{\text{H}}$  (400 MHz; D<sub>2</sub>O) 6.37-5.76 (34 H, m, C=CH<sub>2</sub>), 4.27 (1 H, br.s, C-O-H), 2.73-2.15 (5H, m, C-C-H), 2.11-1.35 (13H, m, C-CH<sub>2</sub>) ppm. Elemental analysis (calc.) (%): C 37.70 (36.20), P 6.95 (8.01), H 5.74 (6.24).

**R70 (70:30):** (0.15 g, 16% yield).  $\delta_{\text{H}}$  (400 MHz; D<sub>2</sub>O) 6.34-5.75 (37 H, m, C=CH<sub>2</sub>), 4.27 (1 H, br.s, C-O-H), 2.75-2.18 (4 H, m, C-C-H), 2.11-1.35 (15 H, m, C-CH<sub>2</sub>) ppm. Elemental analysis (calc.) (%): C 36.93 (39.20), P 9.38 (9.36), H 5.27 (5.14).

**R80 (80:20):** (0.18 g, 19% yield).  $\delta_{\text{H}}$  (400 MHz; D<sub>2</sub>O) 6.36-5.77 (44 H, m, C=CH<sub>2</sub>), 4.26 (1 H, br.s, C-O-H), 2.74-2.13 (1 H, m, C-C-H), 2.12-1.34 (3 H, m, C-CH<sub>2</sub>) ppm. Elemental analysis (calc.) (%): C 34.25 (37.70), P 12.49 (10.41), H 3.56 (5.09).

**R90 (90:10):** (0.28 g, 29% yield).  $\delta_{\text{H}}$  (400 MHz; D<sub>2</sub>O) 6.34-5.77 (57 H, m, C=CH<sub>2</sub>), 4.27 (1 H, br.s, C-O-H), 2.76-2.15 (1 H, m, C-C-H), 2.13-1.36 (5 H, m, C-CH<sub>2</sub>) ppm. Elemental analysis (calc.) (%): C 36.93 (37.80), P 14.83 (12.56), H 5.27 (5.10).

### **A2.3. Synthesis of PVPA-*co*-AA using chain transfer agent (CTA)**

The characterisation data for PVPA-*co*-AA copolymers, with different monomer feed ratios and in the presence of chain transfer agent, are presented below:

**PVPA-20:** (0.78 g, 75% yield).  $\delta_{\text{H}}$  (400 MHz; D<sub>2</sub>O) 4.29 (1 H, br.s, C-O-H), 2.78-2.19 (10 H, m, C-C-H), 2.16-1.28 (22 H, m, C-CH<sub>2</sub>) ppm.  $\delta_{\text{P}}$  (202 MHz; D<sub>2</sub>O) 30.07 (s, C-P=O(OH)<sub>2</sub>) ppm. Elemental analysis (calc.) (%): C 38.09 (39.30), P 5.64 (6.36), H 5.85 (5.04).

**PVPA-30:** (1.36 g, 73% yield).  $\delta_{\text{H}}$  (400 MHz; D<sub>2</sub>O) 4.29 (1 H, br.s, C-O-H), 2.81-2.21 (22 H, m, C-C-H), 2.17-1.28 (67 H, m, C-CH<sub>2</sub>) ppm.  $\delta_{\text{P}}$  (202 MHz; D<sub>2</sub>O) 31.11 (s, C-P=O(OH)<sub>2</sub>) ppm. Elemental analysis (calc.) (%): C 36.54 (35.30), P 9.52 (10.36), H 5.64 (5.04).

**PVPA-60:** (0.78 g, 38% yield).  $\delta_{\text{H}}$  (400 MHz; D<sub>2</sub>O) 4.28 (1 H, br.s, C-O-H), 2.81-2.16 (15 H, m, C-C-H), 2.14-1.21 (33 H, m, C-CH<sub>2</sub>) ppm.  $\delta_{\text{P}}$  (202 MHz; D<sub>2</sub>O) 31.13 (s, C-P=O(OH)<sub>2</sub>) ppm. Elemental analysis (calc.) (%): C 27.92 (31.50), P 17.71 (15.86), H 5.25 (5.34).

**PVPA-80:** (0.60 g, 30% yield).  $\delta_{\text{H}}$  (400 MHz; D<sub>2</sub>O) 4.29 (1 H, br.s, C-O-H), 3.04-2.17 (19 H, m, C-C-H), 2.15-1.24 (51 H, m, C-CH<sub>2</sub>) ppm.  $\delta_{\text{P}}$  (202 MHz; D<sub>2</sub>O) 31.16 (s, C-P=O(OH)<sub>2</sub>) ppm. Elemental analysis (calc.) (%): C 22.62 (26.30), P 22.74 (20.20), H 4.89 (5.05).

#### A2.4 FT-IR spectra of PVPA-*co*-AA copolymers

The FT-IR spectra of PVPA-20 and PVPA-80 copolymers are presented in Figure A2.1.

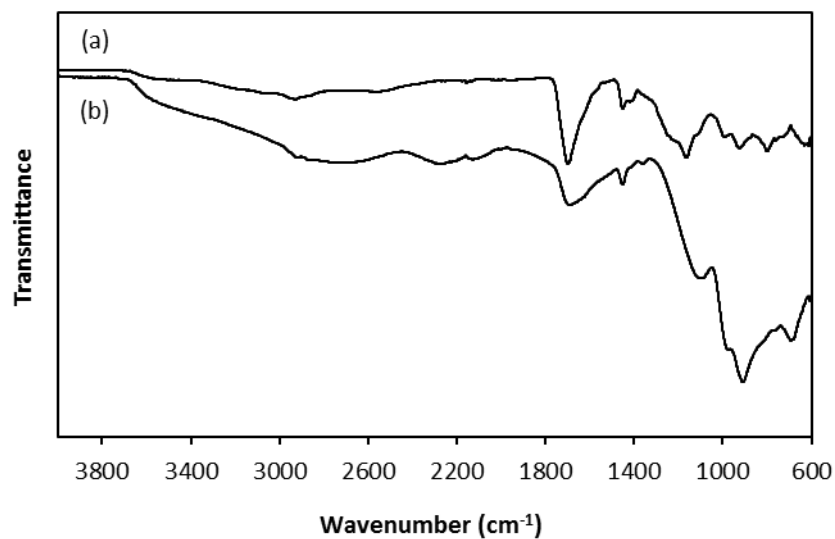


**Figure A2.1.** FT-IR spectra of (a) PVPA-20 and (b) PVPA-80.

### Chapter 3: Calcium binding affinity of PVPA-*co*-AA

#### A3.1 Assessment of calcium binding affinity: calibration

The calibration curve for the determination of calcium chelation by PVPA-30, with respect to polymer concentration, is shown in Figure A3.1.

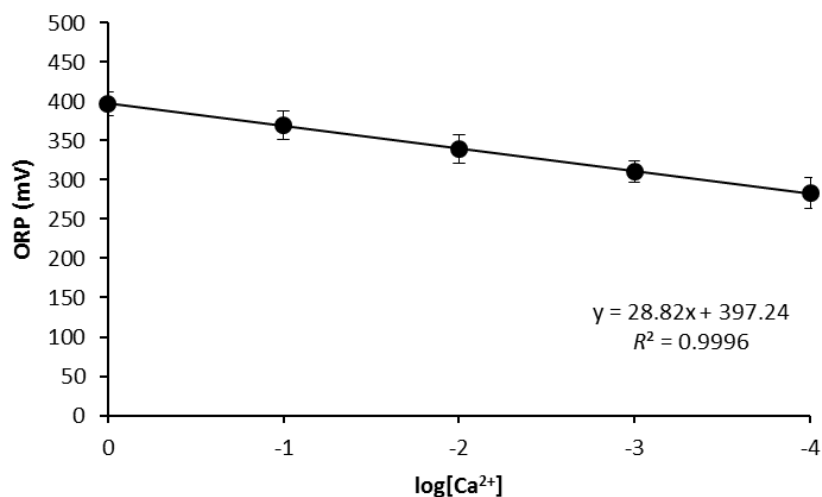


**Figure A3.1.** Calibration curve for the determination of calcium chelation by PVPA-30, with regards to polymer concentration.

The calibration curve for the determination of calcium chelation by PVPA-0, PVPA-30 and PVPA-100, with respect to the ionic strength of the medium, is shown in Figure A3.2.

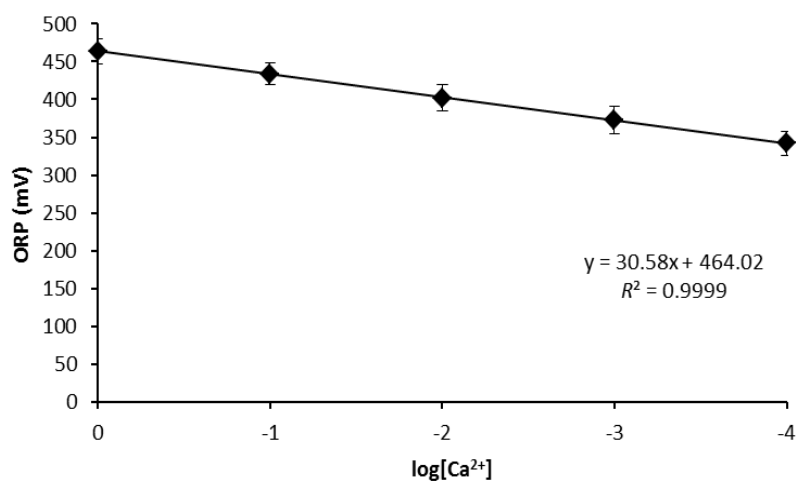


**Figure A3.2.** Calibration curve for the determination of calcium chelation by PVPA-0, PVPA-30 and PVPA-100, with regards to the ionic strength of the medium.

The effect of added  $\text{MgCl}_2$  on the calcium chelation capacity of PVPA-30 is presented in Figure A3.3.

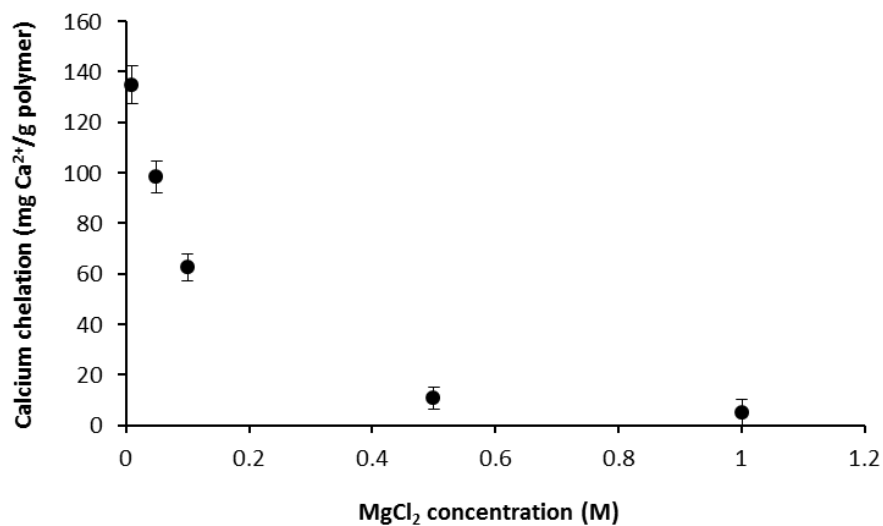


**Figure A3.3.** Calcium chelation capacity of PVPA-30 with increasing  $\text{MgCl}_2$  concentration. Polymer solutions ( $5.0 \text{ mg mL}^{-1}$ ) were prepared in deionised water at pH 7.3.

#### **Chapter 4: Incorporation of PVPA-*co*-AA into electrospun PCL scaffolds**

The calibration curve for the determination of calcium chelation by PCL/PVPA-*co*-AA scaffolds is shown in Figure A4.1.

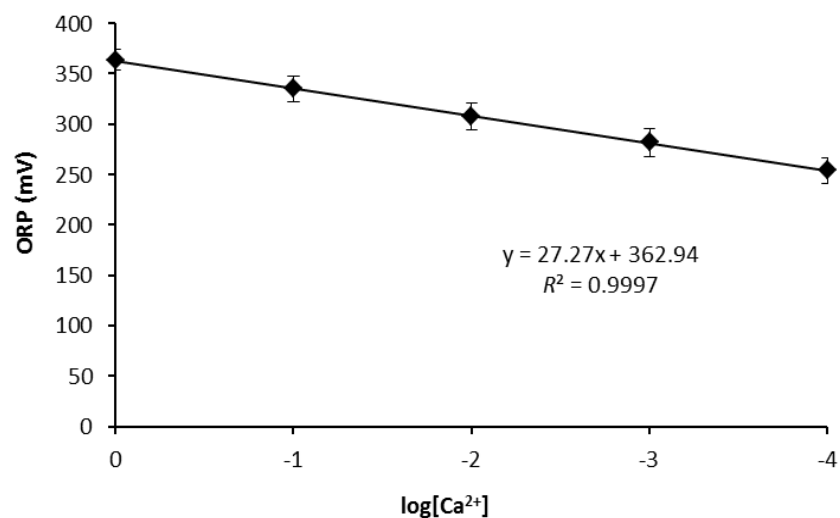


**Figure A4.1.** Calibration curve for the determination of calcium chelation by PCL/PVPA-*co*-AA scaffolds.

The calibration curve for the determination of calcium chelation by PCL/PVPA-*co*-AA scaffolds in osteogenic differentiation media is presented in Figure A4.2.

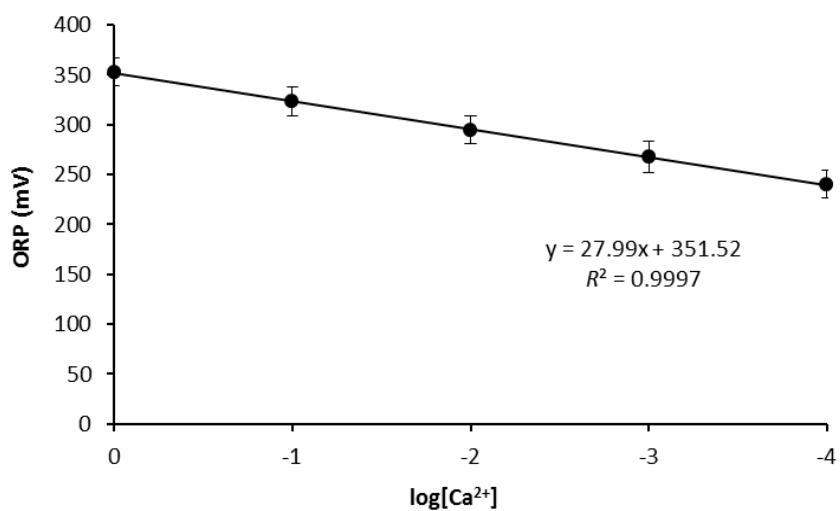


**Figure A4.2.** Calibration curve for the determination of calcium chelation by PCL/PVPA-*co*-AA scaffolds in osteogenic differentiation media.

## Chapter 6: Application of PVPA-co-AA for fluoride removal from groundwater

The storage ( $G'$ ) and loss ( $G''$ ) modulus of PVPA-HA hydrogel is shown in Figure A6.1 across a strain range of 1.0-125%. The linear viscoelastic region (LVR) is between 20 and 100 % strain.

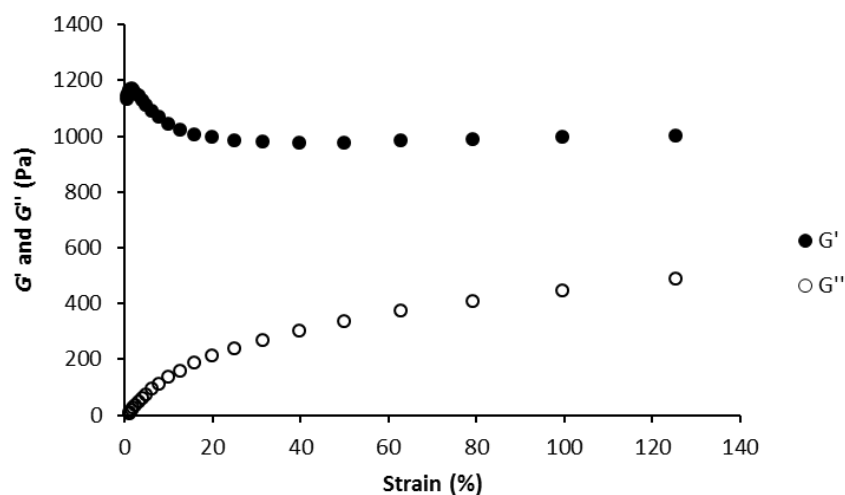


**Figure A6.1.** Storage ( $G'$ ) and loss ( $G''$ ) modulus of PVPA-HA hydrogel, with a nHA concentration of 0.25 mM, across a strain range of 1.0-125%.

The calibration curves for the determination of fluoride uptake by PVPA-HA hydrogels are shown below:

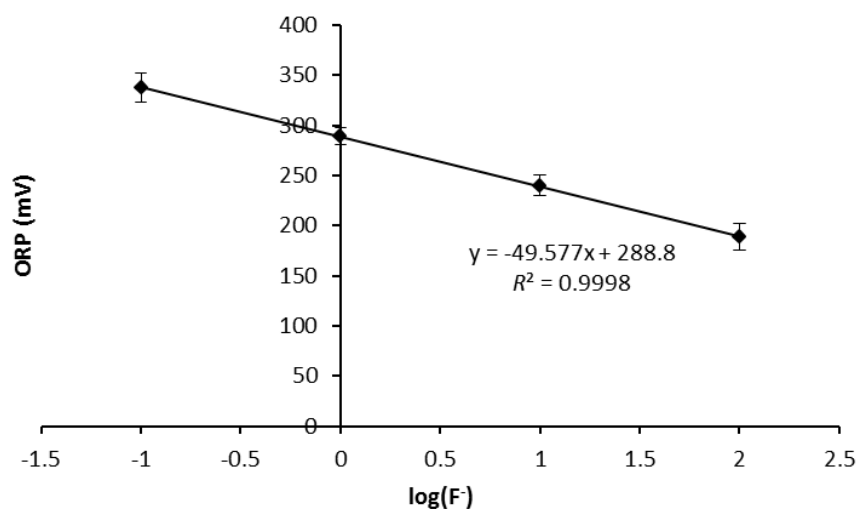


**Figure A6.2.** Calibration curve for the determination of fluoride uptake by PVPA-HA hydrogels.

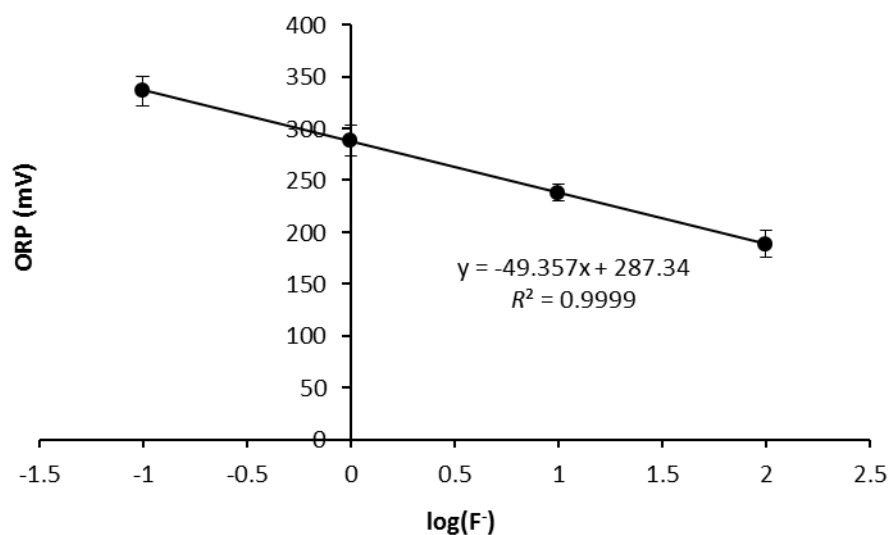


**Figure A6.3.** Calibration curve for the determination of the effect of pH on the fluoride uptake of PVPA-HA hydrogels.

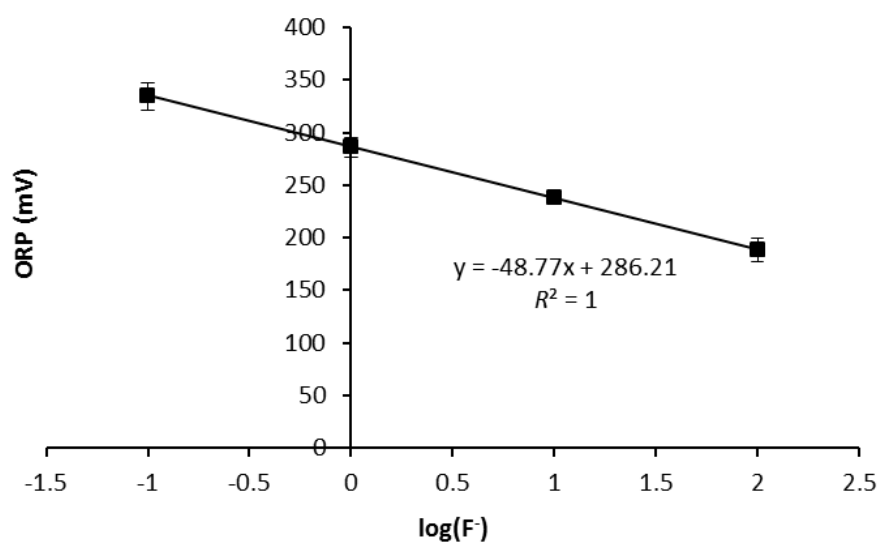


**Figure A6.4.** Calibration curve for the determination of contact time on the fluoride uptake of PVPA-HA hydrogels.

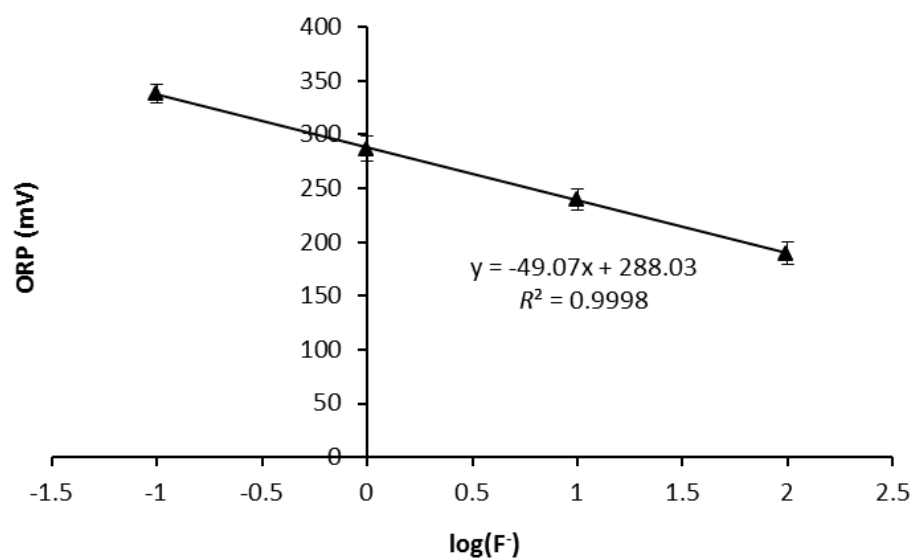


**Figure A6.5.** Calibration curve for the determination of the effect of competing ions on the fluoride uptake of PVPA-HA hydrogels.

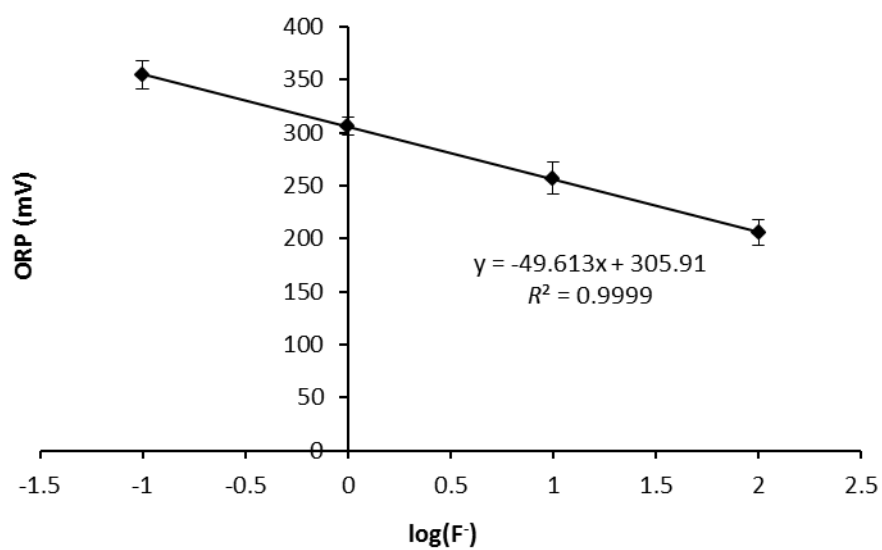


**Figure A6.6.** Calibration curve for the determination of regeneration on the fluoride uptake of PVPA-HA hydrogels.